The Effects of Higher Strength and Associated Concrete Properties on Pavement Performance

PUBLICATION NO. FHWA-RD-00-161

JUNE 2001

U.S. Department of Transportation
Federal Highway Administration

Research, Development, and Technology
Turner-Fairbank Highway Research Center
6300 Georgetown Pike
McLean, VA 22101-2296

FOREWORD

This report documents the investigation of the effect of strength and other associated concrete properties of the long-term performance of concrete pavements. Performance criteria used included joint spalling, faulting and transverse slab cracking. Project variables included pavement age, traffic, climate, distress levels and types, joint spacing and compressive strength. Compressive strength was found to correlate well with permeability. Concrete characteristics found to be desirable include compressive strength in the 45 to 50 MPa range, flexural strength in the 4.5 to 6.0 range, non-alakali reactive aggregate that is freeze-thaw distress resistant, a well-graded aggregate with large top size, water-cement ratio of 0.42 to 0.45 and cement content of approximately 335 kg/m^3. Prototype mixture designs were developed for different climatic regions.

This report will be of interest to those involved in concrete pavement mixture design, as well as those involved in the design, construction and analysis of concrete pavements. Sufficient copies are being distributed to provide 10 copies to each FHWA Resource Center, five copies to each FHWA Division, and five copies to each State highway agency. Direct distribution is being made to the FHWA Division Offices. Additional copies may be purchased from the National Technical Information Service (NTIS), 5285 Port Royal Road, Springfield, Virginia 22161.

T. Paul Teng, P. E.
Director, Office of Infrastructure,
Research and Development

NOTICE

Technical Report Documentation Page

1. Report No. FHWA-RD-00-161	2. Government Accession No.	3. Recipient's Catalog No.	
4. Title and Subtitle The Effects of Higher Strength and Associated Concrete Properties on Pavement Performance		5. Report Date June 2001 6. Performing Organization Code	
7. Author(s) W. Hansen, E.A. Jensen, and P. Mohr		8. Performing Organization Report No.	
9. Performing Organization Name and Address University of Michigan, 2340 G.G. Brown, Ann Arbor, MI 48109-2125		10. Work Unit No. (TRAIS) 11. Contract or Grant No. DTFH61-95-C-00108	
12. Sponsoring Agency Name and Address Federal Highway Administration, Research, Development and Technology; 6300 Georgetown Pike McLean, Virginia 22101-2296		13. Type of Report and Period Covered Final Report 1995-2001 14. Sponsoring Agency Code HRDI-12	

15. Supplementary Notes: FHWA Contracting Officer's Technical Representative (COTR): Dr. Stephen W. Forster
Special thanks are given to the following highway agencies for their assistance in the conduct of this study: California, Georgia, Iowa, Michigan, Minnesota, Ohio, Wisconsin and Washington State.

16. Abstract

The major goal of this project was to develop recommendations for PCC properties and materials characteristics found in higher strength JPCP's with improved long-term performance as determined by joint spalling and faulting, and transverse slab cracking. Primary project variables were pavement age, climate, traffic (4 to 23 million ESAL's), distress levels and types, joint spacing, and compressive strength. Fifteen JPCP's were selected for detailed field and laboratory investigation. The field compressive and tensile strengths (splitting) ranged from 33 to 75 MPa and from 3.1 to 4.5 MPa, respectively.

Regular strength highway concrete with a design flexure strength of about 4.5 MPa can develop excellent long-term joint spalling resistance provided that (1) good sub-surface drainage conditions are present, (2) the concrete reaches low permeability level over time from additional curing (i.e. high resistance to physical and chemical deterioration from rapid chloride and water permeability test), (3) it has good entrained air void system (i.e. 6 to 8.5 percent), and (4) sound aggregate are used in the concrete mix. Several different permeability tests were evaluated, and each showed a good correlation with compressive strength. The compressive strength test is therefore a good indicator of the permeability level. The range of low permeability can typically be achieved at a compressive strength range of 45 to50 MPa. Water-cementitious ratio was found to be the major mix feature controlling compressive strength. This requires a concrete mix with a water-cementitious ratio of 0.42 to 0.45, a cement content of about 335 kg per m^3 (6 sack mix typical for most SHA's), and well-graded quality aggregate. Several aggregate characteristics of the concrete mix were found important to achieve good long-term pavement performance. These included aggregate inertness with respect to AAR and F-T, and strong and large sized coarse aggregate to ensure good cracking resistance and aggregate interlock. In addition, well-graded aggregate were beneficial in reducing the paste volume fraction. This results in low coefficient of thermal expansion and drying shrinkage, which both are important properties for avoiding premature transverse cracking. Given sufficient slab thickness, good long-term resistance to fatigue (transverse) cracking was found at any flexure strength level of 4.5 to 6 MPa, provided that loss of slab support from pumping erosion was not a factor. Joint faulting was found to be a consequence of factors causing pumping erosion and/or slab settlement and it was not affected by PCC strength level.

Prototype mix designs were developed for different climate regions.

17. Key Words Concrete pavement, Higher Strength PCC, Material Characteristics, Durability, LTPP Database.		18. Distribution Statement No restrictions	
19. Security Classif. (of this report) Unclassified	20. Security Classif. (of this page) Unclassified	21. No. of Pages 256	22. Price

Form DOT F 1700.7 (8-72) Reproduction of completed page authorized

SI* (MODERN METRIC) CONVERSION FACTORS

APPROXIMATE CONVERSIONS TO SI UNITS

Symbol	When You Know	Multiply By	To Find	Symbol
	LENGTH			
in	inches	25.4	millimeters	mm
ft	feet	0.305	meters	m
yd	yards	0.914	meters	m
mi	miles	1.61	kilometers	km
	AREA			
in^2	square inches	645.2	square millimeters	mm^2
ft^2	square feet	0.093	square meters	m^2
yd^2	square yards	0.836	square meters	m^2
ac	acres	0.405	hectares	ha
mi^2	square miles	2.59	square kilometers	km^2
	VOLUME			
fl oz	fluid ounces	29.57	milliliters	mL
gal	gallons	3.785	liters	L
ft^3	cubic feet	0.028	cubic meters	m^3
yd^3	cubic yards	0.765	cubic meters	m^3
NOTE: Volumes greater than 1000 l shall be shown in m^3.				
	MASS			
oz	ounces	28.35	grams	g
lb	pounds	0.454	kilograms	kg
T	short tons (2000 lb)	0.907	megagrams (or "metric ton")	Mg (or "t")
	TEMPERATURE (exact)			
°F	Fahrenheit temperature	5(F-32)/9 or (F-32)/1.8	Celcius temperature	°C
	ILLUMINATION			
fc	foot-candles	10.76	lux	lx
fl	foot-Lamberts	3.426	candela/m^2	cd/m^2
	FORCE and PRESSURE or STRESS			
lbf	poundforce	4.45	newtons	N
lbf/in^2	poundforce per square inch	6.89	kilopascals	kPa

APPROXIMATE CONVERSIONS FROM SI UNITS

Symbol	When You Know	Multiply By	To Find	Symbol
	LENGTH			
mm	millimeters	0.039	inches	in
m	meters	3.28	feet	ft
m	meters	1.09	yards	yd
km	kilometers	0.621	miles	mi
	AREA			
mm^2	square millimeters	0.0016	square inches	in^2
m^2	square meters	10.764	square feet	ft^2
m^2	square meters	1.195	square yards	yd^2
ha	hectares	2.47	acres	ac
km^2	square kilometers	0.386	square miles	mi^2
	VOLUME			
mL	milliliters	0.034	fluid ounces	fl oz
L	liters	0.264	gallons	gal
m^3	cubic meters	35.71	cubic feet	ft^3
m^3	cubic meters	1.307	cubic yards	yd^3
	MASS			
g	grams	0.035	ounces	oz
kg	kilograms	2.202	pounds	lb
Mg (or "t")	megagrams (or "metric ton")	1.103	short tons (2000 lb)	T
	TEMPERATURE (exact)			
°C	Celcius temperature	1.8C + 32	Fahrenheit temperature	°F
	ILLUMINATION			
lx	lux	0.0929	foot-candles	fc
cd/m^2	candela/m^2	0.2919	foot-Lamberts	fl
	FORCE and PRESSURE or STRESS			
N	newtons	0.225	poundforce	lbf
kPa	kilopascals	0.145	poundforce per square inch	lbf/in^2

* SI is the symbol for the International System of Units. Appropriate rounding should be made to comply with Section 4 of ASTM E380.

(Revised September 1993)

TABLE OF CONTENTS

VOLUME I: FINAL REPORT

TABLE OF CONTENTS (CONTINUED)

TABLE OF CONTENTS (CONTINUED)

TABLE OF CONTENTS (CONTINUED)

TABLE OF CONTENTS (CONTINUED)

VOLUME II: APPENDIXES

LIST OF FIGURES

LIST OF FIGURES (CONTINUED)

LIST OF FIGURES (CONTINUED)

LIST OF FIGURES (CONTINUED)

LIST OF TABLES

LIST OF TABLES (CONTINUED)

LIST OF ABBREVIATIONS

Abbreviation	Meaning
AASHO	American Association of State Highway Officials
AASHTO	American Association of State Highway and Transportation Officials
AADT	Annual Average Daily Traffic
AAR	Alkali Reaction
ACI	American Concrete Institute
ACPA	American Concrete Pavement Association
ASR	Alkali Silica Reaction
ASTM	American Society for Testing and Materials
ATB	Asphalt Treated Base
CBR	California Bearing Ratio
CRCP	Continuous Reinforced Concrete Pavement
CS	Control Section
CTB	Cement Treated Base
CTE	Coefficient of Thermal Expansion
DCP	Dynamic Cone Penetrometer
DF	Dry-Freeze (climate zone)
DGAB	Dense Graded Aggregate Base
DNF	Dry-No-Freeze (climate zone)
ESAL's	Equivalent Single Axle Loads
FHWA	Federal Highway Administration
FMC	Fracture Mechanics of Concrete
FPT	Field Permeability Test
F-T	Freeze-Thaw
FWD	Falling Weight Deflectometer
GPS	General Pavement Studies (database)
HSC	High Strength Concrete
IMS	Information Management System
JCP	Jointed Concrete Pavement
JPCP	Jointed Plain Concrete Pavement
JRCP	Jointed Reinforced Concrete Pavement
LCB	Lean Concrete Base
LTE	Load Transfer Efficiency
LTPP	Long Term Pavement Performance
LVDT's	Linear Variable Differential Transducers
MDOT	Michigan Department of Transportation
MTS	Material Testing System
MTU	Michigan Technological University
NCHRP	National Cooperative Highway Research Program
NDT	Nondestructive Deflection Testing

LIST OF ABBREVIATIONS (CONTINUED)

Abbreviation	Meaning
PCA	Portland Cement Association
PCC	Portland Cement Concrete
RCPT	Rapid Chloride Permeability Test
RH	Relative Humidity
S/D	Span to Depth ratio
SHA's	State Highway Agencies
SHRP	Strategic Highway Research Program
SME	Soil & Materials Engineering, Inc.
SR	State Road
TAP	Technical Advisory Panel
U of M	University of Michigan
W/C ratio	Water/Cement or Water/Cementitious materials ratio
WF	Wet-Freeze (climate zone)
WIM	Weigh in Motion
WNF	Wet-No-Freeze (climate zone)

LIST OF SYMBOLS

Symbol	Meaning
B	Brittleness number
E or E_{PCC}	Elastic modulus of PCC
ε	Shrinkage coefficient
f'_c	Compressive strength
f_m	Flexural strength
f_{sp}	Splitting tensile strength
G_F	Fracture energy
k	Dynamic modulus of subgrade reaction
K_1	Fracture toughness
K_T	Coefficient of Torrent air permeability (10^{-16} in^2)
K_W	Coefficient of water permeability (in/sec)
ρ	Electrical resistance
s_e	Energy brittleness number

TABLE OF TEST SECTION LOCATIONS

Climate Region	SHRP State Code	Test Section ID		Project location
		SHRP Sections	Other Sections	
DNF	6	3017		NB, SR 2, Glendale, California
	6	3021		WB, I-8, Buckman Springs, California
	6		CS1	NB, I-5,Tracy California Test Road-Control Section
	6		CS3	NB,I-5,Tracy, CA Test Road-Higher Cement Content
	6	7456		NB, I-5, Tracy Test Road-Thickened Section, California
	6		I-10	WB, I-10, Ontario Co., Los Angeles, California
DF	53	3019		EB, I-82, Benton Co., Washington
WF	19	3006		WB, US-30, Clinton Co., Iowa
	19	3055		WB, US-20, Hamilton Co., Iowa
	27	4054		WB, I-90, Winona Co., Minnesota
	39	3801		SB, SR-7, Belmont Co., Ohio
	55	3008		Ozaukee Co., Wisconsin
WNF	53	3011		SB, I-5, Whatcom Co., Washington
	53	3812		NB, I-5,Snohomish Co., Washington
	13		GA15	WB, I-85, Newman Co., Georgia

INTRODUCTION

Background

Many portland cement concrete (PCC) pavements on the Interstate highway system have met or exceeded their original design lives (about 20 years). In many cases, the good performing pavements have carried more than twice their design traffic. The good performance has been manifested by no or very low chemical and physical deterioration and structural distresses, in particular near joints and free edges.

In 1991, Washington State Department of Transportation investigated two urban Interstate PCC pavement sections along State Road (SR) 5 in Seattle and SR 90 in Spokane that had performed exceptionally well (e.g., no cracking or joint faulting). The evaluation showed that the pavement sections had carried 50 percent and 60 percent respectively more Equivalent Single Axle Loads (ESAL's) than could be expected using the American Association of State Highway and Transportation Official's (AASHTO) Design Guide. This unusually good performance was attributed to good foundation design with excellent drainage, mild environmental conditions, high quality aggregates in the mix, and high inplace concrete strength. On SR 5 the average in-place compressive and tensile (splitting) strengths were 78 MPa (11,406 lbf/in^2) and 6.4 MPa (923 lbf/in^2) respectively for 102-mm (4-in) diameter cores. Core strength data for SR 90 was 61.4 MPa (8,894 lbf/in^2) and 5.2 MPa (752 lbf/in^2) in compression and tension, respectively. These values are significantly higher than those typically specified on a paving project (usually in the range of 27.6 MPa (4,000 lbf/in^2) in compression), and were probably obtained through fortuitous circumstances at the time of construction (Mahoney et al., 1991).

With the large number of older PCC pavements now in service, State Highway Agencies (SHA's) must consider either rehabilitation or new construction. It would be optimal if the properties that allowed for such excellent performance in Washington could be reproduced in this upcoming work. In concrete applications other than pavements (e.g., bridges, columns for high rise buildings, off shore structures, etc.), there is a trend toward using higher strength. Design strengths of 55 to 75 MPa (8,000 to 11,000 lbf/in^2) or higher have been utilized with success. The advantages of using high strength concrete (HSC) in structural applications are well understood, as the structural demand on the material is high. In pavements, however, the advantage of higher-strength is less obvious. For this reason, strength is being used only as a measure to indicate which pavements might perform better than others. The focus of this study is the material response of the concrete, and not the structural performance of the pavement system.

Project Objectives

The main objective of this project is to determine the effect of the concrete quality on pavement performance, specifically the effect of increasing strength and altering associated properties. In many current paving specifications quality is defined by flexural strength, compressive strength, and air content. It is possible that PCC properties other than strength and air content may prove to be good or better indicators of improved long-term performance of concrete pavements.

To fulfill the research needs described above, the Federal Highway Administration (FHWA) initiated this project in October 1995. The overall objectives are to:

1. Determine the properties of portland cement concrete of higher strength found in certain inservice pavements which resulted in exceptional long-term performance, particularly as evidenced in freedom from distress near joints and free edges.

2. Identify test methods to measure (quantify) these properties. Also, determine the material characteristics of the concrete constituents and their proportions, which are responsible for the levels of these properties found in the concrete.

3. Develop, if necessary, revised mix design procedures including any additional fresh or hardened concrete tests, and develop recommendations for mix designs that will result in the production of concrete for use in pavements that would possess these properties while still meeting current construction requirements and economic considerations.

Project Phases

The work conducted in this project can be divided into three phases. The first phase of the project consisted of three parts. The first part was a comprehensive state-of-the-art literature review on important PCC properties, their apparent relation to the PCC pavement performance and PCC mix characteristics. The second part of phase one was an evaluation of the Strategic Highway Research Program's (SHRP) Long Term Pavement Performance (LTPP) database for PCC pavements of higher strength and their durability performance near joints and cracks. Finally, the third part was to identify and select up to 12 test sections throughout the United States, from primarily excellent performing concrete pavements, for inservice pavement evaluation.

The second phase consisted of performing and evaluating field tests and condition surveys of each of the selected test sections. At the University of Michigan (U of M), Michigan

Department of Transportation (MDOT), and the Michigan Technological University (MTU) laboratories the PCC properties and material characteristics were measured and determined through standardized and systemized testing procedures.

The third phase was mainly development of recommendations based on the field results and any additional laboratory testing of pavement concretes. The field results were evaluated to identify the required levels of PCC properties and their material characteristics in order to obtain excellent pavement concrete. In addition, controlled laboratory investigations were performed on standard pavement concrete mixes to further establish trends and to fill gaps not answered by field testing.

Advisory Panel

An advisory panel consisting of experienced pavement engineers was assembled to provide guidance to the research team in the collection and evaluation of the PCC properties and material characteristics, and the PCC pavement performance. Members of the advisory panel were:

Dr. Jamshid M. Armaghani, Florida Department of Transportation
Mr. Bill Cape, James Cape & Sons
Mr. Larry Cole, American Concrete Pavement Association
Mr. Jim Grove, Iowa Department of Transportation
Mr. Robyn Moore, Washington Department of Transportation
Mr. Elias H. Rmeili, Texas Department of Transportation, and
Mr. David L. Smiley, Michigan Department of Transportation

Overview of the Report

The results of this project are presented in this final report along with appendixes (separate volume). This report consists of eight chapters. Chapter 1 summarizes the comprehensive literature review of important PCC properties, and their apparent relation to the PCC pavement performance and PCC mix characteristics. It also summarizes an evaluation of the LTPP database for PCC pavements of higher strength and their durability performance near joints and cracks. Chapter 2 presents the outline and methodology for field site selection. Experimental procedures for field and laboratory evaluation of the selected pavements are also presented. Chapter 3 includes a brief site description of each investigated test section, a description of the PCC on a petrographic level, and a presentation of summary data tables obtained from the laboratory tests. Chapter 4 presents an evaluation of the field distress and its causes for the various test sections. Links are made between distress types and concrete properties, and mix characteristics and pavement design factors. The PCC property results from the testing on field

concretes are analyzed and discussed in chapter 5. Chapter 6 presents the PCC material characteristics that resulted in the concrete properties reported in chapter 5. Chapter 7 presents the development of project recommendations.

CHAPTER 1. LITERATURE REVIEW SUMMARY ON "EFFECTS OF INCREASING CONCRETE STRENGTH AND ASSOCIATED PCC PROPERTIES ON LONG-TERM PAVEMENT PERFORMANCE"

1.1 Introduction

In order to determine the role of the concrete on jointed plain concrete pavement (JPCP) performance it must be realized that a pavement structure is a complex system with many interacting components (e.g. Forster, 1997, and Smith et al., 1997). Pavement performance depends not only on traffic loading, portland cement concrete (PCC) properties and environmental factors (which determine exposure conditions such as freeze-thaw and moisture effects on the concrete over time); but it also depends on the influence of subgrade support and subsurface drainage.

It is generally recognized that higher strength concrete with its improved mechanical properties (compressive, tensile, elastic modulus) and more impervious pore system performs better than normal strength concrete in certain structural applications. These applications pertain to structures such as bridges, high rise buildings, off shore structures, etc. However, it is not clear whether this type of concrete is the answer to improved performance in pavement applications. Design compressive strength in structural applications for higher strength concrete is often 55 MPa to 75 MPa or higher. There is very little information in the literature on the performance of higher strength concrete in pavements.

1.2 PCC Properties and Material Characteristics for European Higher Strength JPCP

It is current European practice to construct JPCP's of higher strength concrete compared to JPCP's in the United States. European state highway agencies have for years used higher strength concrete for pavement applications with design compressive strength typically ranging from 35 to 45 MPa. To better understand the role of concrete strength and durability factors on JPCP performance, the FHWA conducted a field tour of selected European pavements. The major findings are documented in a series of FHWA reports based on a 1992 US tour of European Concrete Pavements (e.g. FHWA-SA-93-012-1992; Till et al., 1994; Smiley, 1995,1996, and 1997; Weinfurter et al., 1994; Larson et al., 1993).

This section briefly discusses the observations made on the tour in 1992, and it presents the first US JPCP test section constructed specifically using European construction practices adapted to US conditions.

1.2.1 Required Levels of PCC Properties and Material Characteristics

Table 1.2.1 lists the JPCP design requirements for concrete properties and material characteristics for eight European countries in wet freeze (WF) and wet no freeze (WNF) climate regions. In addition, requirements are given for pavement and base type. The concrete requirements are shown for the 28-day compressive strength, 28-day flexural strength, water/cement (w/c) ratio, cement content, aggregate gradations, cement types, mix proportions, and air content. Not all eight countries have requirements for all parameters. It should be noted that table 1.2.1 represents design requirements from the early 1990's and revisions may have occurred.

Table 1.2.1 shows that the European countries have similar requirements for compressive strength with the exception of Norway which requires strength values from 45 to 75 MPa. However, a wide spread is seen in the flexural strength requirements ranging from 4.3 to as high as 7.0 MPa. The typical value is around 5.0 MPa. The requirements for w/c ratio are between 0.40 and 0.50, while the cementitious contents range from 300 to 350 kg/m^3. Most of the countries allow for cementitious substitutions using slag and fly ash. In Germany fly ash is usually not used due to its variability. The concrete must be freeze-thaw resistant with air contents of 3 to 7 percent. Finally, Germany and France have requirements for the aggregate gradations. It is noteworthy that the mix proportions are typically based on trial mixes. Finally, it should be emphasized that only Norway allows the use of granular bases, and that Germany only allows for bonded cement bases.

The German "autobahn" has for decades been considered to be the best European highway, which has been a result of high quality control. For instance, the minimum specified 28-day strength (as determined on 20-cm cubes) is 35 MPa. Normally, as in most US pavements, the field strength substantially exceeds minimum requirements. In a two-layer pavement the compressive strength is often 65 MPa in the top layer and 50 MPa for the bottom layer. Furthermore, the maximum w/c ratio is 0.42, the minimum cement content is 349 kg/m^3, and the air content is typically about 5 percent. A 5-m joint spacing is used with variably spaced, plastic coated dowel bars. An important feature of the German pavement cross section is the use of a 15-cm lean concrete (LCB) or cement treated base (CTB). Special for the German design is that the CTB is bonded to the slab, thereby achieving a thicker monolithic slab for several years after construction. To prevent reflection cracking, the CTB is pre-notched to match the transverse joint in the slab. To decrease edge stress the concrete pavement extends 0.5 m beyond the traffic lane.

1.2.2 European Concrete Pavement Demonstration Project in Michigan

Based on the European design catalogs, an experimental higher strength rigid pavement section was constructed in Detroit, Michigan, in 1993. The test road was designed as a premium JPCP based on the German design guidelines for the local climate, soil, and traffic conditions. The project used high quality concrete aggregate and higher than normal concrete strengths combined with a nonerodible lean concrete base to limit slab deflections (Larson et al., 1993, Till et al., 1994).

The test road is located on I-75, in downtown Detroit, Michigan. Also known as the Chrysler freeway located between I-375 and the I-94 freeways, this section is one of Michigan's busiest freeways carrying about 111,000 vehicles a day, of which about 11 percent are trucks.

The test pavement is about 1.6 km long. For comparison, a conventional Michigan pavement design was used for the remaining project, which is a jointed reinforced concrete pavement (JRCP), and therefore has much longer joint spacing as compared to the JPCP European pavement (4.57 m). Two typical Michigan JRCP slab designs were used with joint spacings of 12.5 m and 8.23 m. As a result of the longer slab lengths, these panels are expected to develop tight mid-slab transverse cracks or one-third panel cracks within a few years after construction. A reinforcing mesh placed in the middle of the slab of the Michigan design is then used to hold the crack tight such that good load transfer across the crack is maintained. If a crack opens beyond about 0.6 mm the aggregate interlock is significantly reduced and the crack often deteriorates due to spalling and faulting (Hansen et al., 1998)

Heavier legal axle loads in Europe require a stronger and more durable pavement. In Germany for instance, the single axle load is 13 tons as of 1993 compared to 8.2 tons in Michigan. However, Michigan is the only State in the United States that allows 11 axle trucks with a gross truck weight of 74.5 tons. The Federal weight limit is 36.4 tons.

Table 1.2.1 *European specifications for high quality JPCP (concrete properties and mix characteristics).*

Country	Climate Zone	Requirements									
		Pavement Type	**28-day Strength Compressive MPa**	**28-day Flexural MPa**	**Max. w/c Ratio**	**Cement Content kg/m^3**	**Aggregate Gradation**	**Cements**	**Mix Proportions**	**% Air Entrained (Min. and Max.)**	**Base Type**
Austria	WF	JPCP	Min. 40 (upper layer) min. 35 (lower layer) (20-cm cubes)	Min 5.5	Usually <0.43	not spec.	Not Specified	OPC or OPC+20% GGBFS no fly ash	Based on specifications	3.5-5.0%	CTB 250-300 mm
Denmark	WF		None	None	0.40	325	Not specified	Low Alkali, fly ash used	Based on trial mixes	4-7%	CTB 150 mm
Finland	WF		None	7	0.42	350	Project specific	OPC	Based on trial mixes	2-4 %	CTB 120-250 mm
France	WF WNF	JPCP	None	> 5	None	300-350	According to NFP standard	OPC or OPC w Pfa	Based on trial mixes	3-6%	LCB/CTB 120-220 mm
Germany	WF	JPCP	Min. 35 Avg. 40 (20-cm cubes)	min. 5.5	<0.42 or based on spec. comp strength	min 300 typ. 340	According to DIN specs (min 50% crushed stone)	OPC or OPC+GGBFS no fly ash	Based on trial mixes	4% (min 3.5%)	Bonded LCB/CTB 150 mm
Great Britain	WNF	JPCP/ JRCP	40	None	0.5	300	Not Specified	OPC or OPC+GGBFS (<50%) or OPC+fly ash 15-35%	Based on trial mixes	4 or 5% (±1.5%) Agg. size dependent	150 mm
Norway	WF	JPCP	45-75	4.3	0.5	330	Not specified	max 20% fly ash	Based on trial mixes		Granular
Sweden	WF		None	4.8	None	None	Not specified	Special, no fly ash	Based on trial mixes	4.8-7%	CTB 150 mm

European and Michigan Pavement Cross Sections.
The cross sections are briefly discussed for the European JPCP and comparable Michigan JRCP's. The layer thicknesses were selected for the European design from the German design catalog for the climatic, soil and traffic conditions found in the Detroit area. This cross section is illustrated in figure 1.2.1 together with the Michigan standard pavement. The European pavement thickness is 100 mm thicker than the Michigan pavement. It is seen that the combined PCC and base thickness is the same for the two designs, but the European design has a 400-mm non-frost susceptible aggregate subbase where the Michigan design has a 300-mm sand subbase.

Tables 1.2.2 and 1.2.3 show a comparison between the European and Michigan strength and mixture requirements and the mid-slab deflections from field measurements by falling weight deflectometer (FWD). The PCC mix designs are quite different as expected from the discussion in section 1.2.1. The pavement deflections of the European pavement are only about 50 percent of the deflections of the standard Michigan pavement. This is a substantial decrease in overall deflections and is attributed to the higher strength concrete (higher elastic modulus) and the bonded lean base.

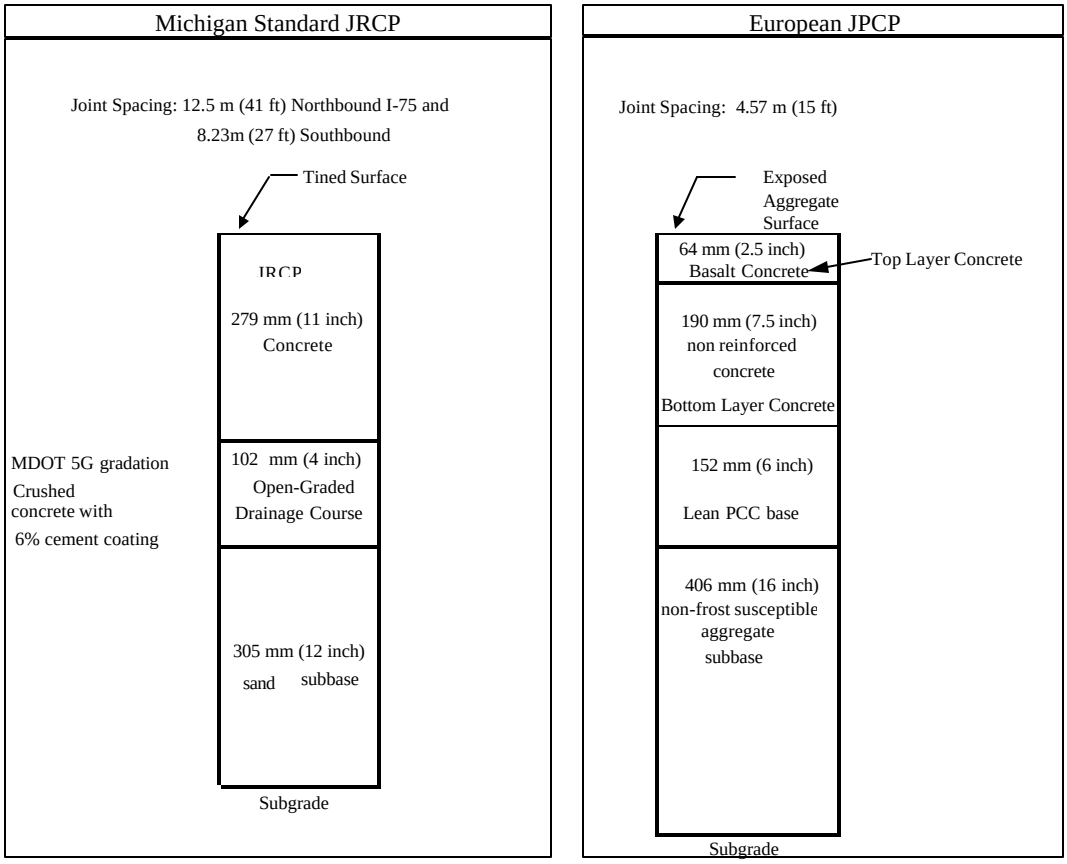

Figure 1.2.1 *Pavement cross section for the European and the Michigan pavements on I-75, Detroit, Michigan.*

Table 1.2.2 *Midslab maximum deflection from FWD on I-75, Detroit.*

Deflections (mm)	Inside Lane		Middle Lane		Outside Lane	
	European	Michigan	European	Michigan	European	Michigan
Average	0.03	0.06	0.03	0.05	0.03	0.05
Maximum	0.04	0.07	0.04	0.06	0.04	0.06
Minimum	0.03	0.05	0.03	0.05	0.03	0.05

Table 1.2.3 *Strength and mix requirements for the European and the Michigan pavements on I-75, Detroit.*

Property	European Test Pavement			Michigan Control Pavement
	Top Layer	Bottom Layer	Lean Base	
28-day Compressive Strength, MPa (lbf/in^2)	37.9 (5500)	34.4 (5000)	17.2 (2500)	24.1 (3500)
28-day Flexural Strength, MPa (lbf/in^2)	None	None	None	4.50 (650)
Maximum w/c	0.40	0.42	0.70	0.50
Minimum Cement Content, kg/m^3 (lb/yd^3)	446 (752)	349 (588)	249 (420)	326 (550)
Maximum Slump, mm (in)	76 (3)	76 (3)	76 (3)	76 (3)
Air Content (±1.5%)	6.5	6.5	6.5	6.5

Preliminary Conclusions

MDOT is monitoring the test sections for up to 5 years for the FHWA. Conclusions based on construction experience and first 5 years of service life are:

- Construction of the European pavement design occurred without any major problems. More familiarity with placing the two-layer concrete mixtures and the exposed aggregate surface would result in faster construction and may reduce cost.
- The top concrete layer should not be less than 7 cm in thickness to avoid poor consolidation and thin surface layer.
- The top layer should not have sand particles larger than 1 mm to allow the coarse aggregate with a nominal diameter of 6-8 mm to lock together better when there is an exposed surface. The coarser sand wears faster than the basalt coarse aggregate, and closer packing is expected to reduce tire noise level.
- Both pavement types are performing as expected. There are no transverse cracks in the short panels of the European pavement, whereas about 28 percent of the Michigan JRCP 12.5 m panels have either one mid panel crack or two transverse cracks at the panel's third points. The cracks are equally scattered across all lanes. This initial crack pattern is typical of Michigan's JRCP's.

This demonstration project has not yet had sufficient traffic and environmental exposure time to warrant a detailed field and laboratory investigation in this study.

However, since the demonstration project, MDOT has developed new design and construction requirements to improve long-term pavement performance. MDOT has modified its concrete pavement mixture to include large size coarse aggregate (62-mm

top size) with lower freeze-thaw dilation values and limits on specific gravity and absorption. MDOT has also included tighter requirements on construction methods for sawing joint relief cuts and allowable concrete mixture temperatures during placement. Furthermore, MDOT now mandates a warranty from the prime contractor on all new or reconstruction projects involving concrete paving. The warranty is a materials and workmanship warranty with condition thresholds on surface distresses.

1.3 Trends in Pavement PCC from the LTPP Database

The LTPP database was originally established by Strategic Highway Research Program (SHRP). As will be detailed in chapter 2, the LTPP database contains a large amount of data from over 200 concrete pavement sites across the United States and Canada. In order to establish overall performance and practice trends, the LTPP database was reviewed as part of this study with special attention given to JPCP pavements (subgroup GPS3 in the LTPP database). This evaluation was done prior to field-testing, and as discussed in chapter 2 of this report, the LTPP database has been used extensively to select the JPCP test sections for detailed analysis in this study. Sections were selected from LTPP which had shown primarily excellent long-term performance (more than 20 years), or which had high or low PCC strength.

1.3.1 Regional PCC Trends in the LTPP Database

There are both general regional trends in the PCC mixture parameters and properties and clear State to State trends (Byrum et al., 1997; and Hansen et al., 1998a). The general trends are likely related to the evolution of PCC mixtures within regions due to different paving conditions. Regions, which are generally hot, such as the southwest and southeast, have evolved mixes that use higher w/c ratio. This general trend may have evolved to ensure adequate workability in such hot conditions. There is also common use of type II low heat of hydration cement in the warmer regions of the southwest and along the West Coast in general. Regions which have considerable freeze thaw cycles, such as the upper mid-west appear to have evolved mixes which have more paste volume with low w/c ratio and higher air and cement contents. Nonfreeze regions that are also cooler and have good aggregates, such as Washington State, have evolved the highest strength mixes. This combination typically results in both high strengths and high stiffness. Similar to the Washington State mixes are the California mixes. These mixes have low paste volume, low air, and high strength aggregate. However, they use high mix water contents and w/c ratio. These mixes often have properties of higher split tensile strength and lower stiffness than would be expected for average concrete. Mixes used in Georgia and Florida have properties of average paste volume, high w/c ratio, and low to medium aggregate strength. The result is a PCC with lower strength and stiffness. Wisconsin PCC uses very high paste volume with low w/c ratio and high air content and lower aggregate strength. This results in higher stiffness and compressive strength but not necessarily higher splitting tensile strength. State to State variations are likely based on variations in SHA mixture specifications and design methodology, variations in primary aggregate types within each state, and variations in placement and curing specifications.

1.3.2 Preliminary Performance Trends in the LTPP Database

A preliminary review of the effects of PCC strength on pavement performance levels in LTPP indicates that the primary pavement deterioration mechanisms are hidden within the foundation layer properties and climate/traffic parameters. This observation warrants a detailed field investigation in order to isolate the effects and the mechanisms of PCC on JPCP deterioration from foundation and environmental factors.

Modeling of faulting, spalling, and transverse cracking using the LTPP database has been performed by several researchers in the last 5 years (e.g. Byrum et al., 1997; and Titus-Glover et al., 1999). These models do incorporate the effect of PCC properties on distress development. Yet, further model improvement must be made if the effect of PCC strength and associated properties on long-term pavement performance is to be better understood.

In general, higher strength concrete may be more sensitive to use in pavement applications. For example, high strength mixes may be more susceptible to developing slab curling. This phenomenon is related to increased PCC elastic modulus. Therefore, extra care must be taken when using higher strength concrete in pavement applications to ensure that a "flat slab" condition is obtained. It appears that if the initial sensitivity can be overcome by stricter temperature control and curing specifications, pavement deterioration will be slower and less severe for higher strength concrete.

While the LTPP database is an excellent tool for developing general trends about performance, it is less effective in evaluating the causes of distress or distress free behavior under specific conditions. This is because such performance can be masked by a multitude of other factors that are not directly evident in the LTPP database. Thus field and laboratory evaluation of selected pavement sections is an indispensable part of this research.

1.4 Concrete Properties with Significant Influence on Jointed Concrete Pavement Performance

In view of the limited number of studies and data available on the effect of higher concrete strength and associated properties on long-term JPCP performance, the literature review focused on the main JPCP variables that affect pavement performance. The JPCP variables to be evaluated include design factors, environmental factors, and concrete properties. However, the review emphasis will still be toward identifying and categorizing the PCC properties that affect JPCP distress development. It is important to keep in mind that the concrete properties and mix characteristics often are not the factors controlling distress initiation. However, they can often be mitigating factors in delaying the distress development.

Concrete pavement design for JPCP's is based on field-calibrated mechanistic design procedures. The design procedures include the pavement response calculated from structural models, durability requirements, distress models to predict the development of distress from the structural response, and distress calibration factors to predict the distresses observed in the field (e.g. PCA, 1984; AASHTO, 1986; and ACI 360R, 1992). The distress models include fatigue cracking models, pumping erosion models, faulting models, and joint deterioration models (e.g. NCHRP Report 1-26, 1990; Van Wiji et al., 1989; Darter et al., 1991; and Titus-Glover et al., 1999). These models include a large number of design factors, environmental factors, and PCC properties.

Table 1.4.1 shows the significant independent variables affecting the various JPCP distresses. These distresses are joint faulting, spalling, transverse cracking and corner breaks. The variables range over design parameters, environmental factors, and PCC properties. The parameters in normal font were also found in a study reported by Owusu and Darter (1994), and the parameters added in italic are additional parameters, which were identified in this literature review. Table 1.4.1 shows that a large number of variables (33) affects pavement distress. This illustrates the complexity and difficulty in quantifying the effects of the individual parameters on pavement performance. The focus of this study is to extract and evaluate the effect of increasing concrete strength and associated properties on pavement performance with emphasis on good long-term performance. Thus, factors leading to premature distress are not emphasized in this study.

The PCC properties affecting distress are listed in bold in table 1.4.1, and it is seen that the properties typically affect more than one distress type. As stated in section 1.3 the effect of PCC properties on pavement distress is often difficult to quantify as factors such as traffic, age, environment, and foundation dominate the overall pavement behavior.

Traditionally, PCC properties are not included in faulting models because factors related to the pavement foundation, traffic, and environmental exposure play primary roles in distress development. Spalling is highly related to PCC durability. The traditional models for prediction of spalling include PCC factors such as D-Cracking and alkali silica reaction (ASR), but not factors such as air void system and permeability. Other prime design factors are traffic, age, and joint spacing.

Table 1.4.1 *Independent variables affecting JPCP performance.*

Independent Variables	Joint Faulting	Joint Spalling	Transverse Cracking	Corner Breaks
Annual Precipitation	X	X	X	X
Average Monthly Temperature Range	X	X	X	X
Base Type**	X		X	
Bearing Stress	X			
Cumulative ESAL's**	X	X	X	X
Corner Deflection	X			
Drainage	X			
D-cracking		X		
Dowel Diameter	X			
Edge Support	X			X
Freeze-Thaw Cycles**		X		
Freezing-Index**	X	X	X	
Incompressibles in Joint		X		
Joint Sealant Type		X		
Joint Spacing**	X	X	X	X
Joint Opening	X	X		
Load Transfer Type**	X	X	X	X
Pavement Age**	X	X	X	X
PCC Flexure Strength**		X	X	X
PCC Compressive Strength**	X			
PCC Elastic Modulus**	X	X	**X**	
PCC Coefficient of Thermal Expansion*	**X**		**X**	
PCC Shrinkage	**X**		X	
PCC Fracture Energy*			**X**	**X**
PCC Permeability*		X		
PCC Air Void System*		**X**		
Pumping**[1]	X		X	X
Reactive Aggregate		X		
Sealant Damage		X		
Slab Stress			X	
Slab Thickness**	X	X	X	X
Subgrade Type**	X		X	X
Static k-value**	X		X	X
Steel Percentage			X	
Thornthwaite Index**	X	X	X	

Parameters in normal font are as listed in Owusu and Darter (1994).
Parameters in italic are added based on this literature review.
Parameters indicated with ** are evaluated in detail in this study.
Bold type indicates concrete properties that affect distress.
[1]Affected by base moisture level, traffic level and load transfer.

The existing models for development for fatigue cracking (bottom-up cracking) show that PCC flexural strength and elastic modulus are included in the design. However, the Portland Cement Association (PCA) and AASHTO design models show that factors such as traffic, design period, load transfer type, drainage, and subgrade and subbase support (k-value) also play primary roles. Yet, in the case of corner breaks (top-down cracking) PCC properties become primary factors for the distress development. The PCC

properties determine the onset of crack initiation and the propagation of full width cracking.

The following sections discuss the key variables affecting faulting, spalling, and transverse cracking.

1.4.1 Crack and Joint Faulting

Faulting is a vertical offset of adjacent slabs at joints or cracks. Faulting and the development of faulting have been observed and investigated by many researchers. It is well-known that a pavement slab will develop severe faulting if the following four conditions occur simultaneously: the joint or crack experiences poor load transfer, heavy traffic is present, free water is present in the slab-base interface, and the base layer is erodible (e.g. Titus-Glover et al., 1999).

Faulting Models

Faulting has traditionally been evaluated through empirical models. The empirical models include the combination of variables that affect the development of faulting (e.g. Darter et al., 1985; and Simpson et al., 1994). The models include some or all of the following parameters: accumulated traffic load, slab thickness, joint spacing, base type, freezing index, precipitation, edge support, pumping, drainage type, load transfer system, and modulus of subgrade reaction. Note that PCC properties are not directly included in these empirical models. For detailed and mechanistic distress analysis the PCC properties and characteristics need to be included. However, it should be noted that PCC compressive strength is included in dowel design (Huang 1993).

PCA developed a mechanistic-empirical model to predict erosion damage at slab corners. This model was based on Miner's damage model of the work induced by traffic load. The model included the expected number of load repetitions, the pressure at the slab-foundation interface, the slab thickness, and the modulus of subgrade reaction. Recently, Titus-Glover et al. (1999) developed another mechanistic-empirical faulting model. The model is based on the concept of differential elastic deformation energy at the crack or joint and incorporates the four prime factors affecting faulting development that were listed previously. The model also incorporates PCC elastic modulus for determining the slab deflections and aggregate interlock.

Crack and Joint Load Transfer

Load transfer efficiency across a crack or joint is controlled by the aggregate interlock, slab stiffness, foundation stiffness, and dowels if any. When cracks develop in JPCP, the structural integrity is only maintained through aggregate interlock aided by compressive stresses (closing forces) that may be present in the slab plane. The vertical stresses are transferred through the aggregate interlock, slab stiffness, and elastic deformation of the sublayers. Traditionally, the effectiveness of aggregate interlock is measured using the load transfer efficiency, LTE. The LTE is quantified by a relative measure of the deflections on either side of the crack or joint, and several models have been developed for quantifying LTE based on slab deflections (e.g. Benkelman, 1933; Teller and

Sutherland, 1936; and Ioannides and Korovesis, 1990). According to the model proposed by Ioannides and Korovesis, LTE is the ratio between the unloaded and the loaded side of the crack. An LTE value of 60 percent is considered the lower limit for medium to heavy truck traffic (Smith et al., 1990).

The mechanism responsible for transferring stresses from the loaded slab segment to the unloaded segment across a crack in a JPCP is rather complex. The mechanism is influenced by crack width, aggregate size and type, slab thickness, slab length, the friction coefficient between the slab and the base, and the magnitude and repetition of the load.

Aggregate interlock provides the shear resistance along the fractured surface. As a load is applied on one side of the crack, vertical deflections of the slab will cause the two crack faces into contact. The opposing crack face will resist the shear loading through bearing and friction of the coarse aggregate along the crack. When a crack is formed in normal strength concrete containing strong coarse aggregate, the majority of the coarse aggregate particles remain embedded in the mortar on either side of the crack. The aggregate/mortar interface zone strength is lower than that of the coarse aggregate, resulting in cracking around the coarse aggregate and forming a rough irregular crack surface. However, if the coarse aggregate is weaker than that of the interface zone, the crack will penetrate through the aggregate resulting in a straight and smoother crack surface. Section 1.5.8 will discuss the coarse aggregate characteristics that affect the load transfer mechanism.

Evaluation of visual distress surveys made in the field shows that the crack widths of the individual cracks vary from hairline to about 1 mm for nondeteriorated transverse cracks. For spalled cracks, the surface crack width is difficult to measure and it is likely very large (e.g. Hansen et al., 1998). Colley and Humphrey (1967) showed for un-doweled pavements that LTE decreases as the joint opening increases. This trend was found in both field and laboratory tests. Hansen et al. obtained the same trend for Michigan JRCP's. Furthermore, Colley and Humphrey showed that for a given crack width, LTE decreases with the number of load repetitions, reaching a plateau determined by the overall system response.

Hansen et al. (1998) evaluated LTE versus crack width for jointed concrete pavements (JCP's) containing different types of coarse aggregates. All sections with gravel and carbonated aggregate showed high and sufficient LTE's ranging from 75 to 100 percent for crack widths smaller than approximately 0.6 mm. This field study also showed that for an increased crack width, in addition to decreasing LTE, the deflection on the loaded slab segment increased significantly.

Joint Opening

The joint load transfer decreases with increasing joint opening. Therefore, an accurate estimate of the joint opening is essential to decide if a dowel system is required at a JPCP joint, or whether aggregate interlock will be sufficient in transferring the wheel loads. For nondoweled JPCP, a joint opening of 0.75 mm is considered as the maximum limit

above which aggregate interlock is insufficient (Kelleher, 1989). This agrees with field and laboratory studies indicating that crack load transfer efficiency typically falls below an acceptable limit for crack widths larger than 0.60 to 0.75 mm (e.g. Colley and Humphrey, 1967; and Hansen et al., 1998).

Joint movement is also a critical factor in the design of a joint sealant as proper design of sealant can significantly reduce joint deterioration. The joint width controls the amount of compression exerted on the sealant during expansion and contraction of the slab. A compressive stress less than the required minimum will provide easy passage for water, while a compression stress beyond the allowable maximum may damage the sealant.

According to Darter and Barenberg (1977), the relationship between joint opening and change in temperature can be written as:

$$\Delta L = C \cdot L(CTE \cdot \Delta T + e) \quad (1.4.1)$$

where *DL* = joint opening (mm).
C = adjustment factor for slab-subbase friction.
L = slab length (mm).
DT = maximum temperature range (temperature at placement/setting time minus lowest mean monthly temperature) (°C).
CTE= PCC coefficient of thermal expansion (/°C).
e = PCC shrinkage coefficient (mm/mm).

The PCC coefficient of thermal expansion and shrinkage are highly dependent on the cement paste content and the aggregate type and content. It should also be emphasized that parameters such as slab length and placement temperature can become very important for climatic zones with very low winter temperatures.

If dowels are needed at the joints, the PCC compressive strength becomes important in determining the overall joint design (dowel diameter and spacing, etc.)

Summary
Based on field investigations and faulting models, the key PCC properties affecting faulting include elastic modulus, compressive strength, coefficient of thermal expansion, and shrinkage. In addition, it was found that the coarse aggregate type and size as a PCC mix characteristic is very important for LTE and in turn for the development of faulting.

1.4.2 Crack and Joint Spalling

Spalling is the deterioration and breaking up of the concrete at longitudinal and transverse edges, joints, and cracks. Spalling is a general term and can be the ultimate manifestation of many forms of deterioration such as freeze-thaw damage, D-cracking, alkali silica reaction (ASR), and poor construction procedures. It should be mentioned that accelerated and severe spalling has been related to D-cracking and ASR susceptible aggregate sources. It is well known that increasing and enhancing the PCC air void system improves the PCC pavement performance in terms of less surface scaling, better sulfate resistance, and less cracking related to alkali-silica reactivity (Kosmatka and

Panarese, 1988). Several detailed studies have documented the D-cracking and ASR phenomena and they are not the focus of this research (e.g. Marks, 1990; Stark, 1991; and SHRP-P-338, 1993).

Furthermore, the transportation of fluids into and out of the concrete is also an important mechanism responsible for deterioration and poor performance (Roy et al., 1995). PCC permeability is considered the best parameter to access long-term durability, or in other words the ability of the concrete to resist deterioration (Schonlin and Hilsdorf, 1988; and Armaghani et al., 1994).

Field studies have shown that coarse aggregate type has been found to relate to concrete spalling. Spalling of continuous reinforced concrete pavements (CRCP's) was investigated and it was found that siliceous gravel mixes had much greater spalling potential than crushed limestone mixes (Senadheera and Zollinger, 1996). Furthermore, a Michigan study found that blended aggregates had highly variable performance (e.g. mix of siliceous and carbonated sources) (Holbrook and Kuo, 1974). In addition, other field studies indicate that the aggregate-matrix bond at an early age is a very important factor in spalling development. The aggregate-matrix bond has typically been evaluated through flexural and tensile strength (Fowler et al., 1996).

Spalling Models

Several empirical models have been proposed for the development of joint spalling. The models generally include parameters such as age, freeze-thaw cycles, ambient temperatures, moisture index, joint spacing, slab thickness, joint opening, joint sealant type, drainage, modulus of subgrade reaction, and concrete elastic modulus (e.g. Simpson et al., 1994; and Yu et al., 1996).

Spalling can also occur due to traffic loading. The mechanism behind this type of spalling is not yet fully understood. However, it is known that loads generally increase the severity and magnitude of spalling. Furthermore, it appears that more movement (either horizontal or vertical) at a crack or joint generally leads to more rapid spalling development. It is typical that during the first few pavement service years, there is almost no development of joint spalling. However, when the deterioration does initiate it usually develops very rapidly. This indicates that spalling can be predicted as a fatigue phenomenon.

Titus-Glover et al. (1999) developed a load based mechanistic-empirical model for slab spalling. The static model is based on the mode of spalling initiation and propagation proposed by Senadheera and Zollinger (1995). The model incorporates concrete properties such as tensile strength, elastic modulus, thermal expansion, and drying shrinkage. Other parameters in the model are tire configuration, tire shear stress, concrete friction coefficient, joint compressive stresses, slab-base friction coefficient, slab thickness, joint spacing, and modulus of subgrade reaction.

Summary
In summary, key PCC properties affecting spalling are elastic modulus, air void system and permeability. In addition, it was found that the early age aggregate-matrix bond is very important for the development of spalling, and it can be evaluated through PCC flexural and tensile strength.

1.4.3 Transverse Cracking and Corner Breaks

Since the 1930's researchers have worked towards understanding, predicting, and modeling transverse cracks and joints in PCC slabs on grade. The work has ranged from field investigations, field-calibrated prediction models, laboratory investigations, and numerical modeling of the crack or joint behavior. Transverse cracks are expected to develop in continuous and jointed reinforced concrete pavements (CRCP and JRCP) due to the combined effect of concrete volumetric changes, and mechanical and environmental loading. However, transverse cracks are not expected or desirable in JPCP's.

Structural behavior of the pavement system and the fatigue strength of the concrete affect transverse cracking (e.g., Bradbury, 1938; Vesic and Saxena, 1969; Darter 1977; Darter and Barenberg, 1977; Packard and Tayabji 1985; Salsilli et al., 1993, and Titus-Glover et al., 1999). The concrete properties affecting the slab response are tensile strength, elastic modulus, fatigue life, coefficient of thermal expansion, and shrinkage. This suggests that transverse cracking is not durability related, but tends to be associated with the mechanical features of the concrete. It is after the crack formation that durability issues become important, affecting deterioration rates for the cracks. Transverse cracking has traditionally been addressed through the life expectancy of the pavement as it is affected by concrete fatigue due to slab edge loading. Recently a mechanistic approach has been proposed based on the theory of fracture mechanics (Titus-Glover et al., 1999).

Fatigue analysis is the classical analysis approach for JCP's. It pertains to slab response to traffic and thermal loading. Fatigue cracking seldom causes structural failure, but it is important since fatigue cracking initiates cracks that may propagate due to external loads and environmental factors (Gillespie et al., 1993). Figure 1.4.1 shows different support and loading configurations for five plates (Bache and Vinding, 1990/1992). Example E can be related to slab-on-grade and this configuration, along with example D, would initiate cracking at peak load, but the plate would not fail in a catastrophic manner as would the plates in examples A, B, and C. For fatigue cracking of slabs-on-grade, as in example E, it is expected that small hairline cracks are initiated and over time they will develop to full width cracks.

PCC fatigue is typically related to PCC flexural strength. PCC fatigue is defined as the stress ratio between applied stress and static flexural strength. Based on beam testing, a very conservative ratio of 0.50 has been suggested by the Portland Cement Association (PCA) if the slab is being subjected to 10 million or more loading cycles. Figure 1.4.2 shows the fatigue results from several beam studies. A recent study on the fatigue of concrete beams and slabs showed that the fatigue resistance was 30 percent higher for

fully supported slabs than for a simple supported beam when the beam flexural strength was used as the reference strength (Roesler and Barenberg, 1998). The main difference between the behavior of the simple supported beam and the fully supported slab was that the beam would fail when a macro crack developed whereas the slab would sustain additional loading during the formation of the macro crack.

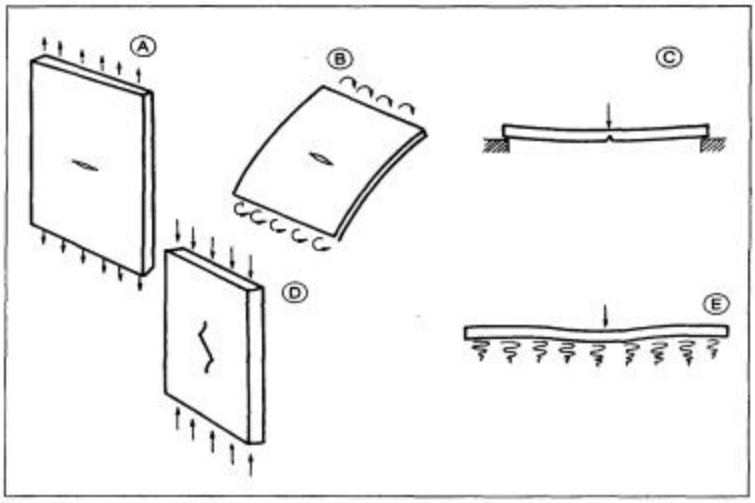

Figure 1.4.1 *Stable and unstable crack and loading configurations for PCC slabs. [After Bache and Vinding (1990/1992)]*

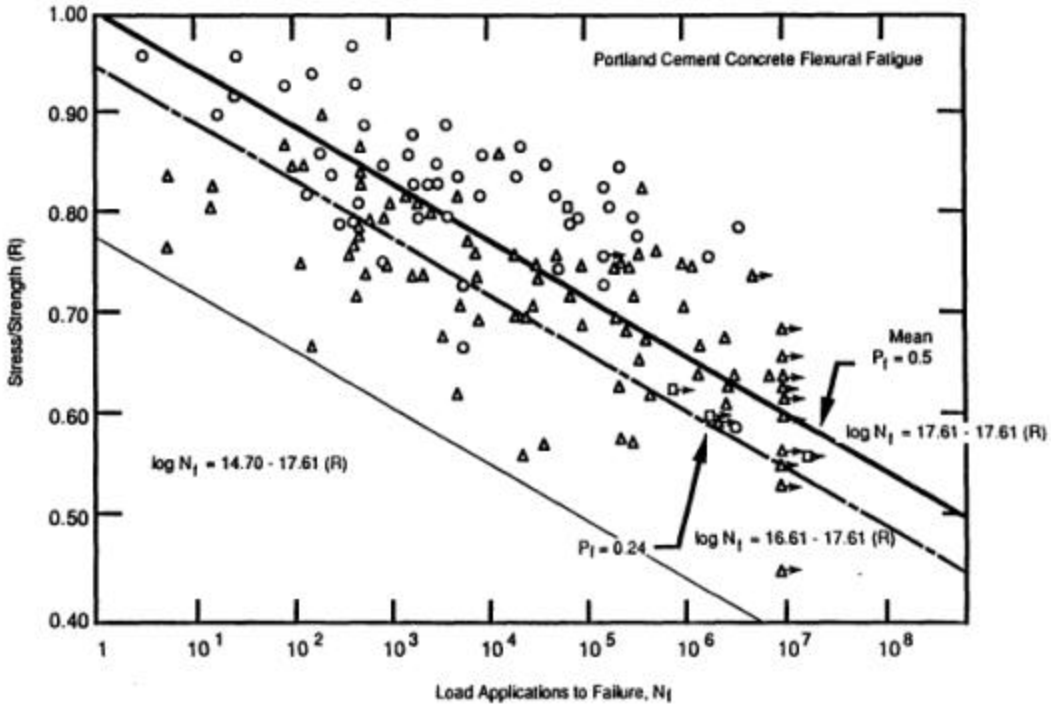

Figure 1.4.2 *Stress/strength ratio versus number of load applications. [After Mahoney et al. (1991)]*

Fatigue cracking can appear in concrete pavement due to the application of a large number of repeated traffic and environmental loads of various amplitudes. The traditional type of cracking is initiated at the bottom of the slab. The cracks induced by concrete fatigue can be transverse cracks initiated at the midslab edges, and longitudinal cracks initiated in the wheel paths at transverse joints (Huang, 1993).

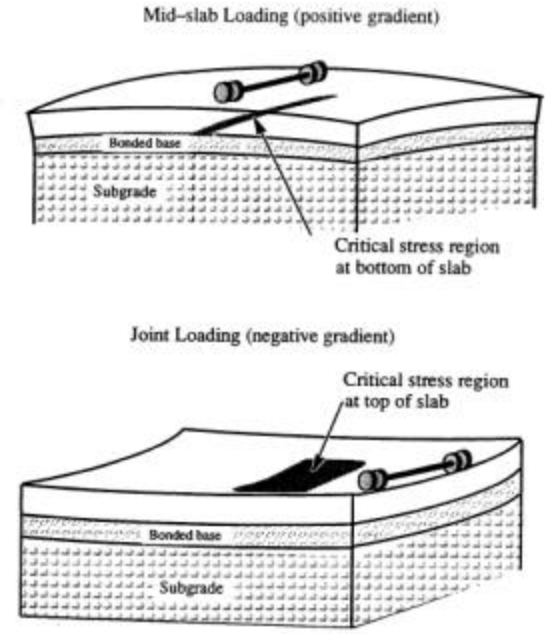

Figure 1.4.3 *Critical loading location with maximum tensile stresses for slabs in a dominantly upward or downward shape. [After Darter et al. (1994)]*

In addition to bottom-up cracking, top-down cracking can also occur. However, top-down cracking is traditionally not included in the structural analysis of the slab. Top-down cracking can be initiated if the slab is subjected to large repeated tensile stresses at the top of the slab. These stress conditions can occur if the slab has a predominantly upward concave shape from curling and warping and/or if the slab experiences loss of support at the joints, causing high tensile stresses from corner loading. (e.g. Teller and Bosley, 1930; Teller and Sutherland, 1935; Rhodes, 1949; Poblete et al., 1991; Poblete et al., 1989; Hansen et al., 1998; and Titus-Glover et al., 1999).

Curling and warping can also contribute to stresses causing bottom-up slab cracking if the slab is in a dominantly curled downward shape. These curling stresses should be added to the edge stresses caused by traffic load. Researchers have been advocating the inclusion of curling stresses when determining the allowable number of load repetitions. However, the execution is complicated as the traffic and curling loading do not appear with the same frequency.

Figure 1.4.3 illustrates the critical stress region for slabs in an upward curled or downward curled shape (Darter et al., 1994). When the slab is curled downward the critical traffic loading is at mid-slab, causing high tensile stresses at the slab bottom.

When the slab is curled upward, the critical loading position is at the slab joint, causing large tensile stresses at the top of the slab at a given distance from the joint.

Conventional Fatigue Concepts - Cracking from the Bottom-Up

The potential for bottom-up transverse cracking is directly or indirectly incorporated in the thickness design of concrete pavement. The PCA design procedure incorporates the fatigue analysis through a standardized load applied at the edges of the midslab (i.e. the fatigue damage is correlated with the flexural strength). The AASHTO design procedure incorporates the fatigue analysis indirectly in design of slab thickness. The procedure is in part empirical, based on experience and data collected from the American Association of State Highway Officials (AASHO) Road Test and in part theoretical (Huang, 1993).

In the classical fatigue analysis, the slab stresses due to traffic loading can be evaluated using the classical Westergaard equations for edge loading (Westergaard, 1926). The equations include the concrete elastic modulus and Poisson's ratio, along with the foundation stiffness and slab thickness. The mathematical equations for stresses due to edge loading of an infinite slab are for Poisson's ratio of 0.15:

$$s_e = \frac{0.803P}{h^2}\left[4\log\left(\frac{l}{a}\right) + 0.666\left(\frac{a}{l}\right) - 0.034\right] \quad (1.4.2)$$

where s_e = stress due to circular edge loading (MPa).
P = edge loading (N).
a = radius of circular loading (mm).
k = modulus of subgrade reaction (kPa/mm).
h = slab thickness (mm).
E = concrete elastic modulus (MPa).
l = length of relative stiffness (mm) expressed as:

$$l = \left[\frac{Eh^3}{12(1-u^2)k}\right]^{0.25} \quad (1.4.3)$$

where u = concrete Poisson's ratio.

Based on these equations it is evident that, for the typical ranges of these parameters, the slab stresses will be mostly affected by the slab thickness followed by the modulus of subgrade reaction and then the elastic modulus. The effect of Poisson's ratio is insignificant.

Top-Down Fatigue Cracking from Combined Curling/Warping and Loss of Slab Support

Top-down cracking can develop if the combined tensile stresses from curling/warping and corner loading exceed the PCC fatigue threshold. The tensile stresses from corner loading are significantly increased if loss of support occurs at the slab joint.

Slab curling is caused by temperature differential through the thickness created by rapid changes in surface temperature. This temperature differential occurs on a daily basis. At night the top is cooler than the bottom. This creates an upward concave shape with corners and edges pointing up. It creates the potential for a gap or void between the slab

and the base. This condition creates tensile stresses at the slab top, which are maximum at mid-slab. The magnitude of this tensile stress depends on several factors as illustrated by the equation below:

$$s_{x(y)} = \frac{E \cdot CTE \cdot \Delta T}{2(1-u^2)}\left(C_{x(y)} + u C_{y(x)}\right) \qquad (1.4.4)$$

where $s_{x(y)}$ = stress in the x or y direction (MPa).
CTE = coefficient of thermal expansion of concrete (/°C).
DT = temperature differential between the top and the bottom of the slab (°C).
C = correction factor for slab geometry in terms of ratio of slab length, L, to radius of relative stiffness l. This factor increases from zero to 1.1 with increasing slab length.

In addition to factors such as temperature gradients, foundation stiffness (k-value), slab length and thickness, the total tensile stress is increased with increasing elastic modulus, as found typically in higher strength concrete. Also, higher CTE is typically found in concretes of higher cement and paste contents.

Field and laboratory testing have shown that the temperature distribution through the slab thickness is highly nonlinear, and model predictions indicate that when taking this into account, the curling stresses are much higher than those determined with a linear temperature distribution. For this reason, temperature curling may be of more importance to pavement design and performance than traditionally believed (Mohamed and Hansen, 1996). This emphasizes the importance of considering curling and warping when estimating the JPCP's fatigue life.

Under the condition where the slab is curled upward, any load near the corner or joint will cause additional tensile stress at the top of the slab. This in turn can lead to corner breaks, diagonal cracks, and transverse cracks in a region from about 1 m from the joint to mid-slab. The crack location depends on the extent of curling, loading, and loss of slab support, if it occurs.

If loss of support occurs, the tensile stresses will be increased under a given traffic load. Figure 1.4.4 illustrates in the case of loss of support at the joint the stress distribution along the slab surface.

AASHTO recommends different reduction factors based on the base type, where the reduction factor decreases as the base becomes stiffer and more stable. (AASHTO, 1986). In the case of loss of support associated with a cement treated base (CTB) with a k-value of e.g. 135 kPa/mm, the effective k-value should be reduced to 46 kPa/mm. In the case of loss of support for a granular base with a k-value of e.g.135 kPa/mm, the effective k-value could in the worst case be reduced to as little as 5 kPa/mm.

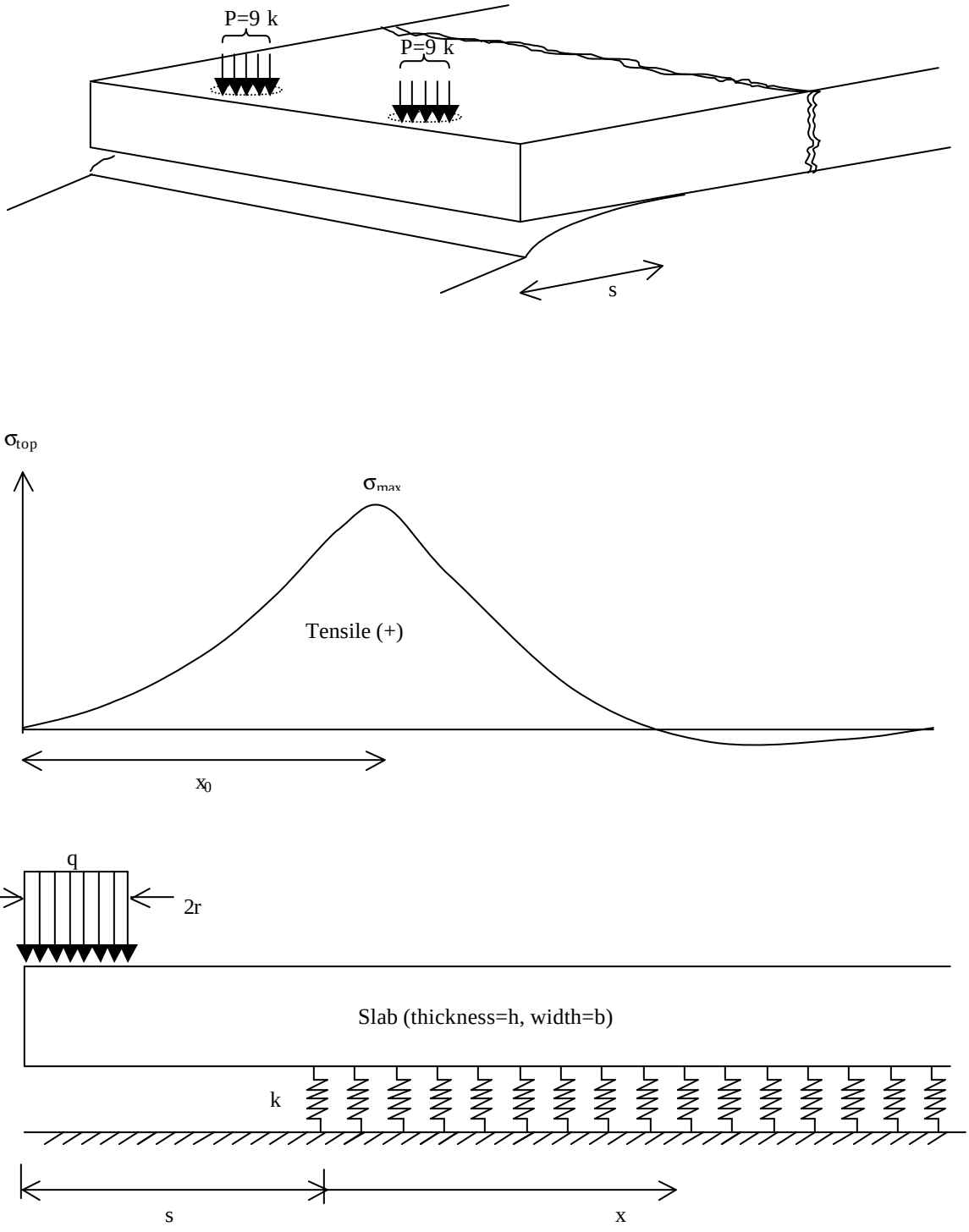

Figure1.4.4 *Schematic of top-down cracking as influenced by foundation loss of support.*

Loss of support comes from any gap or void that may develop over time between the base and the slab, causing increased deflection of the slab surface. Loss of support can have a major impact on pavement performance. Loss of support can have two major components: an intermittent one from daily curling effects, and a permanent one from high temperature construction curling effects and/or long-term effects of pumping erosion and warping.

The pumping action occurs when "… a heavy wheel load approaches a joint or crack, the approach slab deflects and forces water trapped under the slab to transport fine material underneath the leave slab. As the wheel load crosses the joint or crack, the sudden vertical pressure on the leave slab causes pumping or ejection of the water and loose material from beneath the slab through the joint or crack. A large part of the fine material that is eroded from beneath the leave slab is deposited under the approach slab." (Titus-Glover et al., 1999) This action will over time develop faulting at the joint due to the build up of fines under the approach slab. Poblete et al. (1989) found that daily slab curling combined with moisture and heavy vehicle loading appears to be instrumental in developing pumping and warping conditions, which result in permanently upward curved slabs.

Field results from Chile and the United States have shown that premature transverse cracking and corner breaks in JPCP may be the result of top down cracking from curling/warping effects and loss of support factors without signs of pumping (Poblete et al. 1989, and Hansen et al., 1998).

The interaction between slab curling and intermittent/permanent loss of support needs to be better understood to be able to fully analyze the situation of top-down cracking. In the case of corner loading, higher concrete strength (increased PCC elastic modulus, and tensile strength), stiffer foundations with intermittent and/or permanent loss of slab support all are contributing factors for increased tensile stresses away from the joint.

The Role of Concrete Fracture Properties in Transverse Cracking

Bache and Vinding (1990/1992) were some of the first researchers to advocate applying concrete fracture properties in the pavement design to enhance long-term pavement performance. There are two main fracture mechanics concepts: (1) is related to the peak failure behavior, and (2), which is more comprehensive, is based on the complete peak- and post-peak fracture behavior. Bache and Vinding suggested using the PCC fracture behavior in terms of peak- and post-peak response to evaluate the development of transverse cracks, and the use of an additional PCC parameter defined as the specific fracture energy. The peak behavior relates to crack initiation, and post-peak behavior relates to crack propagation.

Titus-Glover et al. (1999) developed fracture mechanic models for the initiation of bottom-up transverse cracking and top-down corner breaks based on the peak load. The approach of using the peak/failure load information to estimate the onset of cracking is more appropriate in the case where a "catastrophic" failure will occur as in the case of early-age joint development. Soares and Zollinger (1997) developed a methodology to

evaluate the saw-cut timing and depth of transverse joints based on the same concept of peak load information.

A recent study showed that the coarse aggregate plays a major role in crack initation and propagation in PCC highway mixes (Hansen and Jensen, 2000; and Jensen and Hansen, 2000). Furthermore, it was found that concrete strength cannot alone predict the concrete fracture behavior because the behavior is largely affected by the material characteristics and in particular by the coarse aggregate type, size, and content. Five aggregate sources were investigated and it was found that concrete containing aggregates such as crushed limestone or blast furnace slag had at early ages higher resistance to crack initiation compared to the investigated glacial gravels. However, at any given point in time the concrete containing gravels had higher resistance to crack development than the investigated dolomitic limestones and blast furnace slag. It is important to keep in mind that PCC fracture properties are dominated by the selected coarse aggregates and that the aggregate properties vary between sources. This indicates that the PCC fracture properties should be evaluated for the project specific coarse aggregate.

Early-age Factors

Early-age transverse cracking is related to the hydration process and the associated temperature rise. During the subsequent cooling process, tensile stresses develop in the slab due to external restraints resulting from friction between the slab and the base, slab weight, tied adjoining lanes, or a combination thereof. Furthermore, increasing joint spacing increases the friction stress. In design, the friction coefficient is typically assumed to be a constant on the order of 1.5 (Huang, 1993).

Tensile stresses may also result from shrinkage as the pavement dries out, or expansion as the pavement becomes wet. It is noted that when calculating joint openings due to shrinkage and seasonal thermal changes, it is recommended to use different adjustment factors for a stabilized base or a granular base (see equation 1.4.1). It is assumed that the joint openings are about 25 percent larger for a granular base than for a stabilized base, which indicates that the friction coefficient for a granular base is smaller than for a stabilized base.

Joint spacing also affects the curling stresses in that increasing spacing increases the tensile curling stresses. Field investigations made by Frabrizzio and Buch (1999) support this theory. They found that the number of transverse cracks per slab increased from 1.0 crack to 3.7 cracks per slab when the joint spacing increased from 4.9 m to 21.6 m, respectively.

Traffic and Environmental Factors

Accumulated traffic and environmental loading affect the initiation of transverse cracks through accumulated fatigue damage. The PCC fatigue is assumed to occur when the combined loading exceeds a fatigue threshold. Typically, proper pavement thickness, strength and stiffness requirements minimize the fatigue cracking (Huang, 1993).

Accumulated traffic and environmental loading also affect the deterioration of transverse cracks. The repeated loading over time can lead to degradation and crushing of the coarse aggregate, reducing the aggregate interlock. The environmental loading through ambient temperature affects the measured LTE as increasing temperature causes the slab to expand and close the crack, whereas decreasing temperatures cause the crack to open (Foxworthy, 1985).

Pavement Age
The pavement age is also a factor in deterioration. It serves as an indicator of the amount of cyclic opening and closing of cracks, the number of freeze-thaw cycles, and the degree of corrosion of reinforcement in JRCP's. The crack deterioration related to cyclic opening and closing of the crack has also been found to be more severe for JRCP's constructed in colder and wetter climates than for those constructed in warmer climates (Pittman, 1996).

Foundation Support
Increasing the base and subgrade support has been found to decrease the transverse crack deterioration rate. Colley and Humphrey (1967) found that increasing the modulus of subgrade reaction from 24 to 123 kPa/mm increased the LTE significantly. In particular, the LTE for larger crack widths of 1.5 to 2.0 mm was higher on the stiffer subgrade.

Summary
In summary, PCC properties are primary factors in the development of transverse cracking in JPCP. The key PCC properties include: flexural strength, elastic modulus, coefficient of thermal expansion, and fracture energy. The PCC resistance to crack development is evaluated through specific fracture energy. (See section 1.5.4 and section 5.5 for details.)

1.5 PCC Properties and Materials Characteristics with Significant Influence on Pavement Performance

Considering the findings of the literature review on PCC properties affecting pavement performance, eight key properties were identified. They include PCC compressive strength, flexural/tensile strength, elastic modulus, fracture energy, coefficient of thermal expansion, permeability, air void system, and shrinkage.

PCC shrinkage was mainly found to affect JPCP joint opening. However, as the subsequent tasks of this study are based on field studies of JPCP, the irreversible field shrinkage cannot be determined.

In addition to these PCC properties it was found in section 1.4 that aggregate characteristics have a major impact on aggregate interlock as related to joint and crack load transfer efficiency. Therefore, mix characteristics affecting joint or crack aggregate interlock are also evaluated in this section.

Each of the remaining seven properties was evaluated in the context of increasing design strength (28-day compressive strength from about 24 to 45 MPa) and relations to the other properties and to material characteristics. Table 1.5.1 identifies for each of the key PCC properties (and aggregate interlock), the PCC mix characteristics which have been found to have a significant influence on these properties. The mix characteristics are coarse aggregate characteristics, w/c ratio, cement type and content, mineral additives, and air entrainment. The category for coarse aggregate is fairly broad as it spans from aggregate size, type, gradation, hardness, angularity, soundness to environmental exposure, and reactivity. As stated in section 1.4, it is beyond the scope of this study to evaluate factors such as aggregate soundness and reactivity.

Water/cement ratio and coarse aggregate characteristics are the most important PCC mix characteristics from the viewpoint of PCC mechanical properties and in turn JPCP structural performance. Water/cement ratio and air entrainment are the most important mix characteristics when considering PCC and JPCP durability. The following sections briefly discuss each of the properties listed in table 1.5.1.

Table 1.5.1 *Primary variables affecting PCC properties.*

PCC Property	Coarse Aggregate Characteristics*	w/c ratio	Cement Type and Content	Mineral Additives	Air Entrain.
Compressive Strength	X	X	X	X	X
Flexural/ Split Tensile Strength	X	X			
Elastic Modulus	X	X			
Fracture Energy	X	X			
Permeability		X	X	X	
Coefficient of Thermal Expansion	X		X		
Air Void System					X
JPCP aggregate interlock	X				

* Coarse aggregate size, angularity, gradation, content, and type.

This section summarizes the detailed literature review performed in the first year of this project. The literature review is reported in "Effect of Higher Strength and Associated Concrete Properties on Pavement Performance," Interim Report, Federal Highway Administration (FHWA), September 27, 1996.

1.5.1 Flexural and Splitting Tensile Strength

The flexure and splitting tensile strength are properties directly related to the performance of PCC pavements. The PCC tensile characteristics directly affect the initiation of transverse cracking and corner breaks. Limited literature exists on the effect on flexure and tensile strength as the compressive strength increases (ACI Committee 363, 1984; and Tachibana et al., 1981). It is believed that the material characteristics, in general, affect the tensile properties in a similar manner as the compressive strength. However, recent literature suggests that factors determining the aggregate-matrix bond are more

important to PCC tensile capacity than compressive strength even in the normal strength range (Forster, 1997; Vervuurt, 1997; and Mohamed and Hansen, 1999).

Model predictions for the relationship between the tensile strength and the compressive strength indicate the influence of mix design parameters. This is also reflected by the relationship between the compressive strength and the flexure strength (ACI Committee 363, 1984; and Carrasquillo et al., 1990). Furthermore, the flexure strength is not a pure material property, but rather a structural property (Neville, 1983).

1.5.2 Compressive Strength

Although compressive failure rarely occurs in the pavement structure, the compressive strength of concrete is perhaps the most comprehensive measure of concrete quality. The compressive strength is directly related to the microstructure of the hardened concrete (Mehta and Aitcin, 1990). Higher strength concrete behaves increasingly as a homogeneous material in pre-peak loading, where the propagation of microcracks does not initiate until just prior to failure. At the same time, the fracture behavior becomes more brittle (Mehta and Monteiro, 1993; and Marzouk and Chen, 1995).

The compressive strength is mainly related to the w/c ratio. As the w/c ratio decreases, the compressive strength increases (Mindess and Young, 1981; Neville, 1983; and Mehta and Monteiro, 1986). Furthermore, strength of the coarse aggregate, mineralogical origin, and quality can become controlling factors at high compressive strengths. In addition, aggregate type influences the characteristics of the aggregate-paste bond at the interfacial transition zone (Mehta et al., 1990; Zia et al., 1991; and Zhou et al., 1995).

Increasing aggregate size generally decreases the water requirements for the same consistency, and should thereby also benefit the strength of the concrete. At the same time, larger aggregate also increases the possibility of defects within the aggregates. For these reasons, aggregate properties become more crucial for higher strength concrete than for normal strength concrete (Mindess and Young, 1981; and Mehta et al., 1990). Aggregate gradation is important to workability, strength, and durability. In general, the sand content is from 40 to 60 percent of the total aggregate content depending on the aggregate type and maximum aggregate size. For higher strength concrete, with higher cement content, the sand should not be too fine because it will increase water requirements (Cramer et al., 1995).

Certain chemical admixtures improve the workability (Aitcin and Lessard, 1994). Entrained air also enhances workability, but decreases the compressive strength (Neville, 1983). Use of entrained air is important from a freeze-thaw durability point of view. Mineral additives such as silica fume and fly ash are commonly used in concrete structures. The mineral additives affect the strength of the concrete. Fly ash is not as effective as cement in increasing early strength, and its effectiveness is dependent on the classification of the fly ash. However, the slow pozzolanic reaction can lead to improved long-term strength. It is recommended that fly ash not exceed approximately 25 to 35 percent of the cementitious material according to American Concrete Institute (ACI)

standard 211.4R (1989). Mainly, the use of fly ash reduces the permeability, thermal cracking, and material costs (Tachibana et al., 1990).

1.5.3 Elastic Modulus

The PCC elastic modulus is an important variable in pavement design as it controls the overall slab deflection from traffic loading and the slab curling stresses. The elastic modulus increases as the compressive strength increases, and it is found that in general the material characteristics affect the elastic modulus in the same manner as the compressive strength. It should be noted that aggregate type and gradation have strong influence on the elastic modulus (Mehta et al., 1990; and Mehta and Monteiro, 1993).

Several relationships between elastic modulus and the compressive strength are presented in the literature (Neville, 1983; Mehta and Monteiro, 1993; Mindess and Young, 1981; and Ahmad, 1994). Use of such a relation has to agree with the conditions under which the original data are obtained. In general, the use of such a relationship for normal strength concrete will not be applicable for higher strength concrete.

1.5.4 Fracture Energy

Concrete strength cannot alone predict the concrete fracture behavior because the behavior is largely affected by the material characteristics and in particular by the coarse aggregate type, size, and content.

A number of studies have been performed evaluating the effect of coarse aggregate properties on the concrete fracture properties (e.g. Petersson, 1981; Kleinschrodt and Winkler, 1986; de Larrard and Malier, 1992; Kan and Swartz, 1995; Zhou et al., 1995; and Giaccio and Zerbino, 1998). It is important to keep in mind that the framework for these studies was traditional structural concrete and not paving concrete.

The concrete fracture energy is given by a combination of the fracture energy of the matrix and the coarse aggregate. For normal strength concrete, the coarse aggregates form the most significant component with a contribution of approximately 85 percent. In other words, the aggregate interlock (bridging and frictional effects) has a significant effect (de Larrard and Malier, 1992; and Bache and Vinding, 1990/1992).

The coarse aggregate is found to be the most important factor for fracture energy. Petersson (1981) reported that the difference in fracture energies lie in the effective crack path. For strong aggregates the crack runs around the aggregate, whereas for weak aggregates the crack penetrates and fractures the aggregates. The crack path also depends on the paste-aggregate bond.

Increasing the aggregate size improves the fracture properties. Studies reported by Petersson (1981), Kleinschrodt and Winkler (1986), and Karihaloo (1995) showed that increasing the coarse aggregate size increases the fracture energy. Karihaloo states that the increased fracture energy is due to the effect of aggregates as “crack obstacles.” The

crack has to change directions to pass around the aggregates, and this requires additional energy compared to that required for a straight-line crack. It was found that only the post-peak response is affected and that increasing aggregate size allows more energy to be absorbed by the concrete.

It has been suggested that a higher volume concentration of particles (aggregates) which are stronger and stiffer than the matrix would also increase the fracture energy (Monterio and Helene, 1994; and Bache and Vinding, 1992). Petersson (1981) did a limited study with cement to aggregate ratio from 0.4, 0.5, and 0.6. He found that the fracture energy did increase with increasing aggregate fraction, but the elastic modulus was more affected. It is important to keep in mind that the framework for these studies was traditional structural concrete and not paving concrete.

Karihaloo (1995) illustrated that aggregate textures affect the fracture energy. However, in contrast to aggregate type, size, and content, the aggregate shape and angularity tend to affect the peak area more than the tail area. Crushed materials tend to reach higher peak stress than rounded materials. In general, the effect of aggregate shape and angularity has less impact on fracture energy than the aggregate type and size.

In general, the load-deflection response for high strength concrete is different from the response of normal strength concrete. The pre-peak response shows that the higher strength concrete generally has a higher load carrying capacity and stiffness than normal strength concrete, and the post-peak response shows that the descending branch is steeper for higher strength concrete than for normal strength concrete. Overall, the total area under the load-deflection curve is larger for higher than for normal strength concrete but the overall response of higher strength concrete is more brittle than the response for normal strength concrete, (Marzouk and Chen, 1995).

The fracture energy value increases as w/c ratio decreases and the area under the load-deflection curve increases (Petersson, 1981; and Kan and Swartz, 1995).

1.5.5 Permeability

Although there is no single standard test for assessing the durability of concrete exposed to different conditions, permeability is generally considered the best parameter for characterizing the ability of concrete to resist deterioration (Schonlin and Hilsdorf, 1988). The permeability of concrete is a measure of the ability of various fluids to be transported through concrete's porous microstructure. Permeability can be an indicator of long-term performance, especially when considered in conjunction with other concrete properties (Armaghani et al., 1992).

The literature has shown that permeability is strongly related to w/c ratio, chemical admixtures, mineral additives, and aggregate properties (e.g. Mobasher and Mitchell, 1988; Schonlin and Hilsdorf, 1988; Mehta, 1990; Kosmatka and Panarese, 1992; and Ollivier et al., 1995). It is widely accepted that lower w/c ratio decreases permeability. Furthermore, replacing cement with ground granulated blast furnace slag and fly ash also

decreases permeability, but these additives can be sensitive to curing conditions. Aggregate type and size have also been shown to affect the microstructure enough to affect permeability results, although individual testing of sources is recommended.

1.5.6 Air Content and Freeze-Thaw Durability

The freeze-thaw durability of the paste is controlled by the air void system of the concrete. Factors affecting the freeze-thaw durability of the concrete are the paste pore system, entrained air, and freeze-thaw resistant aggregates. D-cracking is a freeze-thaw problem directly related to the coarse aggregate, characterized by the aggregate internal pore structure and maximum aggregate size. The durability of aggregate is not covered in this study, as it is already well explained in the literature.

The freeze-thaw durability of normal strength concrete can be estimated from the spacing factor, which indicates the distribution of air voids in the paste (a spacing factor less than 0.2 mm is required for freeze-thaw resistance) (Powers, 1945 and 1949). For higher strength concrete the requirement is not clear, but ACI allows a one-percent reduction in recommended air content for 28-day compressive strength higher than 34.5 MPa. It is not fully understood how the air content affects the freeze-thaw durability for higher strength concrete (ACI 318, 1995).

The air system in the hardened concrete is highly related to the concrete mix and the finishing procedures. For example, decreased w/c ratio, finer ground cement, finely divided mineral additives and high proportion of fines in the fine aggregate all lead to less entrained air (Mindess and Young, 1981). Using air-entraining admixtures with proper mixing, placement and finishing can provide a well-distributed air system. It is found that entrained air reduces bleeding and segregation of the fresh concrete, which minimizes the system of microcracks in the hardened concrete. The disadvantage of entrained air is the associated decrease in compressive strength.

1.5.7 Coefficient of Thermal Expansion

The value of the coefficient of thermal expansion (CTE) is considered very important for joint movement and slab curling (PCA, 1988). The literature review has shown that CTE is highly dependent on the mix composition (Neville, 1975; Addis, 1986; and Van Dam, 1995). The CTE of concrete is determined by the CTE of cement paste and aggregate. Aggregate type has the highest influence on the value of thermal expansion due to the high volume content of coarse and fine aggregate in concrete (Zoldners, 1971). While moisture conditions have significant influence on the thermal properties of the cement paste, the effect is greatly reduced for concrete as a whole (Meyers, 1950). This is thought to be the case for both normal and higher strength concrete.

The methods for measuring CTE of concrete have not been standardized by the American Society for Testing and Materials (ASTM) or AASHTO, although AASHTO recently adapted the FHWA method as provisional standard TP-60-00. In recent years, several methods have been developed for research purposes (Emborg, 1989, and Bjontegaard,

1999). These methods are sometimes specially designed for measuring CTE of early age concrete. Test results from Emborg and Bjontegaard indicate that CTE decreases rapidly with age and becomes almost constant after 28 days. The method used in this research project is not specially designed for early age concrete but allows a relatively quick determination of CTE so that other forms of deformation (autogeneous shrinkage and swelling) can be minimized.

1.5.8 Coarse Aggregate Characteristics Affecting Joint/Crack LTE

Sutherland and Cashell (1945) found that concretes made with rounded gravel had better load transfer characteristics than concretes made with similarly graded crushed limestone. The difference was attributed to the concrete crack face. It was observed that the concrete containing gravel generated a rough surface and the concretes with limestone generated a smoother surface, due to cracking around instead of through the aggregate.

Abdel-Maksoud et al. (1998) evaluated the effect of coarse aggregate type on laboratory specimens subjected to cyclic shear. They found that for a low number of cyclic loadings the responses for limestone, gravel and trap rock were comparable. However, under an increasing number of cycles, the limestone exhibited a rapid increase in displacement compared to the gravel and the trap rock. The difference in behavior was explained by the varying degrees of resistance to degradation and crushing. The authors of the study showed that aggregate properties like Los Angeles abrasion and Crushing Value correlated with these observations. These findings are also in agreement with results reported by Sutherland and Cashell (1945).

In addition to coarse aggregate type, coarse aggregate angularity also affects the load transfer characteristics. Colley and Humphrey (1967) showed that the load transfer characteristics improved significantly from the behavior of a natural gravel to a crushed natural gravel.

Sutherland and Cashell (1945) and Nowlen (1968) studied the effect of coarse aggregate size, and found that by increasing the aggregate size, from a nominal maximum aggregate size of 38 to 62 mm, the load transfer was increased. Abdel-Maksoud et al. (1998) also reported that increasing the nominal maximum aggregate size from 25 to 38 mm decreased the displacement needed to mobilize a given shear stress. Results from gravel and trap rock indicated the same trends. Furthermore, the study also indicated the importance of coarse aggregate size in relation to crack width. They suggested that coarse aggregate size to crack width ratio is a likely controlling parameter for aggregate interlock.

CHAPTER 2. RESEARCH METHODOLOGY FOR DETAILED FIELD AND LABORATORY EVALUATION

The intent of this project is to evaluate the effects of PCC properties and materials characteristics on pavement performance in the context of increasing strength. This chapter focuses on the selection of pavement test sections and the field and laboratory techniques used in their evaluation. Chapter 3 discusses the selected sites and the variables covered.

Due to the limited number of JPCP field sites with PCC of higher strength, it is important that the literature review and succeeding field and laboratory studies are covering as wide a range as possible in the PCC strength and associated properties. Data must be obtained to determine the required levels of the PCC strength and associated properties, which are associated with good long-term performance of the JPCP's. Based on analysis of these data, recommendations can be made for the required levels of PCC properties and mix characteristics necessary for good long-term JPCP performance. Furthermore, because a wide range in PCC strength has been evaluated it is possible for engineers to interpolate and extrapolate within the project database aided by theory and pavement models.

This objective was met by evaluating the FHWA Long Term Pavement Performance (LTPP) database. Based on this preliminary investigation overall PCC and performance trends were established. The following section discusses the observations made from this analysis.

Test section selection has been done primarily using the SHRP LTPP database. Selection criteria are based on concrete strength, geographic location, age, design features, loading history, and performance characteristics. A major goal in test site selection was to identify good and poor performers within each climate type for comparison. Variation of parameters which do not play highly significant roles in performance were minimized, allowing the effects of critical parameters to be better quantified.

Field site surveys were designed to accurately evaluate the current pavement condition of each site, and to specifically identify and quantify distresses and unusual features. Field surveys include distress mapping, site photos, falling weight deflectometer measurements, dynamic cone penetrometer measurements, dipstick surface profile measurements, drainage surveys, general site surveys, concrete sampling and soil sampling.

Laboratory analyses of concrete samples from these test pavements focus on determining their key physical properties and material characteristics. These laboratory tests include concrete strength (compressive and splitting tensile), elastic modulus, transport properties (water and air permeability, rapid chloride permeability test, and water absorptivity), coefficient of thermal expansion, petrographic analysis of distress, air void analysis, aggregate type, size and gradation, cement content, and w/c ratio determination.

2.1 Information on Pavement Performance, PCC Properties, and Material Characteristics Obtained from the SHRP LTPP Database

As was observed in the literature review, the number of variables that affect concrete pavement performance are numerous, and no one or two variables appear to have a dominant impact for any distress mode. The fact that so many interacting variables affect performance of the pavement system would dictate that a large number of test sites covering the full range of each parameter be selected to fully examine the statistical impact each variable has on observed pavement performance. Current studies such as the LTPP Program are investing the resources required to obtain enough data to conduct meaningful statistical analysis of the factors affecting pavement performance. The project team has used the SHRP-LTPP data to examine the impact of each of the critical variables.

2.1.1 Overview of the LTPP Database

The LTPP program was initiated in 1987 and is designed to be a 20-year program. The first 5 years of the program were conducted under the SHRP, and it then was transferred to the FHWA. As stated on the cover of the latest version of the LTPP database, DataPave 97, the LTPP program is expected to be the largest available pavement performance database, with enormous potential for the development of products to improve pavement technology.

The pavement sections in this database are located in all States of the United States and in Canada. In this study pavement sections under the General Pavement Studies (GPS) have been included for investigation. The GPS sections were in service at the time of selection, either in their original design phase or their overlay phase. Furthermore, only the plain jointed pavement sections, identified as GPS-3, have been included for evaluation.

The LTPP Information Management System (IMS) data used for identifying the ranges of concrete properties was requested in October 1995. It is important to emphasize that the database was not complete at that time. A newer version, DataPave, is now available.

2.1.2 Available Information in the LTPP Database

To date, considerable amounts of data have been collected on pavement construction, maintenance, rehabilitation, and performance. The data is stored in the LTPP database, which maintains information on different pavement types. The types of data that may be available for each section include an inventory of design and construction parameters, environmental factors, results of material testing, pavement monitoring parameters (e.g. deflection and distress), traffic, maintenance, and rehabilitation activities.

The environmental data contain a wide variety of information, including both monthly and annual summaries of climatic parameters such as: freezing index values; number of freeze-thaw cycles; maximum, and average air temperatures; precipitation; relative

humidity; and wind speed. In addition, detailed location information is provided for each recorded weather station. Environmental information provides a basis for understanding how climate has impacted pavement performance. Such parameters as climatic zone, number of freeze-thaw cycles, and freezing index have been closely related to pavement performance. Other environmental factors, such as maximum and minimum temperatures, are also thought to play an important role. This information was initially used to evaluate climate effects on performance and to select candidate pavement projects over a variety of climatic conditions for the field investigations in this study.

The inventory information contained in the LTPP database can be divided into two general categories: descriptive/design information, and construction/materials information. Descriptive/design information includes section location and layout, layer thickness, age, joint spacing, percent steel, load transfer type, shoulder configuration, lane width, subdrainage, etc. These types of data are very useful in identifying design features, which may impact pavement behavior. Construction/materials information includes PCC mix design parameters, aggregate type and gradation, and PCC strength and stiffness values obtained during construction.

Under the LTPP Program, each experimental site is being monitored to provide a systematic assessment of the pavement condition. Monitoring activities include nondestructive testing using a falling weight deflectometer (FWD), longitudinal profiling, identification of surface distress, frictional measurements, and transverse profiling. These regularly scheduled monitoring activities are conducted using well-documented techniques and calibrated equipment. Pavement performance, as measured by changes in pavement condition as a function of time, traffic, and climate, can thus be assessed.

Of significant interest to this study are the surface distress data. These data have been collected both manually and through automated means. Manual surveys are conducted in accordance to standardized procedures from SHRP-P-338 (1993). The distresses in this category are cracking, joint deficiencies, surface defects, and miscellaneous distress. Furthermore, the database contains information on joint and crack faulting.

The traffic information was in part generated from estimates and collected on site using weigh in motion (WIM) technology. Considering these data, information can be obtained on growth rate for Equivalent Single Axle Loads (ESAL's), cumulative ESAL's, initial ESAL rate and average ESAL's.

Under the LTPP program, an extensive amount of field drilling, sampling, and material testing has been and continues to be performed. Data has been collected on all the pavement layers including the PCC base, subbase, and subgrade. The information on PCC material properties includes compressive strength, splitting tensile strength, and static elastic modulus. At this point in time no information is available on hardened concrete permeability, air content or flexural strength. The amount of data available under the material testing section is highly variable, and some sections have only limited information. However, the material testing data are instrumental in test site selection.

2.2 Selection of Candidate Pavement Sections

2.2.1 Introduction

It was the task of the project investigators to establish a pavement selection criteria philosophy based on the results of the information search and the limits of the project budget, which maximizes the usefulness of the field study. The following methodology was used during site selection. First jointed plain concrete pavements from the LTPP GPS-3 database were selected based on climate, age, strength, traffic, and distress levels. A few test sites outside the LTPP database were also selected based on recommendations from SHA officials. Then, scatter plots of key parameters were generated and reviewed to determine if any of the selected projects were nonstandard or outliers from typical pavement sections or foundation types. This process was repeated until a set of sections was established which had good balance between distress levels, PCC properties (with emphasis on strength), and mix parameters.

The following discussion considers some of the more critical factors that influence pavement performance, and describes how each was addressed in the selection of proposed candidate pavement sections.

2.2.2 Climate

Climate is indisputably a major factor that contributes to the performance of PCC pavements. Temperature and moisture fluctuations lead to expansion and contraction of the PCC and cyclical upward and downward curling or warping of the slab ends results in ever changing stress patterns and the relative movement at joints and cracks. These effects, combined with load induced stress, strongly control the rate of deterioration of the pavement system.

Many PCC pavement distresses can occur only under the influence of both temperature and moisture extremes. For example, frost heave not only requires below freezing temperatures, it also needs a ready supply of moisture. Furthermore, a distress such as spalling due to aggregate freeze thaw damage can only occur if the poor quality aggregate is in near saturated condition as it freezes.

The classification approach adopted by this study is to define four major climatic regions as follows (Rauhut et al., 1984; and TRB, 1986):

- Wet-Freeze (WF).
- Dry-No-Freeze (DNF).
- Dry-Freeze (DF).
- Wet-No-Freeze (WNF).

2.2.3 Concrete Strength

It has proven difficult to define what constitutes "higher than normal" concrete strength for pavements. In addition, the age at which the concrete is tested also has significant impact on the observed strength. Concrete strength data obtained through testing of cores were available in the LTPP data. It was also observed in the literature that compressive strength is commonly used to distinguish higher strength from normal strength concrete. Thus it was decided to use inservice compressive strength, as obtained from testing of cores of existing pavements as the primary strength parameter in the selection process.

The use of compressive strengths obtained from cores has at least one added advantage. Because the sections selected for evaluation are at least 10 years old, little additional strength gain would be expected. Thus, the compressive strengths obtained could be considered as near ultimate concrete compressive strength. This is an important concept, as there are concerns being voiced in the industry that over time cements have evolved towards higher earlier strength gain with lower additional strength gain after 90 days resulting in lower ultimate strengths.

After examination of relevant literature, a study of the LTPP data, and discussion among the Technical Advisory Panel (TAP), an insitu concrete compressive strength of 48 MPa (7,000 lbf/in^2) was selected as a reasonable estimate of the average long term inservice strength of PCC pavement.

The strength philosophy used for the selection process was to have eight to nine sections of higher than average strength and three to four sections of lower than average strength. Furthermore, the selections were made to obtain a range of performance/distress levels within the different climates.

2.2.4 Distress

Pavement performance, as defined by the initiation and progression of distress over time, is the overriding concern of every pavement designer. Distress level was therefore one of the most important factors used to select pavement sections for further evaluation in this study. As mentioned earlier, the observation of superior performing pavements in the State of Washington was a catalyst for the creation of this study. It was noted that many of these pavement sections had insitu concrete compressive strengths well in excess of that normally encountered, some exceeding 69 MPa (10,000 lbf/in^2). The literature review has indicated that strength may have played a secondary role in performance in the State of Washington. In the case of the Seattle concrete several parameters may have played significant roles in the performance characteristics observed. These include the combination of a thermally stable climate (very little hot or freezing conditions), a moist climate (modest annual precipitation but high number of wet days per year), and good quality aggregate in the foundation layers and in the PCC.

Distress types considered in the selection process include transverse joint spalling, transverse slab cracking, transverse crack deterioration, and faulting. It is noted that sections identified as having durability related cracking were eliminated from consideration, as agreed to during the first meeting with the TAP.

2.2.5 Pavement Age

It was imperative that the selected pavement sections had a sufficient age so that deterioration from climatic and load factors had occured. For about the first 10 years of service, typical well constructed concrete pavements have little observable damage. After this time, superior performing pavements begin to distinguish themselves with far fewer observances of pavement distress. At ages in excess of 20 years, only exceptional pavements are expected to have little or no observable distress.

Thus, pavement sections considered for further analysis in this study were grouped into one of two age categories. The younger sections are between 10 and 20 years old, while the older sections are 20 years or older.

2.2.6 Traffic

All pavement design methods consider traffic loading as an important design variable. Traffic is largely responsible for the rate of development of numerous pavement distresses. Highway traffic consists of a diverse mix of vehicles, each having unique loading characteristics. Researchers who analyzed data collected at the American Association of State Highway and Transportation Officials (AASHTO) road test developed equivalency factors that relate damage induced by various load and axle configurations (as measured by the change in pavement serviceability) to that of a standard 80-kN (18,000-lb) single axle load for various pavement structural sections (AASHTO, 1993). Through the use of these equivalency factors, a diverse mix of traffic can be "converted" to a single metric referred to as equivalent single axle loads (ESAL's). The term ESAL's is the most common traffic index used in the design process and is calculated and reported by most SHA's. It is also one measure of traffic provided in the LTPP data. Because ESAL's are commonly understood and reported, the ESAL was chosen as the traffic variable in the selection of experimental pavement sections.

Each pavement section examined in this study has a different age, making it impractical to use cumulative ESAL's as a selection criterion. Instead, ESAL rate was used; as defined by the total cumulative ESAL's divided by the age in years. Although there is no universally accepted value separating low from medium or high traffic, a rate of 300,000 ESAL's per year was considered appropriate. This is based on the distribution of ESAL rates observed in the LTPP data and the assumption that 6 million ESAL's within a 20 year design life is a good demarcation between a secondary and primary route.

2.2.7 Joint Spacing and Reinforcement

The national trend in PCC pavement design is toward short-jointed, plain, doweled concrete pavements. According the web site of the American Concrete Pavement

Association (ACPA), the majority of States are now building primarily jointed plain concrete pavements (JPCP). Only 9 States currently construct jointed reinforced concrete pavements (JRCP) sections, and 8 construct continuous reinforced concrete pavements (CRCP). Typical slab lengths have also become shorter, with many states using 4.5-m (15-ft) or shorter slabs. Only one State builds JPCP sections with slab lengths greater than 6 m (20 ft).

The literature review and analyses of the LTPP pavement performance data has indicated that pavements with long slab lengths are more sensitive to climate and foundation conditions than shorter sections. It was therefore decided to maximize the applicability of this PCC properties and materials characteristics study by focusing on the analysis of short (~3.6 to 6 m (~12 to 20 ft)) slab JPCP where joint movements are minimized and mixture characteristics play a more significant role in long-term performance. Maximum joint spacing for JPCP is typically less than 6 m (20 ft) and in many instances less than 4.5 m (15 ft) which is well below the critical slab length where maximum curling/warping related bending stress and joint deflection occurs.

2.2.8 Other Design Parameters

There are many other variables that impact concrete pavement performance. These include pavement thickness, base type, subgrade type, drainage conditions, shoulder type, joint sealant, load transfer design, and a multitude of others. Due to the rigorous nature of the proposed testing regime, relatively few sections will be investigated. It was thus attempted to hold other variables within a reasonable range when selecting sections for study.

2.3 Details of Field Evaluation of Selected Pavement Sections

2.3.1 Introduction

The field evaluation portion of this study was conducted to provide valuable information concerning the field conditions of the candidate pavement sections and to supply concrete samples for use in the subsequent laboratory analyses. This evaluation consisted of continued background information collection, onsite visual surveys, core sampling, and evaluation of existing nondestructive deflection testing data.

2.3.2 Background Information

As discussed previously, the majority of the candidate pavement sections selected for study are included in the LTPP database. Therefore, large amounts of information concerning climatic conditions, design, construction, traffic, and maintenance activities are available. These sections have also been monitored and tested for distress, structural response, and strength parameters.

Some of this data was compiled during the site selection process but more was available. The project team utilized that LTPP data in greater detail later, examining materials and construction factors. Structural response data from nondestructive deflection testing was also sought. Specifically, the following types of information were sought, documented, and analyzed:

- Design Information - slab dimensions (thickness, length, and width), load transfer method, type of shoulder, support characteristics (base, subbase, and subgrade), and drainage.
- Material Information - cement type, coarse and fine aggregate types, proportions and gradations, type and quantity of admixtures, and other PCC mixture characteristics.
- Monitoring Information - updated distress, faulting, and nondestructive deflection testing.
- Traffic Information – Annual Average Daily Traffic (AADT), percent trucks, and ESAL's.

2.3.3 General Site Visit

A general site visit was conducted to provide final verification of the suitability of each site for this study through establishing the section's uniformity of construction, drainage, traffic, and performance. It was also important that the 152-m (500-ft) test section was representative of the pavement project as a whole. The LTPP program invested considerable efforts to verify both uniformity within the section and to ensure that the test section was representative of the project. Specifically, the following criteria established in a previous FHWA study were used (FHWA, 1995):

- Horizontal curves less than three degrees and vertical grades less than 4 percent.
- A minimum of cut/fill transitions, either longitudinally or transversely.
- No culverts, pipes, or other substructures within the section (if possible).
- Uniform traffic flow through the project.
- Identification of any other factors that may in any way compromise the safety of the field survey team such as confined space due to barrier walls or guardrail.

The final purpose of the general site visit was to coordinate with the cooperating SHA in scheduling visual distress surveys and field sampling.

2.3.4 Visual Survey

After the general site survey was performed, a detailed visual distress survey was conducted by Soil and Materials Engineers, Inc. (SME) using slight modifications to the procedures outlined in the SHRP Distress Identification Manual for the Long-Term

Pavement Performance Studies (SHRP-P-338, 1993). Copies of the forms used during the distress inspections are shown in figures 2.3.1 and 2.3.2.

These procedures are very rigorous, recording all visible distress including cracking, spalling, scaling, durability related distress, faulting, and lane-shoulder separation and/or drop off. Joint widths are measured and sealant quality recorded. Other pavement features, including patches, core holes, culverts, bridges, etc., are also noted on the form. Joint faulting is measured using the Georgia faultmeter similar to SHRP procedures (SHRP-P-338, 1993).

For this study, spalling and faulting are quantified in greater detail than outlined in the SHRP standard procedures. For spalls, the approximate dimensions of the spall are noted directly on the crack maps for each occurrence. Faulting is measured and recorded to the finest resolution possible by the equipment being used (preferably 0.1 to 0.2 mm (0.0039 to 0.0078 in)). Every discontinuity (crack or joint) is recorded for faulting (zero's included). In addition, all crack widths are measured and noted on the crack maps during the faulting surveys. Profile/roughness measurements, typically conducted with dipstick type devices, are replaced with dipstick measurements which can measure slab warping and/or construction related curling.

In conjunction with the visual distress survey, a drainage survey was also conducted. Ditches were evaluated for standing water, and the presence of vegetation found in swampy areas was recorded. Drainage structures, such as outlets and culverts, were examined and functionality assessed, and pavement and shoulder cross slopes were measured. The drainage field survey form, adapted from a recent FHWA study (FHWA, 1995), is shown in figure 2.3.3.

Site location maps detailing all observations were prepared. The nearest milepost was located, as were all fixed structures including culverts, bridges, and highway exits. All coring locations were also shown.

Field Survey: *General Information*

Project ID: _____

ERES ID: _____

Date of Survey (mm/dd/yy): ___/___/___

Surveyors' Initials: _____/_____/_____

Test Section Location:

	Milemark (MP)	Station (STN)	Section Length, ft
Start Point		+	
End Point		+	

If no MP or STN: Distance from the nearest landmark: _____ ft

Direction FROM the landmark: Line of Traffic / Against Traffic

Landmark description (type/name of structure/interchange/crossroad):

_____

_____

Shoulder: **General Condition:** Good / Fair / Poor / Failed

Shoulder Surface Type

1. Turf 4. Concrete
2. Granular 5. Surface Treatment
3. AC 6. Other: _____

	Type	Width
Outside Shoulder:		ft
Inside Shoulder:		ft

Contraction Joint: Joint Spacing: _____.__ ft Skewed? y / n

Random Spacing: ____-____-____-____ ft ft/Lane: _____

Sealant Type: None HP SI Preform Other: _____

Longitudinal Joint: Method Used to Form Centerline Joint: Saw Cut / Plastic Insert

Sealant Type: None HP SI Preform Other: _____

Roughness and Serviceability:

Roughness Measurement Device Used: _____

		Lane Number*		
		1	2	3
Roughness Index	Trial 1			
	Trial 2			
Roughness Measurement Speed (mph)				
Present Serviceability Rating (mean)				

*Lane 1 is outer lane, Lane 2 is next lane 1, etc.

Figure 2.3.1 *General field survey form.*

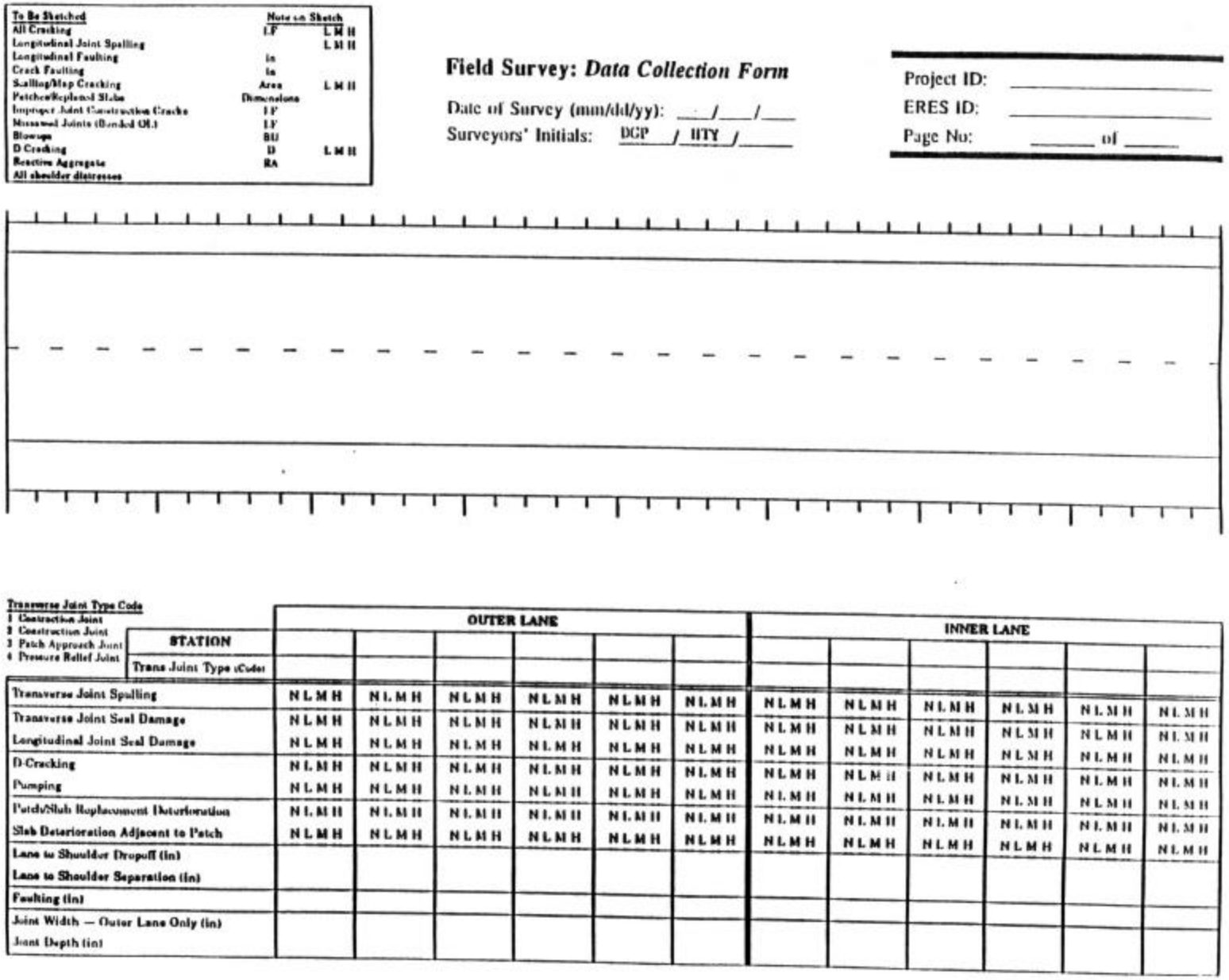

To Be Sketched	Note on Sketch	
All Cracking	LF	L M H
Longitudinal Joint Spalling		L M H
Longitudinal Faulting	in	
Crack Faulting	in	
Scaling/Map Cracking	Area	L M H
Patches/Replaced Slabs	Dimensions	
Improper Joint Construction Cracks	LF	
Measured Joints (Banded Ol.)	LF	
Blowups	BU	
D Cracking	D	L M H
Reactive Aggregate	RA	
All shoulder distresses		

Field Survey: ***Data Collection Form***

Date of Survey (mm/dd/yy): __/__/__

Surveyors' Initials: DGP / HTY /

Project ID: _____

ERES ID: _____

Page No: ____ of ____

Transverse Joint Type Code
1 Construction Joint
2 Construction Joint
3 Patch Approach Joint
4 Pressure Relief Joint

	OUTER LANE						INNER LANE					
STATION												
Trans Joint Type (Code)												
Transverse Joint Spalling	N L M H	N L M H	N L M H	N L M H	N L M H	N L M H	N L M H	N L M H	N L M H	N L M H	N L M H	N L M H
Transverse Joint Seal Damage	N L M H	N L M H	N L M H	N L M H	N L M H	N L M H	N L M H	N L M H	N L M H	N L M H	N L M H	N L M H
Longitudinal Joint Seal Damage	N L M H	N L M H	N L M H	N L M H	N L M H	N L M H	N L M H	N L M H	N L M H	N L M H	N L M H	N L M H
D-Cracking	N L M H	N L M H	N L M H	N L M H	N L M H	N L M H	N L M H	N L M H	N L M H	N L M H	N L M H	N L M H
Pumping	N L M H	N L M H	N L M H	N L M H	N L M H	N L M H	N L M H	N L M H	N L M H	N L M H	N L M H	N L M H
Patch/Slab Replacement Deterioration	N L M H	N L M H	N L M H	N L M H	N L M H	N L M H	N L M H	N L M H	N L M H	N L M H	N L M H	N L M H
Slab Deterioration Adjacent to Patch	N L M H	N L M H	N L M H	N L M H	N L M H	N L M H	N L M H	N L M H	N L M H	N L M H	N L M H	N L M H
Lane to Shoulder Dropoff (in)												
Lane to Shoulder Separation (in)												
Faulting (in)												
Joint Width — Outer Lane Only (in)												
Joint Depth (in)												

Figure 2.3.2 *Distress field survey form.*

Field Survey: ***Drainage Information***

Project ID: _____

ERES ID: _____

Date of Survey (mm/dd/yy): ___/___/___

Surveyors' Initials: _____/_____/_____

Slope Measurements:

	Station	Slope	
		Outer	Inner
Longitudinal Slope (nearest 1/16")	+	/	/
3 measurements, equally spaced along project.	+	/	/
	+	/	/
Transverse Slope (nearest 1/16")	+	/	/
3 measurements, equally spaced along project.	+	/	/
	+	/	/
Shoulder Slope (nearest 1/16")	+	/	/
3 measurements, equally spaced along project.	+	/	/
	+	/	/

Cut/Fill and Ditch Line Depth:

Circle, if Cut/Fill Depth Uniform	Cut/Fill Depth	Station(s)		Depth of Ditch Line
1.	Fill > 40 ft	+	+	ft
2.	Fill 16 - 40 ft	+	+	ft
3.	Fill 6 - 16 ft	+	+	ft
4.	At Grade (5 ft fill to 5 ft cut)	+	+	ft
5.	Cut 6 - 15 ft	+	+	ft
6.	Cut 16 - 40 ft	+	+	ft
7.	Cut > 40 ft	+	+	ft

Lane/Shoulder Joint Integrity:

	Outer Shoulder	Inner Shoulder
Sealant Damage	N L M H	N L M H
Blowholes	N L M H	N L M H
Sealant Type	None HP SI Preform Other:	

Subsurface Drainage (visual):

Type of drainage system present: ____

1. None. 3. Transverse Drains.
2. Longitudinal Drains. 7. Other: _____

Indicators of Poor Drainage:

Cattails or willows growing in ditch: y / n

Drainage outlets clogged: y / n

Drainage outlets below ditch line: y / n

Non-continuous cross section, crown to drainage ditch: y / n

Pumping: N L M H

Other: _____

Figure 2.3.3 *Drainage survey form.*

2.3.5 Coring

Coring of the test sections was done concurrently with the distress surveys. Core locations are established consistent with LTPP practice, which require positioning core locations just outside the boundary of the actual LTPP test section to avoid disturbing it. Thus, it was critical that the chosen test site was located within a uniform pavement project having common design, construction, material, traffic, and performance characteristics.

For each test site, a minimum of 14 cores (if possible) was obtained and tested as indicated in table 2.3.1. Of the 14 cores, 12 need to be intact specimens away from distress. Petrographic specimens included the distressed region if present. All specimens except those for permeability were 150-mm (6-in) diameter cores, whereas the permeability specimens had 100-mm (4-in) diameter cores. An R-meter was used to locate and avoid areas where steel dowels and tie bars are present. If a stabilized base was present, it was also cored.

Table 2.3.1. *Typical core sampling regime for the test sites.*

Test Type	Number of Cores
Compressive Strength	3
Splitting Tensile Strength	3
Coefficient of Thermal Expansion	2
Permeability	2
Petrography *	2

**One core was taken near distressed area if available.*

Each core was labeled as to test site, station, location (i.e., joint or center), core number, and measured thickness. Cores were then stored in plastic molds for delivery to the University of Michigan. Stabilized base material was treated similarly.

After coring, a dynamic cone penetrometer (DCP) test was conducted to provide information concerning the thickness and estimated in situ California Bearing Ratio (CBR) values of each unstabilized, underlying layer to a depth of approximately 1.5 m (5 ft). This information aided in identifying if settlement was causing distress.

2.3.6 Falling Weight Deflectometer

Nondestructive deflection tests (NDT) were obtained using a falling weight deflectometer (FWD). FWD testing was performed at midslab, joints, and at cracks, if any. Furthermore, FWD testing was performed at morning, noon, and afternoon conditions when possible. These results were used to determine midslab deflections, the composite modulus of subgrade reaction, and joint/crack load transfer.

In addition to the standard testing pattern, a new pattern was developed where FWD testing was done every 600 mm (2 ft) along the slab length. Typically three slabs were

tested. Using these data, the effect of intermittent and permanent loss of support and joint load transfer can be assessed.

2.3.7 Dipstick Profilometer Data

In situ slab surface profiles were, when possible, obtained for three or more slabs per test section. Using a Dipstick device, the surface profiles were obtained in the direction of traffic for the outer and the inner wheel-paths along with the slab diagonal. The profiles on the investigated slab(s) were measured in increments of 300 mm (1 ft). A zero beginning elevation was selected at the start point. If the entire test section was measured the site design slopes were removed in order to show small changes in elevation profiles. Furthermore, when possible surface profiles were obtained at morning, noon, and afternoon conditions.

The surface profiles can assess slab permanent shape and temperature curling, joint faulting, and slab rotation.

2.4 Details of Laboratory Evaluation of Selected Pavement Sections

To quantify and verify the observed trends and levels of concrete properties and material characteristics that produce excellent long-term distress free pavement performance, a field sampling and evaluation program for 15 inservice pavements was conducted. The following properties and material characteristics were necessary for detailed study from the field cores.

Physical Properties

- Compressive strength *(also measured by SHRP-LTPP).*
- Splitting tensile strength *(also measured by SHRP-LTPP).*
- Elastic modulus *(also measured by SHRP-LTPP).*
- Fracture energy *(not measured by SHRP-LTPP).*
- Permeability *(not measured by SHRP-LTPP).*
- Coefficient of thermal expansion *(not complete in SHRP-LTPP).*

Material characteristics

- W/C ratio.
- Cement content.
- Coarse aggregate gradation.
- Percent coarse aggregate.
- Coarse aggregate type.
- Coarse aggregate maximum size.
- Air void content.
- Air void size distribution.
- Air void spacing.

These above parameters offer a mix of primary factors and secondary factors which are used to infer critical parameters such as freeze-thaw durability, brittleness, and primary causes of distress. The methodologies of the laboratory analyses are discussed below. Standardized methods are not discussed in detail.

2.4.1 Methods to Determine Compressive Strength, Splitting Tensile Strength, and Elastic Modulus

The PCC properties compressive strength, splitting tensile strength, and elastic modulus are determined according to the following standards:

- Compression Testing: Testing guidelines provided in ASTM C 39-94, "Standard Test Method for Compressive Strength of Cylindrical Concrete Specimens."

- Split Tensile Testing: Testing according to ASTM C 496-90, "Standard Test Method for Splitting Tensile Strength of Cylindrical Concrete Specimens."

- Static Elastic Modulus: Testing according to ASTM C 469-94, "Standard Test Method for Static Modulus of Elasticity and Poisson's Ratio of Concrete in Compression."

2.4.2 Method to Determine Fracture Energy

The PCC fracture energy is proposed as a method to quantify the quality of the coarse aggregate in the concrete. At the same time, the overall PCC fracture behavior can be qualified, as discussed in chapter 7. Fracture energy can be determined from the complete load-deflection response of a notched beam subjected to center-point bending. The RILEM Technical Committee 50-FMC on Fracture Mechanics of Concrete – Test Methods proposed this test method (RILEM, 1985). The procedure is described by several textbooks (Karihaloo, 1995; and Shah et al., 1995). Many researchers have evaluated the test method and it has been found that the beam fracture energy is size dependent. The reason for the size-effect is mainly that the specimen and the loading configuration limit the crack length. However, results can be directly compared when the fracture energy is determined on the same specimen size.

Test Specimen

The recommended specimen size depends on the concrete maximum aggregate size. The notch depth should be equal to half the beam depth ±5 mm, while the notch width at the tip should be less than 10 mm. Further, it is recommended that the notch is saw-cut under wet conditions. Table 2.4.1 lists the recommended sizes for measuring fracture energy. Depth and width dimensions are the most critical dimensions depending on the maximum aggregate size. The ratio between span and depth, S/D, is recommended to range from 4 to 8 (Karihaloo, 1995). For 25-mm maximum aggregate size, this would require a minimum span of 800 mm and a maximum span of 1600 mm.

Table 2.4.1 *Recommended sizes of beams for measuring fracture energy.*

Nom. Maximum Aggregate Size (mm)	Depth (mm)	Width (mm)	Length (mm)	Span (mm)
16.1-32	200±5 mm	100±5 mm	1190±10 mm	1130±5 mm
32.1-48	300±5 mm	150±5 mm	1450±10 mm	1385±5 mm
This study				
25-38	200±5 mm	100±5 mm	1190±10 mm	965±5 mm

During casting, the beams are mechanically vibrated to avoid entrapped air. The beams cure for at least 24 hours before demolding. The beams cure at ambient room temperature of 20 ± 2 °C at 100-percent relative humidity (RH). Furthermore, the beams remain at 100-percent RH until time of testing/sawing. The notch is sawn on a table-saw with a diamond blade. If a table-saw is not available, a hand-held saw can be used with extreme care.

Test Procedure

The beam is tested as a statically determinate beam under constant deformation rate. In the literature it has been recommended that the peak load is reached within 60 seconds from start of test. However, the deformation rate may have to be lower depending on how brittle the material behavior is. The loading rate in this study was such that the peak was typically reached after 4-5 minutes depending on the level of nonlinear deformation before peak. The deformation rate can be controlled either directly from the beam deflection or from the crack mouth opening displacement (or a combination thereof.) Using the crack mouth opening displacement (measured by a clip-gage) induces the most stable test and in particular the peak area is well captured. It is recommended that the beam deflection is measured to the accuracy of at least 0.01 mm, and the load is measured to the accuracy of 2 percent of peak load. Possible nonelastic deformation at the loading and support points is excluded from the beam deflection.

A closed-loop servo hydraulic testing machine test is needed to perform a test in displacement control. If such equipment is not available, the stiffness of the testing machine should be larger than that of the steepest slope on the descending part of the curve. It should be emphasized that the descending part (softening) is very difficult to obtain using this method and expert literature should be reviewed.

Test Results and Calculations

The method to calculate fracture energy depends on the direction of loading. In this case it is assumed that the beam is downward loaded, and therefore the contribution from the beam self-weight and any equipment resting on the beam must be added to the load-deflection curve. The additional load is transformed into an equivalent single point load acting at the center and is added to the measured load. At the same time the associated deflection from the self-weight and any equipment on the beam is estimated using the initial slope of the measured load-deflection curve.

The specific fracture energy is calculated from the work-of-fracture. In this test downward loading occurred. Thus, the contribution from the self-weight and the equipment resting on the beam was included. The specific fracture energy can be calculated as:

$$G_F = G_F^{measured} + G_F^{self-weight} = \frac{\sum \left(F_i + F^{self-weight}\right) \cdot \left(d_i + d^{self-weight}\right)}{A} \quad (2.4.1)$$

where G_F = specific fracture energy (N/mm or N/m).
F_i = load at point i (N).
d_i = deflection at point i (mm).
$F^{self\text{-}weight}$ = load associated with the beam self-weight (N).
$d^{self\text{-}weight}$ = associated estimated deflection (mm).
A = initial cross section area at the notch (mm^2).

The test is typically terminated before complete beam separation occurs. Therefore, it is necessary to estimate the remaining part of the load-deflection curve in order to obtain G_F. This part of the curve corresponds to the area from the last measured deflection to the deflection at zero-load. The energy can be estimated using an analytical beam model for fictitious crack propagation assuming a parabolic descending branch (Ulfkjær et al., 1990). The load-deflection relation is:

$$F_i = F^{last} \cdot \left(\frac{d^{last}}{d_i}\right), F_i \geq F^{last} \quad (2.4.2)$$

where F^{last} = last measured load (N).
d^{last} = associated deflection.

Integrating this relation from d_{last} to $d \Rightarrow \infty$ yields:

$$G_F^{tail} = \frac{F^{last} \cdot d^{last}}{A} \quad \text{(N/mm or N/m)} \quad (2.4.3)$$

2.4.3 Transport Property Test Methods

Rapid Chloride Permeability Test (RCPT)

In this study, chloride ion penetration resistance has been measured using the Rapid Chloride Permeability Test (RCPT), which is designated as AASHTO T 277 and ASTM C 1202. Because this is a standard test procedure, it will not be described here in detail.

The test is a rapid measure of the resistance of concrete to the penetration of chloride ions. It is an electrochemical test, and is in reality not a permeability test. However, RCPT results are often referred to as permeability results. Table 2.4.2 lists the permeability classifications for the RCPT based on coulomb values after 6 hours of testing.

Table 2.4.2 *RCPT classifications.*

Classification	Charge Passed (C)
High	4000+
Moderate	2000-4000
Low	1000-2000
Very Low	100-1000
Negligible	0-100

In the literature, the test sample is typically taken near the top of the concrete. This is because most environmental attacks on the concrete are likely to occur near the pavement surface, and penetrate downward. Thus, this is considered the most critical region of the pavement for protection from the environmental exposure. At the same time, the very top surface of the pavement is avoided because of the prominence of distresses like shrinkage cracks, spalls, and high salt concentrations. Thus, the test sample is taken starting about 12 mm (0.5 in) below the surface. In this study that same procedure is used. However, samples are also tested at other depths within the concrete. This is to measure the through-thickness variation of the RCPT Results within the pavement. Each successive sample is taken immediately below the previous one, with the width of one sawcut separating them. The number of samples taken from a core depends on the pavement depth.

Water Permeability Test

Water permeability in this study has been measured by adapting the Florida Field Permeability Test (FPT) to laboratory samples. The test, developed by the University of Florida in cooperation with the Florida Department of Transportation, was designed for in situ measurements on structural elements in the field (Armaghani and Bloomquist, 1993). In this study, the method is used on laboratory samples under controlled laboratory conditions. Some minor adjustments have been made to the test procedure to account for this difference.

The FPT apparatus consists of a control unit, a pressure regulated nitrogen gas supply, a hand held vacuum pump, a test probe, and a pressurized water tank. Only distilled and deaerated water is used in the test to increase test accuracy.

To perform a test, a 75- to 150-mm (3- to 6-in) deep, 22-mm (0.875-in) diameter hole is drilled into the concrete to be tested. The depth of the test region is adjustable from 32 to 89 mm (1.25 to 3.5 in). The test probe is then inserted into the hole and sealed off. The test probe is a hollow stainless steel shaft with a water outlet hole near the bottom. Neoprene rubber packers seal off the test hole above and below the water outlet hole to isolate the test area. This test set up is shown schematically in figure 2.4.1.

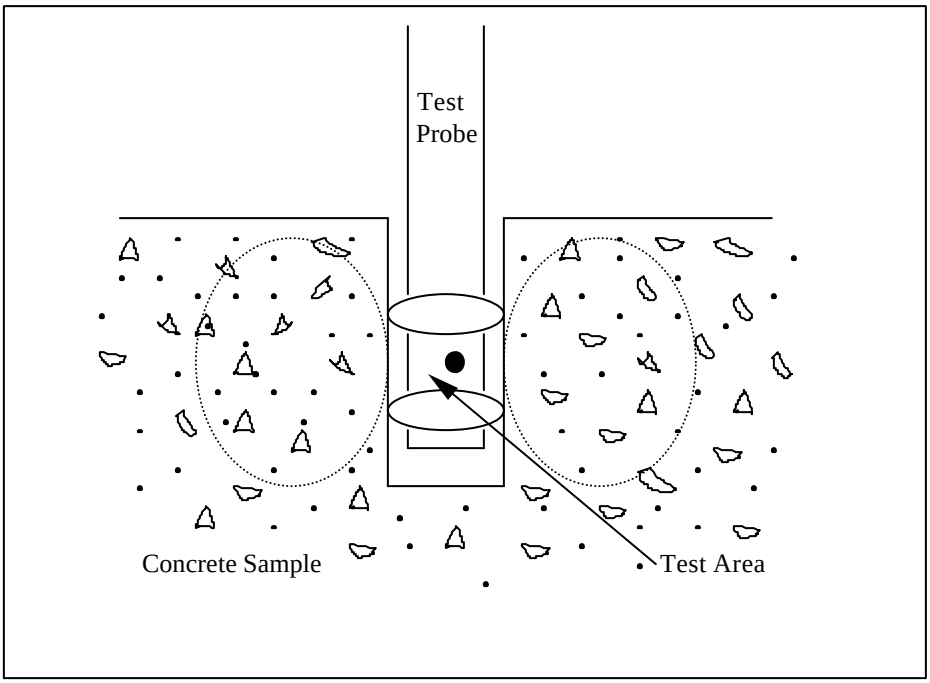

Figure 2.4.1 *Schematic of the water permeability test.*

The test begins by removing air from the system. Pressurized water is then injected into the test area through the water outlet in the probe. The water is forced into the concrete in the test area. The water pressure applied during the test may vary from 0.69 to 2.1 MPa (100 to 300 lbf/in^2), depending on concrete strength and expected permeability. As the test progresses, the water flowing into the concrete is monitored on a manometer loop in the control unit, and recorded at regular time intervals. Intervals from 5 to 30 minutes are allowable. In this study, 10-minute time intervals were used between readings. Readings are continued typically for 2 to 3 hours.

During the test, water flow tends to be rather high at first, and ultimately reaches a steady state condition within 1 to 2 hours. For insitu concretes, it is advisable to presaturate the test region with water under low pressure prior to beginning the test. This increases the speed with which steady-state flow is attained. In this study, concretes were stored underwater before and after the test hole was drilled. Thus, a significant amount of presaturation had already occurred before the sample was ever pressurized. Thus, it was found that the presaturation period could be omitted. Furthermore, steady-state flow was reached more quickly for these concretes. In order to standardize the testing procedure, it was decided to test each sample for 2 hours. The first hour's readings were used to allow the flow to stabilize, and the second hour's readings were used in permeability calculations. As is seen from the data, this approach appears justified.

Permeability is calculated based on the test pressure and flow rate, using the Packer/Lugeon equation to compute the coefficient of water permeability, K_w (FPT User's Manual, 1993). The actual flow pattern into the surrounding concrete is not known (and is likely dependent on the composition of the concrete matrix, as well as size, location, and types of aggregates near the test hole). For the sake of calculation, the flow

pattern is modeled as a sphere emanating from the probe center with ellipsoid shaped equipotential surfaces. The equation is written as the following:

$$K_w = \frac{Q}{2pL_0h}\sinh^{-1}\left(\frac{L_0}{2r}\right) = \frac{Q}{h}C_k \qquad \text{for} \qquad r \le L_0 \le 10r \quad \text{(in/sec or cm/sec)} \qquad (2.4.4)$$

where Q = rate of flow (in^3/sec or cm^3/sec).
h = pressure head (in or cm).
L_0 = length of test region (in or cm).
r = radius of test hole (in or cm).

In this study, the length of the test region is 1.27 cm (0.5 in) and the diameter of test hole is 2.23 cm (0.875 in). The coefficient C_k can be calculated to be 0.0682 cm^{-1} (0.1732 in^{-1}). The pressure applied from the regulator panel, P, has to be converted to equivalent head h by multiplying P by 70.3385. This means that 1 lbf/in^2 is equivalent to 70.3385 cm (27.6923 in) water head. Q can be calculated from the manometer reading of the water flowing into the specimen. The equivalent form of the above equation is:

$$K_w = \frac{Q}{70.3385P}C_k = \frac{Q}{P}\left(\frac{0.0682\frac{1}{cm}}{70.3385cm}\right) = \frac{Q\left(\frac{cm^3}{sec}\right)}{P\left(lbf/in^2\right)}\left[96.95x10^{-5}\frac{lbf/in^2}{cm^2}\right] \qquad (2.4.5)$$

The permeability classifications for the water permeability test are given according to the database of values obtained by Florida Department of Transportation and the University of Florida (Armaghani and Bloomquist, 1994) as shown in table 2.4.3.

Table 2.4.3 *FPT classifications based on Florida database of values.*

Classification	**K_w (x10^{-11} cm/sec)**
Very High	>500
High	150-500
Moderate	75-150
Low	15-75
Very Low	2.5-15
Negligible	<2.5

Air Permeability Test

The Torrent Air Permeability Test was developed in Switzerland as a portable, nondestructive method that is suitable for both field and laboratory measurement of permeability (Torrent, 1992). The method operates under vacuum pressure to pull air out of the concrete pores.

The apparatus features a two chamber vacuum cell, a pressure regulator, and a computer control unit. The vacuum cell is applied to the surface of the concrete. The two vacuum chambers are two concentric rings, as shown in figure 2.4.2. The outer chamber is intended to eliminate edge effects by capturing air flow from the concrete surface near the test area. The inner chamber is the test chamber, which measures air flow from

within the concrete at a right angle to the surface. The coefficient of permeability K_T is calculated from results of the inner vacuum chamber.

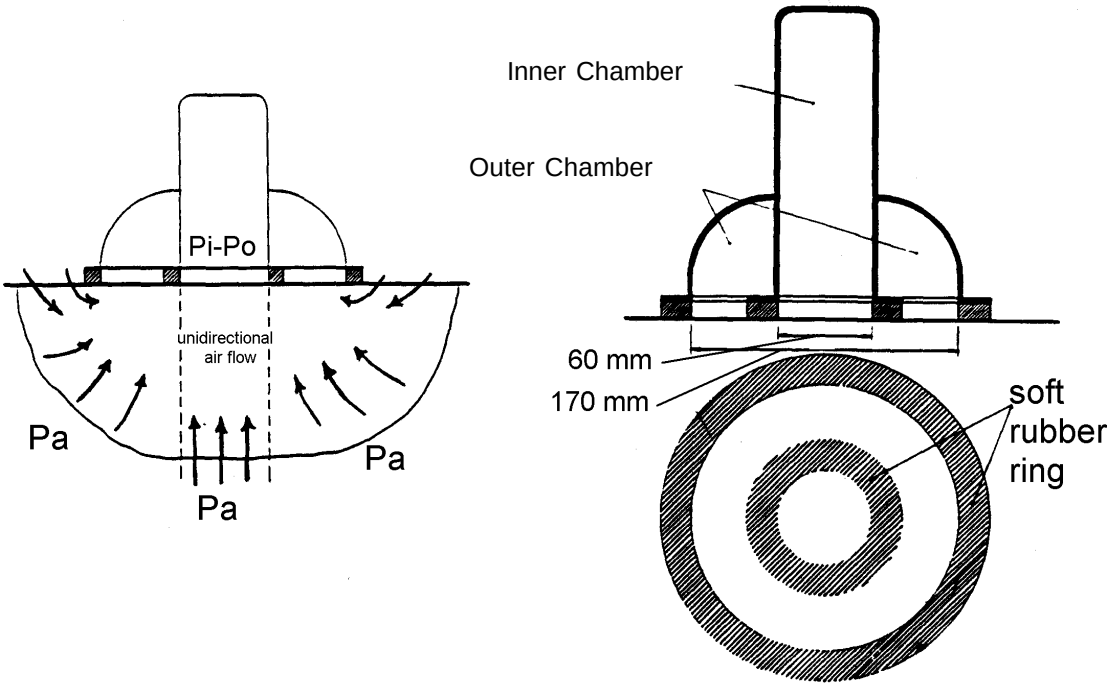

Figure 2.4.2 *Schematic of Torrent air permeability apparatus. [after Torrent, (1992)]*

One permeability measurement takes 720 seconds. During the first 60 seconds, the vacuum pressure is obtained in the inner and outer chambers. A total pressure of 20 mbar or less is typical at the beginning of the test. After the initial vacuuming period, the inner chamber is shut off, and the loss of vacuum pressure over time is recorded. The outer chamber continues to pull vacuum in order to ensure no influence from the edges. The permeability K_T is determined using equation 2.4.3 below.

$$K_T = 4\left(\frac{V_c dP/dt}{A(P_a^2 - P_1^2)}\right)^2 \frac{mP_a}{h}\int\left(1-\left(\frac{P_1}{P_a}\right)^2\right)dt \qquad (\text{x } 10^{-16}\ \text{m}^2) \qquad (2.4.6)$$

where V_c = total volume to which the filling air had access (m^3).
m = viscosity of air (2 x 10^{-5} Ns/m^2).
h = porosity of concrete.
A = area (m^2).
P = pressure (mbars).

It should be noted that moisture in the concrete significantly influences the measured permeability, as water trapped in the pore spaces inhibits the flow of air. The more water present, the lower the measured permeability. Thus, the method is best suited for dry concretes, where moisture does not influence results. When moisture is present, separate

electrical resistance (ρ) measurements are taken into account for the moisture. The K_T and ρ values are then used to determine the concrete permeability quality class.

Concrete quality classes are divided by orders of magnitude of K_T, spanning five orders of magnitude in all, as seen in table 2.4.4. In addition, ρ measurements span three orders of magnitude. This results in effective general classifications of the concrete quality. A high degree of precision within a category, though, is difficult to obtain. In this study it was found that even minor differences in surface roughness of the concrete could lead to perceivable differences within a permeability class.

Table 2.4.4 *Torrent air permeability classifications.*

Classification	K_T (x 10^{-16} m^2)
Very High	10-100
High	1-10
Moderate	0.1-1
Low	0.01-0.1
Very Low	0.001-0.01

Water Absorption Test

It is necessary to pre-dry PCC in order to determine the rate at which water through capillary forces fill the micropores (i.e. gel and capillary pores). To keep effects of specimen drying on moisture gradients and cracking tendency small, an oven drying temperature range between 60°C and 65°C was used as opposed to conventional drying at 105 C. The specimen thickness of 38.1mm (1.5 in.) was selected based on the maximum nominal aggregate size, which in this study was 38.1 mm for specimens outside the WF zone. Weight-loss equilibrium was reached within 7 days of drying in the oven with specimens resting on their edge to facilitate drying from both ends thereby reducing drying time and maximum moisture gradient duration.

To ensure one-dimensional water uptake during the test the specimen perimeter was coated with epoxy, similar to the rapid chloride permeability test. Also, to minimize evaporation effects the specimens were kept in a sealed container during the absorption test.

The Washburn equation for dynamic flow of a porous material containing cylindrical capillaries was used as the basis for analyzing the results.
According to this equation, the volume of liquid uptake (water in this case) by capillary suction per specimen surface area in kg/m^2 is given as:

$$V = k ((r_{(avg)})/ \eta)^{0.5} * t^{0.5} \qquad (2.4.7)$$

Where V is the volume of liquid which will penetrate the sample in the time t. For similar sized assemblage of capillary pores the water uptake is proportional to square root of the time, where $r_{(avg)}$, represents the average capillary pore radii, η is viscosity of the liquid, and k is Reynold's number. The slope of V versus $t^{0.5}$ is therefore correlated to coefficient of permeability. For larger pores (i.e. pores with diameter greater than about

1 micrometer), the capillary suction forces are much smaller. Thus the rate is reduced. For air-entrained PCC which consists of capillary pores, which are substantially smaller than 1 micron, and macro pores greater than 1 micron, this effect results in two distinct curvilinear portions. The initial high rate of filling is associated with capillary filling of micropores. The distinct lower rate of additional pore-filling is due to diffusion of water into the larger airvoids. The V versus $t^{0.5}$ relation is illustrated using the sketch in figure 2.4.3 below.

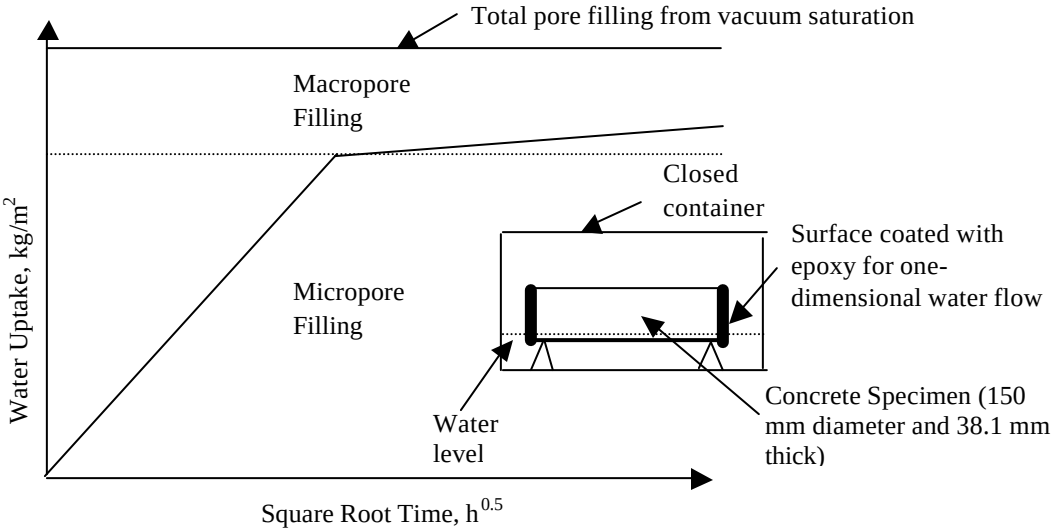

Figure 2.4.3 *Experimental setup for the water absorption test. The specimens rest on thin styrofoam spacers so that the water level is 1-2 mm above the specimen bottom.*

In reality the inflection point marking completion of micropore filling is not as distinct. This point was therefore approximated from a 24 hour soak in water. Complete porefilling of micro and macropores was obtained from a 24 hour vacuum saturation test in which air was removed prior to water filling. The difference in water uptake between these two tests is used to determine total air content in the sample.

2.4.4 Coefficient of Thermal Expansion

Currently, a standard specification on the measurement of the coefficient of thermal expansion (CTE) of concrete is not available. (Note that the updated FHWA test is now AASHTO 2000 provisional standard TP-60-00.) There are, however, several procedures that have been applied and recommended (Alungbe et. al., 1990; and FHWA, 1996). In general, in order to work satisfactorily, the procedure must be easy to do, robust, accurate, and reliable. The following procedure is intended to provide a very accurate and reliable result.

The method used here for determining CTE was originally based on the FHWA recommendation (FHWA, 1996). The design of the test frame shown in figure 2.4.4 is very similar to that described in the FHWA report. However, the test procedure is designed to continuously measure temperatures of the cooling/heating water and deformations of concrete specimens. In the FHWA recommendation, the measurement of

deformations is done at every 10 °C increment. Therefore, the present method may be considered as an improvement from FHWA's procedure.

A high resolution (18-bit) data collection system with sensitive linear variable differential transducers (LVDT's) is used to measure the linear expansion/contraction of concrete due to temperature changes from its surroundings. The concrete specimens are placed in a 190-L (50-gal) water bath connected to a heater-chiller for temperature control. Lab specimens are prepared with thermocouples imbedded in them so that the actual temperature of the specimens can be recorded. Along with the field specimens, a control specimen will also be used. Simultaneous data collection of specimen length change with internal temperature results at the center of a control specimen assumes that CTE is obtained accurately and is not affected by differences in water bath temperature. The data collection system will typically record data for every 0.2 °C change in internal concrete temperature. Thus, about 200 to 300 data points can be collected in each test. Data will be collected for the range of 10 to 50 °C and then for 50 to 10 °C. Once the test is completed, the data for each cycle is plotted separately. A displacement versus temperature plot is used to find the slope and CTE. After several tests with the same specimens, the final CTE for each specimen is found by averaging all the test runs. Figure 2.4.4 illustrates the frame used for measurement together with the position of the concrete specimen and the displacement sensor (LVDT).

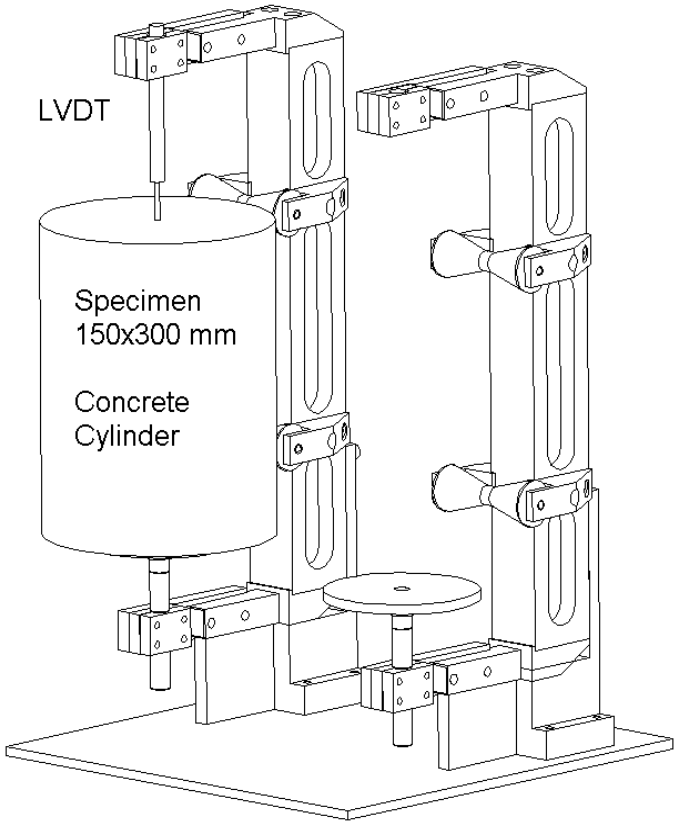

Figure 2.4.4 *Test frame for determination of CTE. [CTA, (1998)]*

The procedure consists of three important steps:
1. Preconditioning and setup.
2. Test execution.
3. Data analysis.

Preconditioning and Setup

Before testing any specimen, it is mandatory that it has been in a water tank (at room temperature) for at least 1 week. The purpose of this is to create a reference moisture content level. Since the CTE varies according to moisture content, all specimens must be soaked in order to minimize the effect of moisture. To compare results accurately, the control specimen should also have been in the water tank for a week before any experimentation.

Remove the specimens from their saturation tank. Measure and record their original length to the nearest 1.6 mm (0.0625 in) and place onto one of the stands in the tank. Each specimen must sit flat on the stand and it should touch the rollers on the stands. The ideal specimen will sit perpendicular to the bottom plate. Adjust the lower platform so that there is about 19-25.4 mm (0.75-1.0 in) gap between the top of the specimen and LVDT holder (by adjusting the lower stand with the entire setup out of the water).

It is recommended that testing also be performed on a reference material with a known coefficient of thermal expansion. This is necessary if one wants to calibrate the LVDT-data acquisition system and to find out the additional deformation due to the stand. If the measured value for the reference material is very close (5- to 10-percent deviation) to the known value, then the measurement system should induce only minor errors. In this project, a stainless steel bar (CTE = 17.3×10^{-6} / $^{\circ}$C) was used as the reference specimen.

For specimens that do not have thermocouples, the temperature reading is taken from a control specimen. In order to assume that the temperature of the control and the testing specimen are equal, the test specimen and the control specimen must be left in the water bath together until the reading for the control reaches equilibrium of 10 $^{\circ}$C. The control specimen is in equilibrium when the LVDT remains fairly constant [$\pm$0.0038 mm ($\pm$0.00015 in)] for at least 20 minutes. Once the test specimens are fully preconditioned, testing may begin.

Test Execution

Testing is commenced through a controller, and data can be saved in a desired file. Then, set the heater temperature to 50 $^{\circ}$C or 10 $^{\circ}$C, depending on the initial concrete temperature. To ensure good water circulation inside the tank and to accurately control the temperature, use a water circulator. The test usually takes about 15 to 22 hours to conduct.

Data Analysis

Once the temperature of the control specimen reaches 50 $^{\circ}$C, the test is complete and can be stopped. (Shut off the heater and close the inlet and outlet valves.)

If one wants to now run the reverse cycle with the same two specimens, no preconditioning is necessary. As long as the water is still near 50 $^{\circ}$C, the down ramp can be started. Save the data to a different file name and reset the heater to 10 $^{\circ}$C.

Convert the data to a spreadsheet (e.g. Microsoft Excel) file and plot displacement vs. interior temperature of the control specimen. Curve fit the plot linearly and then divide the slope of the graph by the original length of the specimen. This value is the linear coefficient of thermal expansion. Acceptable values for concrete range from 7×10^{-6} to 14×10^{-6} /$^{\circ}$C.

The temperature is controlled from a heating-cooling controller that operates under a constant energy rate. This basically means that the time required to heat or cool specimens in the tank depends on the total volume of water plus specimens. In this project the time required to drop or raise the temperature 40 $^{\circ}$C varies from 14 to 22 hours. This is considered slow enough for producing a uniform temperature profile in the concrete specimen. If the heating or cooling time is too fast, the concrete specimen might not deform evenly due to a nonuniform temperature profile inside, which can lead to inaccurate results. A plot illustrating the time-concrete temperature relationship is given in figure 2.4.5. The temperatures shown were obtained from two thermocouples located in the interior (close to centroid) and the exterior (near surface) of the control specimen. It is very clear that these two temperatures are very close to each other. Therefore, the temperature field in the specimen can be considered uniform.

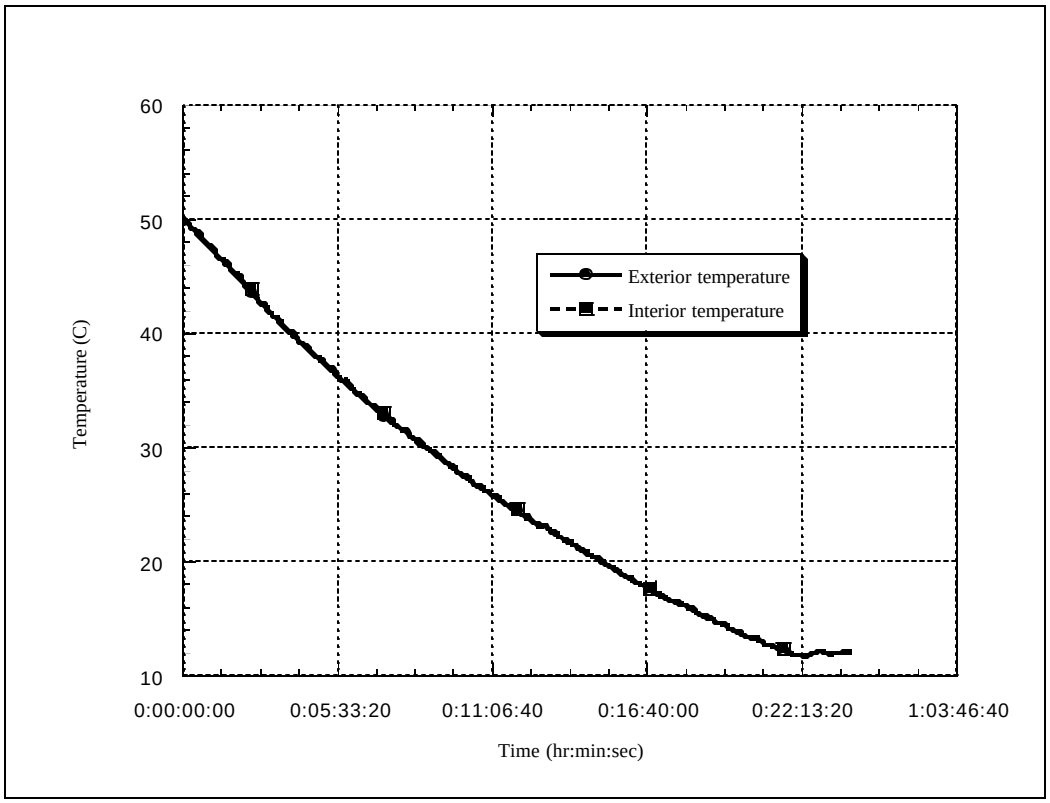

Figure 2.4.5 *Temperature-time relationship of a concrete specimen in the CTE test.*

2.4.5 Petrographic Analysis of Cored Samples

Concrete mix characteristics, which were found to have high influence on concrete distress from the literature review, are determined from the field cores using petrographic analysis. Although the mix design data are contained in the LTPP database, they may not be sufficiently accurate. The literature review indicates that the material characteristics most influential on the concrete pavement distress (spalling, cracking, and faulting) are w/c ratio, coarse aggregate (gradation, content, type) and entrained air. The coarse aggregate characteristics and air void parameters (paste content, total air) are measured on the field cores by the petrographers at the Michigan Department of Transportation according to ASTM C 856. Sample preparation procedures follow the guidelines of ASTM C 457. Petrographic analysis also documents if other internal distresses which have not yet reached the stage of visual detection are present. Such distresses include D-cracking, ASR, plastic shrinkage and drying shrinkage cracking. These distresses are determined using low power stereo microscopy and thin section microscopy.

Estimates of w/c ratio have been made in this study by the Michigan Technological University using the maleic acid technique, as described in appendix C.

CHAPTER 3. RESULTS OF FIELD AND LABORATORY INVESTIGATIONS

This chapter presents the data from laboratory and field investigations on the studied pavements, as collected by the research team. This data will be analyzed and discussed in detail in the following chapters. Section 3.1 gives an overview of each test site, with accompanying site photos. Detailed field evaluations including distress surveys are available in appendix A. Section 3.2 gives a description and petrographic overview of each concrete. Additional microphotographs and petrographic discussions are found in appendix B. Finally, laboratory results for each of the concrete properties measured in this study are presented in section 3.3.

3.1 Field Test Sites

The LTPP database was started in 1987 with the goal of determining ways to increase pavement service life through improvements in design, construction and maintenance practices. By investigating the performance of inservice pavement sections, specific information can be obtained on the various factors and design features that most influence pavement deterioration. In this project the intent was to use the LTPP database on JPCP's (from the GPS-3 database) that are 10 years in age or older, which had exhibited low-distress performance. Major study variables consisted of a range of ages, levels of distress and strength, and climates.

Because a large pool of high strength older pavements was not available, the primary selection criteria were good performing pavements of varying strength levels, with service lives greater than their original design life of 20 to 25 years, located in different climates. A total of 15 pavement sections were selected for study. (Sections 13-GA1-5 and 13-GA1-6 are considered as one section for most discussions. They differ in that 13-GA1-5 rests of a cement treated base while 13-GA1-6 is on an asphalt treated base. Their performance is similar).

Figure 3.1.1 depicts graphically the ages and cumulative traffic volumes in ESAL's for each of the studied test sections. Table 3.1.1 lists key pavement system information for the selected sections. The table includes site information obtained from both the LTPP database and field testing from this study. Ten of the fifteen JPCP's are on CTB's, and that the majority are undoweled. It is noteworthy that the Iowa section 19-3055 and the Wisconsin section 55-3008 have no subbase, and this design feature and the low California Bearing Ratio (CBR) subgrade at those sites have a major effect on faulting.

The PCC slab thicknesses are nearly constant for the tested sites, with average value of 237 mm (9.3 in). The largest slab thickness, 297 mm (11.7 in), was found on the thickened slab section of the experimental test road 06-7456 on I-5 near Tracy,

California. Figure 3.1.2 shows the pavement layer thicknesses of the concrete slab, base and subbase layers for each test section.

The environmental data for the selected sites are shown in table 3.1.2. It is noteworthy that the California pavements are in a mild climate with low freeze index. Consequently, the combined effects from freeze-thaw cycles and deicing salts on PCC durability at joints are not a problem in California.

The investigated test sites are presented in the following sections. First, six test sections from the dry-no-freeze (DNF) region; one test section from the dry-freeze (DF) region; then five test sections from the wet-freeze (WF) region; and finally three test sections from the wet-no-freeze (WNF) region are presented. The general locations of the test sections are shown in figure 3.1.3. Along with the brief site description, a few photographs have been selected to show the overall pavement condition.

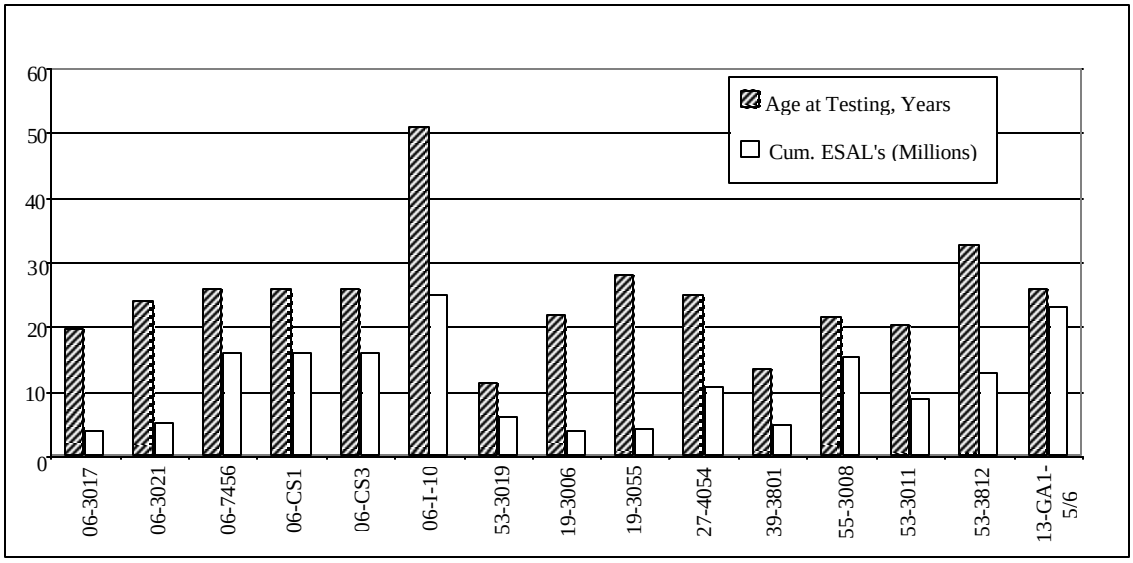

Figure 3.1.1 *Years in service and estimated cumulative ESAL's (millions) for the selected test sections.*

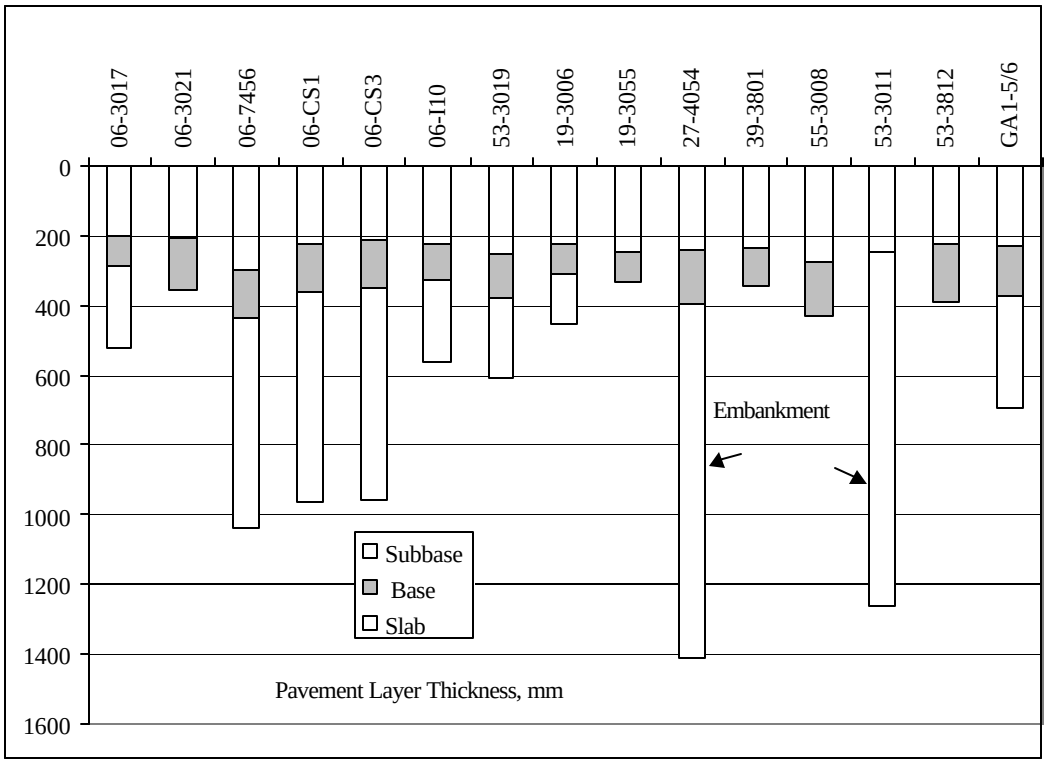

Figure 3.1.2 *Pavement layer thickness for the studied pavements (mm).*

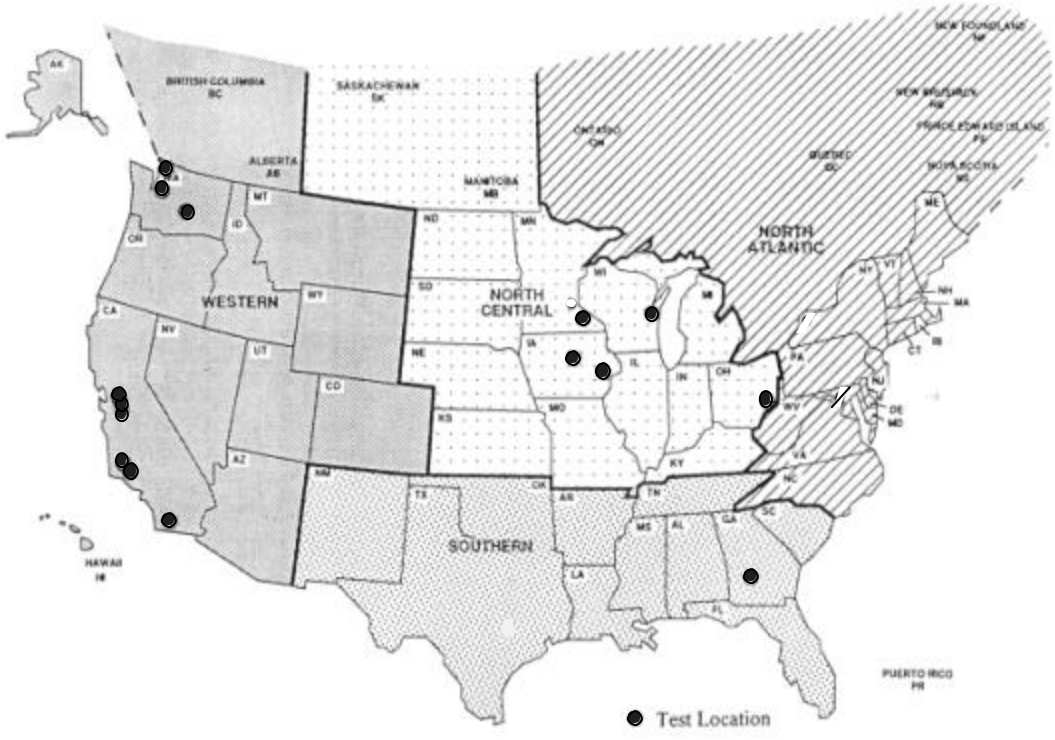

Figure 3.1.3 *General locations of the 15 selected test sections. The shadings indicate the geographical region.*

Table 3.1.1 *Pavement system information for the studied test sections determined from the LTPP database and field investigations.*

Climate	State	Section	Const. Date	Age at Testing (Years)	Estimated Cum. ESAL's (Millions)	Joints			Layer Information				
											Layer Thicknesses		
						Type	Avg. Spacing (m)	Random Spacing (m)	Pavement Type	Base Type	PCC (mm)	Base (mm)	Subbase (mm)
DNF	06	3017	7/1/78	19.50	3.90	Agg	4.7	3.65, 3.96, 5.79, 5.49	JPCP	CTB	202	84	235
	06	3021	4/1/74	24.00	5.25	Agg	4.7	3.65, 5.50, 5.80, 3.95	JPCP	CTB	207	150	No Sub.
	06	7456	12/1/71	26.00	16.00	Agg	4.7	3.65, 5.50, 5.80, 3.95	JPCP	CTB	297	137	608
	06	CS1	12/1/71	26.00	16.00	Agg	4.7	3.65, 5.50, 5.80, 3.95	JPCP	CTB	224	137	608
	06	CS3	12/1/71	26.10	16.00	Agg	4.7	3.65, 5.50, 5.80, 3.95	JPCP	CTB	212	114	608
	06	I-10	1946	51.00	>16.00	Agg	4.7	3.65, 5.50, 5.80, 3.95	JPCP	CTB	224	106	235
DF	53	3019	8/1/86	11.20	6.21	Agg	3.5	2.74, 3.05, 4.27, 3.96	JPCP	CTB	252	127	229
WF	19	3006	11/1/75	21.80	3.97	Dow	6.1	--	JPCP	CTB	225	84	141
	19	3055	8/1/69	28.10	4.27	Agg	6.1	--	JPCP	Gravel-Uncrushed	250	84	No Sub.
	27	4054	10/1/72	24.90	10.70	Dow	8.2	--	JRCP	Crushed Stone	243	151	1016
	39	3801	1/1/84	13.40	4.69	Dow	6.1	--	JPCP	CTB	238	108	No Sub.
	55	3008	12/1/75	21.70	15.20	Agg	4.7	3.96, 5.79, 5.49, 3.65	JPCP	Crushed Gravel	277	152	No Sub.
WNF	53	3011	6/1/77	20.40	8.93	Agg	3.5	4.3, 4.0, 2.7, 3.0	JPCP	-	248	No Base	1016
	53	3812	3/1/65	32.60	12.77	Agg	4.6	--	JPCP	Coarse Soil Agg. Mix	224	165	No Sub.
	13	GA1-5/6	6/1/71	26.10	23.00	Dow	6.1	--	JPCP	CTB (GA1-5) ATB (GA1-6)	232	142	319

27-4054 has 1016 mm (40 in) embankment over loose/soft clayey silt

53-3011 has 1016 mm (40 in) embankment over glacial sandy gravely clay/clayey sand and gravel

* Estimated total traffic

Table 3.1.2 *Environmental data for the studied test sections, primarily from the LTPP database.*

Climate	State	Section	Annual Precipitation (mm)	AVG Days Below 0 °C (32 °F)	AVG Days Above 32 °C (90 °F)	AVG Days Wet per Year	Days with 127 mm (0.5in) Precip. per Year	Yearly Freeze-Thaw Cycles	USCOE Freeze Index
DNF	06	3017	508	1	60	45	12	1	0
	06	3021	447	63	70	53	11	73	2
	06	7456	277	16	70	58	5	22	1
	06	CS1	277	16	70	58	5	22	1
	06	CS3	277	16	70	58	5	22	1
	06	I10	508	1	60	45	12	1	0
DF	53	3019	170	70	35	66	0	64	215
WF	19	3006	848	128	14	135	18	84	1037
	19	3055	828	148	12	117	20	91	1400
	27	4054	846	152	9	134	19	91	1546
	39	3801	1019	110	11	146	25	92	458
	55	3008	861	129	1	165	17	82	891
WNF	53	3011	912	53	0	140	17	54	98
	53	3812	950	19	2	141	21	22	29
	13	GA1-5/6	NA	NA	NA	NA	NA	NA	NA

Of the 15 pavement sections, 11 were chosen from the LTPP database because of the wealth of pavement data available for these sites. The other four pavements were selected outside the LTPP database for various reasons. One of these pavements, the I-10 section by Etiwanda, just east of Los Angeles, was selected based on information by Caltrans that it was constructed in 1946 and had performed well, though it consisted of regular strength concrete. The other three pavements were older JPCP's from experimental test roads in California and in Georgia. The California test road, on I-5 near Tracy, included two sections of interest to this study in addition to section 06-7456 from LTPP database. One was a control section with the same mix design as section 06-7456, but with a decreased slab thickness. The other was a test section of the same thickness as the control section, but with higher strength PCC. For these test sections the same aggregates were used in the mix.

The Georgia section, brought to the attention of the research team by FHWA, was an older JPCP of lower strength concrete. A major design difference was the use of doweled joints on the Georgia test road to control faulting. This pavement turned out to be important for this study as it shared several important characteristics with the control section on I-5 in Tracy, California. Both were without subsurface drainage, JPCP's on CTB's, of the same age (26 years), in mild climates (WNF versus DNF), of the same slab thickness, and subject to high traffic loading (23 million ESAL's versus 16 million for the California test road). The main differences between these two sections are performance related. The Georgia section has virtually no distress. This was even more significant when considering that it consisted of long 6.1-m (20-ft) PCC slabs, which is at the upper recommended limit for design of JPCP to avoid transverse slab cracking. In comparison, the longer of the I-5 JPCP slabs (> 3.96 m (13 ft)) on CTB in California developed low to medium severity transverse cracks over time, except when a much thicker slab design was used as for the 06-7456 section.

Of the studied pavement sections, four were older sections with high distress levels. They were selected in order to better evaluate whether the differences in key PCC properties result in either low or high distress levels in terms of joint/crack faulting, spalling and transverse cracking. Two of these four sections from the WF climate zone were of particular interest. The Wisconsin section 55-3008, was found to have an in-place compressive strength of 62 MPa (9000 lbf/in^2) with the highest level of faulting in the LTPP database. It is undoweled with high cumulative ESAL's. The Iowa section 19-3006, was selected because it had the highest level of spalling according to LTPP. The in-place strength was 56 MPa (8100 lbf/in^2). Both these sections were older pavements of similar age (21.7-21.8 years) at time of testing.

Three high strength concrete pavements with excellent performance were selected from Washington State. These pavements had in-place compressive strengths up to 75 MPa (10,900 lbf/in^2), and contained durable aggregates. At section 53-3812 located near Seattle, WA, on I-5, the pavement was over 30 years old. A previous study had attributed the unusually good performance to combinations of good foundation design, mild environmental conditions, high quality aggregates in the concrete mix, and higher than normal strength. (Mahoney et al., 1991).

3.1.1 Test Sections in the DNF and DF Regions

Test Section 06-3017

Test section 06-3017 is located in California on State Route 2, Glendale. The field investigation was executed on December 10, 1997. The pavement was constructed in 1978 and was about 20 years old at the time of testing. The test section was placed on a tangent/elevated section on a plus grade (uphill) in the direction of traffic, and it is located on a deep fill greater than 12.2 m (40 ft). The pavement section consisted of about 185- to 215-mm (7.25- to 8.5-in) plain concrete on an 85-mm (3.3-in) cement aggregate mixture, and a 150-mm (6-in) coarse soil aggregate mixture subbase. The subgrade consisted of silty sand and gravel. It is possible this was embankment/fill material. Coring showed that there was no bond between the concrete and the base layers. The DCP indicated excellent support conditions. There was no evidence of a subsurface drainage system. The pavement transverse joints were skewed 60 cm (2 ft) per lane, and the load transfer was achieved by aggregate interlock. The joint spacing averaged 4.7 m (16 ft), but varied from 3.65, 5.50, 5.80, and 3.95 m (12, 18, 19, and 13 ft) and repeating. Both the inside and the outside shoulders were constructed with asphalt concrete.

The test section was in excellent condition with only a minor amount of faulting, which was on the order of 0.5 to 2 mm, with two joints having faulting of 5.7 mm. Three longitudinal joints exhibited medium severity of spalling with a total length of 0.8 m (31 in). The concrete surface showed map cracking, but it did not appear to have affected the concrete durability or the concrete surface condition.

Figure 3.1.4 *Overview of test site 06-3017.*

Figure 3.1.5 *Distress free slab and joint in test site 06-3017.*

Test Section 06-3021

Test section 06-3021 was located in California on I-8, Buckman Springs. The field investigation was executed on December 11, 1997. The pavement was constructed in 1974 and was about 24 years old at the time of testing. The test section was placed on a tangent/elevated section on a plus grade (very shallow uphill) in the direction of traffic, and it was located on a cut of about 1.8 to 4.6 m (6 to 15 ft). The pavement section consisted of about 200- to 215-mm (8- to 8.5-in) plain concrete on a 135- to 165-mm (5.25- to 6.5-in) CTB, and coarse grained subgrade of micaceous sand with trace-to-some silt. Coring showed that there was no bond between the concrete and the base layers. The DCP indicated good support conditions. There was no evidence of a subsurface drainage system. The pavement transverse joints were skewed 60 cm (2 ft) per lane, and the load transfer was achieved by aggregate interlock. The joint spacing varied from 3.65, 5.50, 5.80, and 3.95 m (12, 18, 19, and 13 ft) and repeating. Both the inside and the outside shoulders were constructed with asphalt concrete.

The test section was in good condition and had undergone some maintenance work (patching). The test section had only a minor amount of faulting that was on the order of 1 to 3 mm, with the largest faulting of 4.5 mm. About 75 percent of the transverse joints suffered from low severity spalling, and some spalling was observed for longitudinal joints. The concrete surface showed map cracking, but it did not appear to have affected the concrete durability or the concrete surface condition.

Figure 3.1.6 *Overview of test site 06-3021.*

Figure 3.1.7 *Distress free slab at test site 06-3021.*

Tracy Test Road Sections (06-7456, 06-CS1, and 06-CS3)
Three pavement sections were tested from the Tracy Test Road, located in California, near Tracy. These included the SHRP section 06-7456, and two control sections (CS), labeled in this report as sections 06-CS1 and 06-CS3. Sections 06-7456 and 06-CS1 are identical from a concrete materials perspective, though 06-7456 has a thicker concrete section of 30 cm (12 in) compared to 22 cm (8.8 in) for section 06-CS1. Section 06-CS3 has the same pavement cross section design as 06-CS1, but has a mix design with a higher cement content.

Test Section 06-7456 (Tracy Test Road)
Test section 06-7456 is the SHRP LTPP test section from the Tracy Test Road. The pavement was constructed in 1971 and was about 26 years old at the time of testing. The test section was placed on a tangent on a plus grade (very shallow uphill) in the direction of traffic, and it was located in a fill with an estimated thickness of 1.5 m (5 ft). The pavement section consisted of about 300-mm (12-in) plain concrete on a 135- to 140-mm (5.25- to 5.5-in) CTB, and coarse grained subbase of sandy gravel. The natural subgrade was not encountered during sampling. Coring showed that there was no bond between the concrete and the base layers. The DCP indicated very good support conditions. There was no evidence of a subsurface drainage system. The pavement transverse joints were skewed 60 cm (2 ft) per lane, and the load transfer was achieved by aggregate interlock. The joint spacing varied from 3.65, 5.50, 5.80, and 3.95 m (12, 18, 19, and 13 ft) and repeating. Both the inside and the outside shoulders were constructed with asphalt concrete.

The test section was in excellent condition. The test section had only a minor amount of faulting, on the order of 0 to 4 mm.

Figure 3.1.8 *Overview of test site 06-7456, Tracy Test Road.*

Figure 3.1.9 *No slab distress at test site 06-7456, Tracy Test Road.*

Test Section 06-CS1 (Tracy Test Road)

Test section 06-CS1 is the control section of the Tracy Test Road. The field investigation was executed on December 3l, 1997. The pavement was constructed in 1971 and was about 26 years old at the time of testing. The test section was placed on a tangent on a plus grade (very shallow uphill) in the direction of traffic, and it was located in a fill with an estimated thickness of 1.5 m (5 ft). The pavement section consisted of about 225- to 230-mm (8.75- to 9-in) plain concrete on a 135- to 140-mm (5.25- to 5.5-in) CTB, and coarse grained subbase of sandy gravel. The natural subgrade was not encountered during sampling. Coring showed that there was no bond between the concrete and the base layers. The DCP indicated very good support conditions. There was no evidence of a subsurface drainage system. The pavement transverse joints were skewed 60 cm (2 ft) per lane, and the load transfer was achieved by aggregate interlock. The joint spacing varied from 3.65, 5.50, 5.80, and 3.95 m (12, 18, 19, and 13 ft) and repeating. Both the inside and the outside shoulders were constructed with asphalt concrete.

The test section was in fair condition. On the longer slabs, low and medium severity corner breaks and transverse cracks were observed. The shorter slabs were found in very good condition. The test section had only a minor amount of faulting, on the order of 0 to 5 mm. Residue left from pumping of fines at the pavement edge adjacent to many transverse joints was observed. The pumping evidence was also observed at some transverse cracks. The concrete surface showed map cracking, but it did not appear to have affected the concrete durability or the concrete surface condition.

Figure 3.1.10 *Medium severity transverse crack at 06-CS1, Tracy Test Road (control section).*

Figure 3.1.11 *Corner break near approach joint at 06-CS1, Tracy Test Road (control section).*

Test Section 06-CS3 (Tracy Test Road)

Test section 06-CS3 is section 3 of the Tracy Test Road. The field investigation was executed on December 4, 1997. The pavement was constructed in 1971 and was about 26 years old at the time of testing. The test section was placed on a tangent on a plus grade (very shallow uphill) in the direction of traffic, and it was located on a fill with an estimated thickness of 1.1 m (3.5 ft). The pavement section consisted of about 210- to 215-mm (8.25- to 8.5-in) plain concrete on a 75- to 130-mm (3- to 5-in) CTB, and coarse grained subbase of sandy gravel. The natural subgrade was not encountered during sampling. Coring showed that there was no bond between the concrete and the base layers. The DCP indicated very good support conditions. There was no evidence of a subsurface drainage system. The pavement transverse joints were skewed 60 cm (2 ft) per lane, and the load transfer was achieved by aggregate interlock. The joint spacing varied from 3.65, 5.50, 5.80, and 3.95 m (12, 18, 19, and 13 ft) and repeating. Both the inside and the outside shoulders were constructed with asphalt concrete.

The test section was in fair condition. Low to medium severity transverse cracks were observed on 2/3 of the slabs, with only the 3.65-m (12-ft) slabs unaffected. There were two locations with low severity corner breaks. The test section had only a minor amount of faulting, on the order of 0 to 6 mm, with an average of 2 to 3 mm. Residue left from pumping of fines at the pavement edge adjacent to many transverse joints was observed. The concrete surface, the wheel path in particular, showed map cracking, but it did not appear to have affected the concrete durability or the concrete surface condition. This test section, 06-CS3, exhibited twice the number of transverse cracks as compared to the control section, 06-CS1, and also the amount of faulting was higher for this section. However, the spalling of this section was only half of that observed at the control section.

Figure 3.1.12 *Crack only in truck lane at 06-CS3, Tracy Test Road (control section).*

Figure 3.1.13 *Corner break in truck lane at 06-CS3, Tracy Test Road (control section).*

Test Section 06-I-10

Test section 06-I-10 was located in California on I-10, Etiwande, at the Ontario site. The field investigation was executed on December 9, 1997. The pavement was constructed in 1946 and was about 51 years old at the time of testing. The test section was placed on a tangent on a minus grade (very shallow downhill) in the direction of traffic, and it was located in a cut/fill transition. The pavement section consisted of about 215- to 235-mm (8.5- to 9.25-in) plain concrete on a 75- to 120-mm (3- to 4.75-in) CTB, and coarse grained subbase of sandy gravel. The natural subgrade was not encountered during sampling. Coring showed that there was no bond between the concrete and the base layers. The DCP indicated very good support conditions. There was no evidence of a subsurface drainage system. The pavement transverse joints were skewed 60 cm (2 ft) per lane, and the load transfer was achieved by aggregate interlock. The joint spacing varied from 3.65, 5.50, 5.80, and 3.95 m (12, 18, 19, and 13 ft) and repeating. Both the inside and the outside shoulders were constructed with asphalt concrete.

The test section was in good condition. Low to medium severity transverse cracks were observed on 25 percent of the slabs, and tended to occur on the 5.5- and 5.8-m (18- and 19-ft) slabs. About 2/3 of the transverse joints were observed to have low severity of spalling, and most of the joints had minor severity faulting averaging about 2 to 3 mm.

Figure 3.1.14 *Overview of test site 06-I10.*

Figure 3.1.15 *Transverse crack at test site 06-I10 closer to leave joint.*

Test Section 53-3019

Test section 53-3019 was located in Washington on I-82, Benton County. The field investigation was executed on October 6, 1997. The pavement was constructed in 1986 and was about 11 years old at the time of testing. The test section was placed on a tangent section on a plus grade (uphill) in the direction of traffic, and it was located in a fill section with a fill thickness exceeding 12.2 m (40 ft). The pavement section consisted of about 250-mm (9.9-in) plain concrete on a 130-mm (5-in) crushed gravel base, and 90 mm (3.5 in) of silty sand with some gravel subbase. The subgrade consisted of silt with some fine sand. The DCP indicated excellent support conditions. There was no evidence of a subsurface drainage system. The pavement transverse joints were skewed 60 cm (2 ft) per lane, and the load transfer was achieved by aggregate interlock. The joint spacing was 4.3, 4.0, 2.7, and 3.0 m (14, 13, 9, and 10 ft) and repeating. Both the inside and the outside shoulders were constructed with asphalt concrete.

This pavement section was in excellent condition. There was abrasion of the pavement surface in the wheel paths, likely caused by use of tire chains and/or studded tires. The finer aggregate and paste had eroded projecting the coarse aggregate above the surrounding pavement surface. There had been no maintenance activities on the test section. Most transverse joints exhibited low severity spalling, and an isolated longitudinal joint suffered from spalling. Transverse joint faulting ranged from 0 to 1.6 mm.

Figure 3.1.16 *Overview of test site 53-3019.*

Figure 3.1.17 *Typical distress free slab at 53-3019.*

3.1.2 Test Sections in the Wet Freeze Region

Test Section 19-3006

Test section 19-3006 was located in Iowa on US-30, in Clinton County. The field investigation was executed on August 27, 1997. The pavement was constructed in 1975 and was about 22 years old at the time of testing. The test section was placed on a tangent section on a plus grade (uphill) in the direction of traffic, and it was located in a fill section with a fill depth estimated to be between 0.6 to 0.9 m (2 and 3 ft). The pavement section consisted of about 230-mm (9-in) plain concrete on a 115-mm (4.5-in) CTB on about 150 mm (6 in) of silty sand subbase. The subgrade was sandy and silty clays. There was only a slight bonding between the PCC and the base. The DCP indicated poor to marginal support conditions. There was no evidence of a subsurface drainage system. The pavement transverse joints were normal, and the load transfer was achieved through 31.75-mm (1.25-in) dowel bars. The joint spacing was on average 6.1 m (20 ft). Both the inside and the outside shoulders were constructed with a gravel surfacing.

The test section was in very poor condition with all joints exhibiting some degree of spalling. High and low severity spalling with loss of material was noted at 22 of the 26 joints. Transverse joint faulting ranged from about 0.2 to 8.5 mm, with an average of about 3 mm. Previous survey records indicate that this section has been deteriorating rapidly since 1994.

Figure 3.1.18 *Typical transverse joint distress at 19-3006.*

Figure 3.1.19 *Close-up on transverse joint spalling at 19-3006.*

Test Section 19-3055

Test section 19-3055 was located in Iowa on US-20, in Hamilton County. The field investigation was executed on August 28, 1997. The pavement was constructed in 1968 and was about 29 years old at the time of testing. The test section was placed on a tangent section on a minus grade (downhill) in the direction of traffic, and it was located in a fill section with a fill depth estimated to be between 0.6 to 0.9 m (2 to 3 ft). The pavement section consisted of about 250-mm (10-in) plain concrete on a 75-mm (3-in) dense graded aggregate base on sandy clay subgrade. The DCP indicated marginal to poor support conditions. The pavement transverse joints were normal, and the load transfer was achieved by aggregate interlock. The joint spacing was on average 6.1 m (20 ft). Both the inside and the outside shoulders were constructed with an asphalt concrete surface.

The test section was in very good condition with only low severity spalling of the transverse joints and transverse joint faulting ranging from 0 to 6.6 mm with an average of 3 mm. Some of the light spalling may have been due to snow plowing.

Figure 3.1.20 *Typical distress free slab at 19-3055.*

Figure 3.1.21 *Transverse joint in good condition at 19-3055.*

Test Section 27-4054

Test section 27-4054 was located in Minnesota on I-90, Winona County. The field investigation was executed on August 26, 1997. The pavement was constructed in 1972 and was about 25 years old at the time of testing. The test section was placed in a transition between an elevated and a tangent section on a plus grade (uphill) in the direction of traffic, and it was located in a cut section with a cut depth between 1.8 and 4.6 m (6 and 15 ft). The pavement section consisted of about 240-mm (9.5-in) wire mesh reinforced concrete on a 150-mm (6-in) crushed stone base on a sand subbase. This sand was not believed to be the subgrade. The DCP indicated excellent support conditions. There was no evidence of a subsurface drainage system. The pavement transverse joints were skewed 60 cm (2 ft) per lane, and the load transfer was achieved by 25-mm (0.975-in) round dowel bars. The joint spacing averaged 8.2 m (27 ft). Both the inside and the outside shoulders were constructed with asphalt concrete.

The test section was in a relatively good condition except for the faulting, which ranged from 0.8 to 7.5 mm, two small high severity corner breaks, and low severity transverse joint spalling due in part to snow plowing.

Figure 3.1.22 *Overview of test site 27-4054.*

Figure 3.1.23 *Corner break and repair at 27-4054.*

Test Section 39-3801

Test section 39-3801 was located in Ohio on SR-7 in Belmont County. The field investigation was executed on June 5, 1997. The pavement was constructed in 1984 and was about 13 years old at the time of testing. The pavement section consisted of about 210- to 245-mm (8.25- to 9.65-in) plain concrete on a 120-mm (4.65-in) cement-aggregate mixture base, and a subgrade consisting of silty clay with some gravel and trace of sand. The DCP indicated good to excellent support conditions. There was no evidence of a subsurface drainage system. The pavement transverse joints were normal, and the load transfer was achieved by 24.8-mm (0.975-in) round dowel bars. The joint spacing averaged 6.1 m (20 ft). Both the inside and the outside shoulders were constructed with asphalt concrete.

The test section was in good condition. All transverse joints exhibited low severity of spalling, and faulting which ranged from -1.3 to 0.7 mm. Furthermore, a significant amount of low severity longitudinal cracking was observed at dowel bars.

Figure 3.1.24 *Overview of test site 39-3801.*

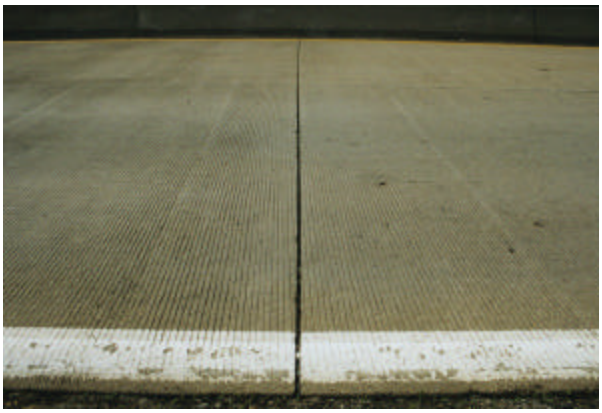

Figure 3.1.25 *Close-up of distress free transverse joint at 39-3801.*

Test Section 55-3008

Test section 55-3008 is located in Wisconsin on I-43, in Ozaukee County. The field investigation was executed on July 29, 1997. The pavement was constructed in 1975 and was about 22 years old at the time of testing. The test section was placed on a tangent section on a plus grade (uphill) in the direction of traffic, and it was located in a cut section with a cut depth estimated to be between 1.8 and 4.5 m (6 and 15 ft). The pavement section consisted of about 265- to 280-mm (10.4- to 11-in) plain concrete. The pavement foundation consisted of a 150-mm (6-in) crushed gravel subbase on a silty clay subgrade. The DCP indicated marginal to good support conditions. There was no evidence of a subsurface drainage system. The pavement transverse joints were skewed 60 cm (2 ft) per lane, and the load transfer was achieved by aggregate interlock. The joint spacing was on average 4.7 m (16 ft) but varied from 3.70 to 5.50 m. Both the inside and the outside shoulders were constructed with asphalt concrete that recently had been surface treated.

The test section was in good condition except for faulting, which ranged from 4.3 to 15.2 mm, and low severity of transverse cracking. In addition the outside lane was faulted 3 to 6 mm relative to the inside lane. One medium severity crack was observed. There was no evidence of pumping of the subgrade, nor had any maintenance been required (except diamond grinding before and after the test section).

Figure 3.1.26 *Overview of test site 55-3008.*

Figure 3.1.27 *Transverse joint at 55-3008 (faulting of shoulder).*

3.1.3 Test Sections in the Wet No Freeze Region

Test Section 53-3011

Test section 53-3011 was located in Washington on I-5, Whatcom County. The field investigation was executed on October 2, 1997. The pavement was constructed in 1977 and was about 20 years old at the time of testing. The test section was placed on a tangent section on a plus grade (uphill) in the direction of traffic, and it was located in a cut section with a cut depth estimated to be between 1.5 and 4.5 m (5 and 15 ft). The pavement section consisted of about 250-mm (9.75-in) plain concrete on a 355- to 380-mm (14- to 15-in) subbase that consisted of coarse-grained soil-aggregate mixture (SAM). The subgrade was silty sand. The DCP indicated excellent support conditions. There was no evidence of a subsurface drainage system. The pavement transverse joints were skewed 60 cm (2 ft) per lane, and the load transfer was achieved by aggregate interlock. The joint spacing was 4.3, 4.0, 2.7, and 3.0 m (14, 13, 9, and 10 ft) and repeating. Both the inside and the outside shoulders were constructed with asphalt concrete.

The test section was in very good condition, and there were no maintenance activities on the test section. Most transverse joints exhibited low severity spalling, and a few isolated longitudinal joints suffered from spalling. The transverse joint faulting ranged from 0 to 5 mm. There was abrasion of the pavement surface in the wheel paths, likely caused by use of tire chains and/or studded tires. The finer aggregate and paste had eroded, projecting the coarse aggregate above the surrounding pavement surface.

Figure 3.1.28 *Overview of test site 53-3011 (above).*

Figure 3.1.29 *Joint core sample in good condition from section 53-3011 (right).*

Test Section 53-3812

Test section 53-3812 was located in Washington on I-5, Snohomish County. The field investigation was executed on September 30 - October 1, 1997. The pavement was constructed in 1964 and was about 33 years old at the time of testing. The test section was placed on an elevated section to the left on a minus grade (downhill) in the direction of traffic, and it was located in a cut section with a cut depth estimated to be between 1.8 and 4.5 m (6 and 15 ft). The pavement section consisted of about 230-mm (9-in) plain concrete on a 150- to 180-mm (6- to 7-in) dense graded aggregate base (DGAB). The subgrade was silty sand with gravel and frequent cobbles. The DCP indicated excellent support conditions. There was no evidence of a subsurface drainage system. The pavement transverse joints were normal, and the load transfer was achieved by aggregate interlock. The joint spacing was 4.6 m (15 ft). Both the inside and the outside shoulders were constructed with asphalt concrete.

This pavement section was in excellent condition. There was abrasion of the pavement surface in the wheel paths, likely caused by use of tire chains and/or studded tires. The finer aggregate and paste had eroded projecting the coarse aggregate (many particles exceeding 25 mm) above the surrounding pavement surface. No maintenance activities had been performed on the test section. Most transverse joints exhibited low severity spalling, and three isolated longitudinal joints suffered from spalling. The transverse joint faulting ranged from -3.0 to 2.5 mm. The faulting appeared to be related to the abrasion of the concrete surface and may not represent true faulting.

Figure 3.1.30 *Overview of test site 53-3812.*

Figure 3.1.31 *Close-up of a distress free transverse joint at 53-3812.*

Test Section 13-GA1-5 and 13-GA1-6

Test sections 13-GA1-5 and 6 were located in Georgia near Newman. The field investigation was executed on July 15, 1997. The pavements were constructed in 1971 and were about 28 years old at the time of testing. The test sections were placed on a tangent section on a minus grade (downhill) in the direction of traffic, and were located in a cut section with a cut depth between 1.8 and 4.5 m (6 and 15 ft). Section 13-GA1-5 consisted of about 230-mm (9-in) jointed plain concrete on a 150-mm (6-in) CTB on about 300 mm (12 in) of sandy gravel subbase. Section 13-GA1-6 consisted of about 230-mm (9-in) jointed plain concrete on a 125-mm (5-in) asphalt treated base on about 350 mm (14 in) of sand subbase. The subgrade for both sections consisted of layered sandy clays and silty sands. The DCP indicated poor to very poor support conditions. There was no evidence of a subsurface drainage system.

The pavement transverse joints were skewed 60 cm (2 ft) per lane, and the load transfer was achieved by 30-mm (1.25-in) round dowel bars. The joint spacing was 6.1 m (20 ft). Both the inside and the outside shoulders were constructed with asphalt concrete.

These pavements were in excellent condition, with negligible faulting which was typically less than 1 mm. Section 13-GA1-6 exhibited very minor transverse joint spalling.

Figure 3.1.32 *Overview of test site 13-GA1-5.*

Figure 3.1.33 *Distress free transverse joint at 13-GA1-5.*

3.2 PCC Sample Description and Petrographic Analysis

Petrographic analysis was performed at the University of Michigan, Michigan Department of Transportation, and Michigan Technological University. The overall petrographic analysis was obtained by characterization of lapped core specimens with the unaided eye and by using a low-power stereo microscope with 80X maximum magnification. The primary aim was to characterize the texture (homogeneity) of the concrete and to determine the aggregate types present in both the coarse (≥ 4 mm) and fine fraction (< 4 mm). The lapped core sections were also analyzed for physicochemical deterioration, such as carbonation depth, dissolution, alkali-silica reactions and cracks. Finally, the volume fraction of coarse and fine aggregates, the cement paste, and the hardened air-void content was determined by the linear traverse method (ASTM C-457) at MDOT.

Selected samples were characterized through microscopic analysis of petrographic thin-sections to evaluate the homogeneity of the cement paste and the extent to which microcracking and formation of secondary phases has occurred in the concrete. These results are explained in detail in appendix B. Figure 3.2.1 shows the typical procedure for cutting the concrete core into a) the lapped section; which is used for overall petrographic analysis and composition by the linear traverse analysis; and b) thin-sections from top, middle and bottom.

The petrographic analysis of each sample is summarized by climatic region in sections 3.2.1 to 3.2.3 hereafter.

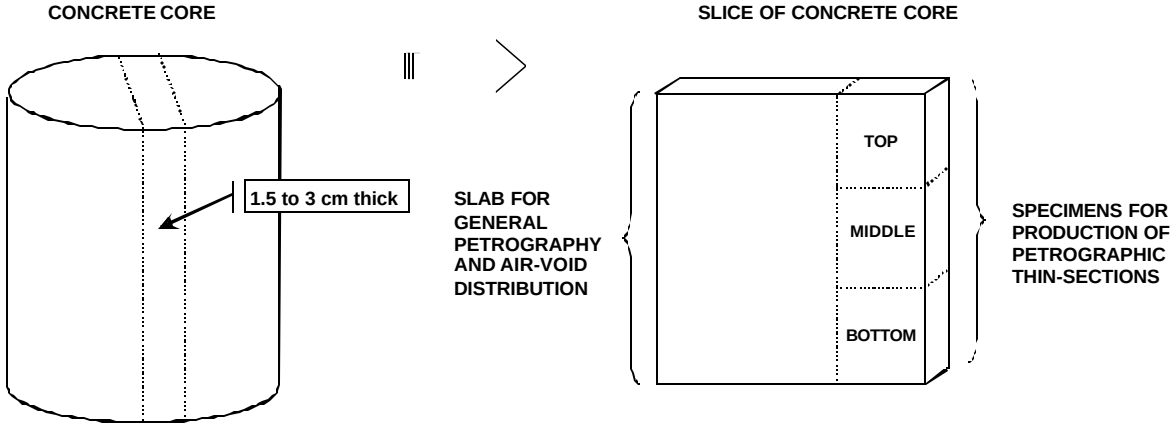

Figure 3.2.1 *Method for cutting the PCC drill-core into the lapped section and three thin-sections used for petrographic analysis.*

3.2.1 Petrographic Characterization of PCC Specimens from the Dry-No-Freeze and Dry-Freeze Regions

The specimens from the DNF region include the sections 06-3017, 06-3021,06-7456, 06-CS1, 06-CS3, and 06-I-10 from California. Section 53-3019, from Washington, is in the DF region. All samples from the dry regions generally appear very well preserved. In two samples (06-3017 and 53-3019), the cement paste had been subjected to partial dissolution at the base of the pavement cores. Two samples (06-CS1 and 06-I-10) had been saw-cut and deterioration analysis at the top and base was not possible.

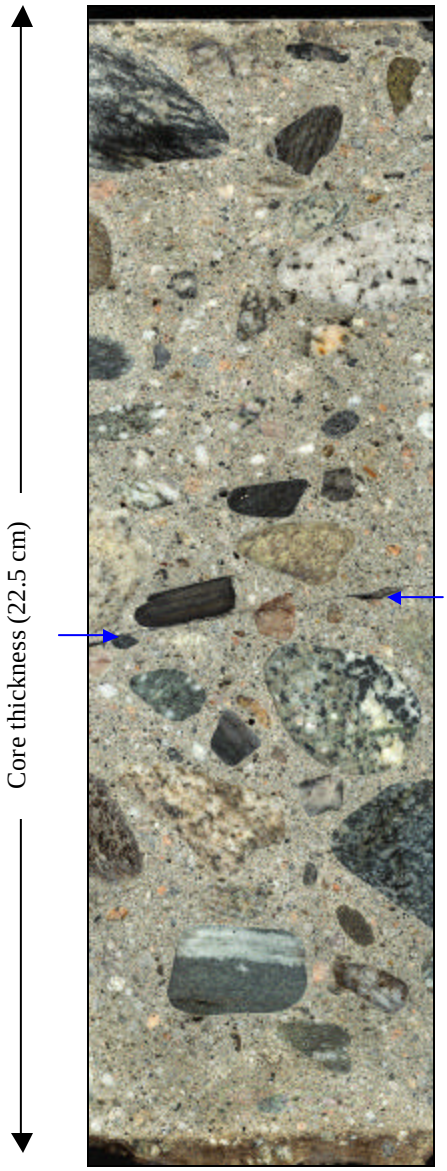

Figure 3.2.2 *Polished cross-section of pavement section 06-3017.*

Section ID: 06-3017
State: California
Climate: DNF

Table 3.2.1 *Mix composition of 06-3017 by linear traverse (ASTM C457).*

Coarse Aggregate	Fine Aggregate	Paste Content	Air Content
49.3 vol.%	29.3 vol.%	14.0 vol.%	7.4 vol.%

The core-sample is 22.5 cm long and consists of rounded gravel in a medium gray cement paste (figure 3.2.2). The gravel consists of various silicate rocks (gabbro, quartz-rich rock fragments, biotite-rich gneiss and other metamorphic rocks). The largest aggregates are 46 mm (1.8 in). The packing of the coarse aggregate appears relatively open.

The fine aggregates mainly consist of angular to rounded quartz and quartz-rich rock-fragments, as well as biotite flakes. The carbonation depth was not determined.

The air voids are well-distributed in the concrete paste. A few large voids (≤17 mm) of trapped air were also observed and typically occurred in connection with the larger aggregates. Locally, a red phase also occurred in these aggregates. Several air voids contain minor amounts of white crystallite precipitates.

The lower 1 to 2 cm of the concrete core is partially dissolved and impregnated with Fe-oxyhydrates. The alteration has left the base fragile and with coarse aggregates partially detached from the concrete paste.

Macro-cracks were not observed in the specimen. The crack observed in the image occurred during shipping of the sample (arrows).

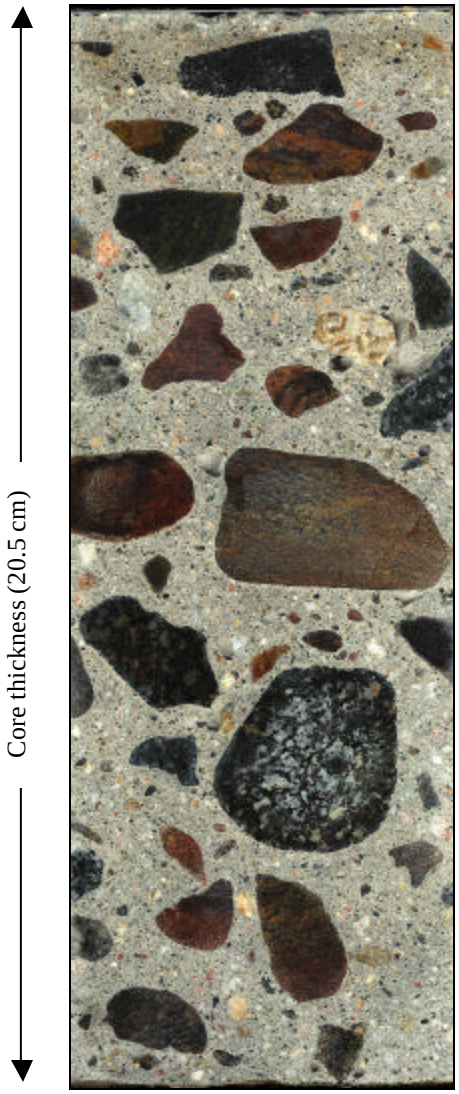

Figure 3.2.3 *Polished cross-section of pavement section 06-3021.*

Section ID: 06-3021
State: California
Climate: DNF

Table 3.2.2 *Mix composition of 06-3021 by linear traverse (ASTM C457).*

Coarse Aggregate	Fine Aggregate	Paste Content	Air Content
28.4 vol.%	43.4 vol.%	25.1 vol.%	3.1 vol.%

The core sample of 06-3021 is 20.5 cm long and consists of angular to rounded gravel in a medium gray cement paste (figure 3.2.3). The packing of the coarse aggregates appears relatively open. The cement paste in the top 15 mm is tanned and did not react with phenolphtalein indicating a deep carbonation depth.

The coarse aggregates (≤ 46 mm) mainly consist of mafic to ultramafic igneous rocks. Minor amounts of coarse quartz and sandstone aggregates were also observed. The mafic aggregates readily rust after lapping indicating a high content of Fe- and/or Fe-Ti-oxides. The coarse aggregates are sometimes partially detached from the paste.

The fine aggregates mainly consist of angular to rounded quartz sand (≤ 2 mm), as well as platy and fibrous aggregates of the mafic and ultramafic rocks observed in the coarse fraction. The fine aggregates are well-distributed in the paste.

The air voids are homogeneously distributed. However, large trapped air voids (≤ 17 mm size) were abundant between 5.8 and 8.7 cm into the core. Several of the air voids contained white precipitates, but the specimen did not show indication of chemical alteration.

A few vertical cracks (≤ 11 mm long) were observed close to the surface. A very fine (<< 1 mm) horizontal crack was observed at 7.5 cm below the surface. This crack is more than 2.5 cm long and runs from a 6-mm wide air void and propagates into the paste, deflecting around a coarse mafic aggregate and disappearing out of the specimen.

Section ID: 06-7456
State: California
Climate: DNF

Table 3.2.3 *Mix composition of 06-7456 by linear traverse (ASTM C457).*

Coarse Aggregate	Fine Aggregate	Paste Content	Air Content
39.1 vol.%	31.1 vol.%	24.7 vol.%	5.1 vol.%

The core sample from section 06-7456 was 29.5 cm long and cut at the base. The concrete is composed of densely packed rounded to well-rounded gravel that is homogeneously distributed in a dark to medium gray cement paste. The carbonation depth was not determined.

The gravel consists of various rock types (gneiss, phyllosilicate-rich metasandstone, other metamorphic rock-types, and quartz-rich rock-fragments. A very thin reaction rim (< 0.5 mm) could be observed around some of the particles containing phyllosilicates as one of the constituent phases. The largest aggregate dimension observed was 7.5 mm, whereas the typical size of the largest aggregates was approximately 30 mm.

The fine aggregates mainly consist of rounded to sub-rounded sand with approximately equal amounts of quartz and rock fragments. The fine aggregates appear well distributed in the cement matrix.

The air voids are generally well distributed, but the total air-void content appears low. Larger air voids are present particularly in the upper 8 cm of the cores. The largest air void was 16 mm long and found in the middle of the section.

Fractures were observed in the upper half of the slab. The largest crack occurs at the very top of the slab and forms a closed loop deflecting at the surface at two larger aggregates at ~ 3.5 cm depth. The fracture may have formed due to cracking of finely layered dark-red siltstone and at detachment of a phyllosilicate-rich metasandstone particle at the very top of the slab. One aggregate of dark-brown shale, however, shows evidence of deleterious reaction with the paste that has resulted in concentric cracks within the aggregate and detachments at its surface. This particle was the only aggregate of this type observed in the slab.

Figure 3.2.4 *Polished cross-section of pavement section 06-CS1.*

Section ID: 06-CS1
State: California
Climate: DNF

Table 3.2.4 *Mix composition of 06-CS1 by linear traverse (ASTM C457).*

Coarse Aggregate	Fine Aggregate	Paste Content	Air Content
40.5 vol.%	24.6 vol.%	30.9 vol.%	4.0 vol.%

The core specimen was 20.1 cm long and cut at top and base. The concrete is composed by close-packed sub-rounded to well-rounded gravel in a dark to medium gray cement paste (figure 3.2.4).

The coarse aggregate mainly consists of fine to medium-grained metapelite, fine-grained gabbro, as well as green and red aggregates, likely to be siltstone. Some of the aggregates contain 1- to 2-mm size voids after dissolved sulfides. Single aggregates also contain up to 1-mm-wide internal cracks. The largest aggregates are more than 76 mm long and have an oblate shape (figure 3.2.4).

The fine aggregates consist of approximately 30 volume percent, quartz sand and 70 volume percent lithic fragments. Most of the fine aggregates appear rounded to sub-rounded and are well distributed in the paste.

The air voids are generally well dispersed. Several large air voids were, however, observed at the assumed base of the drill-core where a more than 15-mm sized air void was observed at the edge of the polished slab. The air voids occasionally contain white precipitates and botryoidal red aggregates.

A sub-horizontal fracture was observed between 7.5 and 9.5 cm into the sample. The crack had one end-point in a cracked aggregate but otherwise runs through the paste where it cuts some of the fine aggregates and deflects around the large aggregates. A small fracture was also observed at the top of the concrete in a sample analyzed at MDOT.

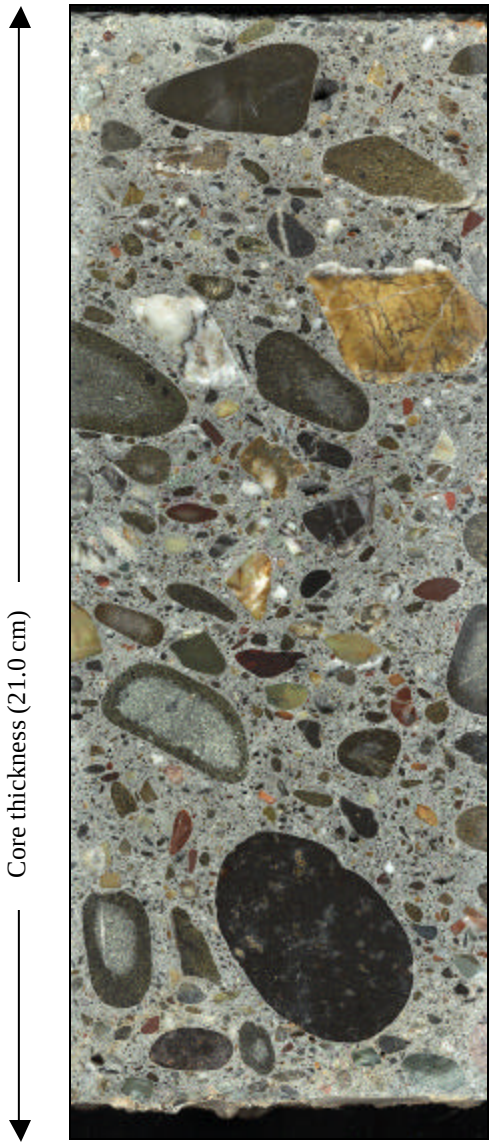

Figure 3.2.5 *Polished cross-section of pavement section 06-CS3.*

Section ID: 06-CS3
State: California
Climate: DNF

Table 3.2.5 *Mix composition of 06-CS3 by linear traverse (ASTM C457).*

Coarse Aggregate	Fine Aggregate	Paste Content	Air Content
30.7 vol.%	39.5 vol.%	25.5 vol.%	4.5 vol.%

This concrete sample is 21 cm long and consists of rounded to well-rounded gravel dispersed in a dark, medium-gray cement paste (figure 3.2.5). Visually, there is tendency to an inhomogeneous distribution of the coarse aggregates (≤ 45 mm). However, this may be caused by the relatively high abundance of larger aggregates. The coarse aggregates appear with a medium degree of packing. The carbonation depth was determined to be 1 to 2 mm.

The gravel consists of dolomitic limestone, sandstone, and siltstone, quartz, basalt, gabbro and metamorphic rocks. The dolomite aggregates contained 2- to 3-mm wide dark rims, probably related to weathering.

The fine aggregates mainly consist of angular to well-rounded quartz and lithic fragments of the same material as the coarse aggregates. Quartz is by far the most abundant aggregate type in the fraction below 1-mm size.

The air voids are well distributed and several air voids contain white precipitates which are inert in 0.1M HCl. Analysis of thin-sections has revealed that the precipitates mainly consist of ettringite. The white precipitates frequently fill the air voids below 9.5-cm depth in the core. Trapped air voids (≤ 14 mm) are observed at all depths in the core.

A 2.1-cm long crack was observed on the surface of the drill-core but could not be traced in depth. At the base of the concrete core, drop-like precipitates had formed suggesting leaching and/or precipitation from trapped water in intergranular cavities below the concrete slab. Minor dissolution has occurred but is negligible.

Figure 3.2.6 *Polished cross-section of pavement section 06 I-10.*

Section ID: 06-I-10
State: California
Climate: DNF

Table 3.2.6 *Mix composition of 06-I-10 by linear traverse (ASTM C457).*

Coarse Aggregate	Fine Aggregate	Paste Content	Air Content
46.5 vol.%	25.7 vol.%	23.9 vol.%	3.9 vol.%

The polished slab from 06-I-10 was 20.7 cm long. The slab did not show the top and base of the drill-core and was not oriented. The concrete is composed by well-rounded gravel and a few angular rock fragments homogeneously dispersed with a relatively open packing in a medium gray concrete paste (figure 3.2.6).

The coarse aggregates consist of various gneiss-types, quartz, and minor amounts of porphyric basalt. The maximum size of the coarse aggregates was 44 mm in diameter. A few of the gneiss aggregates were partially altered.

The fine aggregates consist of angular to sub-rounded quartz sand with approximately 30 volume percent lithic fragments.

The number of air voids appears to be low. The largest air voids are 7 to 10 mm in diameter and mainly occur below 7 cm from the assumed top of the drill-core. Some of the air voids contain precipitates of a white phase.

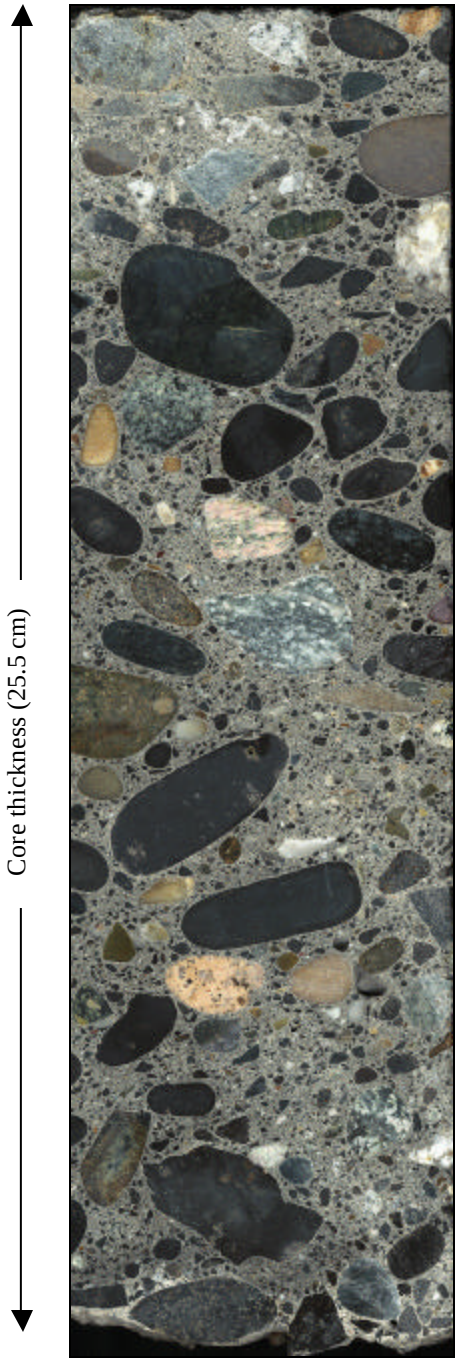

Figure 3.2.7 *Polished cross-section of pavement section 53-3019.*

Section ID: 53-3019
State: Washington
Climate: DF

Table 3.2.7 *Mix composition of 53-3019 by linear traverse (ASTM C457).*

Coarse Aggregate	Fine Aggregate	Paste Content	Air Content
45.9 vol.%	29.5 vol.%	15.5 vol.%	9.4 vol.%

Sample 53-3019 is 25.5 cm long and mainly consists of up to 47-mm sized rounded to well-rounded aggregates of spherical to oblate shape dispersed in a dark gray cement paste (figure 3.2.7). The coarse aggregates show a medium degree of packing with slightly closer packing at the top 13.5 cm of the drill-core. The cement paste has a white coloration at the base of the concrete core and suggests that the paste has been subjected to minor dissolution (figure 3.2.7). The carbonation depth was not determined.

The coarse aggregates mainly consists of porphyric basalt (~ 75 volume percent) and minor amounts (~ 25 volume percent) of coarse-grained gabbro, granite, gneiss, and quartz (figure 3.2.7). A single angular aggregate of "recycled" concrete was also observed. Sometimes, the gneissic and granitic aggregates contained some porosity due to sulfide oxidation and secondary formation of Fe-oxyhydrates. Most of the aggregates were surrounded by fine (<<1-mm-wide) white rims due to increased contents of fine air voids in at their interface. A few aggregates contained microcracks at their rims which resulted in the formation of local air-clusters and detachment of the aggregate from the cement paste.

The fine aggregates consist of angular to rounded quartz sand, as well as angular basalt and minor amounts of other lithic fragments that dominate in the 2- to 4-mm size fractions. The quartz sand strongly dominates in the fraction below 2-mm grain size.

The number of air voids appears to be high and they appear well-distributed in the paste. The largest air voids were 8.5 mm in diameter and located 9 cm below the surface. Most air voids were spherical but large angular pores of trapped air were also observed below 13.5-cm depth in the core.

3.2.2 Petrographic Characterization of PCC Sections from the Wet-Freeze Region

The wet-freeze group consists of two samples from Iowa (19-3006 and 19-3055) and one sample from Minnesota (27-4054), one from Ohio (39-3801), and one from Wisconsin (55-3008). All concretes mainly contain coarse aggregates of carbonate-rocks. However, sample 39-3801 also contains important quantities of silicate rock aggregates. All the sections show dissolution of the paste and/or impregnation with secondary phases at their base. Moreover, paste alteration was prominent in 39-3801.

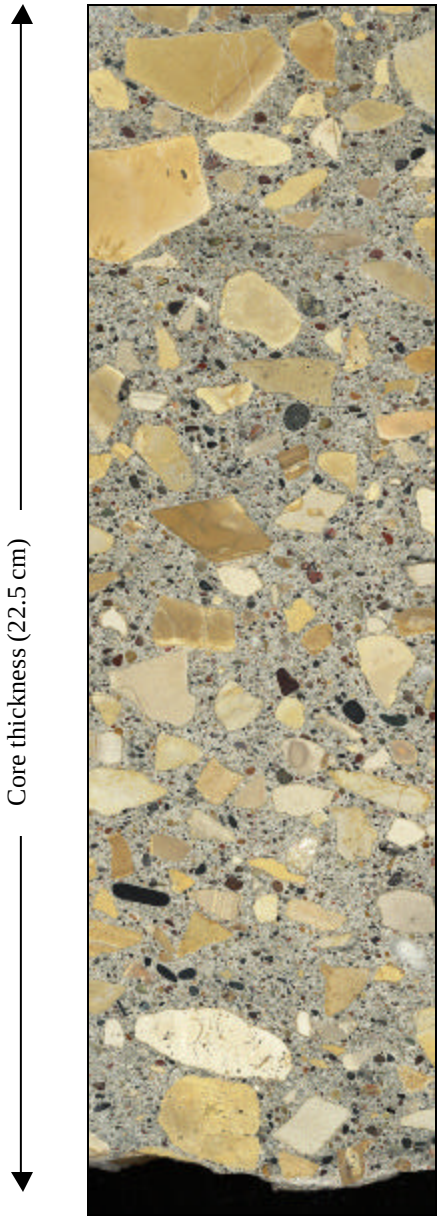

Figure 3.2.8 *Polished cross-section of pavement section 19-3006.*

Section ID: 19-3006
State: Iowa
Climate: WF

Table 3.2.8 *Mix composition of 19-3006 by linear traverse (ASTM C457).*

Coarse Aggregate	Fine Aggregate	Paste Content	Air Content
43.1 vol.%	29.2 vol.%	19.4 vol.%	8.3 vol.%

The drill-core of 19-3006 is 22.5 cm long. The concrete consists of angular and cream-white to beige-colored dolomite and a few fine-grained gabbroic rock-fragments dispersed in a medium gray cement paste (figure 3.2.8). The carbonation depth was 2 to 4 mm. The packing of the coarse aggregates was relatively open with a tendency to a closer packing in the upper 6 cm of the core.

The largest aggregate was 31 mm in diameter. The typical aggregate size was significantly smaller (≤ 15 mm). Some dolomite aggregates have relatively large grain-sizes (≤ 0.25 mm) and are often porous. Several of the beige-colored dolomite aggregates showed a white or weak reddish brown color zoning at the border to the paste. At these aggregates, the paste is typically white and shows increased porosity. The color change may be due to either de-dolomitization of the dolomite aggregate and/or oxidation of microscopical Fe-oxides in the dolomite. Similar observations were made by MTU.

The fine aggregates mainly consist of rounded to well-rounded sand with a typical grain-size below 2 mm. More than 60 volume percent of the sand consists of quartz. The rest of the sand-fraction consists of a wide variety of igneous and sedimentary rocks dominated by fine-grained mafic rocks.

The air voids are relatively small with a maximum size of 6 mm. The largest air voids are most abundant towards the base of the concrete core and typically occur in connection with the coarse aggregates.

A fine horizontal crack was observed at the base of the drill-core. The crack cuts both the paste and embedded aggregates in the concrete.

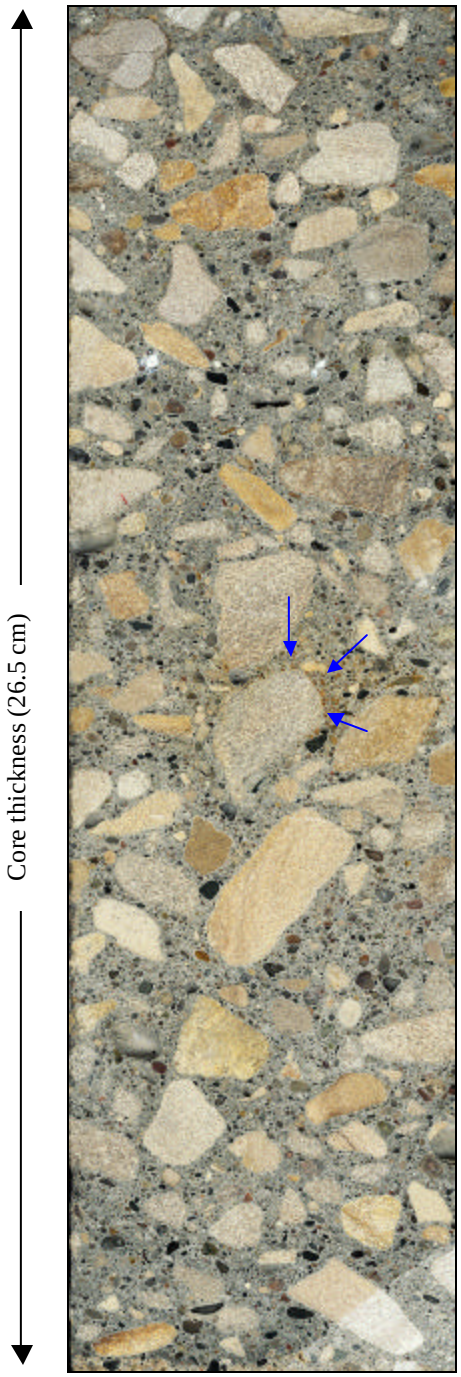

Figure 3.2.9 *Polished cross-section of pavement section 19-3055.*

Section ID: 19-3055
State: Iowa
Climate: WF

Table 3.2.9 *Mix composition of 19-3055 by linear traverse (ASTM C457).*

Coarse Aggregate	Fine Aggregate	Paste Content	Air Content
33.7 vol.%	28.0 vol.%	30.8 vol.%	7.5 vol.%

The drill-core of concrete 19-3055 is 26.5 cm long. The concrete is mainly composed by angular and sub-rounded gray and beige-colored dolomitic limestone embedded in a medium gray cement paste (figure 3.2.9). The coarse aggregates are evenly distributed and close packed. The carbonation depth is 2 to 3 mm.

The coarse aggregates consist of very fine-grained dolomite and more coarse-grained (≤ 1 mm) oomicrite and/or pelmicrite. Minor gabbro aggregates are also present. Some of the coarse-grained dolomitic aggregates are porous and may show minor reaction with diluted HCl. The largest aggregates are up to 42-mm size in diameter. The typical aggregate size appears to be in the region of 15 to 20 mm. A rust-red coloration is locally observed in the paste around the some of the coarse aggregates (example shown at arrow in figure 3.2.9).

The fine aggregates consist of rounded to well-rounded quartz-rich sand and angular grains of dolomite, igneous, and metamorphic rocks. The grain size of the fine aggregates is typically below 2 mm. A few aggregates of dehydrated swelling clays were also observed. MTU identified some of the fine aggregates as the fragments of the "Pierre shale" which they claim is very reactive. MTU also observed minor but insignificant alkali-silica reactions at some of the fine aggregates.

The air voids are up to 11-mm size and generally homogeneously distributed in the paste. A few air voids contain white precipitates. Some of the precipitates were calcite. MTU reported that ettringite was abundant among the precipitates.

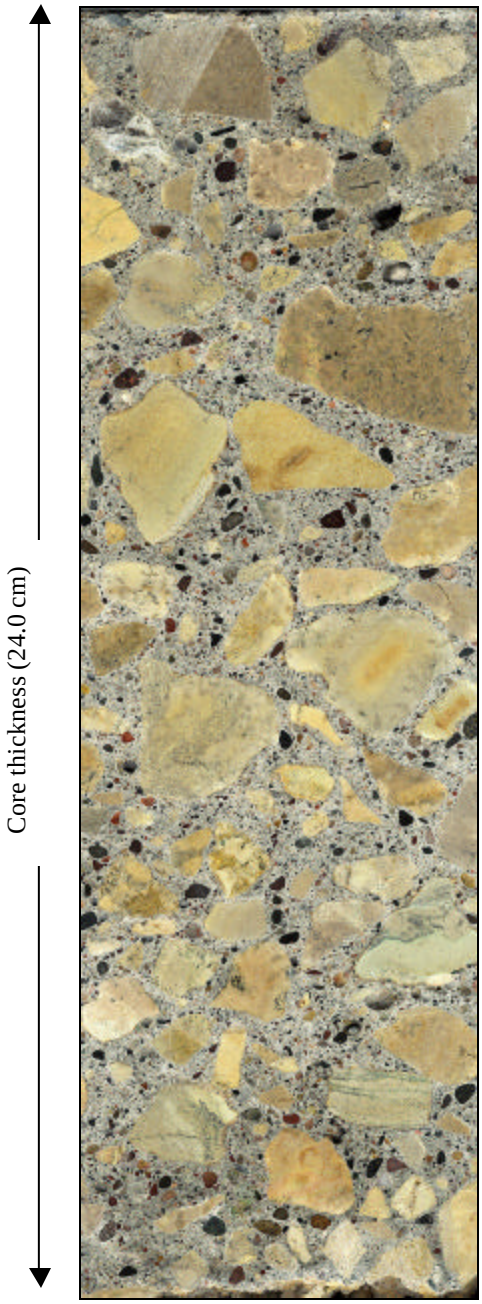

Figure 3.2.10 *Polished cross-section of pavement section 27-4054.*

Section ID: 27-4054
State: Minnesota
Climate: WF

Table 3.2.10 *Mix composition of 27-4054 by linear traverse (ASTM C457).*

Coarse Aggregate	Fine Aggregate	Paste Content	Air Content
55.4 vol.%	17.9 vol.%	20.5 vol.%	6.2 vol.%

The drill-core of pavement 27-4054 is 24.0 cm long and mainly consists of angular to sub-rounded dolomitic limestone in a light medium-gray cement paste (figure 3.2.10). Minor amounts of gabbro and other aggregate types are also present. The carbonation depth is 2 to 4 mm. The base of the concrete shows some sign of deterioration by partial dissolution of the cement paste and replacement with a yellow to red-brown brown phase(s).

The coarse aggregates are homogeneously distributed and appear to be relatively closely packed. The slab specimen showed the presence of more coarse aggregates at the top of the pavement section. This was, however, not confirmed by analysis of other sections from this site. The largest aggregate was more than 40 mm in diameter while the typical aggregate size appears to be 20 to 30 mm. Most of the coarse aggregates are porous, probably due to the volume reduction which occurs during dolomitization of calcite. Some of the coarse aggregates are rimmed by a 1- to 2-mm-wide reddish or white reaction rim.

The fine aggregates consist of sub-rounded to well-rounded quartz-rich sand with approximately 20 volume percent lithic fragments dominated by mafic rocks. Single nodules of swelling clays, up to 1 mm in size, were also observed in the paste. MTU observed reactive chert with idiomorphic carbonate inclusions in the sand fraction.

The air voids are usually small reaching a maximum size of approximately 7 mm. A few of these larger air voids were observed at 1.8 to 5.2 cm and 18.8 and 20.5 cm into the drill-core. The air voids contain minor amounts of colorless and white precipitates. The white precipitates are most abundant in the lower half of the pavement section.

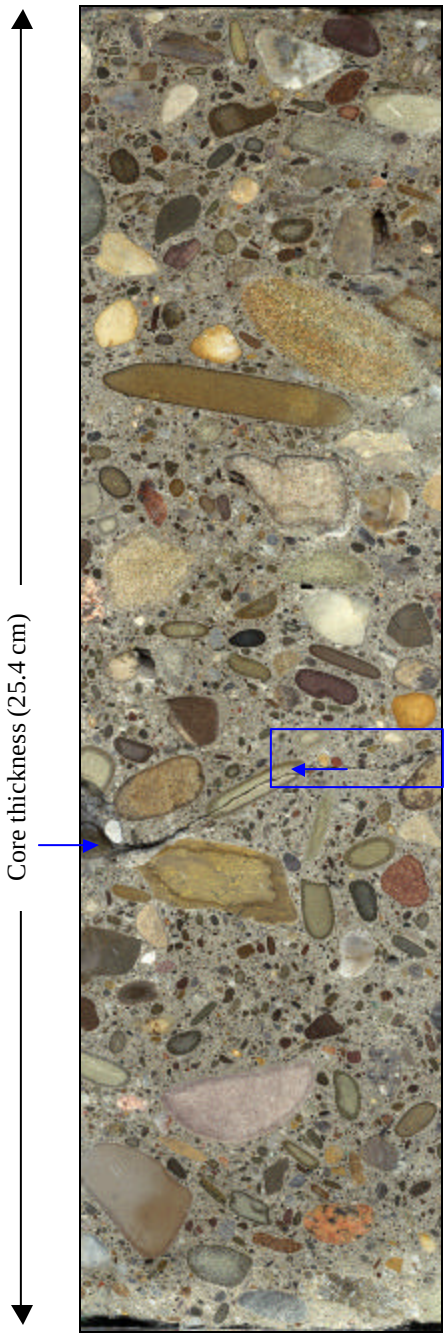

Figure 3.2.11 *Polished cross-section of pavement section 39-3801.*

Section ID: 39-3801
State: Ohio
Climate: WF

Table 3.2.11 *Mix composition of 39-3801 by linear traverse (ASTM C457).*

Coarse Aggregate	Fine Aggregate	Paste Content	Air Content
41.9 vol.%	24.9 vol.%	26.8 vol.%	6.4 vol.%

Pavement section 39-3801 is 25.4 cm thick and consists of rounded to well-rounded gravel embedded in a dark medium gray cement paste (figure 3.2.11). The coarse aggregates display a relatively close packing. The carbonation depth was up to 1 mm deep.

Approximately 50 volume percent of the gravel aggregates consist of dolomitic limestone and tan siltstone. The limestone may show weak reaction with 0.1M HCl. The limestone aggregates contained a dark reaction rim, up to 5 mm wide, which is related to natural weathering. The remaining 50 volume percent of the coarse aggregates consist of a mixture of igneous rocks, quartz-grains and sandstone. A few flint-like aggregates were also observed but appeared to have remained inert. The maximum recorded size of the coarse aggregates was 27 mm.

The fine aggregates consist of equal amounts of sub-rounded to well-rounded quartz-sand and dolomitic limestone. The fine limestone aggregate dominates in the fraction between 2 and 4 mm while the quartz-rich sand dominates in the size fraction below 2 mm.

Large air voids (≤ 11 mm) were present below 3-cm depth in the sample where a cluster of trapped air was observed at the edge of the polished slab. Below 6-cm depth, the air voids normally contained white precipitates and most air voids were filled with these precipitates below 11-cm depth into the sample.

One of the slabs studied contained a horizontal open crack between 14.2- and 14.5-cm depth into the core (see arrows in figure 3.2.11). Note the wide crack in the boxed region formed after cutting and characterization of the slab. The maximum crack width (<< 1 mm) was observed around a larger air void in the sample. The crack cuts both paste and aggregates.

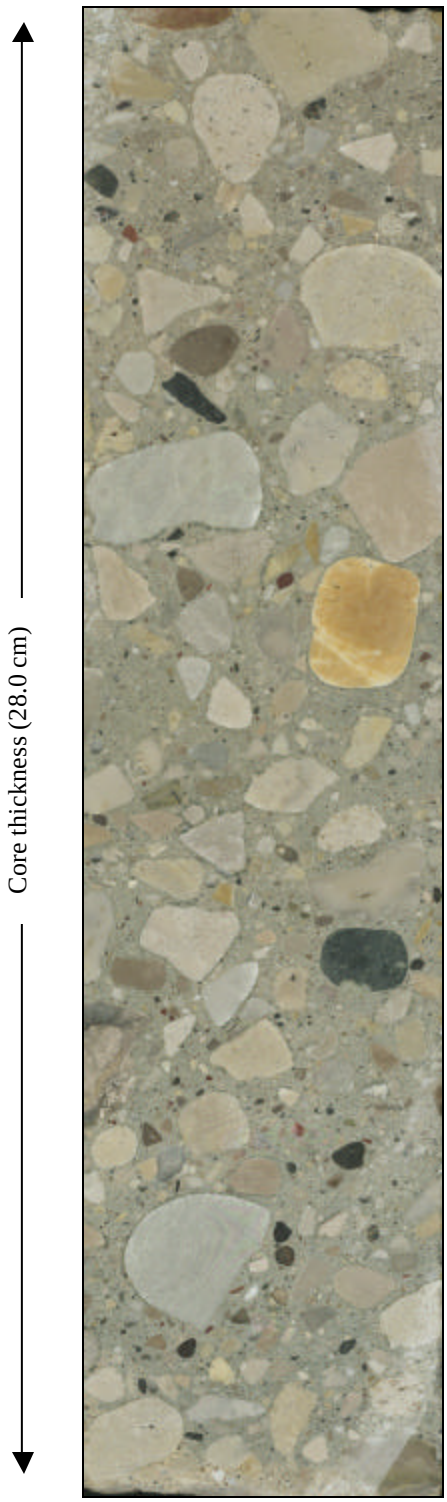

Figure 3.2.12 *Polished cross-section of pavement section 55-3008.*

Section ID: 55-3008
State: Wisconsin
Climate: WF

Table 3.2.12 *Mix composition of 55-3008 by linear traverse (ASTM C457).*

Coarse Aggregate	Fine Aggregate	Paste Content	Air Content
51.9 vol.%	29.7 vol.%	12.2 vol.%	6.2 vol.%

Pavement section 55-3008 is 28 cm thick, the thickest section studied. The concrete is made up of angular and rounded coarse dolomite and minor gabbro aggregates in a medium gray cement paste (figure 3.2.12). The coarse aggregates display a medium to open packing with denser packing in the central part of the pavement section. Carbonation was not observed.

Some of the dolomite aggregates are relatively coarse-grained (up to ~1 mm) and are sometimes porous. A white and very porous paste often surrounds the porous aggregates. The maximum aggregate size is 43 mm while the normal coarse aggregate size appears to be around 15 mm.

The fine aggregates mainly consist of sub-rounded to well-round quartz-sand with a typical grain size of approximately 1 mm. Minor amounts of dolomite, fine-grained gabbro, and other silicate rocks are also present.

The air voids generally become larger and more abundant towards the base of the pavement section. In the polished slab, a large (~ 40-mm) and more or less horizontally oriented air void was located at intermediate depth on the backside of the slab and indicates problems with compaction.

3.2.3 Petrographic Characterization of PCC Sections from the Wet-No-Freeze Region

Three samples from the WNF region were analyzed in this study. Two samples (53-3011 and 53-3812) were collected from Washington and the third sample (13-GA 1-5) was collected from Georgia. Similar to the previous samples, the concretes from the WNF region are well preserved. However, both the samples from Washington show evidence of a relatively advanced dissolution at their base.

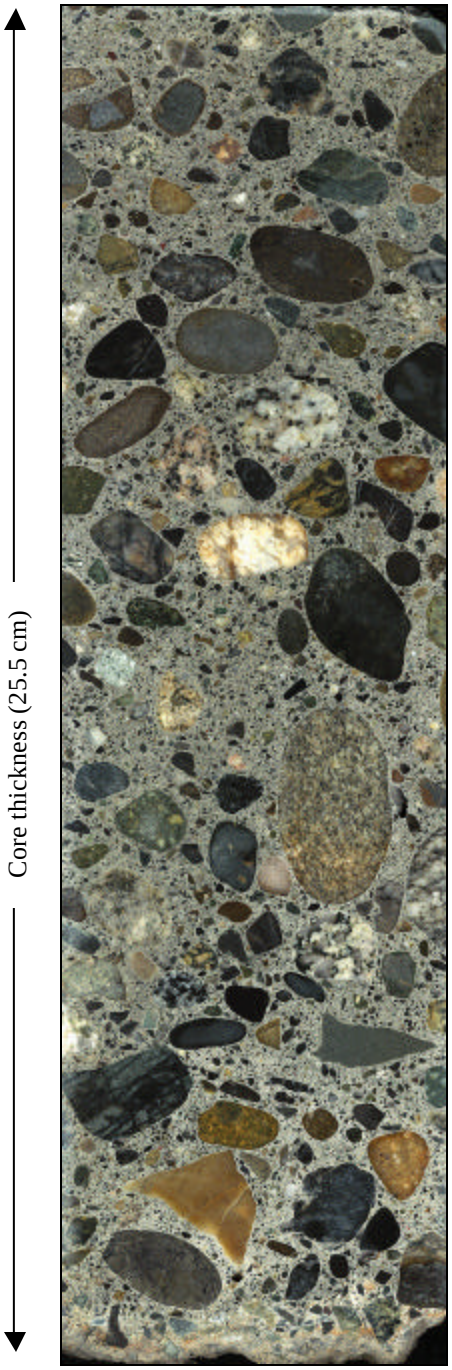

Figure 3.2.13 *Polished cross-section of pavement section 53-3011.*

Section ID: 53-3011
State: Washington
Climate: WNF

Table 3.2.13 *Mix composition of 53-3011 by linear traverse (ASTM C457).*

Coarse Aggregate	Fine Aggregate	Paste Content	Air Content
33.4 vol.%	34.5 vol.%	23.5 vol.%	8.6 vol.%

The core of pavement 53-3011 is 25.5 cm thick and consists of dense packed rounded to well-rounded gravel in a dark medium gray colored paste (figure 3.2.13). The carbonation depth was determined to be less than 1 mm. In the polished slab, the concrete paste showed a darker color at the top 16 to 17 cm of the core.

The composition of the gravel is complex and includes basalt, gabbro, granite, quartz-biotite, and metamorphic rocks. A few sandstone aggregates were also observed. The largest aggregate was 38 mm in diameter. A few aggregates were partially detached from the cement matrix, and there was also a tendency to the presence of higher concentrations of air voids at the interface with the coarse aggregates.

The fine aggregates consist of equal amounts of angular to rounded quartz and fine-grained mafic rock fragments. A few aggregates in the sand fraction may consist of chalcedony which have reacted during hydration of the cement paste. Some flint-aggregates may also be present.

The number of air voids appears to be relatively high. Larger air voids (≤ 8 mm) were observed in the top 7 cm, as well as the lower 11 cm of the core. The air voids in the lower 8 cm of the core were frequently partially filled with white precipitates which sometimes occurred with needle-shaped morphology.

Figure 3.2.14 *Polished cross-section of pavement section 53-3812.*

Section ID: 53-3812
State: Washington
Climate: WNF

Table 3.2.14 *Mix composition of 53-3812 by linear traverse (ASTM C457).*

Coarse Aggregate	Fine Aggregate	Paste Content	Air Content
41.0 vol.%	31.7 vol.%	23.9 vol.%	3.4 vol.%

Pavement section 53-3812 is 22.5 cm thick and consists of rounded to well-rounded gravel in a medium gray cement paste (figure 3.2.14). A few angular grains were also observed. The coarse aggregates are medium to close-packed. No carbonation was noted.

The coarse aggregates are up to 32 mm in diameter and consist of granite, fine-grained gabbro and well-consolidated sedimentary rocks. A light colored rim often surrounds the aggregates due to the accumulation of very fine air voids at their interface. A few aggregates were partially detached from the concrete paste.

The fine aggregates consist of rounded and angular sand with 30 to 40 volume percent quartz. The rest of the fine aggregates consist of the same material as the coarse aggregates.

The amount of large air voids in 53-3812 appears very low. Only 5 to 7 pores larger than 5 mm in diameter were observed in the cross-section. A few air voids contained precipitates.

A single “semi-vertical” crack was observed in the specimen analyzed by MDOT. The crack was observed at the top of the drill-core and ran through the paste without cutting the coarse aggregates.

Figure 3.2.15 *Polished cross-section of pavement section 13-GA1-5.*

Section ID: 13-GA1-5
State: Georgia
Climate: WNF

Table 3.2.15 Mix composition of 13-GA1-5 by linear traverse (ASTM C457).

Coarse Aggregate	Fine Aggregate	Paste Content	Air Content
38.0 vol.%	32.0 vol.%	22.1 vol.%	7.9 vol.%

The drill-core of pavement 13-GA1-5 is 22.5 cm long and shows a concrete composed by crushed rock-fragments embedded in a pale gray cement paste (figure 3.2.15). Carbonation was not noted. The packing of the coarse aggregate appears close.

The coarse aggregates consist of a coarse-grained granitic to granodioritic rock. A few coarse aggregates of a biotite schist are also present. The largest aggregate observed was more than 36 mm in diameter.

The fine aggregates consist of the same material as the coarse aggregates. Notably, the fine aggregates also include numerous evenly dispersed biotite flakes (≤ 1 mm) in addition to the crushed rock particles.

The air voids are not homogeneously distributed and the vesicles often occur in clusters. The largest air voids (≤ 10 mm) are mainly observed between 9- and 15-cm depth in the sample where both spherical and angular voids are observed. The larger air voids were rarely observed at the top 9 cm of the sample. The air voids frequently contain fine-grained white and gray precipitates. According to the MTU report the precipitates in the air-void structure mainly consist of ettringite.

3.2.4. Summary of Petrographic Analysis

A summary of the petrographic analysis is shown in table 3.2.16. As reported, most of the concretes are homogeneous in their structure with some variations in their degree of packing. Most of the concretes show dense aggregate packing but a few, particularly samples 06-3021, 06-3017, and 19-3006 show open aggregate packing.

Most of the samples contain coarse aggregates of silicate rock gravel. However, the coarse aggregates in sections 19-3006, 19-3055, 27-4045, and 55-3008 from the wet freeze regions consist almost entirely of dolomitic limestone. Based on the morphology of the coarse aggregates, samples 19-3006 and 13-GA1-5 are the only concrete samples that contain considerable amounts of crushed aggregates (dolomitic limestone and granitic to granodioritic rocks, respectively). All the other concretes contain rounded to well-rounded gravel aggregates indicating that they have been subjected to some degree of natural reworking (maturation). The maximum size of the aggregates is normally below 46 mm. Sample 06-CS1, however, contains very large aggregates exceeding 76 mm. The smallest maximum aggregate size (27 mm) was observed in sample 39-3801 from the wet freeze region.

Table 3.2.16 *Summary of petrographic results.*

Climate Region	LTPP	ID	Carbonation Depth (mm)	Coarse Aggregate Type	Max Aggregate Dimension (mm)	Max Size Air void (mm)	Crack Position	Dissolution at Base
DNF	06	3017	-	gravel (mix)	46	17	N.D.	< 2 cm
	06	3021	≤15	gravel (mafic)	46	17	top, internal	negligible
	06	CS1	-	gravel (mix)	76	>15	internal	N/A
	06	CS3	≤2	gravel mix incl. dol.	45	14	top	negligible
	06	I-10	-	gravel (mix) [1]	44	10	N.D.	N/A
DF	53	3019	-	gravel (mafic) [1]	47	9	N.D.	~ 1 cm
WF	19	3006	≤4	dol. limestone [2,3,4]	31	6	base	very thin
	19	3055	≤3	dol. limestone [4]	42	11	N.D.	< 0.5 cm
	27	4054	≤4	dol. limestone [4]	40	7	N.D.	negligible
	39	3801	≤1	gravel + dol. limestone	27	11	internal	negligible
	55	3008	not observed	dol. limestone [4]	43	40	N.D.	< 1 cm
WNF	53	3011	≤	gravel (mix)	38	8	N.D.	< 2 cm
	53	3812	N.D.	gravel (mix)	32	7	top	< 2 cm
	13	GA1-5	N.D.	granite/granodiorite [2]	36	10	N.D.	negligible

Abbreviations: - unknown, N.D. not detected
[1] recycled concrete observed
[2] crushed rock
[3] relatively soft aggregates
[4] with minor gabbro

Despite their ages (15 to 32 years), the petrographic analysis suggests that all the pavement concretes generally are in a good state without severe deleterious reactions. The aggregates are of good quality and have mainly remained inert. A few examples, though negligible, were observed where alkali-silica reactions may have occurred. A more typical feature was the presence of reaction rims. However, the reaction rims were

not observed to have caused “problems” with respect to the performance of the concrete. In fact, the reaction rims appear to be related to weathering rather than in situ reactions.

The atmospheric weathering of the concretes results in carbonation through reactions between CO_2 and the $Ca(OH)_2$ and cement hydrates in the paste. According to St. John et al. (1998), when the depth of carbonation is great enough (> 0.5 mm), carbonation shrinkage is induced at the surface and microcracks develop. In the analyzed pavement concretes, the carbonation depth was normally less than 3 to 4 mm when observed. However, one sample, 06-3021, did show evidence of deep surface carbonation (≥ 15 mm). Microscopic analysis of thin-sections also suggests that extensive carbonation has occurred around the air voids in 39-3801 and 13-GA1-5. In 39-3801, carbonation appears to have formed in association with microcracking in the lower half of the concrete.

Both the dolomite and silicate rock aggregates were occasionally porous. The porosity was either caused by the presence of vesicles in the volcanic aggregates, altered mineral phases, or intergranular porosity/cavities in the dolomite aggregates. However, these pore types are normally not interconnected and do not result in a high permeability. Hence, the observed aggregate porosity is not important with respect to freeze-thaw durability.

3.3 Presentation of Field and Laboratory Results on Concrete Properties

3.3.1 Compressive Strength, Splitting Tensile Strength, and Elastic Modulus

This section presents the laboratory results for strength and elastic modulus testing on the concrete from the test sections in this study. The field compressive strengths are substantially higher than the generally required 28-day strengths for pavement concrete, which are typically in the range of 24 to 28 MPa. Tables 3.3.1 and 3.3.2 list the mechanical properties obtained in this study for the field concrete with respect to compressive strength, elastic modulus, and splitting tensile strength. The samples range from 11 to 51 years old, with an average age of 25 years at the time of testing. The average compressive strength is 49 MPa (7,105 lbf/in^2), and ranges from 33 MPa (4,785 lbf/in^2) for California section 06-3021, to 75 MPa (10,875 lbf/in^2) for Washington section 53-3812.

Table 3.3.1. *Measured compressive strength, split tensile strength, and elastic modulus for cored samples from each of the test pavement sections of the DNF and DF regions. Note, values in bold are the average values for each test section.*

Region	Database		Measured Compressive Strength		h/d[1]	Corrected Compressive Strength		Measured Split Tensile Strength		Measured Elastic Modulus	
	State ID	Section ID	MPa	lbf/in^2		MPa	lbf/in^2	Mpa	lbf/in^2	MPa	lbf/in^2
DNF	06	3017	38.8	5633	1.40	36.8	5340	3.64	528	26821	3889000
			40.3	5842	1.30	38.1	5527	3.72	539	26666	3866500
			42.4	6155	1.34	39.9	5791	3.35	486	24117	3497000
			40.5	**5877**		**38.3**	**5552**	**3.57**	**518**	**25868**	**3750833**
	06	3021	34.0	4930	1.41	32.3	4680	3.15	457	22686	3289500
			34.5	5007	1.38	32.7	4735	3.77	547	25769	3736500
			36.7	5320	1.32	34.5	5003	3.39	492	22686	3289500
			35.1	**5086**		**33.1**	**4806**	**3.44**	**499**	**23714**	**3438500**
	06	7456	36.7	5317	1.88	35.9	5211	3.63	526	25710	3728000
			37.7	5472	1.85	37.0	5363	2.93	425	24086	3492500
			37.2	**5395**		**36.5**	**5287**	**3.28**	**475**	**24898**	**3610250**
	06	CS1	46.9	6807	1.45	44.8	6494	3.48	505	32634	4732000
			47.8	6937	1.40	45.4	6576			30224	4382500
			47.4	**6872**		**45.1**	**6535**	**3.48**	**505**	**31429**	**4557250**
	06	CS3	56.1	8137	1.34	52.8	7655	4.18	606	33738	4892000
			67.9	9846	1.36	64.0	9287	3.36	487	35621	5165000
			62.0	**8992**		**58.4**	**8471**	**3.77**	**547**	**34679**	**5028500**
	06	I-10	39.4	5711	1.46	37.6	5455	4.30	623	28321	4106500
								3.70	536		
			39.4	**5711**		**37.6**	**5455**	**4.00**	**580**	**28321**	**4106500**
DF	53	3019	52.3	7589	1.70	51.1	7407	4.21	611	39086	5667500
			61.9	8970	1.65	60.1	8719	3.95	573	42017	6092500
								4.63	671		
			57.1	**8280**		**55.6**	**8063**	**4.26**	**618**	**40552**	**5880000**

[1] h/d is the height to diameter ratio used for strength correction according to ASTM specifications

Table 3.3.2. *Measured compressive strength, split tensile strength, and elastic modulus for cored samples from each of the test pavement sections of the WNF and WF regions. Note, values in bold are the average values for each test section.*

Region	Database		Measured Compressive Strength		h/d[1]	Corrected Compressive Strength		Measured Split Tensile Strength		Measured Elastic Modulus	
	State ID	Section ID	MPa	lbf/in^2		MPa	lbf/in^2	MPa	lbf/in^2	MPa	lbf/in^2
WF	19	3006	49.6	7199	1.40	47.1	6825	3.97	576	32469	4708000
			50.2	7276	1.49	48.1	6976	3.20	464	30621	4440000
			44.8	6494	1.36	42.2	6125	3.34	485	31607	4583000
			48.2	**6990**		**45.8**	**6642**	**3.51**	**508**	**31566**	**4577000**
	19	3055	43.7	6338	1.47	41.8	6062	3.61	523	25510	3699000
			42.6	6181	1.68	41.5	6023	2.22[2]	322	26007	3771000
			43.2	**6260**		**41.7**	**6042**	**2.91**	**423**	**25759**	**3735000**
	27	4054	61.5	8918	1.50	59.0	8561	3.32	481	40614	5889000
			50.2	7276	1.52	48.3	6997	3.44	499	37969	5505500
			57.8	8377	1.59	55.9	8102	4.31	625	38559	5591000
			56.5	**8190**		**54.4**	**7887**	**3.69**	**535**	**39047**	**5661833**
	39	3801	51.1	7406	1.50	49.0	7110	3.39	491	24779	3593000
			49.6	7197	1.52	47.7	6921	3.90	566	25041	3631000
			41.5	6023	1.43	39.5	5731	3.89	564	25917	3758000
			47.4	**6875**		**45.4**	**6587**	**3.73**	**540**	**25246**	**3660667**
	55	3008	62.6	9074	1.75	61.3	8893	4.62	670	42862	6215000
			59.9	8684	1.83	59.1	8566	4.54	658	45090	6538000
			65.8	9544	1.68	64.1	9300	4.33	628	46538	6748000
			62.8	**9101**		**61.5**	**8919**	**4.50**	**652**	**44830**	**6500333**
WNF	53	3011	62.2	9023	1.55	60.0	8698	3.71	538	40310	5845000
			61.5	8918	1.55	59.3	8597	3.97	575	43179	6261000
			61.9	**8971**		**59.6**	**8648**	**3.84**	**557**	**41745**	**6053000**
	53	3812	76.1	11030	1.56	73.4	10642	4.05	588	49007	7106000
			81.3	11790	1.36	76.7	11120	4.75	689	44855	6504000
			78.7	**11410**		**75.0**	**10881**	**4.40**	**638**	**46931**	**6805000**
	13	GA1-5	33.1	4798	1.40	31.4	4549	3.27	474		
			47.1	6833	1.66	43.7	6341	2.72[2]	394	28366	4113000
			36.7	5320	1.48	35.1	5094	3.00	435	21614	3134000
			39.0	**5650**		**36.7**	**5328**	**3.00**	**434**	**24990**	**3623500**

[1] h/d is the height to diameter ratio used for strength correction according to ASTM specifications

[2] data point in question

Overall, the test results for mechanical properties from this study and LTPP are in good agreement, as seen in table 3.3.3. However, the LTPP database does in general show higher compressive strength values by an average of 17 percent. This is likely related in part to the use of smaller specimen sizes (100- by 200-mm cores) in the LTPP database. This study uses 150- by 200- to 250-mm cores with an additional correction for height-to-diameter ratio. Specimen size affects the measured strength, with smaller specimens yielding higher strength (e.g. Price, 1951).

Table 3.3.3 *Compressive strength, splitting tensile strength, and elastic modulus for each test section. (Data is from this study and from the LTPP database (DataPave 97). Values reported are averages of all specimens tested for each test section.)*

Climate Region	LTPP		Section Age		Compressive Strength			Elastic Modulus			Split. Tensile Strength		
	State ID	Section ID	LTPP (Yrs)	This Study (Yrs)	LTPP (MPa)	This Study (MPa)	% Diff.	LTPP (MPa)	This Study (MPa)	% Diff.	LTPP (MPa)	This Study (MPa)	% Diff.
DNF	06	3017	19	20	44	38	13	28276	25868	9	5.0	3.7	26
	06	3021	18	24	44	33	25	21034	23714	-13	5.1	3.5	32
	06	7456	20	26	50	37	26	29138	24898	15	5.7	3.3	43
	06	CS1	20	26		45			31429			3.5	
	06	CS3	20	26		58			34679			4.2	
	06	I-10		51		38			28321			4.3	
DF	53	3019	6	11	64	56	13	34138	40552	-19	6.2	4.2	32
WF	19	3006	19	22	58	46	22	31552	31566	0	3.4	3.5	-3
	19	3055		28	59	42	29	23966	25759	-7	3.9	2.8	28
	27	4054	19	25	57	54	5	38276	39047	-2	4.0	3.7	7
	39	3801	11	13	59	45	23	25862	25246	2	3.2	3.7	-15
	55	3008	19	22	72	62	14	46897	44830	4	4.7	4.5	5
WNF	53	3011	15	20		60		36379	41745	-15	7.0	3.8	45
	53	3812	27	33	79	75	5	45690	46931	-3	6.2	4.4	28
	13	GA1-5/6		26		37			24990			3.0	
Avg			18	25	59	48	18	32837	32638	-3	4.9	3.7	21
Max			27	51	79	75	29	46897	46931	9	7.0	4.5	45
Min			6	11	44	33	5	21034	23714	-19	3.2	2.8	-15

3.3.2 Fracture Energy

Fracture energy was measured in this study from test beams from four California test sections. The beams were tested according to the RILEM 50-FCM test procedure as was described in sections 2.4 and 5.5. The results are listed in table 3.3.4.

The beams were cut directly from the insitu pavement slabs. Thus, the beam height is the slab thickness. Because the slabs from the different test sections were of different thickness, the notch-to-depth ratio in the test beams varied somewhat. This variation is taken into account when calculating the fracture energy. The variation of the fracture energy values within each site is within the expected variation for fracture energy beam testing. See section 5.5.

The laboratory mixes used for development of recommendations were designed to investigate the effect of coarse aggregate type and size using the fracture energy test. The results from the laboratory mixes are also discussed in section 5.5. Considering the laboratory mix results, the fracture energy results obtained from the field are what would be expected for highway concretes containing gravel as coarse aggregate. This observation is important because fracture energy results are not available in the LTPP database for comparison.

Table 3.3.4 *Summary of fracture energy testing results from the tested study sections.*

Climate Region	LTPP State	LTPP Section	Specimen	Fracture Energy N/m	Notch to Depth Ratio
DNF	06	3017	#1	250	0.43
			#2	175	0.44
			#3	249	0.43
			Mean	**225**	**0.43**
	06	3021	#1	179	0.42
			#2	241	0.40
			#3	184	0.42
			Mean	**202**	**0.41**
	06	CS3	#1	286	0.47
			#2	284	0.45
			Mean	**285**	**0.46**
	06	I-10	#1	199	0.37
			#2	261	0.35
			Mean	**230**	**0.36**

3.3.3 Transport Properties

Permeability is not determined in the LTPP database, so all data reported here was measured in this study, using various test methods. Chloride ion penetration resistance and air permeability are measured at three depths within the concrete. For the Rapid Chloride Permeability Test (RCPT), the top sample is taken 12 mm beneath the concrete surface, extending 50 mm below that. The middle and bottom samples are taken successively below that one. Air permeability is measured at approximately 12 mm beneath the surface for the top reading. Middle and bottom readings are taken at approximately 100 and 200 mm beneath the surface where possible. Water permeability readings are taken at two depths, roughly 30 to 40 mm below the surface for the top reading and 130 to 140 mm below the surface for the bottom reading. Water sorption tests were performed on two 38 mm thick samples, one at the pavement surface, and one immediately beneath the first sample. The transport property test methods have been described in detail in chapter 2.

RCPT results were highly repeatable for the concretes that were studied. On the other hand, the water permeability results were questionable for a number of the samples due to observed leaking during the test. It was not clear whether the cracks were caused by the test or had been present beforehand. The questionable data points have not been reported. While there is some variability in the air permeability results this is expected. Air permeability values can span five orders of magnitude so only broad classifications are generally made. Water sorption is perhaps the simplest test procedure, and it yields very useful results, as will be discussed further in Chapters 5 and 6. Tables 3.3.5-3.3.10 show the results from the various tests.

Table 3.3.5 *Rapid Chloride Permeability Test results for the DNF and DF climate regions. Results are for successive test specimens cut with increasing depth in each core sample tested.*

Climate	Section ID		State		RCPT Results (Coulombs)			
	State	Section		Sample	1st (Top)	2nd from Top	3rd from Top	4th (Bottom)
DNF	6	3017	California	1	6680	4146	1564	--
				2	6062	2555	1077	--
				3	4558	3526	1857	--
				4	4918	4361	3485	--
				AVG	**5555**	**3647**	**1996**	--
				STDev	**987**	**810**	**1044**	--
	6	3021	California	1	4720	5854	4173	--
				2	6563	5132	5638	--
				3	3318	3617	2067	--
				4	3843	3878	2637	--
				AVG	**4611**	**4620**	**3629**	--
				STDev	**1424**	**1055**	**1608**	--
	6	7456	California	1	2324	3017	990	921
				2	3163	2046	1389	1593
				AVG	**2744**	**2532**	**1190**	**1257**
				STDev	**593**	**687**	**282**	**475**
	6	CS1	California	1	1719	1916	387	--
				2	2191	1862	673	--
				3	1999	1133	639	291
				AVG	**1970**	**1637**	**566**	**291**
				STDev	**237**	**437**	**156**	--
	6	CS3	California	1	1406	751	530	--
				2	1197	971	444	--
				3	1433	667	323	--
				AVG	**1345**	**796**	**432**	--
				STDev	**129**	**157**	**104**	--
	6	I-10	California	1	3526	3187	1096	--
				2	3891	2886	1508	--
				3	3890	3480	1056	--
				AVG	**3769**	**3184**	**1220**	--
				STDev	**210**	**297**	**250**	--
DF	53	3019	Washington	1	557	105	71	29
				2	287	76	106	56
				3	356	--	--	215
				AVG	**400**	**91**	**89**	**100**
				STDev	**140**	**21**	**25**	**101**

Table 3.3.6 *Rapid Chloride Permeability Test results for the WF and WNF climate regions. Results are for successive test specimens cut with increasing depth in each core sample tested.*

Climate	Section ID		State		RCPT Results (Coulombs)			
	State	Section		Sample	1st (Top)	2nd from Top	3rd from Top	4th (Bottom)
WF	19	3006	Iowa	1	2497	1237	785	--
				2	1633	865	577	--
				3	1855	1744	--	--
				AVG	**1995**	**1282**	**681**	--
				STDev	**449**	**441**	**147**	--
	19	3055	Iowa	1	1656	1023	1242	973
				2	4203[1]	1829	1850	2338
				AVG	**1656**	**1426**	**1546**	**1656**
				STDev	**--**	**570**	**430**	**965**
	27	4054	Minnesota	1	1184	725	766	229
				2	3782[1]	810	592	445
				AVG	**1184**	**768**	**679**	**337**
				STDev	**--**	**60**	**123**	**153**
	39	3801	Ohio	1	1802	1533	790	709
				2	1207	1217	1792	947
				AVG	**1505**	**1375**	**1291**	**828**
				STDev	**421**	**223**	**709**	**168**
	55	3008	Wisconsin	1	225	288	312	324
				AVG	**225**	**288**	**312**	**324**
				STDev	--	--	--	--
WNF	53	3011	Washington	1	652	390	--	251
				2	606	288	301	456
				3	779	363	442	279
				4	1112	500	351	283
				AVG	**787**	**385**	**365**	**317**
				STDev	**229**	**88**	**71**	**94**
	53	3812	Washington	1	448	530	345	--
				2	561	354	318	--
				3	443	214	208	--
				4	257	237	202	--
				AVG	**427**	**334**	**268**	--
				STDev	**126**	**144**	**74**	--
	13	GA1-5	Georgia	1	7030	2349	1653	--
	13	GA1-6	Georgia	1	6825	6268	4248	4157
				AVG	**6928**	**4309**	**2951**	**4157**
				STDev	**145**	**2771**	**1835**	**--**

[1] *Data point in question.*

Table 3.3.7 *Air Permeability Test results for the DNF and DF climate regions.*

Air Permeability							
Climate	**State**	**Section**	**Measurement Location**	**Air Permeability Kt (10-16 m^2)**	**Penetration Depth L (mm)**	**Electrical Resistance (kohm cm)**	**Permeability Class**
DNF	06	3017	Top	1.032	53.1	--	Bad
			Middle	0.175	28.5	135	Normal
			Middle	0.200	30.6	155	Normal
			Bottom	0.015	8.5	184	Good
	06	3021	Top	4.426	77.6	--	Bad
			Middle	1.047	53.4	293	Bad
			Middle	0.134	25.0	223	Normal
			Bottom	0.172	28.3	310	Normal
	06	CS1	No Test				
	06	CS3	No Test				
	06	I-10	Top	1.632	56.4	--	Bad
			Middle	0.449	44.9	307	Normal
			Middle	0.599	46.9	216	Normal
			Bottom	0.086	20.1	207	Good
DF	53	3019	Top	0.893	51.0	--	Normal
			Middle	0.016	8.7	--	Good
			Middle	0.038	13.4	560	Good
			Bottom	0.017	8.9	--	Good

Table 3.3.8 *Air Permeability Test results for the WF and WNF climate regions.*

Air Permeability							
Climate Region	**State**	**Section**	**Measurement Location**	**Air Permeability Kt (10^{-16} m^2)**	**Penetration Depth L (mm)**	**Electrical Resistance (kohm cm)**	**Permeability Class**
WF	19	3006	Top	0.693	47.9	243	Normal
			Middle	0.308	37.9	177	Normal
			Middle	0.013	7.8	176	Good
			Bottom	0.009	6.3	195	Very Good
	19	3055	Top	0.033	12.5	77	Good
			Middle	0.067	17.7	63	Good
			Middle	0.107	22.3	52	Normal
			Bottom	0.114	23.0	54	Normal
	27	4054	Top	0.125	24.1	116	Normal
			Middle	0.070	18.0	140	Good
			Middle	0.088	20.3	113	Good
			Bottom	0.046	14.6	123	Good
	39	3801	Top	0.086	20.0	92	Good
			Middle	0.026	11.1	61	Good
			Middle	0.039	13.5	56	Good
			Bottom	0.008	6.3	56	Very Good
	55	3008	Top	0.042	14.0	169	Good
			Middle	0.019	9.4	179	Good
			Middle	0.037	13.1	150	Good
			Bottom	0.034	12.6	116	Good
WNF	53	3011	Top	7.103	91.1	210	Bad
			Middle	0.006	5.5	--	Very Good
			Middle	0.001	2.4	151	Very Good
			Bottom	0.029	11.6	--	Good
	53	3812	Top	0.22	32.1	313	Normal
			Middle	0.017	9	212	Good
			Middle	0.042	14	205	Good
			Bottom	0.02	9.8	214	Good
	13	GA1-5	Top	0.399	43.2	60	Normal
			Middle	0.039	13.6	34	Good
			Middle	0.595	46.9	58	Normal
			Bottom	0.172	28.4	69	Normal

Table 3.3.9 *Water permeability test results.*

Climate Region	LTPP		Water Permeability ($cm/sec x 10^{-11}$)	
	State ID	Section ID	Top	Bottom
DNF	06	3017	303.4	--
	06	3021	--	--
	06	7456	--	--
	06	CS1	--	--
	06	CS3	--	--
	06	I-10	--	--
DF	53	3019	56.1	--
WF	19	3006	117.2	81.0
	19	3055	--	50.4
	27	4054	53.6	--
	39	3801	--	38.2
	55	3008	48.7	--
WNF	53	3011	42.9	--
	53	3812	16.9	--
	13	GA1-5	155.1	99.3

Table 3.3.10 *Water absorption rate results from water sorption test.*

Climate Region	Test Section ID	Absorption Rate	
		Top Sample $kg/m^2/h^{0.5}$	2nd Sample $kg/m^2/h^{0.5}$
DNF	06-3017	0.82	0.79
	06-3021	0.93	1.48
	06-7456	0.91	0.81
	06-CS1	0.85	0.71
	06-CS3	0.47	0.40
	06-I10	0.88	0.76
DF	53-3019	0.38	0.27
WF	19-3006	0.56	0.59
	19-3055	0.71	0.82
	27-4054	0.72	0.72
	39-3801	0.55	0.57
	55-3008	0.43	0.41
WNF	53-3011	0.40	0.38
	53-3812	0.40	0.51
	13-GA1-5	1.30	1.47

3.3.4 Coefficient of Thermal Expansion

Coefficient of thermal expansion is not complete in the LTPP database. Thus, all data presented is from field cores in this study. The coefficient of thermal expansion was tested according to a recommended procedure from FHWA as described in chapter 2. The procedure was modified for continuous measurements of temperature and deformations of the concrete for improved accuracy.

The values measured in this study fall within the acceptable range for concrete coefficient of thermal expansion, as seen in table 3.3.11. The concretes have a relatively narrow range of values. Results are measured against a stainless steel reference bar to ensure testing accuracy. The coefficient of thermal expansion is averaged from the value obtained with increasing temperature and the value obtained from decreasing temperature. Note that the coefficient of thermal expansion may differ 10 to 20 percent between two temperature cycles.

Table 3.3.11. *Measured coefficient of thermal expansion for cored samples from each of the tested pavement sections of this study.*

Climate Region	LTPP State ID	LTPP Section ID	Specimen ID	α (10-50 C) ($*10^{-6}$)	α (10-50 C) ref. ($*10^{-6}$)	α (50-10 C) ($*10^{-6}$)	α (50-10 C) ref. ($*10^{-6}$)	Average α ($*10^{-6}$)
DNF	06	3017	-	-	-	-	-	NA
	06	3021	-	-	-	-	-	NA
	06	7456	C7	9.1	-	10.5	-	9.8
			C8	9.2	-	11.3	-	10.3
	06	CS1	C4	9.9	17.1	9.7	16.2	9.8
	06	CS3	C19	13.1	16.3	14.2	16.4	13.7
	06	I-10	C6	8.2	17.3	8.5	17.6	8.4
	DNF Region Average: 10.4							
DF	53	3019	C3	9.8	17.4	8.5	17.4	9.2
			C8	8.4	16.9	8.6	17.4	8.5
	DF Region Average: 8.9							
WF	19	3006	-	-	-	-	-	NA
	19	3055	C11	9.8	-	9.7	-	9.8
			C19	8.3	-	8.7	-	8.5
	27	4054	C4	9.1	-	8.4	-	8.8
			C5	9.7	16.5	9.3	16.9	9.5
	39	3801	C3	11.3	17.5	11.9	17.9	11.6
	55	3008	C12	9.7	17.1	9.5	-	9.6
			C15	8.8	18.0	8.8	19.0	8.8
	WF Region Average: 9.5							
WNF	53	3011	-	-	-	-	-	
	53	3812	C17	9.9	17.1	8.3	17.2	9.1
			C10	13.3	17.3	12.5	16.6	12.9[1]
	13	GA1-5	C14	9.5	17.0	8.5	16.3	9.0
	WNF Region Average: 9.1							

[1] Data point in question

CHAPTER 4. PAVEMENT PERFORMANCE

4.1 Introduction

The main purpose of this study has been to investigate relationships between higher strength and associated properties of concrete, its effect on pavement performance, and its added resistance to chemical and physical deterioration. In the context of increasing strength, the objective is to identify the key concrete properties and mix characteristics associated with the improved pavement performance.

The preliminary evaluation of the effects of PCC strength on pavement performance levels, based on the LTPP database, indicated that some of the primary pavement deterioration mechanisms are hidden within the foundation layer properties and climate/traffic parameters. See chapter 1. Therefore, a detailed field investigation was undertaken to isolate the effects and the mechanisms of PCC on JPCP deterioration from the effects of foundation and environmental factors.

The review of the LTPP database and other available information from various SHA's revealed only a few in-service concrete pavements of high strength (45 to 50 MPa or above) and sufficient age (> 20 to 25 years) in different climatic zones for evaluation in this study. Three out of the fifteen test sections selected for detailed field and laboratory investigation had high in-service compressive strength. These three sections were located in different climatic zones. The Washington State LTPP section 53-3812, in the WNF zone, was selected as it had the highest field compressive strength of 75 MPa (10,875 lbf/in^2) and had excellent long-term performance. The higher strength JPCP near Tracy, California, 06-CS3, located in the DNF zone, had field compressive strength of about 58 MPa (8,410 lbf/in^2). The third high strength project was the Wisconsin LTPP section 55-3008 located in the WF zone, with a field compressive strength of 62 MPa (8,990 lbf/in^2).

In each of these climate zones, other projects were selected to cover a range in strength levels and performance. The complete test matrix includes seven projects from the DNF and DF zones, five from the WF zone, and three from the WNF zone. Chapter 3 presents key pavement information, climate data, PCC properties, and summary site and petrographic descriptions. Appendixes A through E provide the detailed results obtained by the project team and include field surveys, mechanical properties (strength and stiffness), air void characteristics and concrete composition, permeability, mix compositions, and additional petrographic analysis.

The selected 15 test sections span the low, medium and high strength range for jointed plain concrete pavements found in the LTPP database as discussed in section 5.1.

4.1.1 Pavement Distress at the Time of Field Testing

Summary distress survey results, collected during the field investigation portion of this project, are shown in table 4.1.1 and 4.1.2. At the time of field testing, 10 out of the 15 sections had not developed any significant amount of distress in terms of joint faulting,

spalling and transverse cracking. The fifteen pavements represent a range in concrete strength, joint spacing, traffic levels, age, and climatic regions. Eight sections represent pavements, which have low long-term distress. They are 20 to 25 years old or older. Five sections were 22 years old or older and have developed various distress types and levels. The remaining two sections were included because they have developed the highest amount of joint faulting and joint spalling in the LTPP database. The Wisconsin LTPP section 55-3008 had developed an average of 9.0 mm joint faulting. The Iowa LTPP section 19-3006 had the highest amount of joint spalling in the database with 20 out of 23 joints in the high level spalling category. For a JPCP on CTB, this section had also developed a significant amount of joint faulting with an average of 4.2 mm. In addition, 5 of its 22 slabs had developed low severity transverse cracking.

Among the investigated pavements was an older California PCC pavement experimental project, which was constructed in 1971. Four different pavement designs were included to study the effect of joint spacing, slab thickness, PCC strength, and base type (CTB versus LCB) on pavement performance (Wells and Nokes, 1991). They are undoweled JPCP designs with random, skewed, and nonsealed transverse joints. All sections have a 137 mm (5.4 in.) base with three sections resting on cement treated base (CTB) and one section resting on lean concrete base (LCB). All sections have a 610 mm (24 in.) aggregate subbase. In this project three northbound sections were selected for detailed field and laboratory investigation, as their original design had not been altered. They include the control section, the higher PCC strength section, and the thickened section. The latter is also an LTPP section (06-7456). The experimental sections had carried substantial heavy vehicle loading (about 16 million ESAL's) at time of investigation.

The experimental test road is of major interest to this project as the effect of increased PCC strength on pavement performance can be evaluated relative to a control section. The higher design strength was achieved by increasing the cement content from 307 to 418 kg/m^3 (5½ to 7½ sacks per yd^3). It will be shown that increasing the cement content instead of reducing the w/c ratio has had a detrimental effect on pavement performance. For the control section, 06-CS1, seven slabs were cracked, averaging about 21 percent slab cracking for the section. Of the 32 slabs in test section 06-CS3, 23 had developed low to medium-severity full lane-width transverse cracking. The thickened test section, 06-7456, had developed a significant amount of joint faulting (2.6 mm) for a JPCP on CTB, but without the associated transverse cracking. Only one slab out of 33 had transverse cracking.

The following sections discuss the major findings on the development of faulting, spalling, and transverse cracking. Faulting and spalling are evaluated in terms of development over an extended period of time, and the data represent the time-series of distress available in the LTPP database combined with the last distress survey conducted at time of field testing. The observed transverse cracking is discussed based on intermittent and permanent loss of support.

Table 4.1.1 *Observed faulting determined in this study and overall foundation stiffness. (The joint spacings can be found in table 3.1.1.)*

Climate	Section ID	Age (Years)	Traffic (KESAL)	Base Type	Joint LTE System	Joints (#)	Ave. Faulting (mm)	Subgrade Stiffness (CBR)
DNF	06-3017	20	3900	CTB	Agg.	31	0.6	86
	06-3021	24	5250	CTB	Agg.	33	1.6	46
	06-7456	25	16000	CTB	Agg.	33	2.6	NA
	06-CS1	26	16000	CTB	Agg.	33	0.0	74
	06-CS3	26	16000	CTB	Agg.	32	1.1	72
	06-I10	51	>16000[1]	CTB	Agg.	33	1.6	67
DF	53-3019	11	6200	Granular	Agg.	43	0.4	57
WF	19-3006	22	3975	CTB	Dowels	23	4.2	6
	19-3055	28	4265	Granular	Agg.	25	2.9	10
	27-4054	25	10700	Granular	Dowels	19	2.7	NA
	39-3801	13	4685	CTB	Dowels	25	0.4	44
	55-3008	22	15220	Granular	Agg.	34	9.0	7
WNF	53-3011	20	8935	Granular	Agg.	43	2.2	83
	53-3812	33	12765	Granular	Agg.	34	1.0	81
	13-GA1-5/6	25	23025	CTB/ATB	Dowels	26	2.0	4

[1] estimated.

Table 4.1.2 *Observed joint spalling and transverse cracking in this study.*

Climate	Section ID	Age (years)	Traffic (KESAL)	No. of Joints	Transverse Joint Spalling Indicated in levels of low, moderate, and high. (L,M,H)						Transverse Slab Cracking Indicated in levels of low, moderate, and high. (L,M,H)					
					L (m)	No.	M (m)	No.	H (m)	No.	L (m)	No.	M (m)	No.	H (m)	No.
DNF	06-3017	20	3900	31	0.5	3	0	0	0	0	0	0	0	0	0	0
	06-3021	24	5250	33	5.4	24	0	0	0	0	6.9	2	0	0	0	0
	06-7456	25	16000	33	1.9	4	0	0	0	0	0	1	0	0	0	0
	06-CS1	26	16000	33	3.2	20	0	0	0	0	23.6	7	0	0	0	0
	06-CS3	26	16000	32	1.4	11	0	0	0	0	82	23	0	0	0	0
	06-I10	51	>16000[1]	33	2.7	22	0	0	0	0	28.6	8	0	0	0	0
DF	53-3019	11	6200	43	10.0	42	0	0	0	0	0	0	0	0	0	0
WF	19-3006	22	3975	23	24.1	20	4.0	7	25	20	18.5	5	0	0	0	0
	19-3055	28	4265	25	19.0	24	0	0	0	0	0	0	0	0	0	0
	27-4054	25	10700	19	9.5	16	0	0	0	0	2.4	1	0	0	0	0
	39-3801	13	4685	25	8.6	25	0	0	0	0	0	0	0	0	0	0
	55-3008	22	15220	34	47.5	33	0	0	0	0	4	1	0	0	0	0
WNF	53-3011	20	8935	43	11.1	41	0	0	0	0	0	0	0	0	0	0
	53-3812	33	12765	34	10.4	30	0	0	0	0	0	0	0	0	0	0
	13-GA1-5/6	25	23025	26	0	0	0	0	0	0	0	0	0	0	0	0

[1] estimated.

4.2 Joint and Crack Faulting

Faulting can be caused either by slab settlement or by the accumulation of loose material beneath the slab near the approach joints. This distress type is important as it controls the ride quality. Observations of faulted joints by Neal et al. (1985) show that a thicker accumulation occurs under the approach slab (upstream side of the joint), causing this end to lift. Material accumulates under the approach slab when the leave slab deflects from wheel loading. When the leave slab is deflected by wheel load, the fines and free water under the joints are ejected towards the approach joint side, where the fines accumulate and gradually lift up the joint, causing faulting. In order to create this type of joint or crack faulting, these factors must occur simultaneously: heavy vehicle loading, free water at the slab-base interface, fines and/or erodible base material, poor load transfer, and curling/warping.

Analysis of field and laboratory data showed that Wisconsin section 55-3008 had developed the highest amount of joint faulting in the LTPP database due to slab settlement and pumping. The JPCP rests on a granular base over a very soft foundation. The data and surface profile measurements using the dipstick device suggest that the substantial pavement upward curvature in the higher strength PCC has occurred over time, and that the foundation has been able to conform to the slab's shape as it settled. In this case the faulting had developed without transverse cracking and corner breaks, indicating that the slab settlement did not induce permanent loss of slab support by the foundation. The data suggests that the foundation had been able to conform to the slab's shape as it settled.

The data obtained for the experimental test sections near Tracy in California showed that these sections developed faulting as a result of pumping erosion with associated accumulation of fines near the approach joint. The erosion had formed a gap under the leave slab and the slab had de-bonded from the base. This condition, combined with temperature curling, can over time induce fatigue transverse cracking starting at the top of the slab. The cracking phenomenon is discussed in detail in section 4.3.

The following sections include a discussion of the variation of joint and crack faulting along a test section, and a discussion on the development of faulting for JPCP's depending on traffic and foundation characteristics.

4.2.1 Joint Faulting from Slab Settlement or Pumping Erosion

Slab Settlement of the Wisconsin Section 55-3008

Surface elevation profiles for the Wisconsin section 55-3008 show joint faulting of 4.3 to 15.2 mm. Figure 4.2.1 shows a faulted joint in this section. Despite the severe faulting, only 1 out of 33 slabs for the 153-m test section has developed transverse cracking of low severity. See also table 4.1.2. Figure 4.2.2 shows the surface elevation profiles for three 30-m sections starting at the beginning of the test section. The surface profiles were obtained in the direction of traffic for both the outer and the inner wheel-paths using the Dipstick device. The 153-m section was measured in increments of 0.3 m (1 ft) starting

at the white painted marker located in this case 0.9 m (3 ft) before the beginning of the first transverse joint. A zero beginning elevation was selected at the start point for both the outer and the inner wheel paths, and the site design slopes were removed as well in order to show small changes in elevation profiles. These results show quantitatively the amount of faulting of each joint. Also, the slabs are noticeably rotated from faulting at the joints with the approach side of the joint turned upward and the leave side of the joint turned downward. Furthermore, the profiles also show that the slabs are of varying length and that only one slab is cracked (located 75 to 80 m from the start of the test section).

In addition to the rotation, the slabs are curved upward at approach joints, consistent with pumping of fines in the presence of water from the leave side to the approach side of a joint. The foundation is forgiving, which has allowed the slab to settle and develop substantial permanent upward curved shape, thereby reducing loss of support. Excellent agreement was obtained between the profiles in the outer and inner wheel paths.

Figure 4.2.1 *Faulted transverse joint in test section 55-3008.*

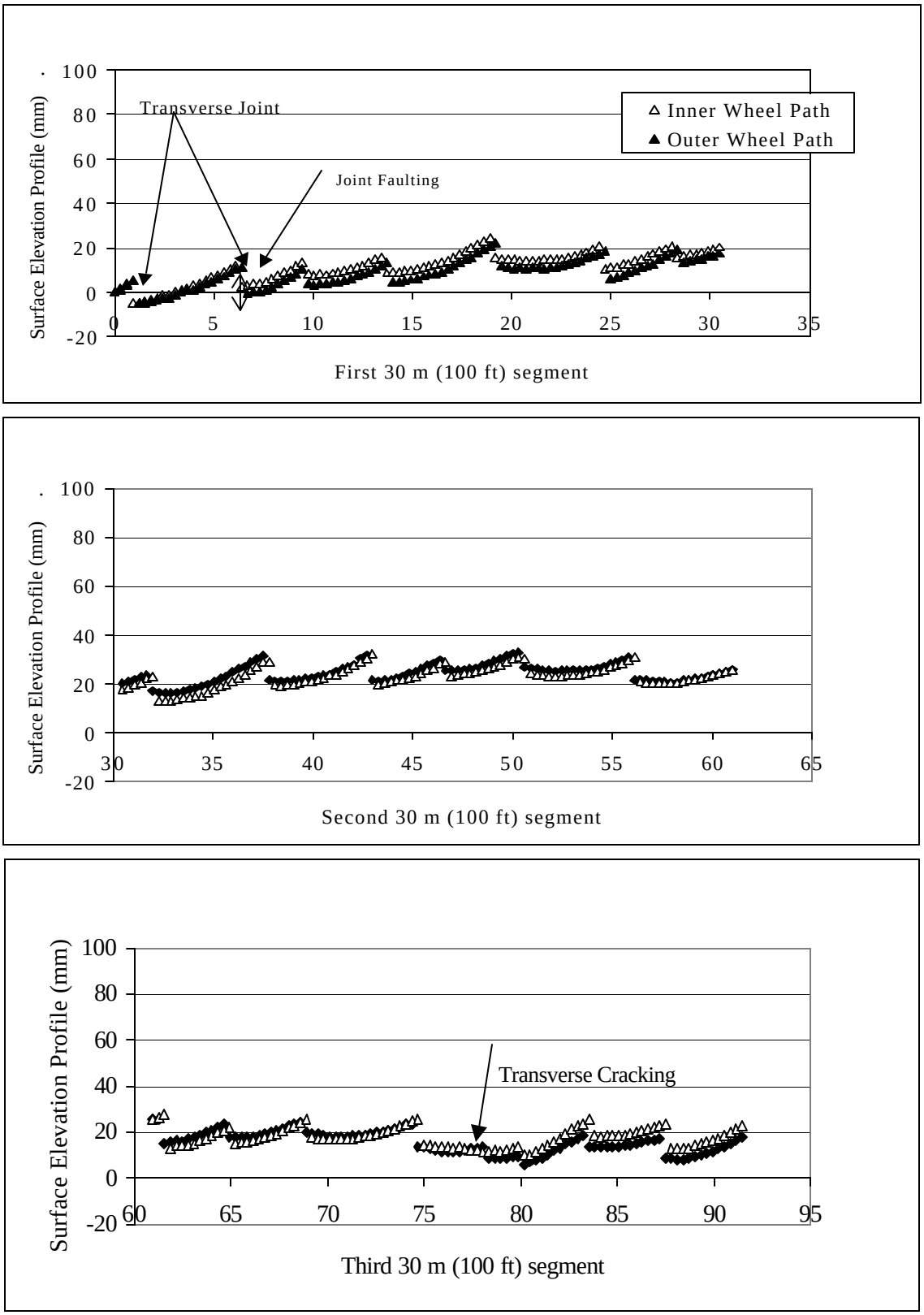

Figure 4.2.2 *Surface profiles for test section 55-3008 with random joint spacing.*

Pumping Erosion on Experimental Test Road near Tracy, California

Surface staining on the shoulder close to joints from pumping was evident for the Tracy Test Road sections 06-CS1 and 06-CS3 as seen from figure 4.2.3. Surface elevation profiles of individual slabs show the effects of pumping with a tendency for the approach side of each transverse joint to develop a permanent concave upward shape. See figure 4.2.4 for Tracy Test Road Section 06-7456. Neal et al. (1985) studied this buildup of fines under slabs in detail. They used tracer sand under the pavement and the shoulder to locate movement of fines, and demonstrated that the source of fines was the adjacent shoulder and the CTB surface. This is consistent with figure 4.2.5, which shows a depressed shoulder. Pumping erosion leads to de-bonding of the CTB from the concrete slab.

Figure 4.2.3 *Surface staining on the shoulder close to joints from Tracy Test Road (06-CS1).*

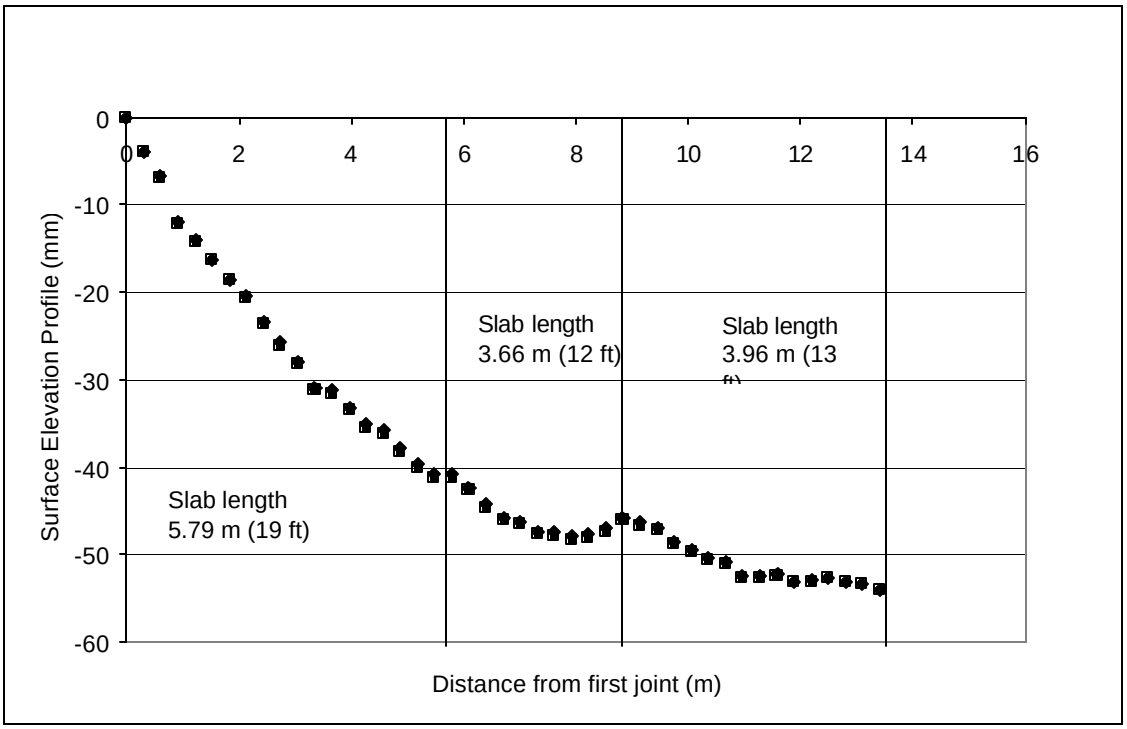

Figure 4.2.4 *Surface elevation profiles for 06-7456 at Tracy. The design slope is not extracted from the profiles.*

Figure 4.2.5 *Depressed shoulder in test section 06-CS3 from pumping of fines. Transverse cracking in outer and inner lane.*

4.2.2 Individual Joint/Crack Faults versus Section Average

Faulting is typically evaluated in terms of one single average section value. The drawback of using one average value is that it can obscure the true faulting, as both negative and positive faulting values occur.

Figures 4.2.6, 4.2.7, and 4.2.8 illustrate the variability in joint faulting measured along the outer wheel path in the direction of traffic for the 153-m test section as illustrated for three different projects. The test sections are 06-I-10, 06-7456 and 06-CS3 in California. Fault measurements were made using the Georgia Faultmeter. The typical coefficient of variation for this distress type is about 50 percent. Note that no clear relation between joint spacing and the level of faulting has been detected from the faulting data.

The effect of environment on faulting is noticeable for the 51 year old I-10 project in San Bernadino Co., California. For this project fault measurements were conducted near the inner wheel path to avoid a section exposed to surface grinding. The faulting data along this test section illustrate the effect of local conditions on overall faulting. See figure 4.2.6. In the first 120 m of the 153-m test section the joint and crack faulting varies between –1.5 and 4.2 mm. However, at the bridge overpass on Etiwanda Ave. the faulting data stabilizes at a level of 1 mm. This is substantially smaller compared to the rest of the test section. It is believed that the reduced faulting is associated with the absence of water under the bridge overpass. Free water is one of the necessary components for faulting development due to pumping erosion. This agrees with findings by Wells (1993). He also showed that traffic and climate are the major factors with respect to joint fault development for several California JPCP's, and that a stable non-erodible LCB tends to reduce fault development. Wells and Nokes (1991) showed, based on fault measurements, that the PCC pavement on LCB of the experimental test sections on I-5, near Tracy, was most resistant to pumping erosion. This was confirmed by a recent investigation by Caltrans on the performance of these sections (Long and Shatnawi, 2000).

It is important to determine fault measurements for each joint and crack along a project length and to monitor the fault development over time as transverse cracks relieve slab stress. The presence of cracks may skew the average project fault value downward as faulting of cracks has not developed over the same time period as that of the joints. Crack faulting may even be negative (i.e. approach crack side lower than leave side) due to slab rotation. This is illustrated for section 06-CS3 in figure 4.2.7. The fault values for this section vary between -2.5 and 5.6 mm with an average value of 1.1 mm. However, the majority of the crack fault data falls below the section average. In addition, it is noticeable that the thickened section at the Tracy Test Road, 06-7456, has a higher overall section fault of about 2.6 mm, and that the fault data ranges from about -1 to 9 mm, see figure 4.2.8. It is suggested that the higher joint faulting is because these thicker slabs have not yet cracked. Furthermore, these sections with variable joint spacing (3.6 to 5.8 m) did not show any correlation between slab length and faulting, which indicates that joint faulting is a local problem controlled by pumping. See figure 4.2.9. This is also

in agreement with surface profile measurements for the three project sections 06-CS1, 06-CS3, and 06-7456.

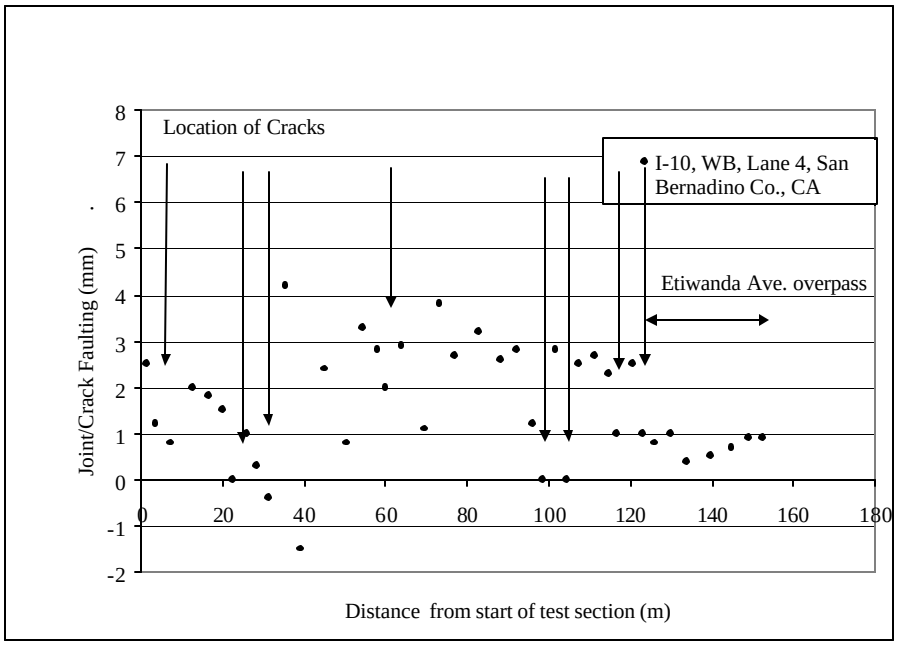

Figure 4.2.6 *Joint/crack faulting measured along the outer wheel path in the direction of traffic for the 153-m test section, 06-I10 in California.*

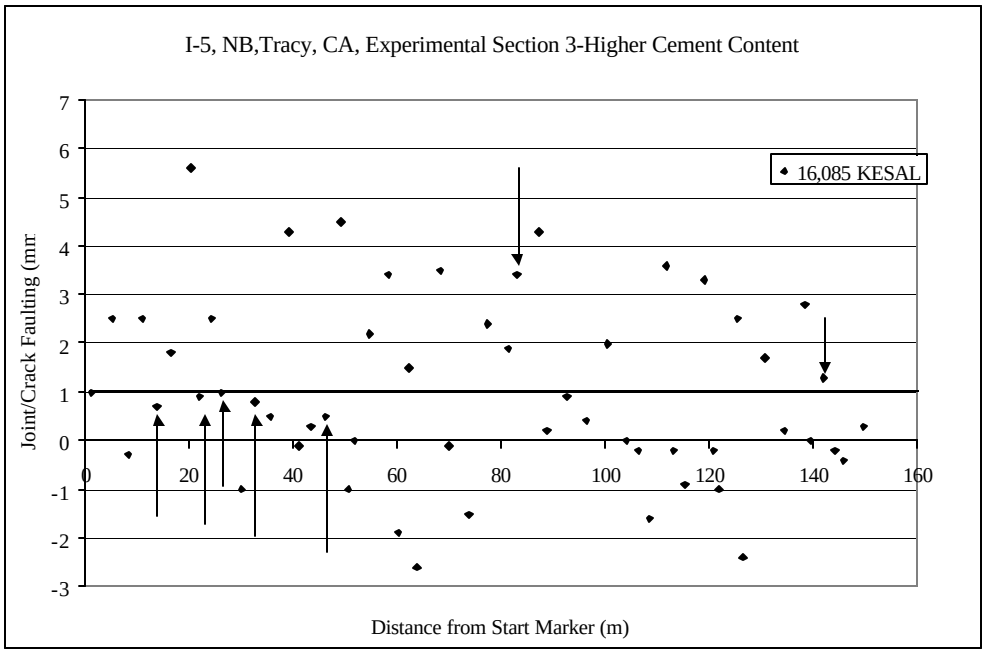

Figure 4.2.7 *Joint/crack faulting measured along the outer wheel path in the direction of traffic for the 153-m test section, experimental test road 06-CS3 near Tracy, California.*

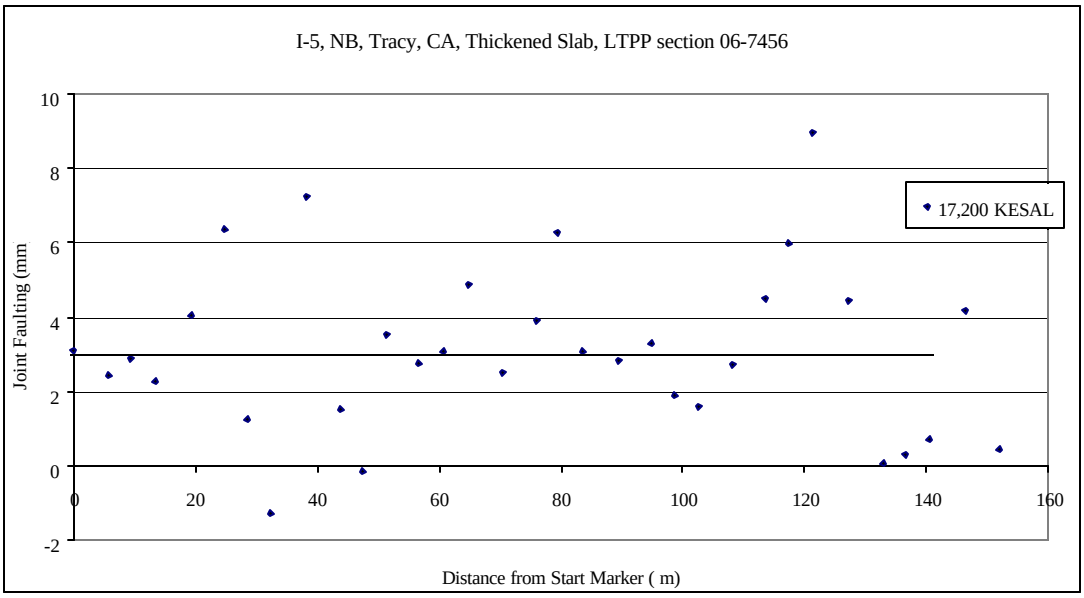

Figure 4.2.8 *Joint/crack faulting measured along the outer wheel path in the direction of traffic for the 153-m test section experimental test road 06-7456 near Tracy, California.*

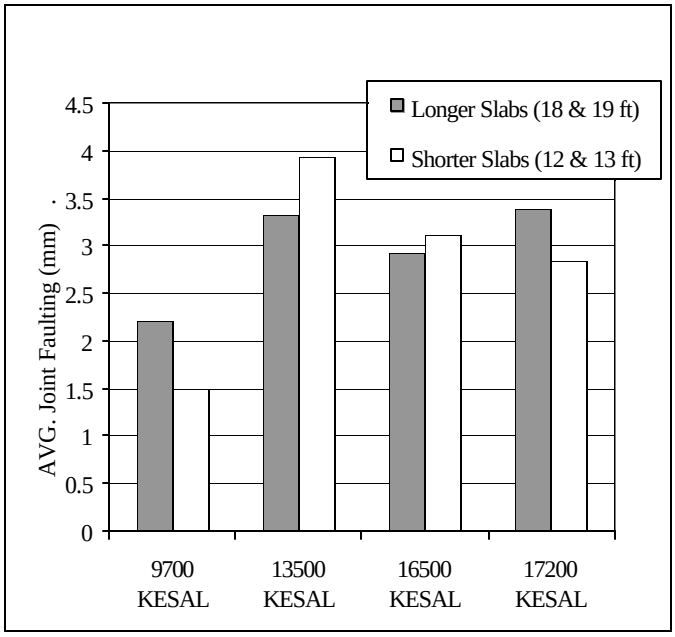

Figure 4.2.9 *Joint faulting for slabs of various lengths for experimental test road 06-7456 near Tracy, California at different cumulative traffic levels.*

In cases where pumping erosion does not occur, fault development for substantial traffic loading (17,000 KESAL's) is negligible for JPCP's on CTB or ATB. This is shown in figures 4.2.10 and 4.2.11 for the Georgia experimental test sections 13-GA1-5 (JPCP on CTB) and 13-GA1-6 (JPCP on ATB).

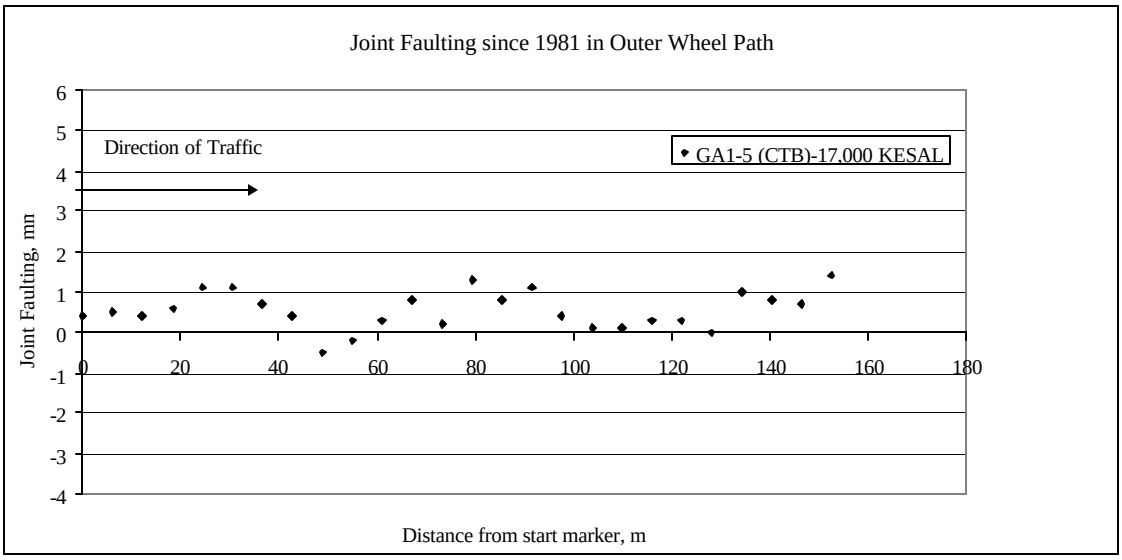

Figure 4.2.10 *Joint faulting measured along the outer wheel path in the direction of traffic for the 153-m test section Georgia Test Road section 13-GA1-5.*

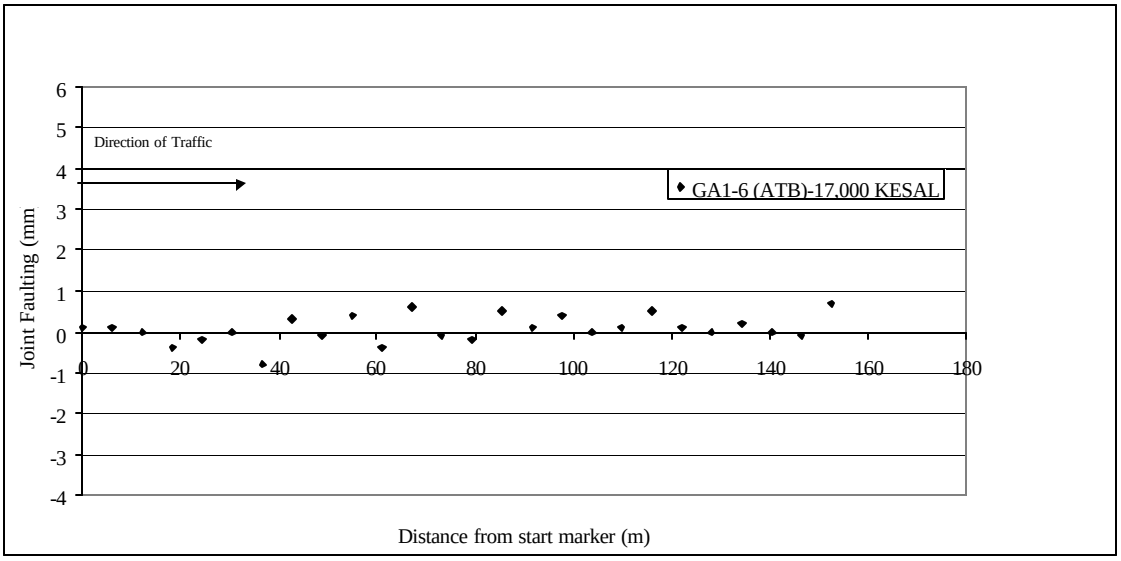

Figure 4.2.11 *Joint faulting measured along the outer wheel path in the direction of traffic for the 153-m test section Georgia Test Road section 13-GA1-6.*

4.2.3 Development of Faulting

Faulting is primarily controlled by the cumulative traffic and base type, and faulting is linearly related to cumulative ESAL's. For granular bases, the rate of faulting increases substantially with decreasing subgrade CBR. Faulting of a JPCP on CTB increases with pumping, and the rate of faulting is controlled by the CTB and not the subgrade CBR. This is shown in figures 4.2.12 and 4.2.13. Overall the observed trend is in agreement with other studies.

Figure 4.2.12 shows the fault development versus traffic for pavements on granular bases. The data represent the time-series of distress available in the LTPP database combined with the last distress survey conducted at time of field testing. The data show a high degree of faulting for section 55-3008 versus traffic. The most plausible reason is settlement of the slab on the soft sandy lean clay subgrade (CBR=7). The rate of increase follows the same trend as section 19-3055, which rests on a foundation with similar characteristics. However, section 19-3055 has not yet experienced the high traffic of section 55-3008.

For other sections on granular bases, where the foundation is much stiffer, faulting develops at a much lower rate. When the faulting of these sections (in figure 4.2.12) is compared to the faulting of sections on stiff CTB's (in figure 4.2.13) the rate of development is found to be similar. Thus, the rate of faulting appears to be independent of base type provided there is uniform stiff support for the pavement slab.

Figure 4.2.13 shows the faulting development versus traffic for sections on CTB's. It can be seen that the overall rate of faulting development is very low. However, there is also a relation between faulting development and the occurrence of pumping in these sections. Pumping of CTB foundations leads to loss of slab support and higher vertical slab displacement. Loss of slab support on a stiff foundation such as a CTB can result in premature transverse cracking, as will be discussed later.

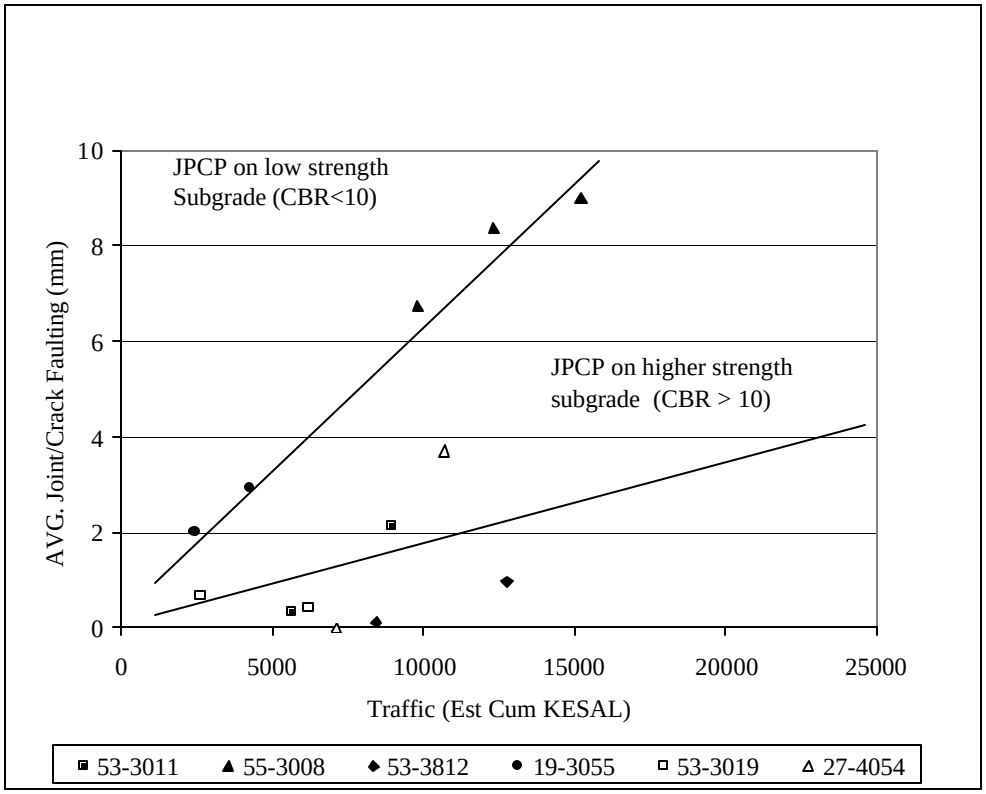

Figure 4.2.12 *Faulting development versus traffic for JPCP on granular bases.*

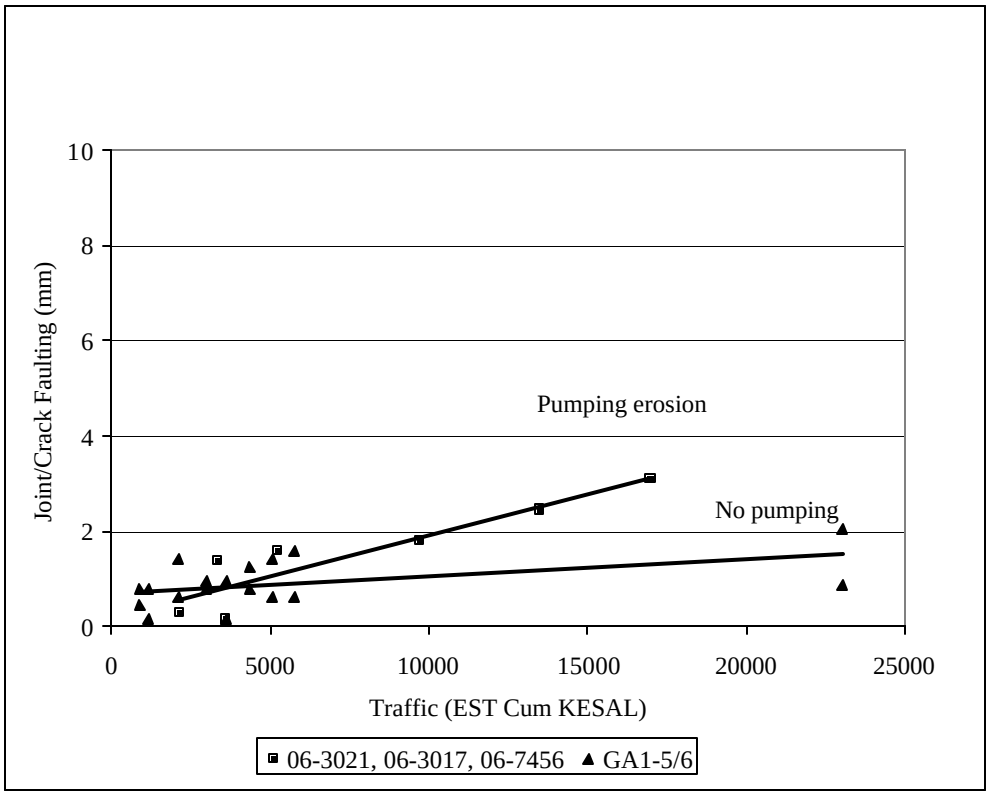

Figure 4.2.13 *Faulting development versus traffic for JPCP on CTB.*

4.2.4 Aggregate Interlock and Pavement Performance

Joint and crack load transfer efficiency (LTE) is often quantified using a relative measure of the deflections on either side of the crack or joint. Several formulas have been developed for quantifying LTE based on slab deflections. The LTE measure proposed by Ioannides and Korovesis (1990) is applied. The equation is:

$$LTE = \frac{d_u}{d_l} \cdot 100\% \qquad (4.2.1)$$

where LTE = load transfer (%)

δ_u = deflection of the unloaded side of the crack or joint (mm), and

δ_l = deflection on the loaded side of the crack or joint (mm).

In this study the LTE was obtained at joints and the values are tabulated in table 4.2.1. Most of the sites have an average site LTE exceeding the suggested 60 percent limit for medium and heavy truck traffic (Smith et al., 1990).

The LTE data show that there is greater variation in LTE values with lower average LTE for a project. This indicates that local joint phenomena are controlling the behavior. The key factors that affect LTE are faulting, spalling, pumping-erosion, crack width, and coarse aggregate type (e.g. Colley and Humphrey, 1967; Nowlen, 1968; Bruinsma et al., 1995; Abdel-Maksoud et al., 1998; and Buch et al., 2000).

One site worth noting is test section 06-I10, in California, where all LTE values were high (78 to 95 percent.) This concrete had very large gravel-like aggregates with a maximum size of 50 to 62 mm. The use of these aggregates would be expected to yield very high load transfer even at large joint openings (e.g. Colley and Humphrey, 1967; Nowlen, 1968; and Abdel-Maksoud et al., 1998).

In general, the LTE is low for the test sections where pumping erosion occurs and only aggregate interlock provides the shear load transfer. The experimental test road near Tracy with the three sections (06-7456 thicker slab, 06-CS1 control section, and 06-CS3 higher cement content) show that the 06-7456 had maintained high LTE compared to the other two sections. The loss of LTE on those sections is likely related to pumping erosion and faulting. However, when LTE is only determined at one point in time the values can only indicate an overall trend, as the coarse aggregate characteristics and the crack width also affect LTE.

The two undoweled Washington sections 53-3011 and 53-3019 on granular bases both have low average LTE of about 34 to 46 percent. However, these sections hardly developed any faulting. It is likely that the high subgrade stiffness and the good subsurface drainage prevented severe fault development in these sections. The subgrade CBR values were on the order of 57 to 83, see table 4.1.1. Table 4.1.2 shows that all joints had started to develop spalling, which is typical for joints with very low LTE.

The lower joint LTE values are associated with fracture through rather than around the coarse aggregates. See also figure 3.1.29. The high early strength in these concretes has likely contributed to the fracture of the coarse aggregates. In such cases, LTE is not improved by using larger size coarse aggregates.

The Iowa test section 19-3055 has also maintained very high joint load transfer (average 86 percent) through its 28 years of service life. This is remarkable since it is an undoweled JPCP's on granular bases over a foundation with relative low subgrade stiffness (CBR of 10). However, the excellent performance is likely due to the low traffic volume, and the avoidance of pumping-erosion and faulting. See figure 4.2.12.

Table 4.2.1 *Average load transfer and its variation along with key design and coarse aggregate information.*

Climate Region	LTPP		Aggregate Characteristics		Traffic (KESAL)	Base Type	Joint Load Transfer System	Load Transfer Efficiency (LTE)			
	State	Section	Max. Aggregate Size[1] (mm)	Type				Section Avg. (%)	Stan. Dev. (%)	Max. (%)	Min. (%)
DNF	06	3017	38.1	gravel (mix)	3900	CTB	Agg.	85	14	98	46
	06	3021	38.1	gravel (mafic)	5250	CTB	Agg.	37	13	59	14
	06	7456	38.1	gravel (mix)	16000	CTB	Agg.	84	NA	NA	NA
	06	CS1	38.1	gravel (mix)	16000	CTB	Agg.	43	15	82	27
	06	CS3	38.1	Gravel mix incl. dol.	16000	CTB	Agg.	56	13	79	39
	06	I-10	50-62	gravel (mix)	>16000[2]	CTB	Agg.	88	6	95	78
DF	53	3019	38.1	gravel (mafic)	6200	Granular	Agg.	46	23	83	23
WF	19	3006	25.4	dol. limestone	3975	CTB	Dowels	80	2	82	77
	19	3055	25.4	dol. limestone	4265	Granular	Agg.	85	1	86	83
	27	4054	25.4	dol. limestone	10700	Granular	Dowels	73	17	94	48
	39	3801	19.1	Grav.+dol. Limestone	4685	CTB	Dowels	67	12	100	58
	55	3008	38.1	dol. limestone	15220	Granular	Agg.	NA	NA	NA	NA
WNF	53	3011	25.4	gravel (mix)	8935	Granular	Agg.	34	20	73	12
	53	3812	38.1	gravel (mix)	12765	Granular	Agg.	NA	NA	NA	NA
	13	GA1-5	38.1	Granite/granodiorite	23025	CTB/ATB	Dowels	78	17	90	37

[1] Based on sieve analysis of thermally decomposed cores.

[2] Estimate

4.3 Transverse Cracking

4.3.1 Effect of Higher Cement Content on Transverse Cracking

Early transverse cracking occurred in the higher cement content section (06-CS3) of the experimental test project near Tracy, California. Caltrans distress surveys (Wells and Nokes, 1991) showed, that 42 percent of the slabs in the higher cement content (06-CS3) section were cracked within the first year after construction, while none of the other sections had developed cracking. Within this time period the project had carried a total of 2.34 million ESAL's. They suggested that slab cracking was due to factors such as thermal shrinkage and drying shrinkage combined with base restraint and/or late joint sawing. This is supported by findings of this study, where this concrete was found to have about 40 percent higher CTE, and estimated to have about 20 percent higher drying shrinkage as compared to the control concrete. This is because the relative volume of shrinking paste increased from 25 percent in the control section 06-CS1 to about 28 percent in section 06-CS3 due to 40 percent higher cement content. At the time of this investigation section 06-CS3 had developed 23 transverse cracks (72 percent) whereas 06-CS1 had developed only 7 cracks (21 percent) as seen from table 4.1.2. See section 5.8 for further discussion on drying shrinkage and CTE values.

4.3.2 Transverse Cracking of JPCP on CTB due to Pumping-Erosion

Upward curled/warped slabs and pumping erosion at joints lead to faulting, and result in uneven slab support. This in turn can cause transverse cracking (Wells and Noke, 1991). This has occurred for some of the test sections on the California experimental project, sections 06-CS1 and 06-CS3, mainly in the longer slabs (i.e. > 5.5 to 5.8 m (18 to 19 ft)). The exception is the thickened section 06-7456, which at the time of this investigation had not developed the associated transverse slab cracking despite the high amount of joint faulting. This is probably due to the greater bending resistance of this thicker section compared to the thinner control section. Figure 4.3.1 shows an overview site photo of the thickened test section, 06-7456. See also table 4.1.2.

Figure 4.3.1 *Overview of the experimental test road at Tracy. Thickened test section 06-7456 with low distress levels.*

4.3.3 Location of Transverse Cracking

For the experimental test road near Tracy, the transverse cracks develop closer to the leave side of the joint than to the approach side of the joint. The same crack pattern had developed in the Ohio test section 19-3006, which had an average joint spacing of 6.1 m. Figures 4.3.2 through 4.3.4 each show the distance to the transverse crack from the approach and leave joint for test sections 06-CS3, 06-I-10, and 19-3006, respectively. The cracks are closer to the leave joint consistent with a greater loss of support near the leave joint. Cracks are typically about 2 to 2.5 m from the leave joint. Figure 4.3.5 shows a typical example of the location of transverse crack for section 19-3006.

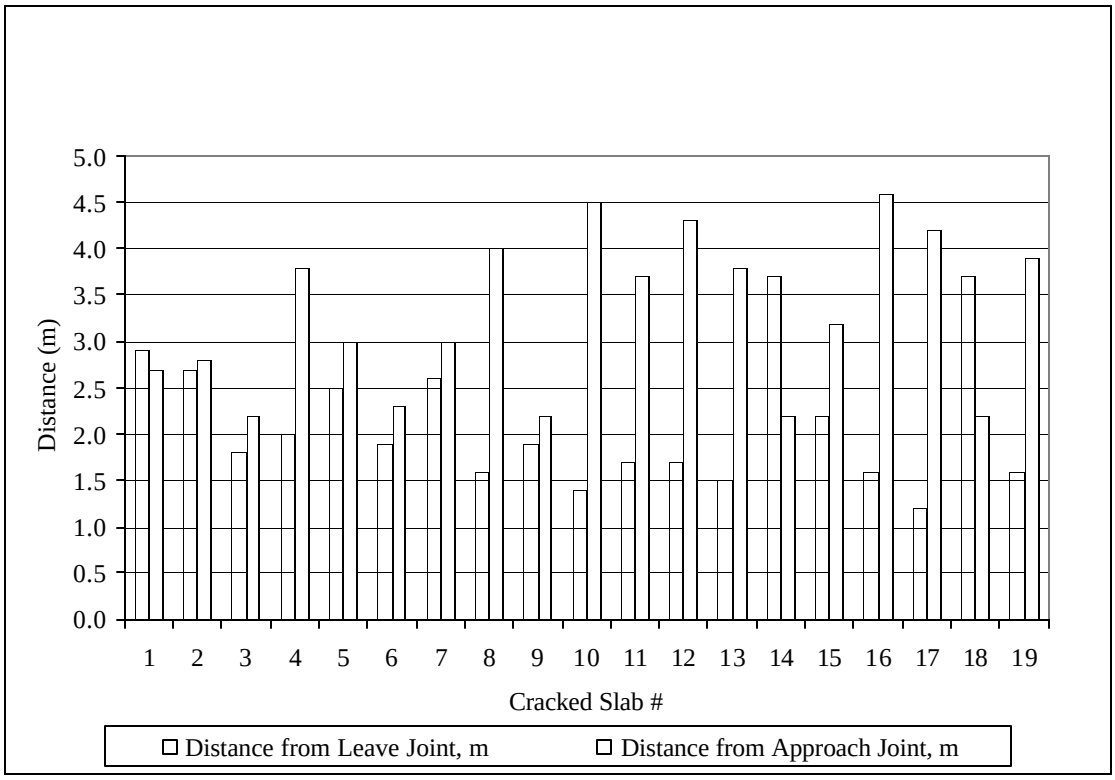

Figure 4.3.2 *Location of transverse cracks from joints for section 06-CS3.*

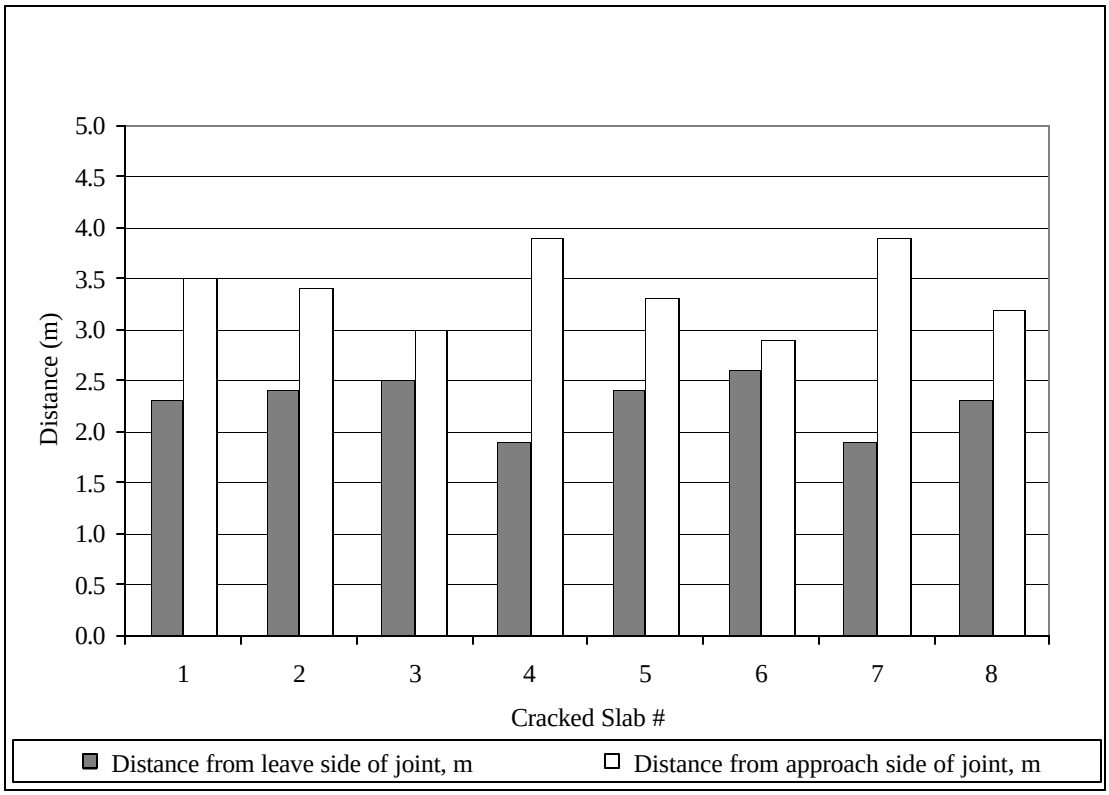

Figure 4.3.3 *Location of transverse cracks from joints for section 06-I10.*

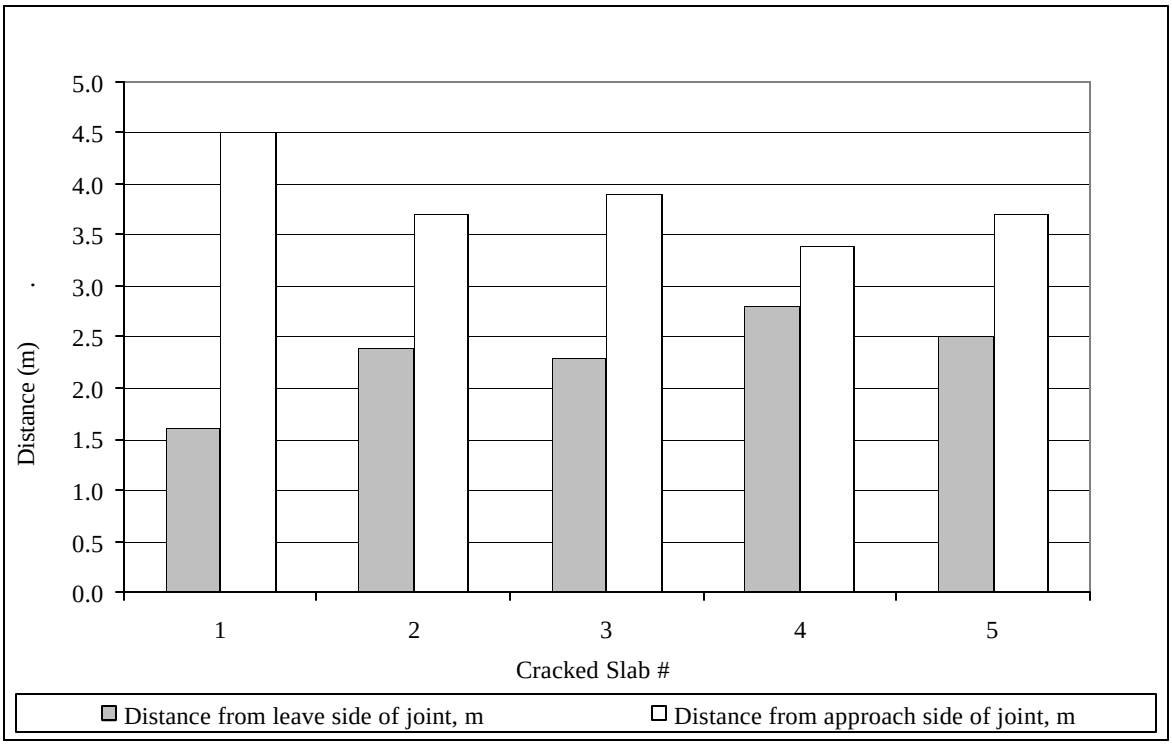

Figure 4.3.4 *Location of transverse cracks from joints for section 19-3006.*

Figure 4.3.5 *Transverse cracking closer to the leave joint for the Iowa section 19-3006.*

4.3.4 Extent of Loss of Joint Support in JPCP on CTB from FWD Testing.

Data obtained from falling weight deflectometer (FWD) testing can illustrate permanent loss of joint support. This is demonstrated in figures 4.3.6 through 4.3.8 for the California experimental test sections. The slab deflection profile was obtained for 40 kN

loading at 0.6 m (2 ft) intervals along the outer wheel path in the direction of traffic for two consecutive slabs.

The effect of intermittent loss of support on joint deflection from daily curling appear to be small, as surface heating of slabs did not change the joint deflection significantly. This is based on the fact that a wide range in surface temperatures occurred during FWD slab testing as seen from the recorded slab surface temperature data in figure 4.3.9.

Permanent loss of joint support increases joint deflection, causing a significant bending stress at the slab surface about 1.5 m to 2.0 m from the joint. This is in addition to the internal tensile stress from curling that will occur in the slab. The observed location of transverse cracking, as discussed, is consistent with these FWD slab deflection profiles. Large (200-250 µm) joint deflections were found in the three sections from the Tracy Test Road in California, consistent with loss of support. See figures 4.3.6-4.3.8.

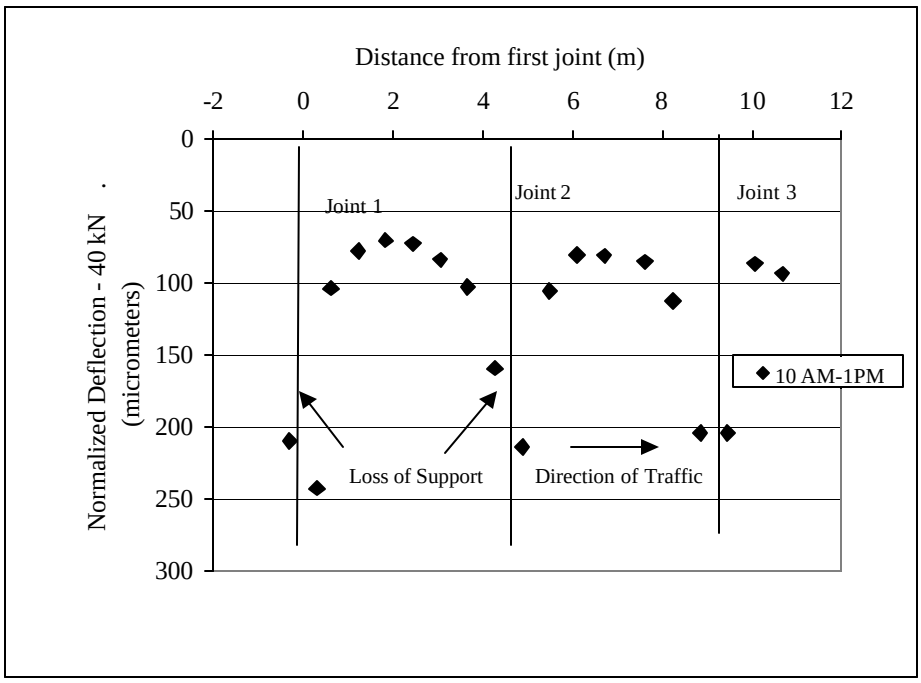

Figure 4.3.6 *FWD slab profile for two slabs on 06-7456 near Tracy (thickened slabs). (Increased edge deflections indicate loss of support.)*

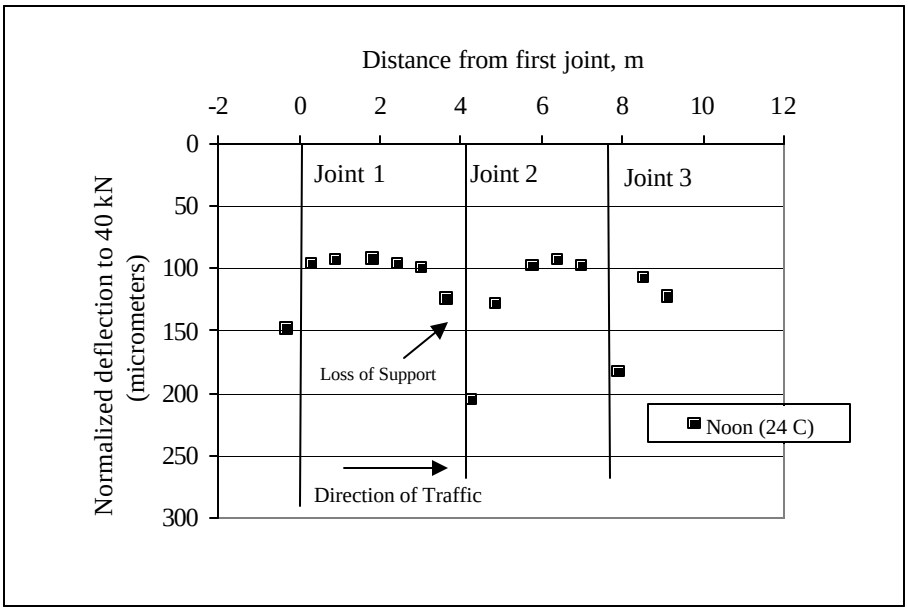

Figure 4.3.7 *FWD slab profile for two slabs on 06-CS1 near Tracy. (Increased edge deflections indicate loss of support.)*

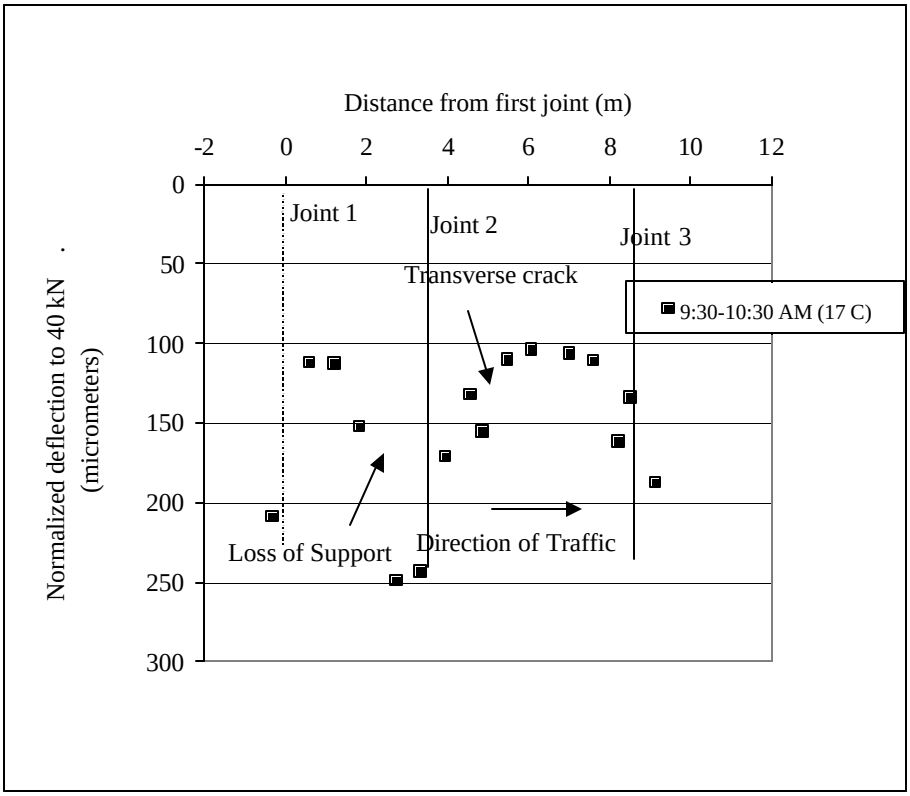

Figure 4.3.8 *FWD slab profile for two slabs on 06-CS3 near Tracy (higher cement content). (Increased edge deflections indicate loss of support.)*

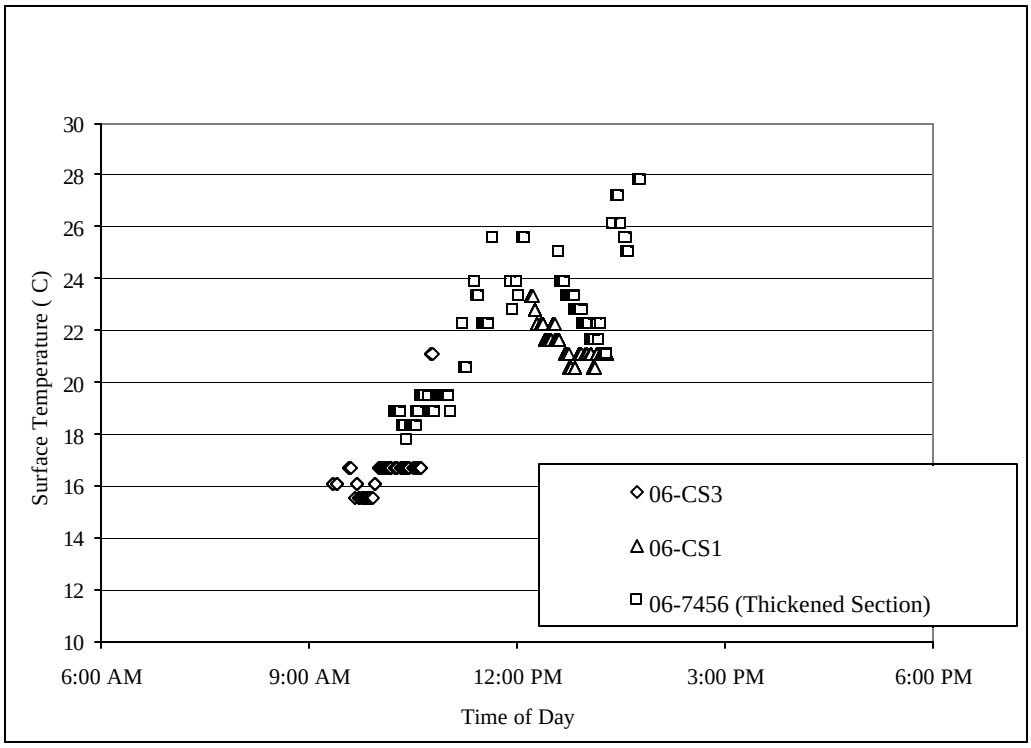

Figure 4.3.9 *Slab surface temperatures during FWD testing.*

4.3.5 When Pumping Erosion Does Not Develop

The relatively long 6.1 m (20 ft) normal strength JPCP slab design in Georgia supported on CTB/ATB has not developed appreciable faulting or any transverse cracking. Figure 4.3.10 shows an overview of the Georgia site.

Figure 4.3.10 *Overview of the Georgia test section, 13-GA 1-5.*

Surface profile measurements showed the slabs were not curved upward, and this is shown in figure 4.3.11. In this case the longer slab length of 6.1 m has performed well.

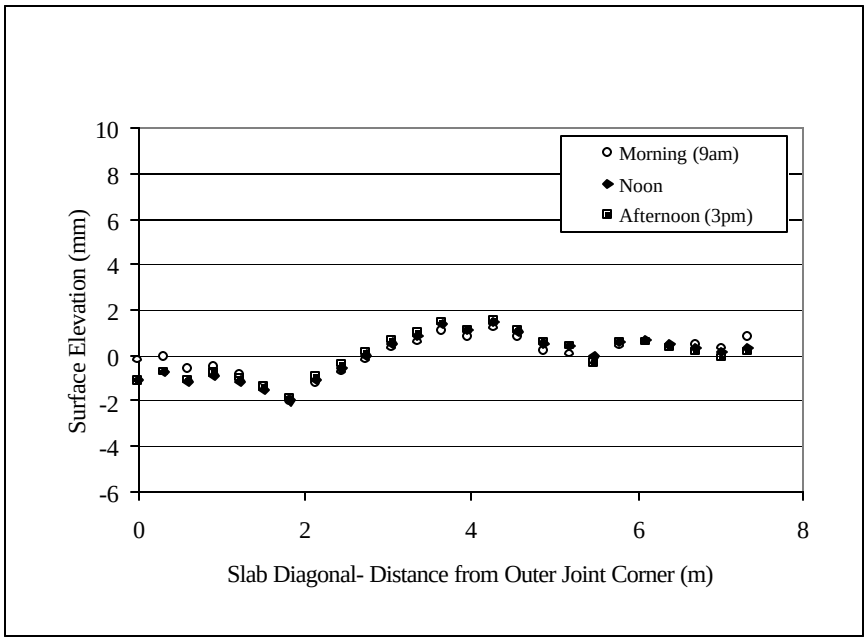

Figure 4.3.11 *Surface elevation profile for 13-GA1-5.*

The Iowa project 19-3055 and the Wisconsin section 55-3008 have overall the same foundation and joint characteristics. Yet, 19-3055 has not nearly developed the same amount of faulting. This is likely due to the much lower traffic volume. Furthermore, section 19-3055 is resting on a granular base with good subsurface drainage. Thus, pumping of fines is not expected. The section has gradually developed a slight permanent downward curvature at the joints as illustrated in figure 4.3.12. The figure shows Dipstick profiles for two 30-m sections for both outer and inner wheel paths. The PCC adapts to this shape without permanent loss of support or cracking. Figure 4.3.13 shows an overview of this test section.

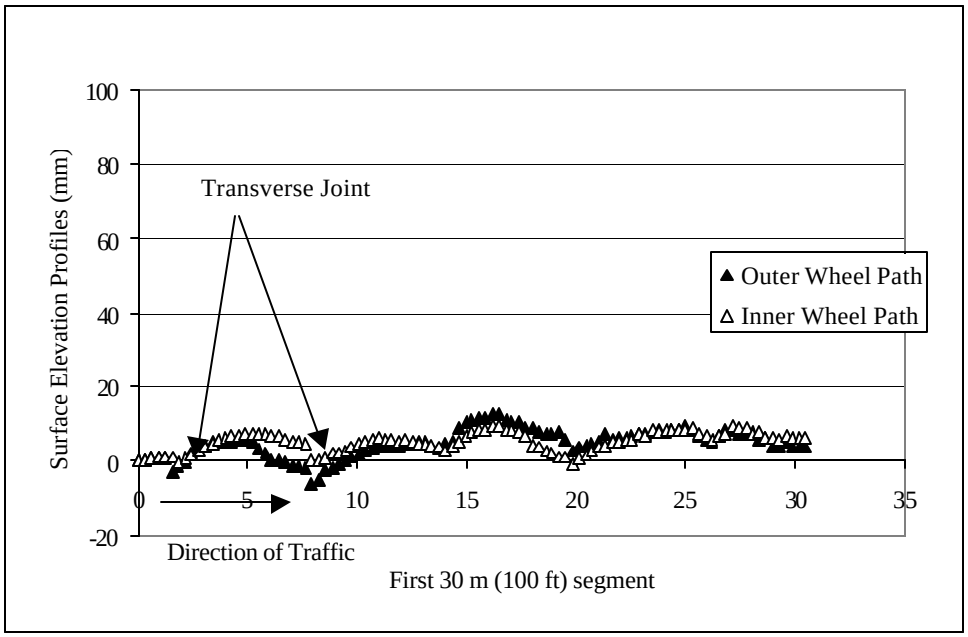

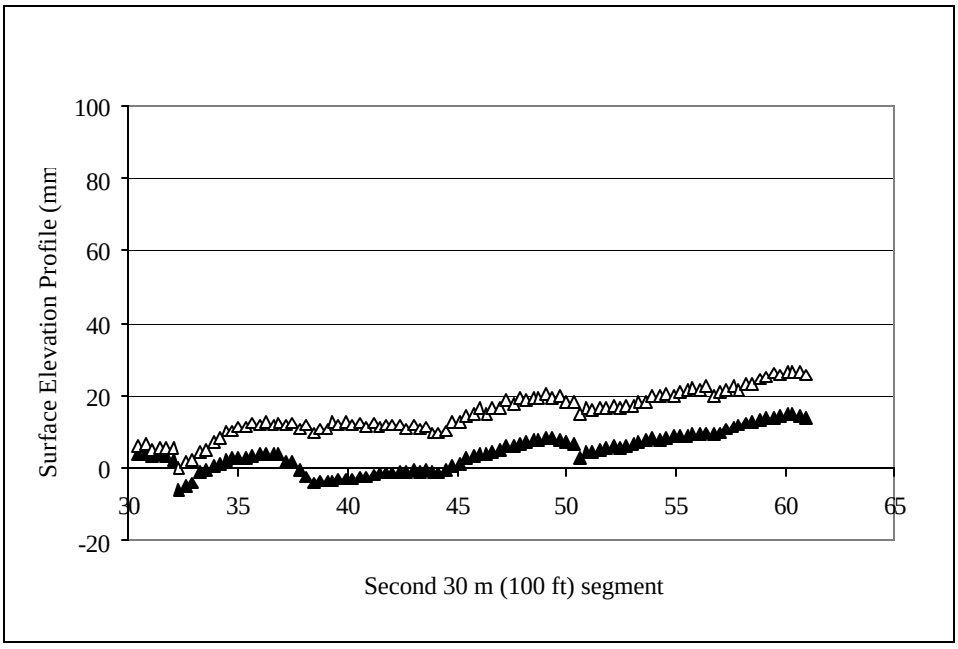

Figure 4.3.12 *Surface profiles for test section 19-3055.*

Figure 4.3.13 *Overview of test section 19-3055.*

4.4 Factors Affecting Joint Spalling

One test section was chosen for investigation because of its spalling deterioration. Section 19-3006 in Iowa has developed high severity joint spalling and is the highest spalling pavement in the LTPP GPS-3 database. It is also the most severely spalled of the pavement sections investigated in this study, as is illustrated in figure 4.4.1. It has also experienced transverse cracking from loss of slab support.

The type of distress observed in this test section is not typical. It is reminiscent of "D" cracking, but without the conventional surface patterns near the edges. Full depth and lane width cracking is observed running about 0.3 m (1 ft) parallel to each transverse joint on either side of the joint. This is illustrated in figure 4.4.2. Core sampling around the deteriorated joint areas, as seen in figure 4.4.3, shows that PCC deterioration started at the bottom of the slab, where high moisture conditions are prevalent.

The concrete itself has been exposed to a severe micro-environment near the joints (i.e. combined effects from prolonged high moisture content, deicing salts, freeze-thaw cycles and about 4 million ESAL's of traffic loading). The cores have a macroscopic crack pattern parallel to the surface as seen in figure 4.4.3.

The combined effects of pumping erosion from truck traffic, high moisture content at the joints due to poor drainage, and moisture warping over time have resulted in a permanently upward curved slab. The warping is especially pronounced at the approach joints. A detailed discussion of the mechanisms causing this type of joint distress is found in section 5.7.

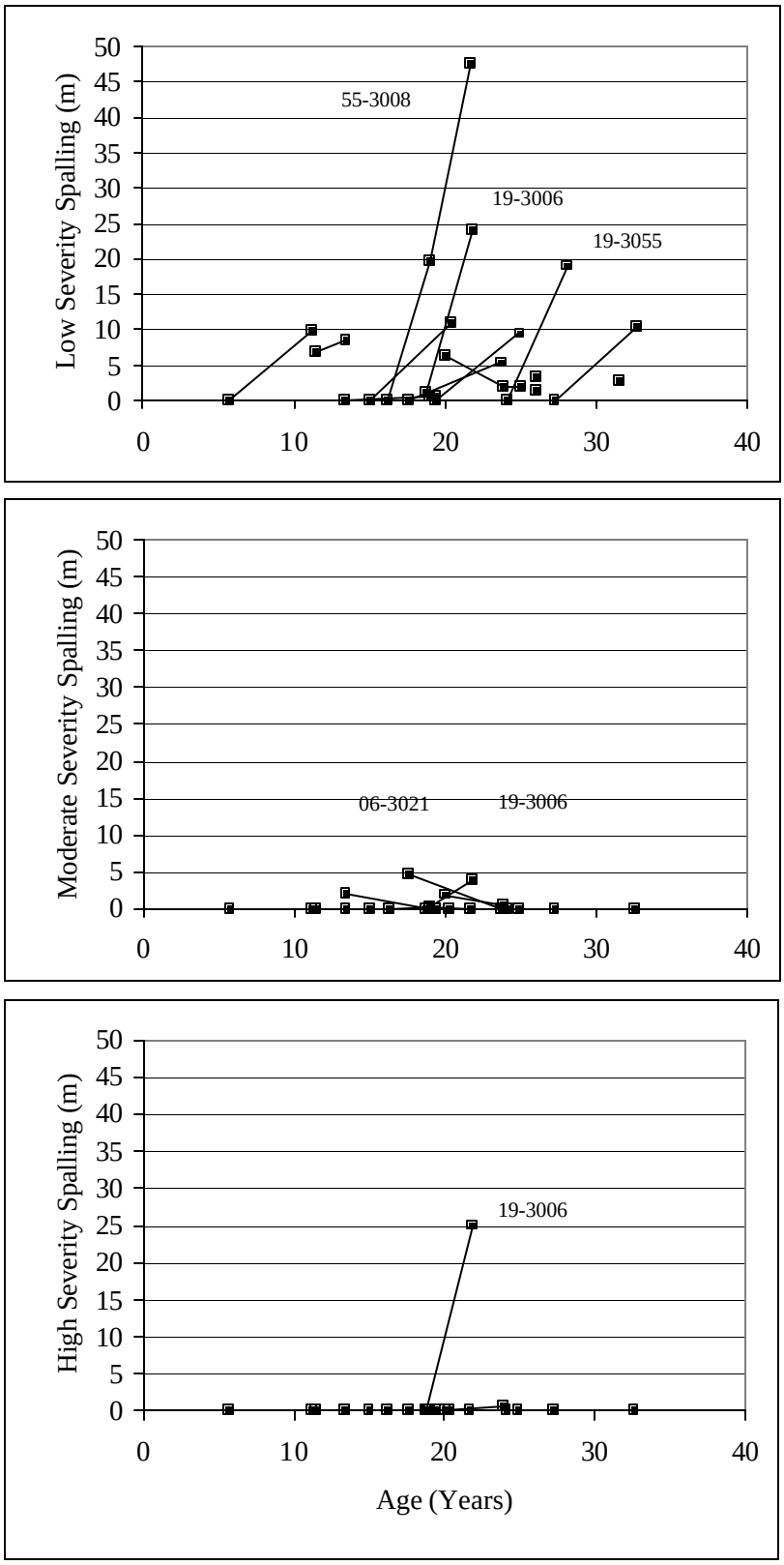

Figure 4.4.1 *Development of spalling over time for the investigated test sections. (Spalling is categorized as low, medium, and high severity.)*

Figure 4.4.2 *Spalling crack running parallel with the joint in a distance of about 0.3 m.*

Figures 4.4.3 *Close-up photos of joint deterioration from test section 19-3006.*

CHAPTER 5. CONCRETE PROPERTIES

5.1 Investigated Strength Range

As seen from figure 5.1.1 the LTPP sections in this study cover nearly the entire flexure and compressive strength range of JPCP's found in the LTPP database (GPS-3 in DataPave 97). The majority of the LTPP test sections have field compressive strength values between 30 and 70 MPa with a few exceptions, and flexural strength values between 4.5 and 7.0 MPa. It should be noted that the field flexural strength values have been estimated from the field splitting tensile strength values using the approximation used by Mahoney et. al. (1991).

$$f_m = 1.02 \cdot f_{sp} + 1.45 \qquad (5.1.1)$$

where f_m = flexural strength (MPa), and
f_{sp} = splitting tensile strength (MPa).

Of the 15 test sections, 11 are found in the LTPP database, of which 9 have strength values listed. Four of these projects were from the lower strength range around 5 MPa. Two projects were from the mid-range of 5.5 MPa, and three projects were selected from the upper strength range of 6.3 MPa.

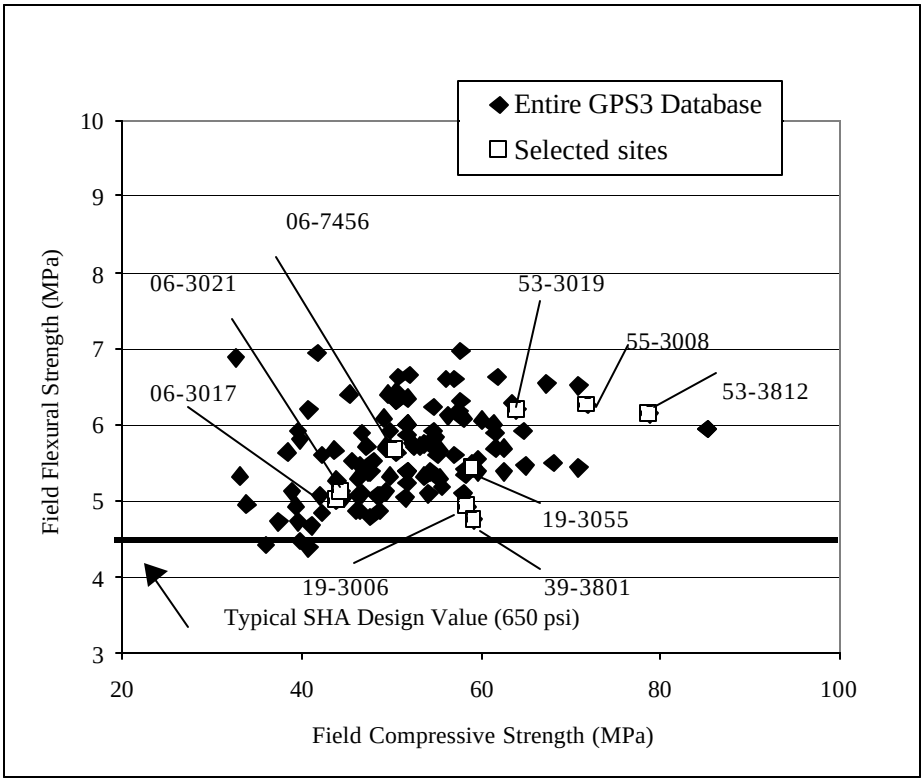

Figure 5.1.1 *Field flexural strength versus compressive strength for the test sections available in the LTPP database.*

5.1.1 Field and LTPP Comparison of PCC Mechanical Properties

In chapter 3, table 3.3.3 lists the average mechanical properties obtained in this study for the field concrete with respect to compressive strength, f_c; elastic modulus, E; and splitting tensile strength, f_{sp}. The LTPP database values are also listed. Overall, the test results for mechanical properties from this study and LTPP are in good agreement. However, the LTPP database does in general show higher f_c and f_{sp} values compared to the values obtained in this laboratory study, see chapter 3. This is likely related in part to the fact that the LTPP uses smaller specimen sizes of 100- by 200-mm cylinders. This study used 150- by 200- to 250-mm cylinders. According to the well-known Weibull effect, this difference in specimen size can account for a difference of 6 percent or higher.

For this laboratory study the average field concretes were about 25 years of age at time of testing. The test matrix ranges from 11 to 51 years old. The average compressive strength is 49 MPa, and ranges from 33 MPa for California section 06-3021, to 75 MPa for Washington section 53-3812. The average elastic modulus is 32,638 MPa, and ranges from 23,714 to 46,931 MPa (same sections as mentioned above). The average splitting tensile strength is 3.7 MPa and ranges from 2.8 to 4.5 MPa.

Figures 5.1.2a, b, and c show graphically the values for compressive strength, flexural strength, and elastic modulus obtained in this study compared to the values available in the LTPP database. As stated above, it is seen that there is overall good agreement with the LTPP database values.

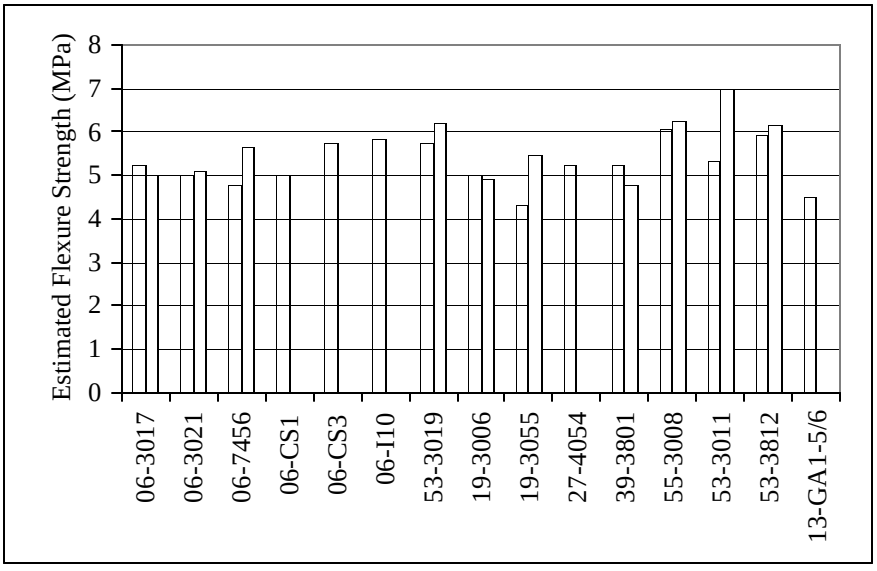

Figure 5.1.2a *Field flexural strength for this study and the LTPP database. (Shaded data bars are from this study, and the clear bars are from the LTPP database.)*

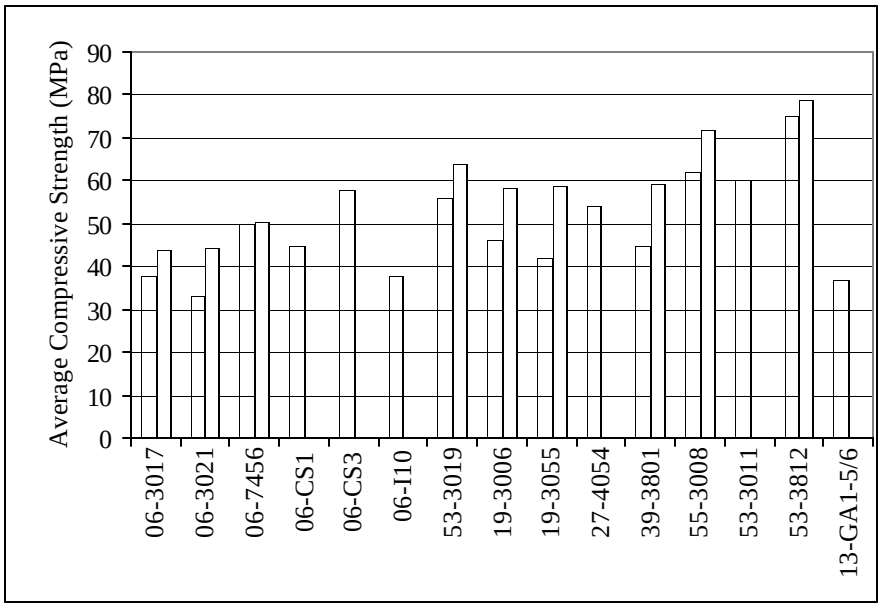

Figure 5.1.2b *Field compressive strengths for this study and the LTPP database (Shaded data bars are from this study, and the clear bars are from the LTPP database.)*

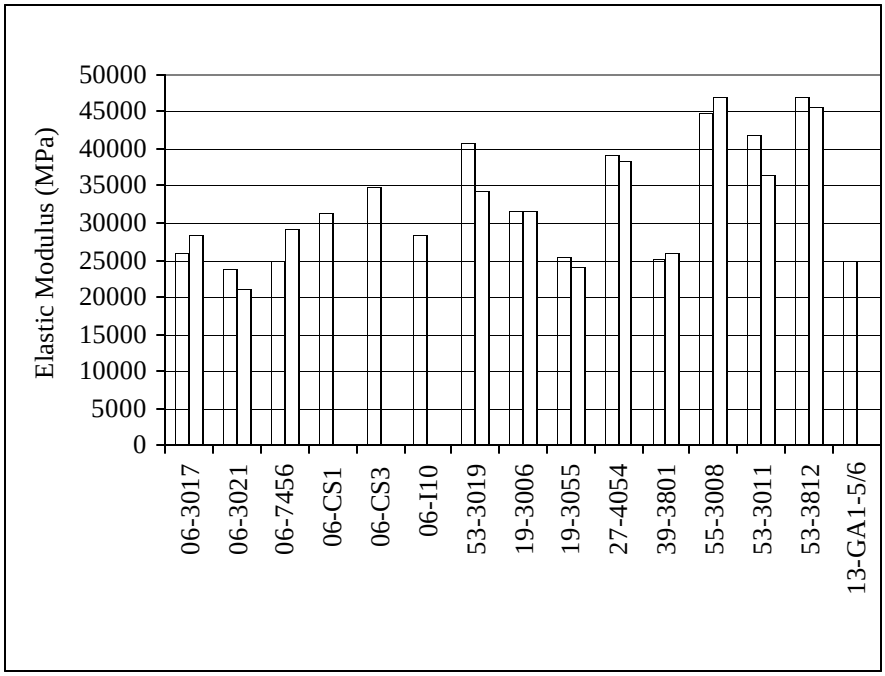

Figure 5.1.2c *Field elastic modulus for this study and the LTPP database. (Shaded data bars are from this study, and the clear bars are from the LTPP database.)*

5.1.2 Estimated Flexural Strength versus Compressive Strength for This Study

Most SHA's use compressive strength and flexural strength as their main PCC design requirements. Therefore, it is important to identify the relation between these two PCC parameters. Figure 5.1.3 shows the estimated flexural strength versus compressive

strength as obtained in this study. Six pavement projects were in the lower strength range with insitu flexural strength ranging between 4.3 MPa and 5.0 MPa. Four projects were close to the average strength of 5.26 MPa. Five projects were in the high-end range of 5.5 MPa to 6 MPa.

The compressive strength range varied between 33 MPa and 75 MPa. From these results it is apparent that the practical range for tensile strength used in fatigue-based design for plain concrete (i.e. without steel or fibers) is relatively narrow, spanning between 4.0 and 6.5 MPa. It is noteworthy that the investigated strength ranges for flexure as well as for compressive strength fall in the expected average range for these values when considering the ACI upper and lower-bound limits. A few exceptions were observed in the lower compressive strength range. In the lower range, a few sections were found to have very high flexure strength. In the upper strength range, when the field compressive strength increases above 60 MPa, it appears that the flexure strength has reached a threshold of approximately 6.5 MPa.

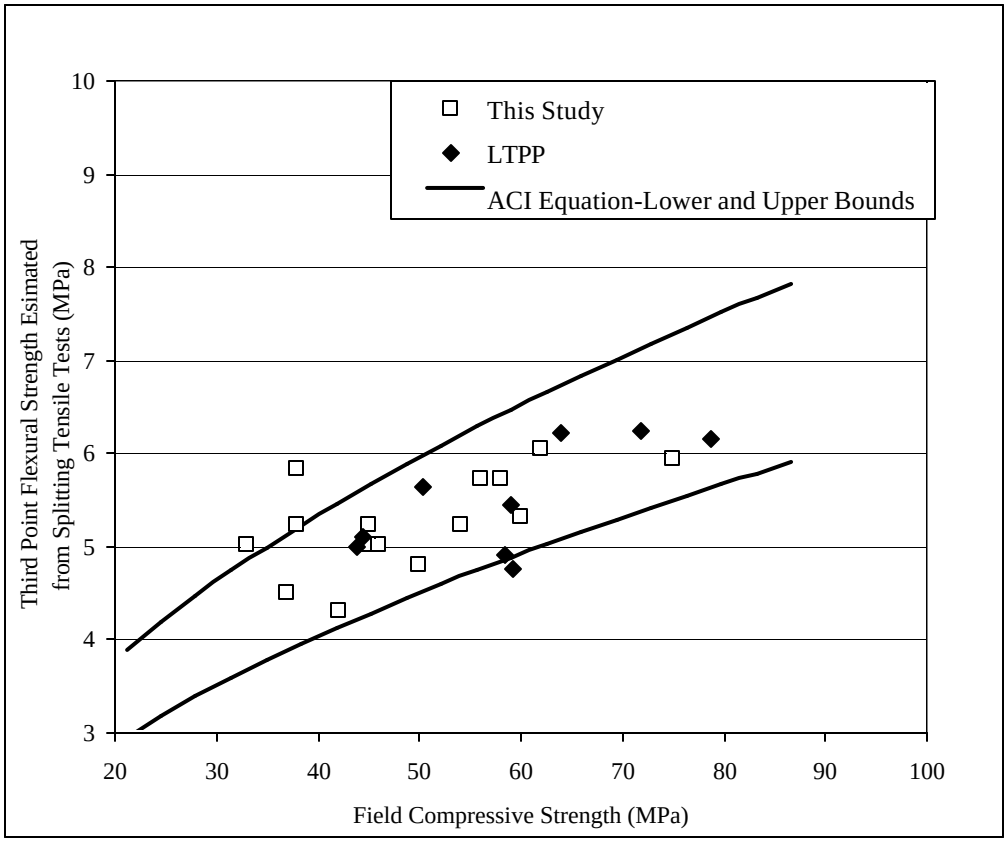

Figure 5.1.3 *Estimated field flexural strength versus field compressive strength for the 15 test sections in this study.*

The 15 different test sections have an average value of 5.26 MPa for their ultimate flexure strength. This corresponds to an estimated 28-day flexure strength of approximately 4.7 MPa, which is based on a well established rule of thumb that long-term tensile strength is about 10 percent higher than the 28-day strength. The average 28-

day flexure strength value agrees well with the 28-day flexure strength of 4.5 MPa used by most SHA's in the United States for pavement design. As discussed in chapter 4, this is an adequate limit for ensuring good long-term pavement performance.

5.1.3 Ultimate versus 28-day Design Compressive Strength

In order to evaluate the overall effect of increasing compressive strength on pavement performance it is necessary to have an estimate of the 28-day design value. The LTPP database does not contain these values for all test sections. Instead the 28-day strength value is evaluated using overall strength gain.

In order to make this estimation, the LTPP GPS-3 database was used to evaluate the increase in compressive strength of field concrete over the 28-day strength. A total of 37 of the LTPP GPS-3 sections had been in service for 10 years or longer, and had 28-day field as well as long-term data available. These results are shown as a density function in figure 5.1.4. The data fall into two normal distribution curves. The lower peak represents 12 concrete sections from climates other than the WF climatic zone. Their average strength gain was estimated to be 28 percent. The major peak shows an average of long-term strength gain of 68 percent. This peak represents 25 pavement sections from the WF climatic zone.

Using these averages, the 28-day compressive strength values can be estimated for the test sections in this study. The 28-day strengths of the two Washington State sections in the WNF climate were also estimated based on a 68-percent long-term strength gain because the curing environment in that region is nearly ideal. Based on the field compressive strength data, listed in tables 3.3.1 and 3.3.2, the estimated 28-day values for the test sections in this study range from about 24 MPa to 45 MPa. The JPCP's located in the dry regions fall in the lower end of the scale and the JPCP's in the wet regions fall in the higher end of the scale. These estimates indicate that the concretes used in these JPCP's all fall in the category of normal strength concrete using the definition of the American Concrete Institute (ACI). Based on figure 5.1.4, the concretes in WF and WNF regions have probably gained more compressive strength over time than the concrete pavements in the DNF climate such as in California.

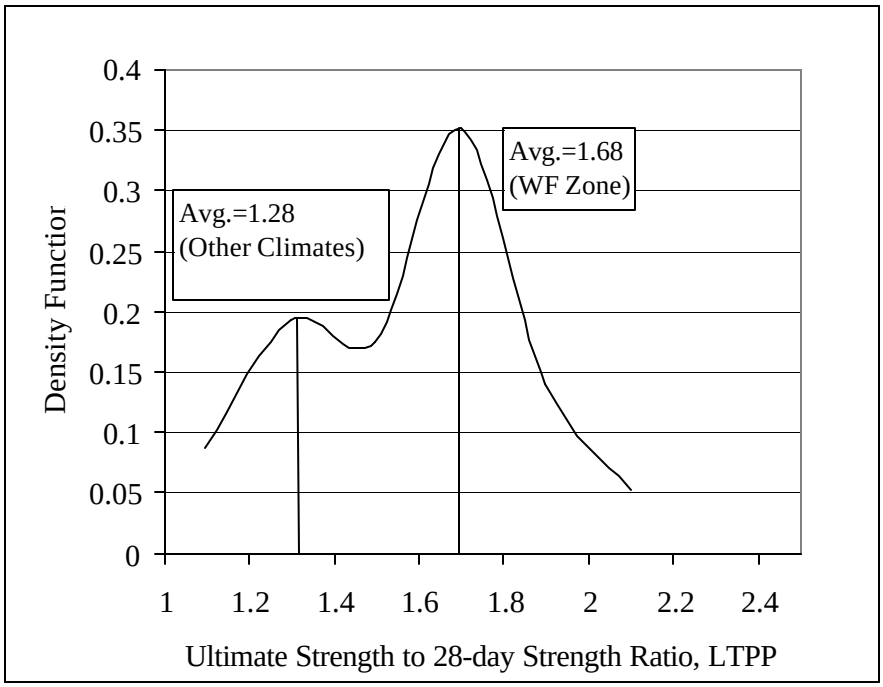

Figure 5.1.4 *Density function of the ultimate strength to 28-day strength ratio for data available in GPS-3 in the LTPP database. (DataPave 97.)*

5.2 Compressive Strength

Although compressive failure is extremely rare in the pavement structures, the compressive strength of concrete is perhaps the most comprehensive measure of concrete quality (Ahmad, 1994). Compressive strength is strongly related to the hydrated paste porosity. This is the reason behind considering the compressive strength to specify, control and evaluate the concrete quality. Although the mode of failure of concrete specimens under other loading schemes is quite different, many of these properties can be correlated to compressive strength.

Table 1.5.1 listed the PCC mix characteristics that were found to significantly affect the PCC compressive strength. They were w/c ratio, coarse aggregate characteristics, cement type and content, mineral additives, and air entrainment.

The results from this study confirm the influence of w/c ratio and the cement content on the PCC compressive strength. However, no correlation with coarse aggregate characteristics or air entrainment could be established. Because the studied pavements predate the common use of mineral additives, all contained only ordinary portland cement (OPC). Thus, it was not possible to evaluate the effect of mineral additives from the field study. The role of mix characteristics on concrete properties is discussed in detail in chapter 6.

5.3. Effect of Increasing Compressive Strength on the Splitting Tensile Strength

Tensile strength represents one of the most important mechanical properties of concrete as it relates to PCC's resistance to crack initiation. As discussed in chapters 1 and 4, the fatigue transverse cracking and corner breaks are directly related to the PCC tensile properties (e.g. flexural strength). If tensile stresses induced by wheel loading, environmental effects, or both, exceed the concrete tensile strength, cracks will form. PCC flexural strength is typically 25 percent higher than the PCC splitting tensile strength. The flexural strength and splitting tensile strength can be considered to be proportional with an initial offset of about 1.50 MPa as was described in section 5.1. This section discusses only splitting tensile strength as determined from the field cores in this study.

The relation between the compressive strength and the splitting tensile strength from this study is shown in figure 5.3.1. A good correlation is obtained between the field splitting tensile strength and the compressive strength, irrespective of air void characteristics. Note that a scatter band of 1 MPa is not uncommon even for field compressive strength values around 35 to 40 MPa. From this figure it is observed that the increase in the concrete compressive strength is not associated with an equal percentage increase in the splitting tensile strength. This is in agreement with the literature on this subject. As the compressive strength increases from 30 to 75 MPa (125-percent increase), the increase in tensile strength is limited to 2.8 to 4.4 MPa, which is only a 56-percent increase.

The fact that there is not an equal percentage increase in tensile strength with increasing compressive strength suggests that increasing the compressive strength for pavement applications beyond the conventional 28-day strength range of 24-28 MPa has limited benefit on increasing the splitting tensile strength. Figure 5.3.2 shows the ratio between the splitting tensile strength and the compressive strength versus the compressive strength. The strength ratio decreases as compressive strength increases and follows a power curve behavior. As is illustrated in the figure, the R^2 value is high at about 0.85. For compressive strengths of about 30 MPa the tensile strengths reach about 10 percent of the compressive strength value. However, for compressive strengths around 60 MPa the tensile strengths only reach about 7 percent of the compressive strength.

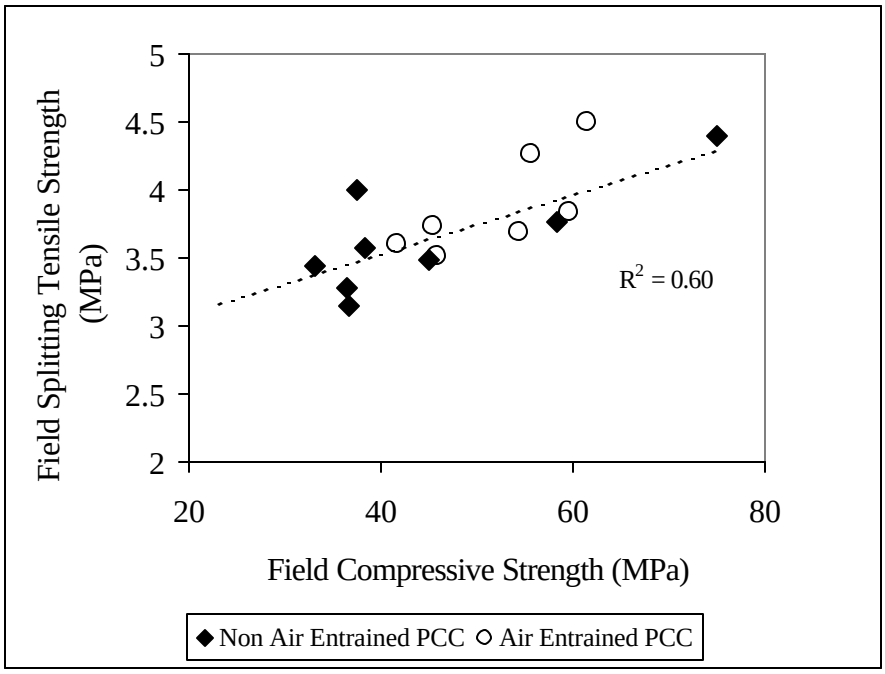

Figure 5.3.1 *Ultimate splitting tensile strength versus ultimate compressive strength for field specimens.*

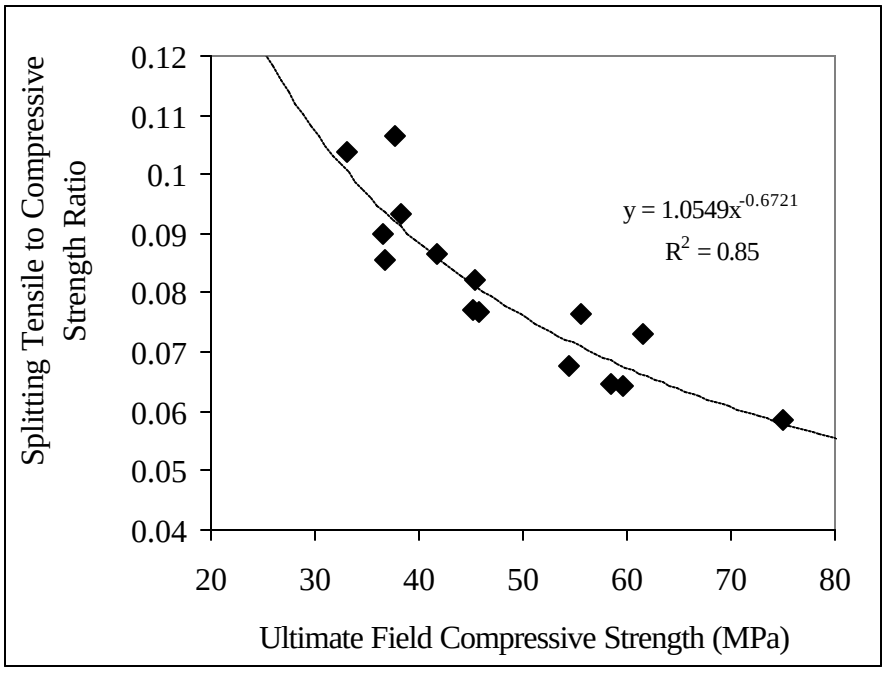

Figure 5.3.2 *Ratio of the splitting tensile strength and compressive strength versus the ultimate compressive strength.*

When compared to the results from this study, the LTPP database shows a much higher degree of scatter between splitting tensile and compressive strength for the same field concretes. This is illustrated in figure 5.3.3. The reasons are not clear, but may be

associated with the use of very different test specimen sizes. The LTPP database shows use of 100-mm by 75- to 200-mm samples according to DataPave 97. This study used 150-mm by 200- to 250-mm depending on the slab thickness. See also section 3.3.

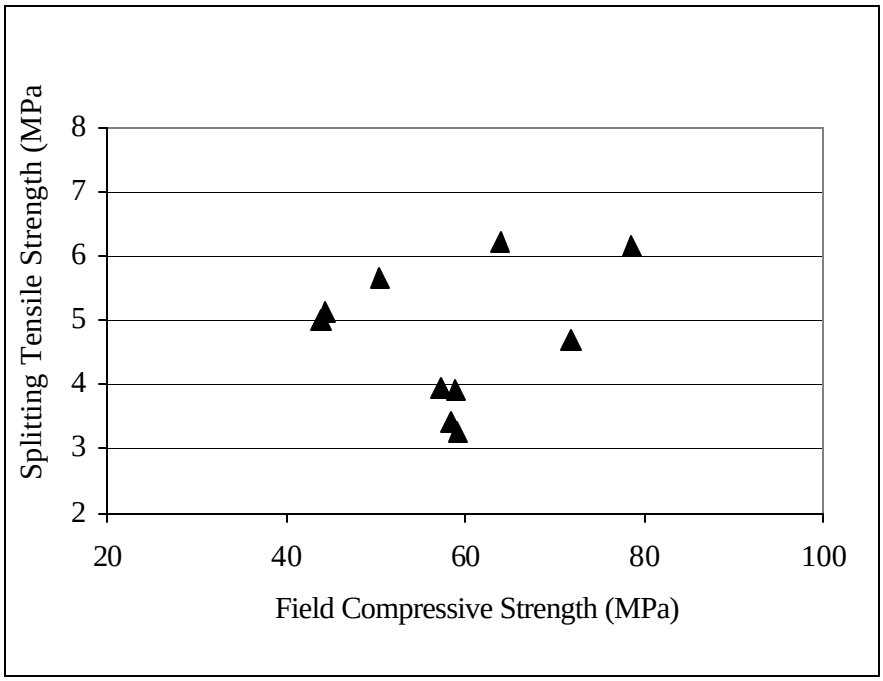

Figure 5.3.3 *LTPP database values for splitting tensile strength versus compressive strength for sections in this study.*

5.3.1 Prediction of Splitting Tensile Strength From Compressive Strength

The commonly used ACI equation for predicting the tensile strength, f_{sp}, as a function of the compressive strength, f'_c (ACI Committee 363, 1984), was found to slightly overestimate the splitting tensile strength of the field concretes from this study. This equation reads

$$f_{sp} = 0.59\sqrt{f'_c}\,. \qquad (5.3.1)$$

This indicates that the pavement designer should use such an equation with caution. As was indicated earlier, splitting tensile strength cannot fully be predicted by compressive strength, and general equations will only provide rough strength estimates. Actual laboratory tests should be conducted during the mix design process to ensure that desired tensile strength is obtained.

5.4. Effect of Increasing Strength on Elastic Modulus

Elastic modulus, E, of concrete has a pronounced effect on the pavement deformation and curling stress. As E increases, the pavement slab deformation due to wheel loading will

decrease. However, as discussed in chapter 4 the potential for increased curling stresses can not be ignored.

A strong correlation was obtained between long-term f_c and E as seen from figure 5.4.1. The same trend was obtained using the LTPP data for these same pavements, but again, as seen for f_{sp}, with a higher degree of scatter. See figure 5.4.2. The laboratory data from this study increases the confidence in the observed trend.

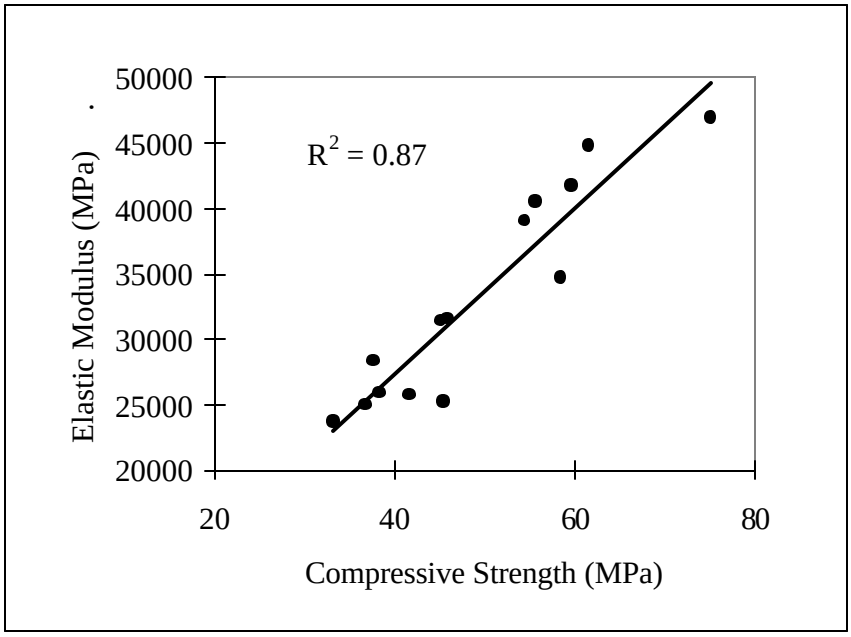

Figure 5.4.1 *Elastic modulus versus compressive strength for field samples.*

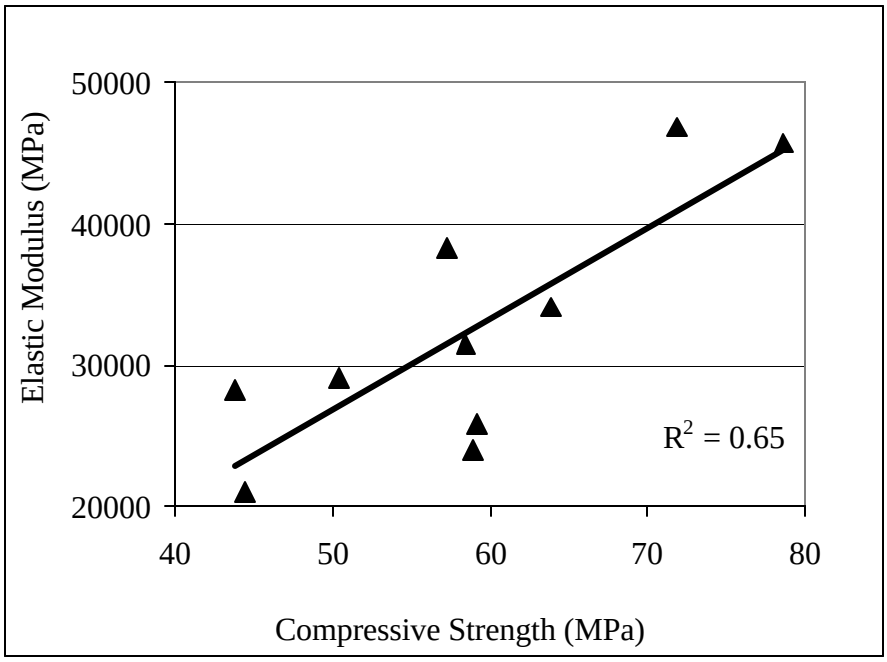

Figure 5.4.2 *Elastic modulus versus compressive strength. LTPP results on field concrete.*

5.4.1 Prediction of Elastic Modulus from Compressive Strength

If the E is predicted based on the ACI equation for normal strength concrete (ACI Committee 363, 1984), the elastic modulus is greatly underestimated for compressive strengths higher than 50 MPa. The ACI equation is written as:

$$E = 4733.6 \cdot f'_c \qquad (5.4.1)$$

It should be noted that this equation is based on 28-day data, which can be a part of the reason why the values are underestimated. It should also be noted the equation was developed based on a large database and there was a significant amount of scatter. As with tensile strength, it appears that E cannot be fully predicted from f'_c, and that the relationship is at least in part mix specific. This suggests that it is preferable to measure E on the design concrete, rather than predict it from a generalized equation.

5.4.2 Increasing Elastic Modulus and Splitting Tensile Strength

The expected relation was obtained between f_{sp} and E. Figure 5.4.3 shows that increasing tensile strength is related to increasing elastic modulus. As elastic modulus increases about 80 percent from 25,000 to 45,000 MPa, the splitting tensile strength only increases about 50 percent from 3.0 to 4.5 MPa.

For pavement applications this indicates that increasing the PCC resistance to fatigue crack initiation by increasing tensile strength significantly increases the PCC elastic modulus. This has a positive and a potentially negative effect on pavement performance as related to slab deformations and slab curling, respectively. This complex relation is discussed in chapter 4.

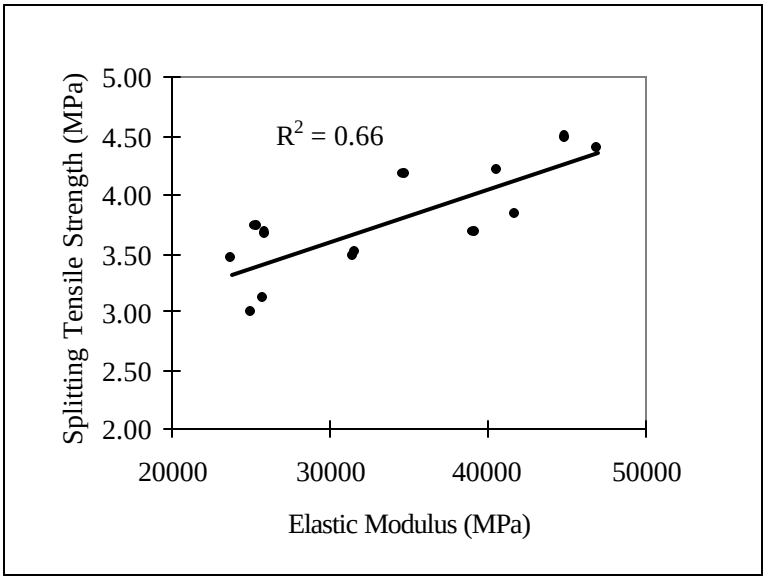

Figure 5.4.3 *Splitting tensile strength versus elastic modulus for field specimens.*

5.5 PCC Fracture Resistance

The PCC fracture behavior is another important characteristic to evaluate when investigating the effect of increasing PCC strength on pavement performance. Increasing the concrete flexure strength increases the concrete's resistance to crack initiation. However, the increased strength can also be detrimental for plain concrete as it may result in increased brittleness during fracture.

Evaluation of PCC brittleness requires measurements of the PCC fracture energy (G_F). Fracture energy was obtained from four California test sections. With help from Caltrans, large beams were obtained from the California test sections 06-3017, 06-3021, 06-I10, and 06-CS3. The tests were performed as described in chapter 2. Fracture energy cannot be determined for the other 11 sites in this study, for which field beams could not be obtained.

The ultimate PCC fracture properties obtained for the four California test sites are valuable. However, these properties alone cannot clarify what mix characteristics control fracture energy or what the effect of increasing strength is on the PCC fracture behavior. These gaps are addressed using results from an ongoing study at the University of Michigan, performed for the Michigan Department of Transportation, MDOT (Hansen and Jensen, 2000, and Jensen and Hansen, 2001). The ongoing study evaluates the effect of coarse aggregates on the PCC fracture behavior for typical pavement mixes.

5.5.1 Resistance to Crack Initiation

The most apparent improvement from increased PCC strength is the increased resistance to crack initiation. The resistance to crack initiation can be estimated for a given material using the linear elastic fracture mechanics concept of fracture toughness, K_I. Fracture toughness is determined from the peak load, and the specimen and load configuration. For a center-notched beam subjected to three-point bending, K_I can be calculated as:

$$K_I = \frac{2}{3} g(a) \cdot P \cdot l \cdot \frac{\sqrt{a}}{W \cdot h^2} \qquad (5.5.1)$$

where P = maximum load (N).
l = beam span (mm).
a = crack length (mm).
h = beam height outside the notch (mm).
W = beam width (mm).
$g(\alpha)$ = geometric factor depending on span-to-depth and notch-to-depth ratio. Expressions for $g(\alpha)$ can be found in fracture mechanics handbooks.

Figure 5.5.1 shows the effect of concrete matrix strengthening in terms of fracture toughness versus compressive strength. Generally, the fracture toughness increases about 50 percent when the compressive strength increases 100 percent. This is the same order of magnitude as observed for splitting tensile strength as discussed in section 5.3. The data shown here represents a large range of compressive strengths (20 to 60 MPa) from the field concretes in this study and normal strength concretes at different ages (7, 28 and

91 days) from the ongoing MDOT study. Note that the concrete from the Tracy experimental test road (test section 06-CS3) with higher cement content (418 kg cement per m^3) follows the same trend as the other concretes that contain 280 to 335 kg cement per m^3.

As the concrete matures, the matrix becomes stronger and the strength increases, resulting in increased resistance to crack initiation. This trend is observed for concretes containing rounded as well as crushed coarse aggregate. The only difference between the concretes is that the ones containing crushed aggregates tend to develop higher 7-day strength than the ones containing rounded aggregates. The improved early strength is likely due to the fact that crushed aggregates in general have improved matrix-to-aggregate bond over rounded aggregates. Thus, concretes containing crushed aggregates will typically have improved resistance to crack initiation at early age.

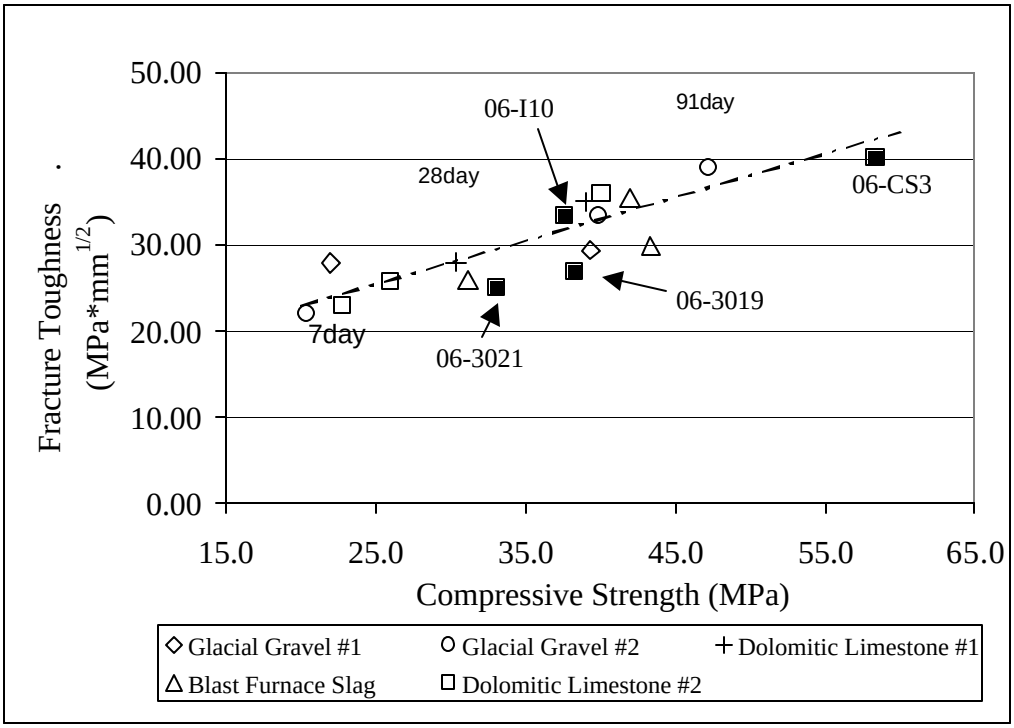

Figure 5.5.1 *Fracture toughness versus compressive strength based on data from this study and the Michigan study (965-mm span,204-mm height, 102-mm width, 102-mm notch).*

The concrete strength (compressive or flexure) depends largely on the strength of the mortar and on the interface bond between the mortar and aggregate. The PCC strength is also affected by the strength of the aggregate, but most normal weight aggregates have strengths much higher than the strength of the mortar with which they are used (e.g. normal strength concretes). However, considering the ACI committee report on high strength concrete, the PCC strength is limited by the strength of the coarse aggregates, as the bond between the matrix and the aggregates reaches an upper limit above which additional matrix strength would not increase the concrete strength (ACI 363R-7).

The coarse aggregate gradation also affects the PCC strength. It should be emphasized that in high strength concrete the maximum aggregate size is recommended to be kept at a minimum to obtain the optimum bond between the aggregates and the matrix. This makes it potentially more difficult to justify high strength concrete for highway pavements, as decreasing the maximum aggregate size tends to increase the PCC brittleness and the potential for low aggregate interlock at joints and cracks. However, if high quality aggregates are used (e.g. hard aggregates) the increased brittleness may be avoided. These aspects are discussed in the following sections. Of course aggregate durability to environmental attacks must also be considered, as will be discussed in chapter 6.

5.5.2 PCC Brittleness Models

Hillerborg (1983) defined a brittleness number, B, that considered the ratio of fracture energy over the elastic energy stored in a specimen at peak load. The brittleness number is based on the behavior of PCC subjected to uniaxial tension, and B is defined as

$$B = \frac{l_{ch}}{D} = \frac{EG_F}{f_t^2 D} \tag{5.5.2}$$

where l_{ch} = characteristic length (mm).
D = critical structural dimension (mm).
E = elastic modulus (MPa).
G_F = fracture energy (N/m).
f_t = tensile strength.

Carpinteri (1986) simplified the Hillerborg brittleness number to the energy brittleness number, s_e, defined as

$$s_e = \frac{G_F}{f_t D} \tag{5.5.3}$$

The consideration is that the PCC elastic modulus and the tensile strength increase at similar rates for increasing PCC strength. Based on these equations, it is of key importance to optimize a higher strength mix for maximum fracture energy.

5.5.3 Fracture Energy from Field Concretes

As mentioned earlier, fracture energy was obtained for four California test sections. Table 5.5.1 lists the key PCC properties representing the four sites. As discussed in chapter 3, the concretes were designed as normal strength concrete. However, due to their ages (20 years or older), they have matured and their in situ compressive strengths range from 33-58 MPa. The dominant coarse aggregate type for the four sections is gravel. The average fracture energy values range from 200 to 285 N/m for the four sections. Section 06-CS3 yields the highest value and section 06-3021 yields the lowest value. It is to be expected that the G_F value is highest for 06-CS3, when considering that the coarse aggregate type,

content, and maximum size are similar for the four California sections, and that this section has the highest compressive strength and the lowest w/c ratio.

The fracture energy values obtained in this study ranged in the high end of what is typically reported for concrete in the literature. This can be due to the larger size aggregates and well-developed bond between the coarse aggregate and the matrix (and for 06-CS3 due to high strength and lower w/c ratio).

Table 5.5.1 *Key ultimate PCC properties for the four investigated sections in California.*

LTPP Section ID	Age (Yrs)	Compressive Strength (MPa)	Splitting Tensile Strength (MPa)	Elastic Modulus (MPa)	Fracture Energy (N/m)
06-3017	19	38.3	3.68	25868	224
06-3021	24	33.1	3.46	23714	201
06-CS3	26	58.4	4.18	34679	284
06-I10	51	37.6	4.30	28321	230

5.5.4 PCC Brittleness and Fracture Energy

Recall from chapter 2 that the fracture energy is the work-of-fracture and is equal to the area under a complete load-deflection curve. It was stated above that the fracture energies from these field concretes were significantly higher than expected from results reported in the literature. Figure 5.5.2 shows the load-deflection curve from the California test section at Tracy that contains very large gravel-like aggregates (maximum aggregate size about 38 mm) and two concretes from the ongoing laboratory study containing glacial gravels and dolomitic limestone, respectively. The laboratory beams are 28 days old at testing. The field concrete yields the highest fracture energy and splitting tensile strength. However, considering equation 5.5.3, the field concrete is less brittle than the laboratory concrete containing dolomitic limestone, but only slightly more brittle than the laboratory beam containing glacial gravel.

This can also be illustrated by plotting the fracture energy versus splitting tensile strength. Figure 5.5.3 shows this for the four field concretes and for several laboratory concretes. The mixes are all normal strength concrete pavements where the main difference is the coarse aggregate type.

The straight line in the plot represents an equilibrium brittleness line. The line was generated based on the laboratory concretes containing glacial gravel using equation 5.5.3. Using this equilibrium line, it is clear that the old field concretes exhibit excellent fracture behavior not only in terms of fracture energy, but also in terms of relative brittleness.

Fracture energy plotted versus the compressive strength does not show a similar clear picture of brittleness. The reason is that the fracture energy is related to a PCC tensile failure and not a compressive failure. The excellent fracture behavior of these old field

concretes is due to the use of very hard gravel-like coarse aggregate that over time have developed excellent bond to the concrete matrix. The aggregates serve as crack obstacles, where the crack either will penetrate the aggregate at a given load or will be forced to propagate around the aggregate.

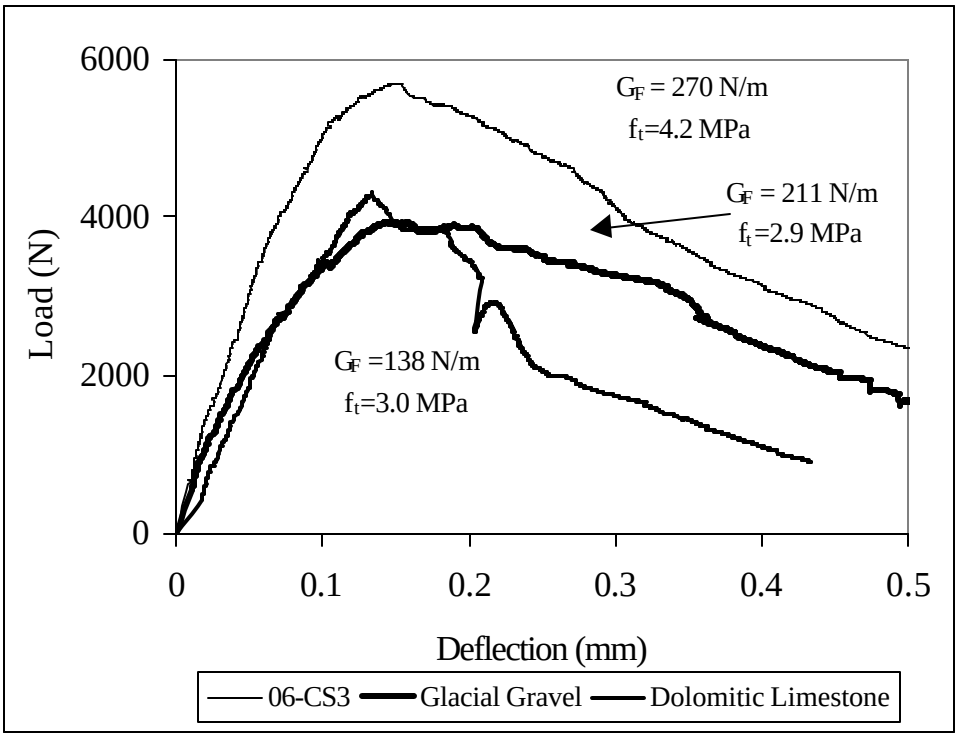

Figure 5.5.2 *Load versus deflection for laboratory and field concretes of same dimensions.*

It is commonly believed that cracks penetrate the coarse aggregate in cases where the properties at the interface, the zone between the coarse aggregate and the matrix, are close to the matrix properties, as in high strength concrete (ACI 363R-7). However, experimental and numerical results reported in the literature show that the phenomenon of crack patterns through or around the aggregates is more complex (e.g. Vervuurt, 1997; and Mohamed and Hansen, 1999). Results show that for increasing interface-to-matrix strength ratio (approaching 1) the specimen peak tensile capacity increases, keeping all aggregate and matrix properties the same. At the same time, it was shown for interface-to-matrix strength ratios approaching 1, that the crack penetrates the coarse aggregates when the aggregate tensile strength is lower than that of the matrix. This occurs irrespective of the fracture energy ratio between the aggregate and the matrix. Yet, the overall specimen 'toughness' increases when aggregate-to-matrix fracture energy ratio increases. Furthermore, in the cases where the tensile strength of the aggregate equals the strength of the matrix, the fracture energy ratio between the aggregate and the matrix is the dominating factor for whether or not the crack penetrates the aggregates. For ratios lower than 1, cracks will penetrate the aggregates, and for ratios higher than 1 the crack will not penetrate the aggregates.

This discussion magnifies the importance of selecting high quality aggregates if higher strength concrete is used in pavement design.

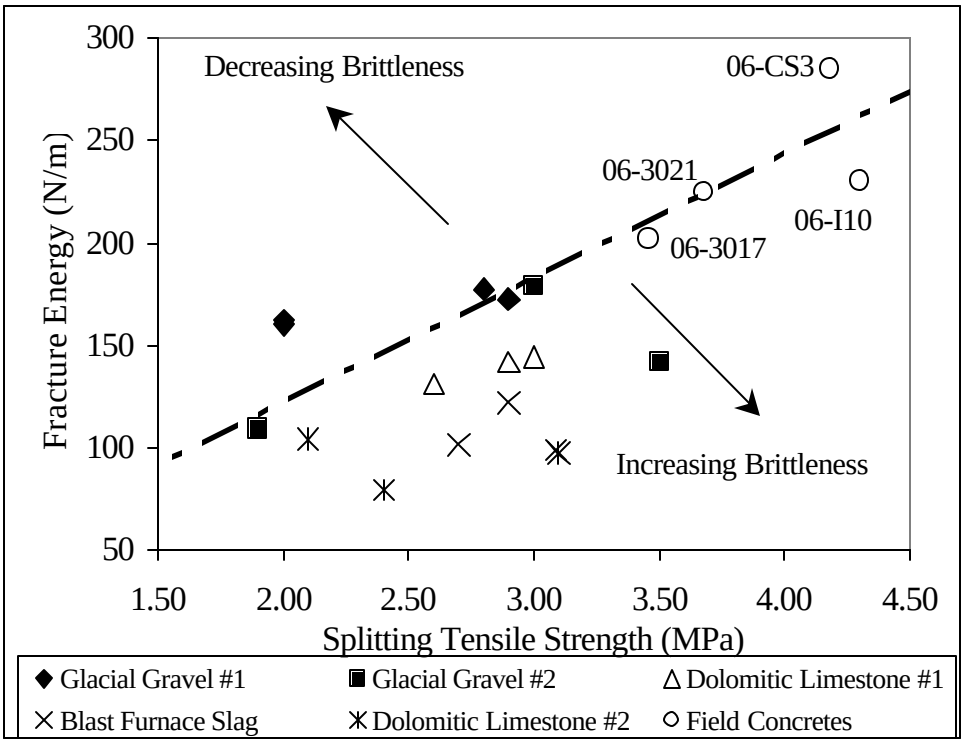

Figure 5.5.3 *Fracture energy versus splitting tensile strength.*

Figure 5.5.3 also shows that the resistance to cracking described by G_F varies greatly, which is related to the coarse aggregate fracture properties. The five aggregates used in the laboratory study yielded 28-day G_F values ranging from 80-170 N/mm, which is an increase of 100 percent from the "softest" aggregate sources to the "hardest" sources. It is also important to emphasize that f_c, E, and f_{sp} were very similar for these mixes. The average bulk properties at 28 days were: f_c = 39 MPa, f_{sp} = 2.9 MPa, and E = 31,000 MPa. In the ongoing study it was found that aggregates' Los Angeles abrasion values were inversely related to G_F for the same strength mixes.

In addition, it appears that fracture energy is in general independent of the PCC's strength level in the age range of 7, 28, and 91 days. However, for increased PCC tensile strength, as seen for the field concretes, it appears that the fracture energy does increase with strength. This suggests that the PCC tensile strength reaches a level where the bond between the aggregates and the matrix becomes increasingly important to the absolute fracture energy.

This shows that for normal strength concrete as designed for highway pavements, the fracture energy property is controlled by the coarse aggregate at early ages, and that as the concrete matures, the effect of the aggregate-to-matrix bond becomes increasingly important. This is in part due to the very high coarse aggregate content in highway mixes

compared to regular structural concrete mixes. Hence, G_F is an important concrete property and it is a quantitative measure of the energy absorbed during crack propagation.

In the Michigan study it was observed that increasing the maximum aggregate size from 25 mm to 38 mm for a glacial gravel and a dolomitic limestone introduced a 10- to 15-percent increase in G_F (at 28 days). It is apparent that increasing the coarse aggregate size improves the concrete resistance to crack propagation. However, the effect is less significant compared to the improvement achievable from selecting another aggregate source. This is in agreement with literature as discussed in chapter 1.

Visual evaluation of the fractured beams clarifies why a concrete containing one type of coarse aggregate yields a higher G_F value than another type. A qualitative relation was observed between the crack path roughness and G_F for the laboratory beams. The crack path for concrete containing glacial gravel is very rough and the majority of the coarse aggregates remain intact. This type of crack path generates large G_F values. The crack path for concrete with the dolomitic limestone or blast furnace slag showed smooth and straight-line crack path with a high percentage of fractured aggregates. For a same strength mix, this type of crack path generates low G_F values.

5.6 Effect of Higher Strength on Concrete Transport Properties

The purpose of determining the transport properties in this study is to investigate relationships between the higher strength and its added resistance to physical and chemical deterioration as measured by a variety of transport property tests. These results will be used to develop recommendations for the desired transport property levels needed for good performance, by either direct measurement or by association with a typically measured property such as compressive strength.

Permeability is generally considered the property which best characterizes the resistance of concrete to deterioration (Schonlin and Hilsdorf, 1988). Thus permeability can be an indicator of long-term durability (i.e. performance) of the concrete at joints, cracks and free edges, where exposure conditions to moisture and deicers are more severe. The literature review and evaluation of the LTPP database also indicate that concrete transport properties like permeability and diffusivity play important roles in spalling.

Permeability and diffusivity are distinguished in that the former measures of the movement of a fluid through the concrete, while the latter measures the diffusion of chemical ions through the concrete. These properties are similar enough in mechanism that they are often (though incorrectly) used interchangeably, such as the Rapid Chloride Permeability Test (RCPT), which is actually an index test relating to chloride ion diffusion. In this report the distinction will be drawn where it is critical to understanding the experimental results.

In view of the varied transport properties governing the durability of concrete with regard to chemical and physical deterioration (Bentz, et al. 1999) different permeability tests were used in this study. They include the RCPT, which is a measure of the concrete's resistance to ionic diffusion of chlorides. Water permeability was determined using the Florida Field Permeability Test. Air permeability was determined using the Torrent Air Permeability Test. The resistance of PCC to water uptake from capillary forces was investigated from the water absorptivity test method. These test methods are described in greater detail in section 2.4.3.

Most deterioration mechanisms are associated with prolonged exposure to high moisture levels, which exist primarily at joints and cracks. Therefore climatic factors, such as annual precipitation, number of freeze-thaw cycles, and subsurface drainage conditions are important, as they control the severity of exposure and the exposure duration. Consequently PCC in the WF climate would be expected to benefit the most from lower permeability. However, irrespective of climate, resistance to ASR or ACR as an example, would be improved with lower permeability as well.

In this investigation, the 15 studied pavements span a wide range in strength and permeability. All have typical mix designs for pavements, and none contain mineral additives. While these studied pavements represent only a minute fraction of in service pavements, they do provide significant clues to permeability's importance.

5.6.1 Effect of Higher Strength on PCC Transport Properties

Concrete compressive strength and elastic modulus were the only two PCC properties found to correlate well with permeability. Both of these mechanical properties correlate to the pore characteristics of the hardened paste (i.e. capillary porosity, pore size, and the pore connectivity) (Hearn et al., 1994; Garboczi, 1990). Shown below in figures 5.6.1-5.6.4 are the results and best fit curves with compressive strength for the different transport property test methods. Other researchers have reported similar relations using the RCPT method (Armaghani, et al., 1992).

It can be seen from these results that the resistance to physical and chemical deterioration improves dramatically with increasing strength and that the strength range from lower strength (33 MPa) to high strength (75 MPa) covers three to four permeability classes ranging from high to very low. These classes are commonly accepted for the rapid chloride, water and air permeability methods. Thus for highway concrete the compressive strength is a good indicator of permeability level. This is significant as PCC mixes can be designed for a permeability level based on compressive strength versus w/c ratio relations at different times. This is illustrated in figure 6.2.1. for results of long-term compressive strength versus w/c ratio from the test sections in this study.

RCPT

In figure 5.6.1, the chloride penetration resistance (RCPT result) vs. compressive strength relation is plotted for the field specimens. In this figure the average compressive strength for each test section is plotted against average RCPT results for each section.

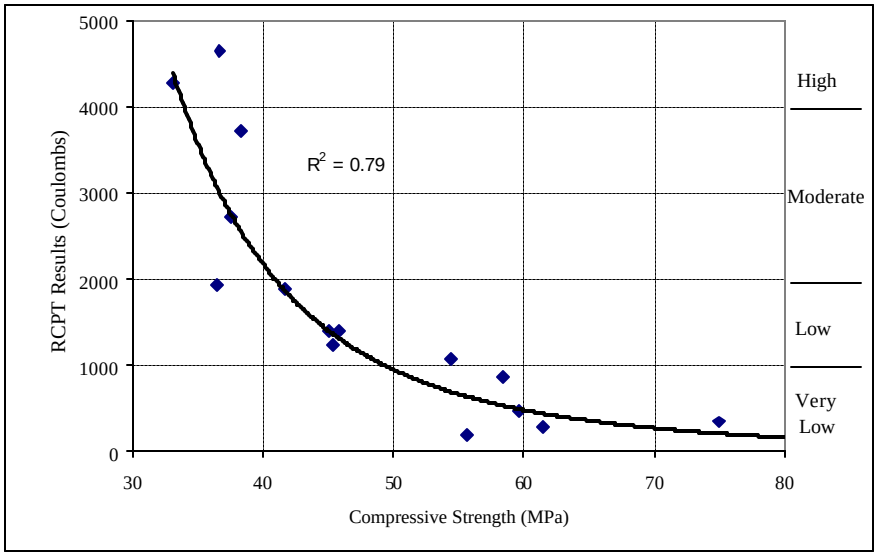

Figure 5.6.1. *Long term RCPT results versus compressive strength relation for pavement concretes from field study.*

A power law regression fit of the data yields a strong correlation (R^2 = 0.79). The RCPT results suggest that compressive strength can be used as a predictive measure for chloride diffusivity or permeability of OPC pavement concretes. Specifically, it is seen that

RCPT results can be greatly reduced with moderate increases in strength. By moving from 35 to 45 MPa compressive strength, the RCPT results can be expected to decrease from over 4000 to under 2000 coulombs (a drop of two RCPT classes). At high strength, however, the benefits to chloride penetration resistance are less pronounced. The RCPT result decrease above 60 MPa is minor. This is important in several ways, primarily for economic reasons, as increased strength is usually associated with increased cost. In addition, these high strength levels can lead to negative effects on other concrete properties, such as increased brittleness, high early (autogeneous) shrinkage and greater thermal deformations at early ages.

A similar permeability trend was found by Armaghani et al. (1992). They also noted the tight relation at higher strength and lower RCPT results, with increasing scatter at the lower strength end of the relation. Shilstone et al. (1992) also found a strong relation between strength and permeability, indicating that both high strength and low permeability were needed to ensure good performance.

The RCPT is criticized for the fact that high chloride penetration samples tend to heat up during the 6-h test duration. High RCPT samples such as the Georgia and some of the California sections were found to heat up by as much as 30^{o}C or more during the test. That heating is believed by some scientists to alter the testing conditions, causing an overestimation of the amount of charge that would be passed if the temperature had remained constant. Recently, however, researchers have been suggesting the use of initial current measurements can accurately predict the charge passed after 6 hours. Indeed, when the initial current data from this study's samples is plotted against the 6-h charge values, a straight line correlation with an R^2 value of 0.98 is observed, as seen in figure 5.6.2. Similar correlations have been shown by other researchers for both normal and high strength concretes (eg. Aldea et al., 1999). This indicates that the heating of the samples during the test does not significantly change the results. Furthermore, the use of initial current readings as opposed to measuring 6-h charge passing appears to be a credible modification to the RCPT method

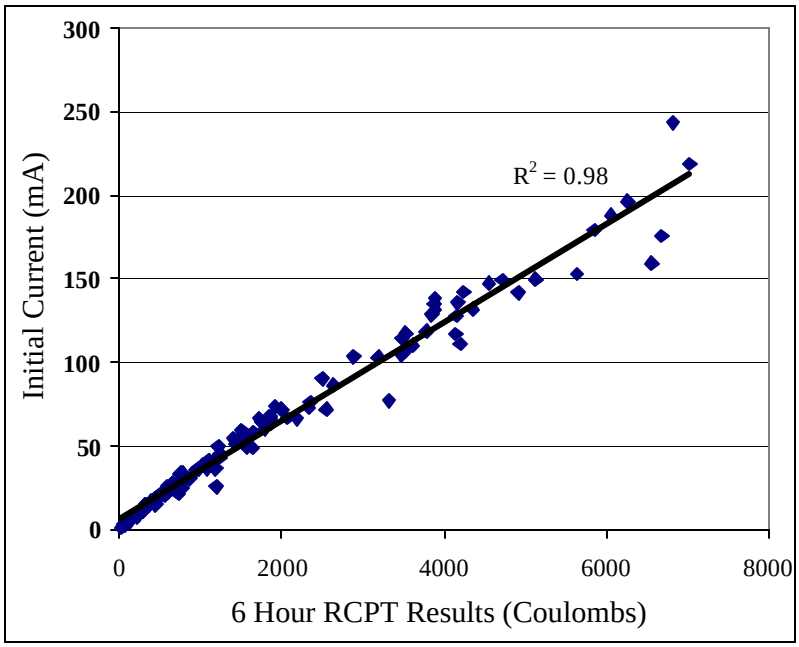

Figure 5.6.2 *Initial current values versus 6-h charge passed using the RCPT method.*

Water Permeability

Water permeability is measured at two depths in the concrete, once near the top surface, and once closer to the bottom surface, as has been described earlier. As with air permeability and chloride penetration resistance, a good correlation is seen with field compressive strength ($R^2 = 0.73$). In figure 5.6.3, water permeability at the top of the concrete is shown versus compressive strength. As before, the compressive strength is averaged over the entire concrete thickness. All values plotted are averages for each pavement section.

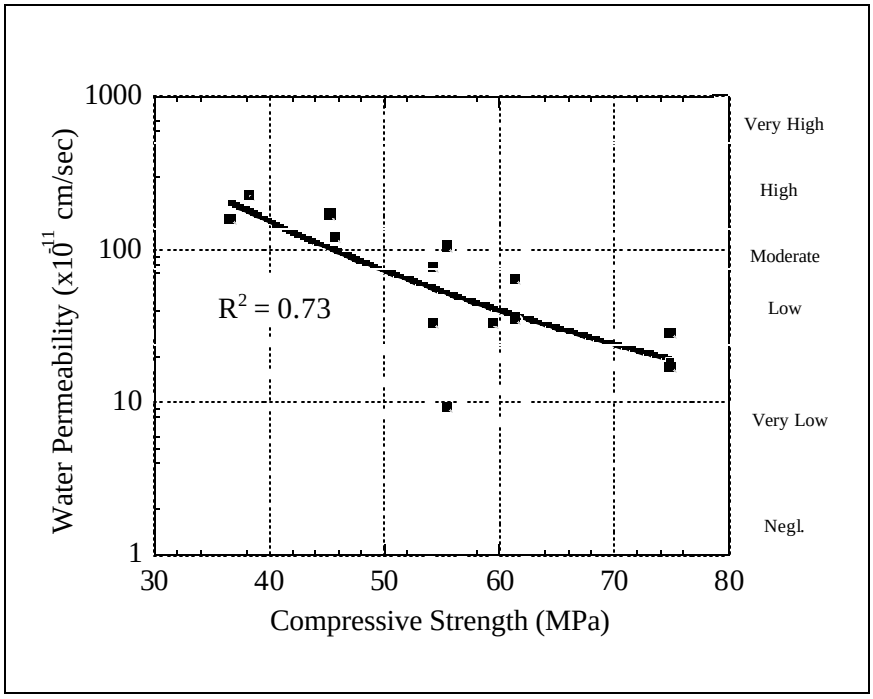

Figure 5.6.3. *Water permeability versus compressive strength for the pavement specimens near the top of the sample.*

The permeability data is plotted on a log scale to cover the several orders of magnitude in readings, and a logarithmic function is used in the regression analysis. Considerably higher scatter in the water permeability data is observed as compared to the RCPT results. This is likely due to the configuration of the test setup, which measures only a small test area (1.25 cm high circular area, 2.2 cm in diameter) as seen in figure 5.6.4. This leads to higher variability in the data because of inhomogeneity in the concrete samples. Figure 5.6.4 demonstrates how the positioning of large aggregate piece can influence the results.

As with the RCPT and Torrent air permeability tests, the results of the water permeability method also span four permeability classes. In this case, the moderate-low boundary appears to be slightly higher at 50 MPa.

It should be noted that there are several different water permeability test methods. The results of each method are dependent on the test configuration and theoretical assumptions (Armaghani and Bloomquist, 1994). The water permeability results therefore should be used as relative values for classification purposes, and not as intrinsic material property measurements.

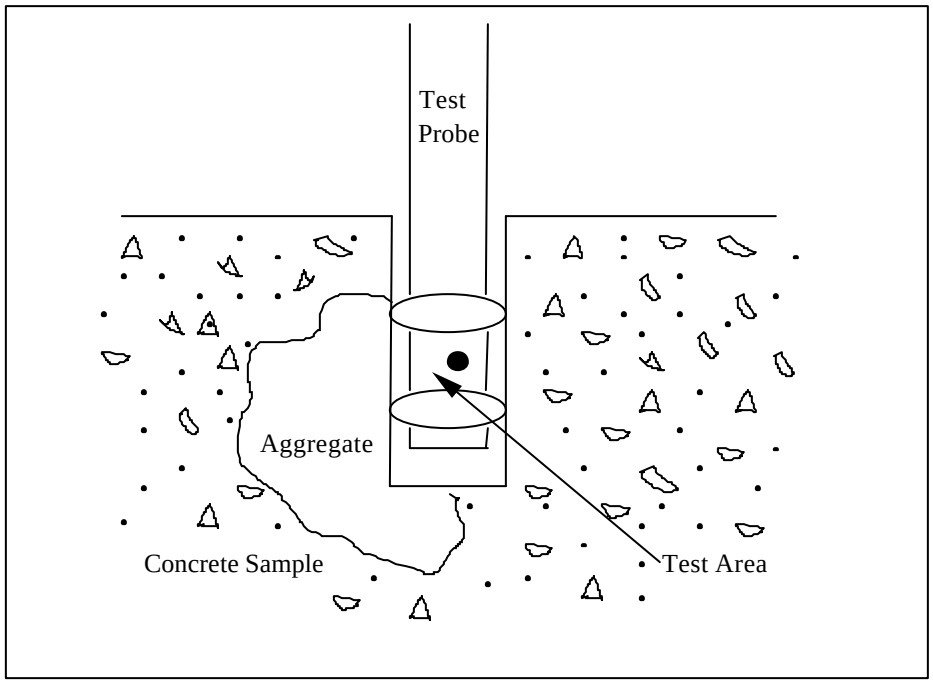

Figure 5.6.4. *Schematic of the potential influence of a large aggregate piece on the water permeability test.*

Air Permeability

The Torrent air permeability test results support the RCPT and water permeability-strength correlation as seen in figure 5.6.5. Air permeability, similar to water, is plotted on a log scale because the technique spans five orders of magnitudes in its results. An excellent strength correlation is achieved using this method ($R^2 = 0.83$). In both the RCPT and Torrent tests, the transition from moderate to low permeability levels occurs at approximately 45 MPa. The fact that RCPT, water and air permeability tests all require similar strengths to reach low permeability levels adds confidence to the strength versus permeability relations.

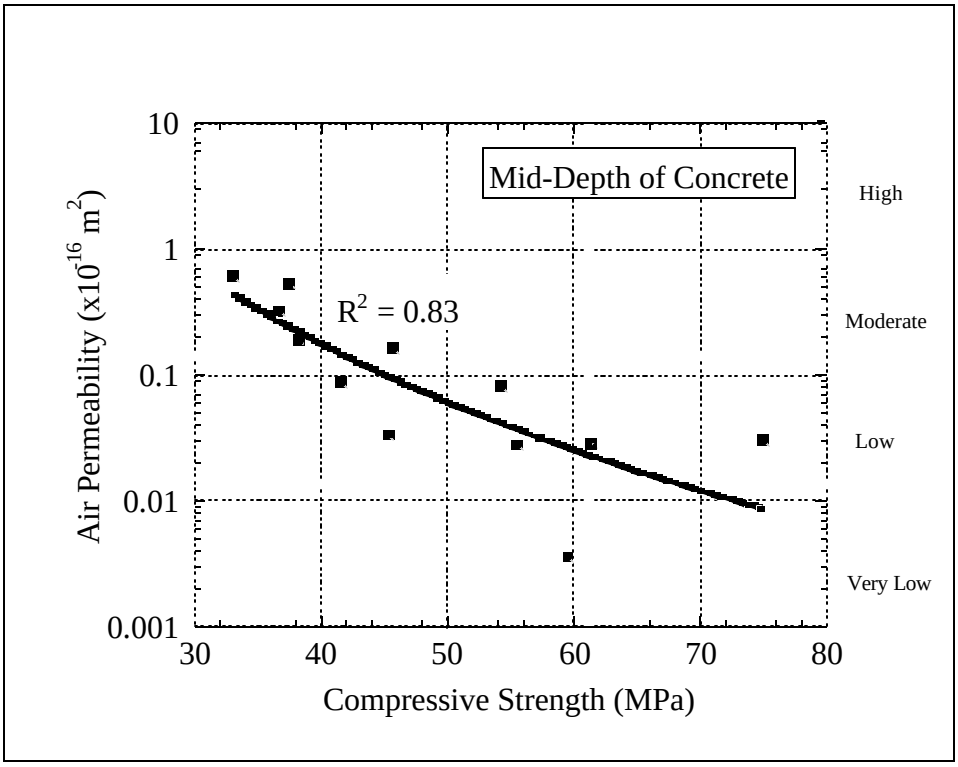

Figure 5.6.5 *Long-term air permeability at the mid-depth of the concrete versus long-term compressive strength for the pavement specimens.*

Water Absorptivity Test

The water absorptivity test was used as it provides important insight into the moisture transport properties during non-steady state conditions, which often exist when dried concrete is in contact with water. Water filling in the micropores (i.e. gel and capillary pores) occurs through capillary suction forces followed by a much slower macropore filling of the much larger air voids.

In this case 150 mm diameter field cores were used. Specimen thickness of 38.1 mm (1.5 in.) was selected to account for the large aggregate size of these concretes. To minimize cracking during heat drying the specimens were dried at 60 to 65^{o}C from both sides until constant weight was reached. This was achieved after 7 days of drying. The specimen sides were then coated with epoxy to ensure one-directional water uptake. Figure 5.6.6 illustrates the test setup in the closed container during the water absorption test.

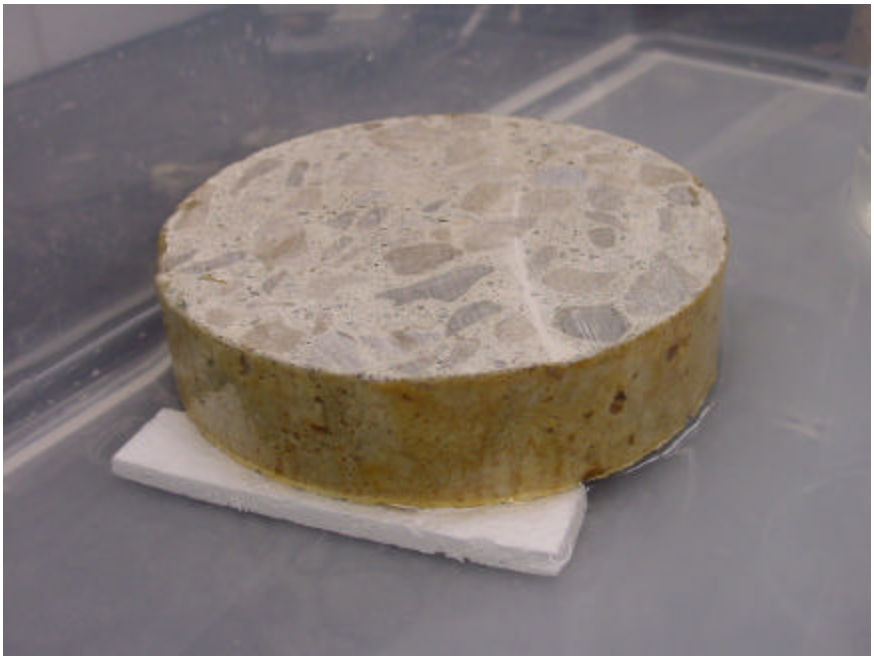

Figure 5.6.6 *Close-up of water absorptivity test.*

The water absorption rate obtained from the initial linear part of the water absorption test of water uptake versus square root time is a measure of concrete permeability and it follows the same trend with compressive strength as the other permeability tests. To illustrate this, the results for the WNF region concretes are shown in figure 5.6.7. The slope of the initial linear part of the water uptake curve (to 3.5 $h^{0.5}$) is plotted versus compressive strength in figure 5.6.8.

The other major features of this test are that it can be used to accurately determine the total air content and the w/c ratio of the sample. This is shown in Chapter 6. It can also be used to determine the exposure time for critical saturation level, which is important for freeze-thaw resistance and for drainage considerations. The latter is discussed in the following section.

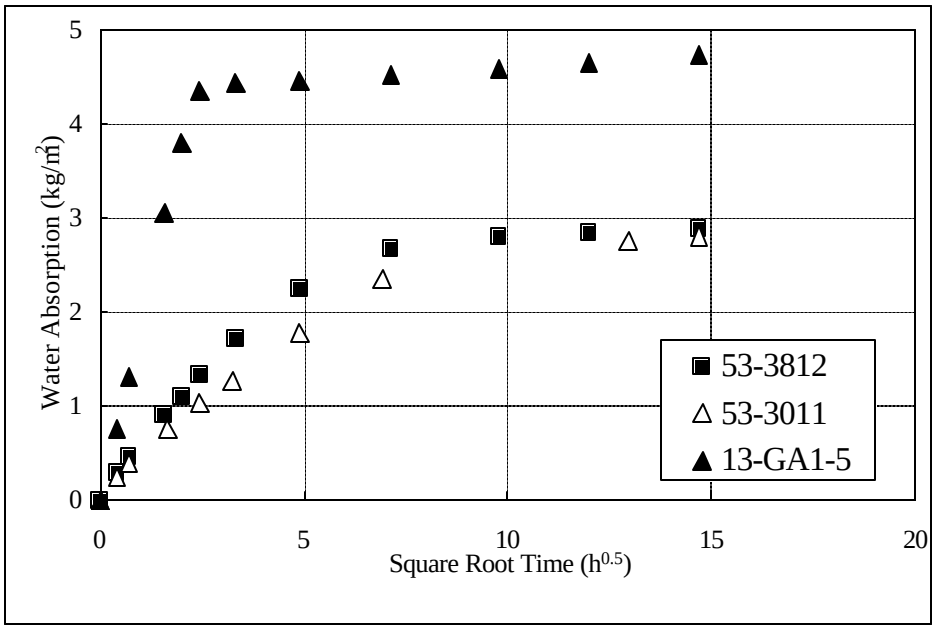

Figure 5.6.7 *Water uptake versus square root time during the water absorptivity test for the WNF region concretes.*

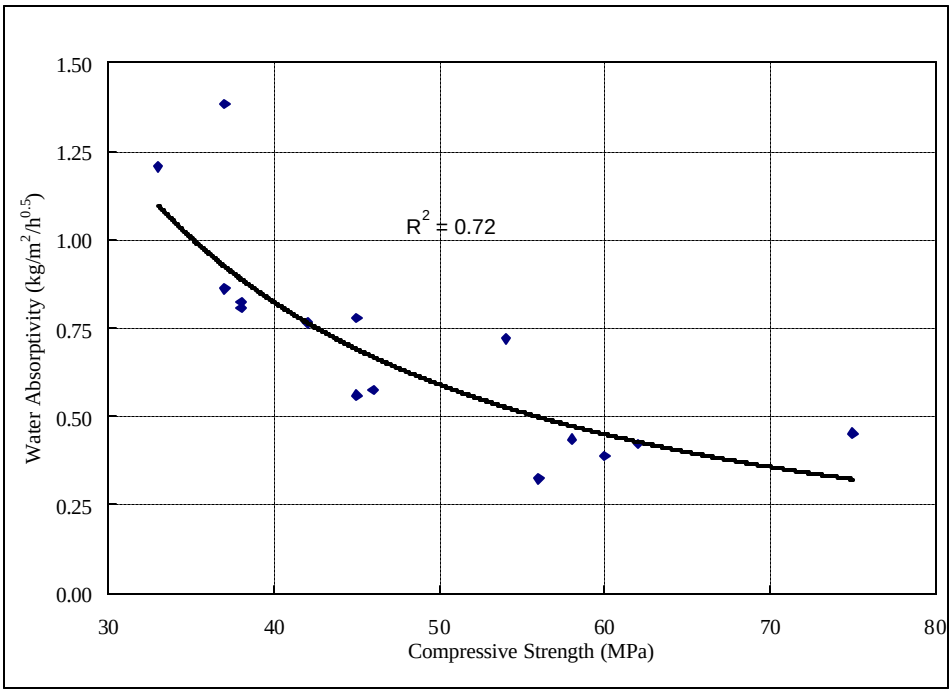

Figure 5.6.8 *Water absorptivity test results versus compressive strength for the studied test sections.*

5.6.2 Effect of Climate and Drainage

The LTPP database was used to determine the effect of long-term field curing on compressive strength. A bi-modal normal density function was obtained showing a substantial increase (68 percent) in compressive strength for the WF region over the 28-

day field compressive strength. In other climates the average increase was much less (28 percent). Consequently, concrete pavements in the WF region have probably reached the low permeability level, associated with a compressive strength of about 45 MPa, within 1 to 2 years after construction. The estimated average 28-day field compressive strength is about 35 MPa. This corresponds to a moderate to high permeability class at the age of 28 days. These concretes were found to have a w/c ratio range of about 0.42 to 0.46 as will be illustrated in table 6.2.1

Moderate to high permeability level is typical for older concrete pavements in California, as they generally have higher w/c ratio (0.47 to 0.56) based on the LTPP database and a lower strength gain over time, as they are located in the DNF climate region. Thus in DNF region concretes containing non-deleterious aggregates, permeability is not as critical as for concrete in the WF zone. Permeability, however may become a factor when mix components favor ASR or ACR as high moisture levels in the PCC trigger these reactions. Petrographic evaluation of the California concretes showed that the aggregates were non-deleterious. The Georgia concrete section located in the WNF region was also lower strength and high permeability, without any signs of durability related distress.

Higher strength concrete such as the three Washington State pavements located in the WNF and the DF regions and the Wisconsin pavement in the WF region were found to have low to very low permeability levels, and thus high internal resistance to physical and chemical deterioration. These pavements had no durability related distresses.

However, in the WF zone very low permeability is not sufficient to guarantee good long-term durability. It appears that adequate subsurface drainage is a prerequisite. This can be inferred from the two Iowa sections (19-3006 and 19-3055). Section 19-3055 was 28 years old at time of this investigation and was found to be distress free, whereas section 19-3006 had deteriorated rapidly during the last 5-6 years, as seen from figure 4.4.1. At the time of the field investigation for this project the section was 22 years old and had developed the highest level of high severity joint spalling in the LTPP database. This section was found to have poor subsurface drainage associated with a CTB and no longitudinal edge drains.

Water absorptivity measurements show that if this concrete is subjected to saturated conditions, which is believed to be the case, high internal moisture levels will develop within 3-4 months due to slow filling of air voids. This can be seen from figure 5.6.9. Initially the smaller capillaries are filled rapidly from capillary suction. Continued exposure to water will gradually fill the air voids, although at a much lower rate. When a critical saturation level corresponding to about 88 percent or higher (Neville, 1997) is reached the PCC loses its frost protection. In other words the air void system is rendered ineffective.

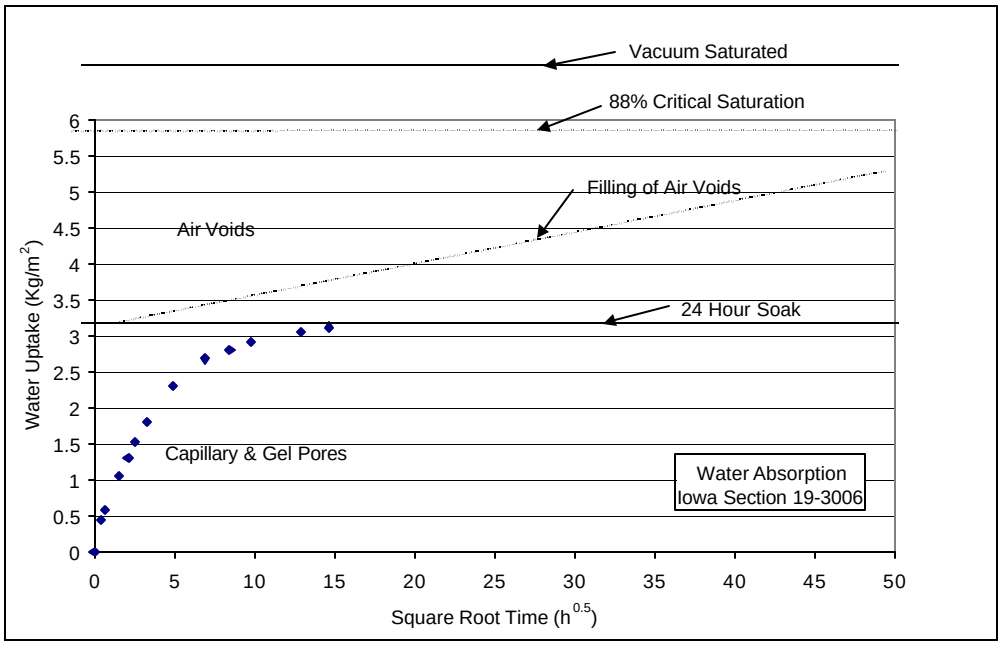

Figure 5.6.9 *Pore filling of test section 19-3006 in saturated conditions from water absorptivity test results.*

As discussed in section 5.7 the Iowa concrete, section 19-3006, has excellent air void characteristics (i.e. air content, spacing factor and specific surface). However, petrographic evaluation of joint cores showed that the air-voids were rendered ineffective as they contained substantial amounts of precipitated material. No visible signs of "D-cracking" patterns were observed on the surface, and petrographic evaluation of the distressed PCC did not implicate the coarse aggregate as the source of deterioration.

For same WF climate conditions, the older Iowa pavement section, 19-3055, has no durability related distress. This concrete was also low in permeability. The combination of a well draining base (e.g. granular base) and low permeability concrete has been effective in avoiding prolonged exposure to high moisture levels. When poor drainage conditions exist, low permeability can at best delay the onset of rapid joint deterioration.

5.6.3 Variation in Permeability with Depth Below the Slab Surface

Several of the test sections were found to have decreasing permeability within the first 100 mm (4 in) from the surface. This is seen from figure 5.6.10 a-e for RCPT results of selected test sections. Similar trends are seen in the Torrent air permeability data. This phenomenon was especially pronounced in the higher w/c ratio concretes from California and Georgia, as seen in figure 5.6.10 a and b. Shrinkage cracking, surface moisture loss, and poor finishing can all contribute to permeability gradients. However, differences in w/c ratio between the top and bottom of a slab are likely the greatest contributing factor to the permeability gradient. In a high w/c ratio concrete some consolidation of the paste can be expected. This results in a denser concrete near the base, and a more porous microstructure near the surface. Mercury intrusion porosimetry results for the Georgia

(13-GA1-5) and California (06-3017) concretes confirm that total pore volume decreases with increasing distance from the concrete surface, as seen in table 5.6.1.

The higher strength, lower w/c ratio concretes were more uniform and did not exhibit permeability gradients through their thicknesses, as illustrated in figure 5.6.10 c and d for Washington State section 53-3812, and Wisconsin section 55-3008. Low w/c ratio concretes are less susceptible to variability in w/c ratio, and thus have more uniform properties through their depth.

Table 5.6.1 *Total porosities and RCPT values at different depths of selected test sections from mercury intrusion porosimetry.*

Depth in Slab	06-3017		53-3812		13-GA1-5	
	Avg RCPT	Avg. Total Porosity %	Avg RCPT	Avg. Total Porosity %	Avg RCPT	Avg. Total Porosity %
Top	5555	8.40	427	5.86	6928	10.38
Middle	3647	7.26	334	5.86	4309	8.60
Bottom	1996	6.18	268	4.85	2951	7.38

As is seen here, within a cross section permeability can vary by as much as two permeability classes. This is significant for the deteriorated Iowa section 19-3006, as this concrete has achieved very low permeability (i.e. <1000 Coulombs) at its base. See figure 5.6.10 e. Nonetheless, bottom-up freeze-thaw deterioration has occurred anyway. Thus, in WF climate concretes, good drainage is a prerequisite for good long-term PCC durability at joints.

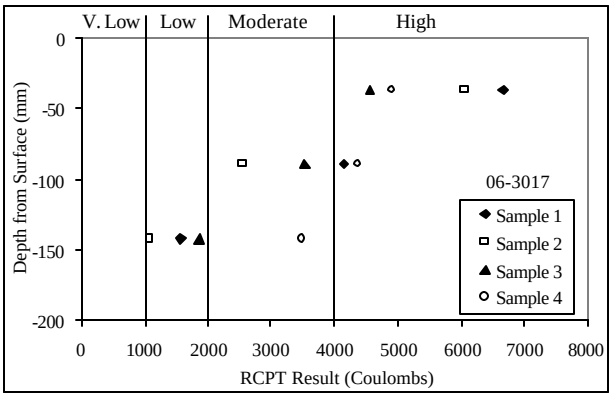

a. Test section 06-3017, California.

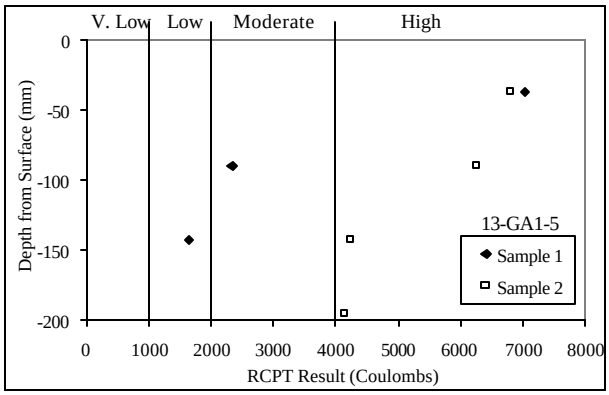

b. Test section 13-GA1-5, Georgia.

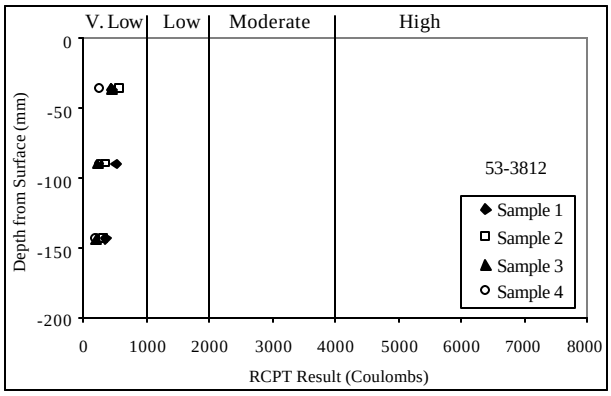

c. Test section 53-3812, Washington.

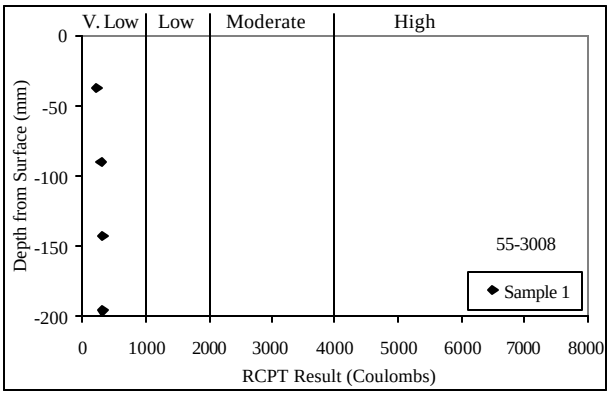

d. Test section 55-3008, Wisconsin.

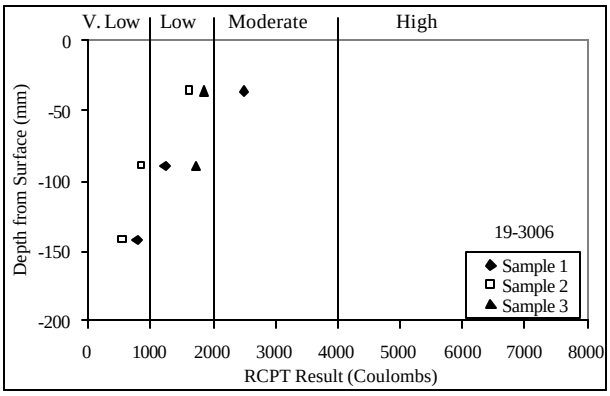

e. Test section 19-3006, Iowa.

Figure 5.6.10 *Through-thickness RCPT gradients in selected test sections.*

5.7 Air Void System and Freeze-Thaw Resistance

Freeze-thaw deterioration in concrete is due to the 9 percent volume expansion of water when it solidifies during freezing. The vulnerability of mature and conventional strength PCC (i.e. 28-day design strength of 24 MPa (3500 psi)) to freezing, in the context of durable aggregates, is a function of the pore structure of the cement-paste, and the moisture condition of the PCC when it is exposed to freezing (Philleo, 1986).

During freezing the entrained air voids, consisting of discontinuous air filled macro-pores, provide a reservoir and pressure relief for the expanding water in the micro-pores of the hardened cement paste. Several studies have shown that the degree of saturation, determined as the ratio of micro-pores to total available pore volume, including the air voids, is a measure of frost protection (Neville, 1997). The critical degree of saturation is reached when the degree of saturation reaches about 88 percent and above, provided that the aggregate are freeze-thaw durable.

Factors affecting the freeze-thaw durability of a concrete pavement are the paste pore system, entrained air, and freeze-thaw resistance of aggregates. D-cracking is a freeze-thaw problem directly related to the coarse aggregate, characterized by the aggregate's internal pore structure and maximum aggregate size. It was beyond the scope of this project to investigate D-Cracking.

Assuming non-deleterious aggregates are used, the freeze-thaw durability of normal strength concrete can be estimated from a spacing factor, which indicates the distribution of air voids. A spacing factor less than 0.2 mm is often required for freeze-thaw resistance (Powers, 1945 and 1949). For higher strength concrete the requirement is not clear, but ACI allows a 1-percent reduction in recommended air content for compressive strength higher than 34.5 MPa (5,000 lbf/in^2). It is not fully understood how the air content affects the freeze-thaw durability for higher strength concrete (ACI 318-95, 1994).

5.7.1 Air Void System of Higher Strength Concrete in the WF Region

The concretes investigated in the WF region are regular strength highway mixes with an average water-cement ratio of about 0.42 to 0.46 based on the LTPP database and this study. Therefore, the average air content is typical of normal strength concrete (6.2 percent based on water absorption test and 6.9 percent from ASTM C 457).

Table 5.7.1 *Summary of air-void analysis from ASTM C457-90.*

Climate Region	LTPP State ID	LTPP Section ID	Air (%)	Spacing Factor (Microns)	Specific Surface (mm^2/mm^3)
DNF	06	3017	7.4	127	14.1
	06	3021	3.1	305	18.5
	06	CS1	4.0	330	16.4
	06	CS3	4.5	279	17.2
	06	I-10	3.9	305	16.9
DF	53	3019	9.4	76	22.1
WF	19	3006	8.3	102	22.4
	19	3055	7.5	152	26.7
	27	4054	6.2	127	24.4
	39	3801	6.3	178	22.4
	55	3008	6.2	51	40.6
WNF	53	3011	8.6	76	31.0
	53	3812	3.4	229	24.3
	13	GA1-5	7.9	127	23.9

The five concretes in the WF region all have good air void characteristics (spacing factor, air content and specific surface area) based on ASTM C 457 as seen from table 5.7.1. Total air ranged between 6.2 and 8.3. The spacing factor varied between 51 microns and 178 microns, and specific surface of the entrained air varied between 22.4 and 40.6 mm^2/mm^3. Only two test sections fell slightly below the minimum recommended specific surface of 24 mm^2/mm^3. These measurements were conducted by the Michigan Department of Transportation (MDOT).

Table 5.7.2 lists total air content obtained three ways. Generally good agreement is obtained between results from the water absorption test on hardened concrete and the LTPP results on fresh concrete. The ASTM C 457 values are generally higher. Based on the water absorptivity test results and LTPP it appears that the California concretes are not air entrained. The same appears to be the case for the Washington State LTPP section 53-3812 and the Georgia concrete. These concretes have total air less than 4 percent.

Table 5.7.2 *Air void contents from the LTPP database, ASTM C457, and water absorptivity test.*

Climate Region	State	Section	Average Air Content		
			Absorptivity Test (%)	LTPP Database (%)	ASTM C-457 (%)
DNF	6	3017	2.9	-	7.4
	6	3021	2.6	-	3.1
	6	7456	3.7	3.9	5.1
	6	CS1	2.9	3.0	4.0
	6	CS3	2.3	2.5	4.5
	6	I10	2.5	-	3.9
DF	53	3019	4.8	4.3	9.4
WF	19	3006	7.5	6.4	8.3
	19	3055	5.9	5.9	7.5
	27	4054	5.8	-	6.2
	39	3801	6.9	-	6.3
	55	3008	4.9	6.5	6.2
WNF	53	3011	4.2	6.2	8.6
	53	3812	2.4	3.4	3.4
	13	GA15	1.8	-	7.9

5.7.2 When the Air Void Structure is Rendered Ineffective

The Iowa concrete, LTPP section 19-3006, has excellent air void characteristics. Therefore this concrete should have adequate freeze-thaw resistance. However, petrographic examination of the upper half of a 150-mm diameter core taken from the deteriorated joint area shows that the smaller air voids (< 75 microns) are lined with a white clear crystalline deposit, which has rendered the voids ineffective. The air void spacing in this area is deficient based on a threshold value of 200 microns as recommended by ACI for freeze-thaw durability. A value of 221 microns is obtained for the spacing factor, as measured by linear traverse according to ASTM C457. The specific surface area of air voids is 17.6 mm^2/mm^3, which is less than the 24 mm^2/mm^3 recommended by ACI. Although the sample has a total air content of 7.2 percent, the spacing factor is high because of high paste content (27.9 percent).

A core sample from the mid-slab region away from the distressed area was found to have total air content of 8.3 percent, and an estimated spacing factor of 102 microns, well below the ACI threshold value. The specific surface area of air voids is 22.4 mm^2/mm^3, which is slightly below ACI recommendations. Thus it appears that freeze-thaw resistance has been compromised in the joint area due to prolonged exposure to water and deicing salts at the slab bottom.

In addition to the filling of air voids with precipitates, reaction rims have formed near the surfaces of several of the coarse aggregates. These rims are likely caused by partial de-dolomitization of the dolomite aggregates and are associated with highly carbonated paste at the aggregate-paste interface. Some associated cracking is observed in some of these large aggregates. Some of the larger cracks run through the large aggregates, but

deflect around the fine aggregates in the paste. Gan et al. (1996) observed this same de-dolomitization mechanism in dolomite aggregates in several other Iowa pavements.

The distresses in section 19-3006 near the joint are shown in figure 5.7.1 a-d using low power stereomicroscopy and thin section microscopy in plane polarized light.

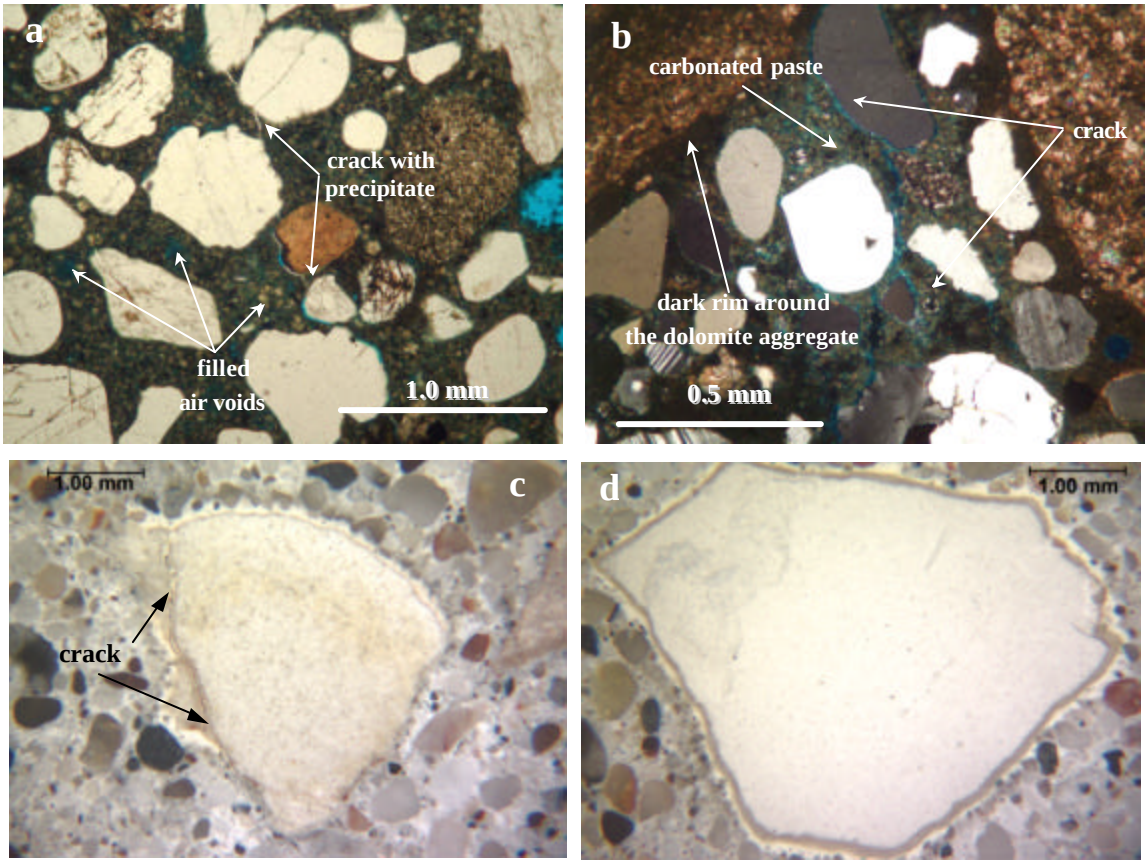

Figure 5.7.1 a, b, c, and d) *Distresses shown in section 19-3006 near the joint using low power stereomicroscopy and thin section microscopy in plane polarized light.*

Based on the condition survey of section 19-3006 performed 3 years earlier in August of 1994, the site conditions have deteriorated rapidly since that time. It appears that joint deterioration and spalling started out as corner spalls rated as corner breaks with some low severity spalls along the joints.

Away from the deteriorated areas this concrete is found to have low permeability (<2000 coulomb). This may have played a role in delaying deterioration, but the severe microenvironment near the joints has prevailed. In view of this, it is doubtful that the use of higher strength concrete for this pavement would have eliminated joint distress.

Joint deterioration and spalling in the WF climate should also consider whether the large aggregates in the slab are susceptible to freeze-thaw damage and D-cracking. The more

water there is available to saturate the slab over long periods of time, the greater the extent of D-cracking. (Peshkin et al., 1994). Pavement sections in Michigan on impermeable bases (i.e. asphalt treated bases and full-depth asphalt concrete shoulders) result in bathtub-type designs, from which water does not readily drain. The Clare test road in Michigan is an example of sudden deterioration of the concrete at the joint starting from the bottom up. This section was found to have no distress after 17 years in service based on the LTPP database, but deteriorated rapidly since then and has now been decommissioned.

Such joint deterioration in WF climates starting at the slab base without the traditional "D" cracking pattern has been reported in several States.

5.8 Concrete Shrinkage and Coefficient of Thermal Expansion

In pavement design, shortening of a slab on grade associated with drying and cooling is of primary interest, as it over time controls joint movement and cracking tendency. Concrete drying shrinkage is a dimensional change due to loss of water, whereas the coefficient of thermal expansion (CTE) is used to determine the dimensional change from temperature effects.

Maintaining small crack and joint opening is critical for long-term pavement performance as it affects the performance in terms of load transfer, faulting, and spalling. A tight joint/crack width (<0.6 mm) maintains high load transfer capacity of the pavement. Joint movements are controlled by the PCC drying shrinkage characteristics and the coefficient of thermal expansion.

Resistance to transverse slab cracking from restrained slab movement is also strongly controlled by thermal and drying shrinkage and the elastic modulus of the concrete. The tensile stress associated with temperature and drying is produced by internal and external restraints. The general thermal and shrinkage stress analysis of pavement slabs is very complex. However, lowering the drying shrinkage and CTE of concrete could minimize the risk of cracking and problems related to exposed cracks.

In this study the CTE property was directly measured on 150-mm diameter field specimens using a modified FHWA procedure (FHWA, 1996) presented in detail in chapter 2. In general, the CTE was found to be very similar for the investigated concretes despite the range of investigated aggregate types. One section, Tracy test section 06-CS3, stands out because of its high cement content.

Drying shrinkage is an irreversible property, which has already taken place for the field concretes of this study. Thus it could not be obtained from laboratory testing. However, the drying shrinkage is estimated based on an approximate relationship between shrinkage and the splitting tensile strength.

5.8.1 Drying Shrinkage

Shrinkage occurs mainly in the cement paste, and is highly related to the w/c ratio and the cement content. For decreasing w/c, the shrinkage will decrease. However, for increasing cement content, the shrinkage will increase. The coarse aggregate counteracts the shrinkage of the cement paste. Increasing stiffness of the aggregate leads to reduced shrinkage. For higher strength concrete with high cement content and/or low coarse aggregate volume it is therefore increasingly important to minimize the shrinkage effects.

Table 5.8.1 lists the estimated relative shrinkage of the different sites based on their estimated 28-day splitting tensile strength (AASHTO, 1993). The 28-day splitting tensile strength is assumed to be 90 percent of the ultimate strength. See also section 5.3. The concrete used in the Tracy test section with increased cement content had 20 percent higher paste content than

the control section. The relative shrinkage has been adjusted accordingly. See chapter 7 for a detailed discussion.

The typical 28-day shrinkage values for JPCP's range within 400 to 800x10^{-6} mm/mm. In table 5.8.1 the shrinkage is given relative to the conservative shrinkage value of 800x10^{-6} mm/mm. Despite the inaccuracy of the estimate, it appears that the drying shrinkage have been in the expected range for JPCP's. However, it should be pointed out that the relative shrinkage in the dry regions is likely being underestimated.

Table 5.8.1 *Estimated relative shrinkage based on the estimated 28-day PCC splitting tensile strength.*

Climate Region	State ID	Section ID	Estimated 28-day Splitting Tensile Strength Mpa	Estimated Shrinkage Relative to 800x10^{-6} mm/mm
DNF	06	3017	3.37	0.57
	06	3021	3.18	0.62
	06	7456	2.98	0.68
	06	CS1	3.18	0.62
	06	CS3	3.82	0.82[1]
	06	I-10	3.91	0.42
DF	53	3019	3.82	0.45
WF	19	3006	3.18	0.62
	19	3055	2.55	0.82
	27	4054	3.37	0.57
	39	3801	3.37	0.57
	55	3008	4.09	0.38
WNF	53	3011	3.45	0.54
	53	3812	4.00	0.40
	13	GA1-5	2.73	0.76

[1]Adjusted for high cement content (paste content)

5.8.2 CTE Test Results and Ranges for the Pavements Investigated

The cement paste and the aggregate have different CTE (Neville, 1997). The coefficient of thermal expansion of the hydrated cement paste varies between 11 to 20E-06 /^{0}C which can be substantially higher than the CTE of the coarse aggregate (Forster, 1997). Typical CTE values of different rock types, as reported by Lane (1994), are shown in table 5.8.2.

The concrete's CTE is a resultant of the two values, but is very sensitive to the cement paste content as the hydrated paste is, despite the smaller volume fraction (about 25 percent) the continuous matrix in which the aggregates are embedded. Thus, for most cases the PCC CTE value are controlled by the cement paste.

Table 5.8.2 *Typical CTE values of different rock types. [after Lane (1994)]*

Rock	CTE value ($x10^{-6}/^oC$)
Quartzite, silica shale, chert	11.0-12.5
Sandstones	10.5-12.0
Quartz sands and pebbles	10.0-12.5
Argillaceous shales	9.5-11.0
Dolomite, magnesite	7.0-10.0
Granite, gneiss	6.5-8.5
Syenite, andesite, diorite, phonolite, gabbro, diabase, basalt	5.5-8.0
Marble	4.0-7.0
Dense, crystalline, porous limestone	3.5-6.0

In this study no strong correlation was detected between aggregate types and PCC CTE. However, the Tracy test section with higher cement content, 06-CS3, containing 40 percent more cement than the control section, 06-CS1, had a 40 percent higher thermal expansion. All CTE values obtained by the procedure described above are shown in table 3.3.11. The average value for each climate region is:

- DNF: 9.93E-06/^{0}C
- DF: 8.9E-06/^{0}C
- WF: 9.49E-06/^{0}C
- WNF: 9.10E-06/^{0}C

These results show that the coefficients of thermal expansion of concrete in different climate regions do not differ significantly from each other. Compared to values obtained from the literature on normal strength concrete, these results can be considered in the range of low to normal.

For sections tested, the average CTE values vary from 8.83 to 10.27 E-06 /^{0}C except for two sections. The variation of CTE of sections tested can be considered quite narrow and close to the expected median CTE value (Neville, 1997). The same finding has also been reported Alungbe et al. (1990). However, the key similarity of these concretes is that the aggregate volume contents were very close at about 75 percent.

Higher CTE values have been identified for two sections from different climatic regions. The highest CTE was determined for section 06-CS3 in the DNF region (13.64E-06 /^{0}C) followed by 39-3801 in the WF region (11.27E-06 /^{0}C). The high CTE in test section 06-CS3 can be attributed to its high cement content (418 kg per m^3 compared to 307 kg per m^3 for the control section 06-CS1). The higher CTE of the Ohio section, 39-3801, compared to the other

PCC's containing dolomitic limestone is likely due to the fact that 50 percent of the coarse aggregate is sandstone and quartz which both have about twice the CTE of limestone.

CHAPTER 6. CONCRETE MIX CHARACTERISTICS

6.1 Introduction

It was shown in the interim report and in chapter 1 that the mix characteristics (such as w/c ratio, cement content, aggregate size and gradation, aggregate content and type) have a varied influence on several of the key mechanical and durability properties of concrete. These properties, in turn, were found to affect pavement performance. This section presents the relations between the mix characteristics and concrete properties obtained from laboratory testing of field cores.

Extensive laboratory evaluation of the concretes cored from the 15 pavement test sections in this study was undertaken to determine the role of mix proportions on the strength level, associated properties, and pavement performance. The data gleaned from petrographic studies, LTPP database values, and historical information available on these test sections confirm that no special mix designs were used, even for the very high strength pavements studied. The high strength and performance levels were achieved not through special mixes, but primarily through careful attention to selection of high quality materials, proper design, and fortuitous placement and environmental conditions.

The concrete mix composition for each of the field projects is shown in table 6.1.1. In general, the mix designs are typical pavement mixes.

Table 6.1.1 *Mix designs for the investigated test sections.*
(Values reported are from the LTPP database except where otherwise indicated.)

Climate Region	State	Section	Cement (kg)	Cement Type	Water (kg)	W/C Ratio	Air Content (%)	Coarse Aggregate (kg)	Fine Aggregate (kg)	C/F Ratio
DNF	6	3017	282	Type II	160[1]	0.57[1]	2.9[2]	1195	703	1.7
	6	3021	335	Type II	188	0.56	2.6[2]	1186	648	1.8
	6	7456	307	Type II	144	0.47	3.9	1208	699	1.7
	6	CS1	307	Type II	144	0.47	3.0	1208	699	1.7
	6	CS3	418	Type II	140[3]	0.35[3]	2.5			
	6	I10	252[3]	--	121[3]	0.48[3]	2.5[2]	1218[3]	681[3]	1.8
DF	53	3019	335	Type II	114	0.34	4.3	1222	730	1.7
WF	19	3006	335	Type I	141	0.42	6.4	1001	832	1.2
	19	3055	358	Type I	154	0.43	5.9	943	806	1.2
	27	4054	320	Type I	147	0.46	5.8[2]	1280	564	2.3
	39	3801	356	Type IA	135	0.38	6.9[2]	1005	683	1.5
	55	3008	335	Type I	134	0.40	6.5	1201	646	1.9
WNF	53	3011	335	Type II	134	0.40	6.2	1222	729	1.7
	53	3812	335	Type IIA	131	0.39	3.4	1222[4]	729[4]	1.7
	13	GA1-5	310[4]	--	152[4]	0.50	4.0[4]	1180[4]	662[4]	1.8

[1] Water content estimated from LTPP database

[2] Air content from water absorptivity test

[3] Water-cement ratio estimated from water absorptivity test (assuming 90% hydration)

[4] Mix design estimated from other test sections in the same state. (Data entry error for LTPP section, 53-3812, Washington State.

From table 6.1.1 it is noteworthy that the mix designs vary with climate region and locally available materials. These variations represent shifts in emphasis to different areas of the mix design to reflect the exposure conditions.

For example, the wet freeze region concretes tend to have smaller coarse aggregate sizes (generally up to 25.4 mm nominal max. size) consistent with the need to avoid durability related aggregate distresses such as freeze-thaw deterioration and D-cracking. In the other climates, larger aggregates (about 38 mm nominal max. size) are used. Large high quality aggregates tend to improve concrete fracture properties and load transfer efficiency after cracking.

Similarly, w/c ratios are generally lower in the wet freeze climate concretes than in those from other climate regions. Low w/c ratio helps to densify the microstructure and reduce permeability and transport properties. This in turn protects the concrete from the ingress of water and salts that can lead to durability related distresses in freeze-thaw susceptible climates. In the other climate regions, higher w/c ratios are observed. It is believed that the workability of the concrete at time of construction in these hot climates is likely the overriding consideration for these pavements.

In general cement contents are held to typical ranges in these mixes, irrespective of climate region. It is noteworthy that one site in California used increased cement content to increase compressive strength. However, this was an experimental section that is atypical of California mix designs. Very high strength can be achieved using normal cement contents on the order of 335 kg/m^3.

6.2 Water-Cement Ratio

Sellevold (1986) has pioneered the w/c ratio prediction in hardened concrete using the capillary sorption method and the Powers-Brownyard equation shown below. The water absorption technique was used in this project to evaluate the transport properties, air content, and the water-cement ratio as well.

In table 6.2.1, the w/c ratio values are shown for each test section based on the LTPP database, the ASTM C1084 maleic acid method, and as predicted using the Powers-Brownyard (1948) equation below, and using the absorptivity results for micro-pore volumes:

$$W/C = (0.317 \cdot P + 0.172 \cdot \alpha) / (1-P) \qquad (6.2.1)$$

where P = normalized micro pore volume (i.e. relative ratio on a paste content basis)
α = degree of hydration (relative amount from 0 to 1).

On average, the binder content by volume from the LTPP database was estimated at 25 percent. This value was then used to normalize micropore volume from absorption tests on the concrete to paste (i.e. binder) porosity.

The estimated w/c ratio was calculated for three different hydration values, 80, 90 and 95 percent. This results in a range of predicted w/c ratios typically within 0.05 from 80 to 95 percent hydration. Overall, good agreement was obtained with the LTPP database values and the maleic acid method, with only a few exceptions. Using the Powers-Brownyard equation, the w/c ratio values for the sections not included in the LTPP database were estimated as well based on the assumption of a 25 percent binder volume. These results appear to be appropriate based on the compressive strength versus w/c ratio curve shown in figure 6.2.1. This curve follows the expected Abram's relation well.

The maleic acid method is based on ASTM C1084, "Standard Test Method for Portland-Cement Content of Hardened Hydraulic-Cement Concrete." The method uses a solution of maleic acid in methanol to dissolve the cement paste from a concrete specimen. The approach involves accurately weighing a sample of ground concrete, dissolving the concrete in the methanol-maleic acid solution, and filtering the mixture after allowing time for settling. The solid residue resulting after dissolution is weighed, and the weight loss is taken as the cement paste content of the concrete. To get cement content, the bound water must be determined and subtracted from the cement paste content. While the method gives generally good approximations of cement content and w/c ratio, it is known that the maleic acid solution also attacks some carbonate aggregates while not dissolving carbonated cement pastes. This may account for differences in cement contents and w/c ratios observed in table 6.2.1. The methanol-maleic acid test was conducted by MTU.

Table 6.2.1 *Water-Cement Ratios of the studied test sections from the LTPP database, maleic acid test, and water absorptivity test.*

Climate Region	LTPP		w/c Ratio				
	State ID	Section ID	LTPP Database	Maleic Acid	Absorptivity Test		
					80% Hyd	90% Hyd	95% Hyd
DNF	06	3017	0.57	0.46	0.43	0.46	0.48
	06	3021	0.56	0.50	0.63	0.67	0.69
	06	7456	0.47	--	0.49	0.52	0.54
	06	CS1	0.47	0.47	0.43	0.46	0.47
	06	CS3	--	0.37	0.33	0.35	0.37
	06	I-10	--	0.45	0.45	0.48	0.50
DF	53	3019	0.34	0.43	0.43	0.46	0.49
WF	19	3006	0.42	0.32	0.40	0.43	0.44
	19	3055	0.43	0.26	0.51	0.54	0.55
	27	4054	0.46	0.49	0.39	0.41	0.43
	39	3801	0.38	0.48	0.46	0.49	0.50
	55	3008	0.40	0.67	0.33	0.35	0.37
WNF	53	3011	0.40	0.38	0.37	0.39	0.41
	53	3812	0.39	0.38	0.32	0.35	0.36
	13	GA15	--	0.49	0.53	0.56	0.57

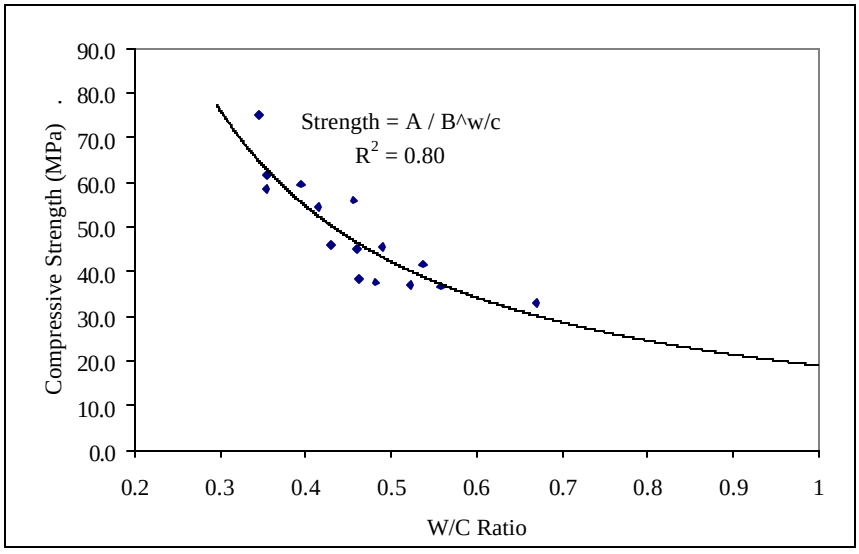

Figure 6.2.1 *Ultimate compressive strength versus w/c ratio from absorptivity test results.*

6.3 Cement Type and Content

The cement types and contents were obtained from the LTPP database and using the maleic acid method. It is significant that although various strength levels were achieved in the field, all of these concretes contain ordinary portland cements (type I and II). In addition, it is noteworthy that none of these concretes contain mineral additives such as fly ash or slag. From the LTPP database, it is seen that for most of the sections, cement contents fall within a relatively narrow range of 307 kg/m^3 to 358 kg/m^3 (517 lb/yd^3 to 604 lb/yd^3). The exceptions are test sections 06-CS3, 06-3017, and 06-I-10. As can be derived from table 6.3.1, the average cement content for all sections is 331 kg/m^3 (557 lb/yd^3). The average within each climatic zone is 332 kg/m^3 (559 lb/yd^3) for DNF, 341 kg/m^3 (573 lb/yd^3) for WF, and 313 kg/m^3 (528 lb/yd^3) for WNF. It can be seen that these average cement contents do not vary significantly from the overall average.

Section 06-CS3 at Tracy, California was an experimental section designed to test the effect of higher cement content on performance. The cement content is 418 kg/m^3 (705 lb/yd^3), and is not typical of the mixes studied. As seen earlier, the higher cement content of the 06-CS3 concrete has produced an increase in compressive strength to 58.4 MPa (8,471 lbf/in^2), as compared to the control mix in section 06-CS1 at the Tracy site. That section has a cement content of 306 kg/m^3 (517 lb/yd^3) and field compressive strength of 45 MPa (6,535 lbf/in^2). However, the increase in cement content has only increased the tensile strength by about 8 percent, from 3.48 MPa (505 lbf/in^2) for the 06-CS1 to 3.77 MPa (547 lbf/in^2) for the 06-CS3. The moderate increase in tensile strength has not been able to counteract the effect of increased shrinkage and CTE on pavement performance. See chapter 4 and section 5.8.

Table 6.3.1 *Cement Types and Contents for the studied sections based on LTPP database and mix design data.*

Climate Region	LTPP		Cement	
	State ID	Section ID	Type	Content Kg/m^3
DNF	06	3017	Type II	282
	06	3021	Type II	335
	06	7456	Type II	307
	06	CS1	Type II	307
	06	CS3	Type II	418
	06	I-10	-	252[1]
DF	53	3019	Type II	335
WF	19	3006	Type I	335
	19	3055	Type I	358
	27	4054	Type I	320
	39	3801	Type IA	356
	55	3008	Type I	335
WNF	53	3011	Type II	335
	53	3812	Type IIA	335
	13	GA1-5	-	326[1]

[1] calculated from volume distribution of coarse and fine aggregates and paste as determined by ASTM C-457.

In addition to strength observations, cement content can also affect thermal expansion in the concrete. Test section 06-CS3, has a high value of CTE at 13.64E-06 /^{0}C. This high CTE is thought to be caused by higher cement content used in the mix. As has been reported (Neville, 1997), a mix having higher paste content tends to give a higher CTE value. Although having almost the same mix composition as 06-CS3 except for cement content, 06-CS1 gives a moderate CTE of 9.79E-06 /^{0}C. This suggests that the cement content significantly influences the thermal expansion of concrete.

An important finding when comparing tables 6.2.1 and 6.3.1 is that the higher strength concretes from Washington and Wisconsin, sections 53-3812, 53-3011, 53-3019, and 55-3008, do not contain high cement contents. Their cement contents are all 334 kg/m^3 (564 lb/yd^3). The high strengths were instead obtained by using low w/c ratio (0.4 or lower).

Figure 6.3.1 shows the cement content as a weight percentage of the concrete mix for each pavement as determined from the LTPP database and the maleic acid method. It is noteworthy that the maleic acid method yields slightly higher cement contents for almost all test sections. This is likely because some dissolution of the aggregates has occurred using the maleic acid method.

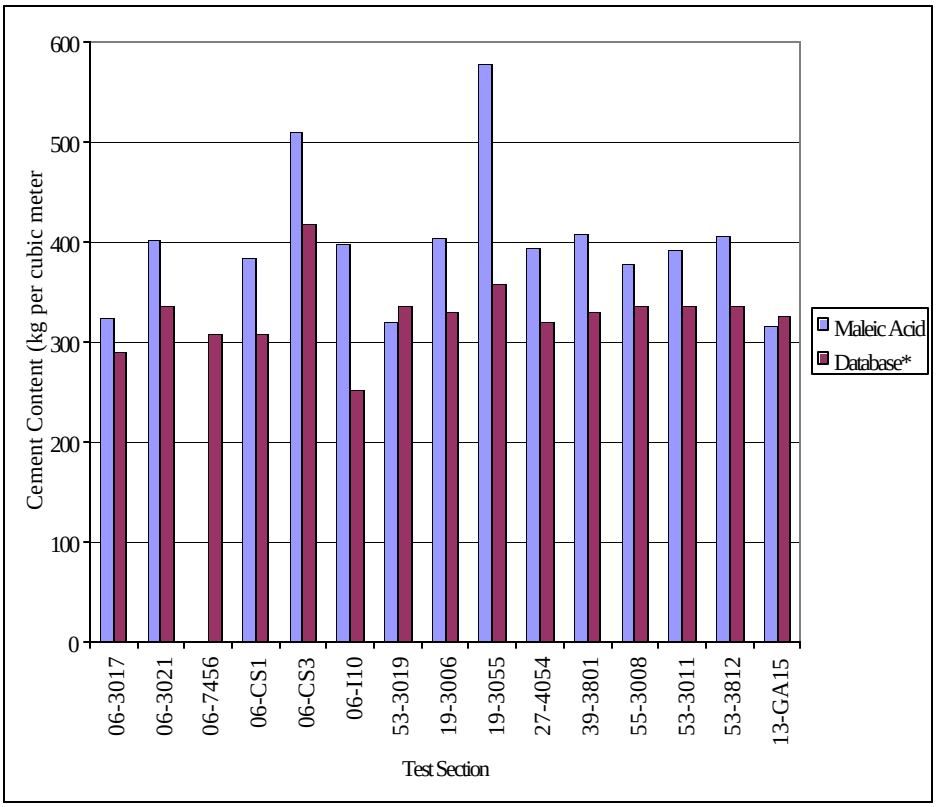

*As determined from the LTPP database and mix design data

Figure 6.3.1 *Cement content as a weight percentage of the concrete mix for each pavement as determined from the LTPP database and the maleic acid method.*

6.4 Aggregates

Coarse and fine aggregate types were determined from petrographic analysis. These results for the coarse aggregates are shown in table 6.4.1. Principally, three different coarse aggregate types were used in the studied concretes: silicate rock gravel, dolomite/limestone, and crushed silicate rocks. The dolomite/limestone aggregates were exclusively used in concretes for the WF zone (19-3006, 19-3055, 27-4054, 39-3801, and 55-3008). The Ohio section 39-3801 also contained a significant amount of sandstone and quartzite. Section 13-GA1-5 contained crushed granitic to granodioritic aggregates while the other concretes (06-3017, 06-3021, 06-7456, 06-CS1, 06-CS3, 06-I-10, 53-3019, 53-3011, and 53-3812) contained gravel of silicate rocks.

The 06-I-10 (in San Bernadino County, California) concrete is composed of a natural silicate gravel mix (gneiss, quartz, and minor basalt) (see section 3.2). These aggregate types are well-known for their high strength and durability. Similar aggregate types were found in other California concretes including, 06-3017, 06-3021, 06-7456, and the other experimental sections investigated on I-5 at Tracy (control section 06-CS1 and higher cement content section 06-CS3). The maximum nominal aggregate size in most of these pavements was 38.1 mm (1.5 in). Silicate gravel was also found in sections 53-3019, 53-

3812, and 53-3011. The Georgia section (on I-85, test section 13-GA1-5) had crushed granite-granodiorite rock in the coarse and the fine fraction. This aggregate contains numerous microcracks. Because these cracks are only present within the aggregate they must have formed during processing.

In the WF region dolomitic limestone was associated with excellent concrete quality. It appears that this is related to the use of high quality limestone with low microporosity. These aggregates generally had smaller nominal aggregate sizes (19.1-38.1 mm). The smaller maximum aggregate size found in the WF region is probably due to general consideration of the effects of coarse aggregate size on concrete D-cracking susceptibility.

At this point there is no clear evidence as to whether a dolomite or a silicate gravel would have a different durability in different climates. However, the durability of an aggregate is highly dependent on its particular source, and cannot be generalized to aggregate type.

Table 6.4.1 *Coarse aggregate characteristics obtained from laboratory analysis.*

Climate Region	LTPP		Coarse Aggregate			
	State ID	Section ID	Shape	Type	Max Nominal Aggregate Size[1] mm	Max Aggregate Dimension [2] Mm
DNF	06	3017	Rounded	gravel (mix)	38.1	46
	06	3021	Rounded	gravel (mafic)	38.1	46
	06	7456	Rounded	gravel (mix)	38.1	75
	06	CS1	Rounded	gravel (mix)	38.1	76
	06	CS3	Rounded	gravel mix incl. dol.	38.1	45
	06	I-10	Rounded	gravel (mix)	50-62	44
DF	53	3019	Rounded	gravel (mafic)	38.1	47
WF	19	3006	Angular	dol. Limestone	25.4	31
	19	3055	sub-rounded	dol. Limestone	25.4	42
	27	4054	sub-rounded	dol. Limestone	25.4	40
	39	3801	Rounded	grav.+dol. Limestone	19.1	27
	55	3008	Rounded	dol. Limestone	38.1	43
WNF	53	3011	Rounded	gravel (mix)	25.4	38
	53	3812	Rounded	gravel (mix)	38.1	32
	13	GA1-5	Angular	syenite/granodiorite	38.1	36

[1] Based on sieve analysis of dissolved cores
[2] Based on petrographic analysis

6.4.1 Coarse Aggregate Characteristics

Coarse Aggregate Fracture in Higher Strength PCC

High fracture energy values were obtained for the four California test sections 06-3017, 06-3021, 06-I-10, and 06-CS3. The values ranged from 200 to 280 N/m. These sections all had high content of strong coarse aggregate of a gravel mix, and a significant amount of the coarse aggregate exceeded 25.4 mm (1 in). From the literature review it was found

that the coarse aggregate type and the aggregate-to-paste bond have significant impact on the PCC fracture energy. Field beams from these few sites gave insight into the level of fracture energy that can be achieved over time. These concretes contained very tough large-size coarse aggregates, which improved the PCC fracture behavior.

Coarse Aggregate Gradations

The aggregate gradations for coarse and fine aggregate were determined on the field cores by thermal decomposition of the concretes and manual separation of the aggregate from the paste. The nominal maximum aggregate size used in these pavements ranges from 25.4 mm for the WF zone to 50 mm for the DNF zone. These values are greater than those typically used today for PCC pavements. Over the years there has been a trend toward using smaller maximum aggregate size.

The coarse aggregate size has also a significant effect on the deterioration of cracks. In a field study, discussed by Yu et al. (1998) it was shown that decreasing the maximum aggregate size from 38.1 to 25.4 mm increased the deterioration of cracks by 15 percent. Further decrease in aggregate size to 12.7 mm increased the deterioration another 100 percent. This indicates that the coarse aggregate sizes above 12.7 mm are the main contributors to aggregate interlock and load transfer.

Figure 6.4.1 shows the coarse aggregate gradation curves for the investigated sections. The gradation curve for 06-7456 was not determined, but is assumed similar to 06-CS1. The gradation curve for test section 06-I-10 was not available due to a limited number of core samples available from the site.

The California gradations were very coarse with 30 to 40 percent retained on the 25.4 mm sieve, and only 15 to 20 percent passing the 12.7 mm sieve. Also, the gradation curves between the projects were very similar. In the WF region the gradation curves are significantly finer than in the DNF region. Typically the maximum aggregate size in the WF zone is 25.4 mm as observed for the Iowa (19-3006, 19-3055), Minnesota (27-4054), and Ohio (39-3801) concretes. At the same time, these concretes had a higher percent passing the 12.7 mm sieve (on the order of 35 to 55 percent). It is worth noting that the Wisconsin concrete has a coarser gradation, with about 20 percent retained on the 25.4 mm sieve. The coarse aggregate here was a dolomitic limestone, and the concrete was in excellent conditions with no trace of freeze-thaw damage. The Wisconsin coarse aggregate gradation is very similar to the gradations used in Washington State (53-3011, -3019, and –3812) and in Georgia (13-GA1-5/6). These sections in the WNF and DF region had typically 20 percent retained on the 25.4 mm sieve and about 25 to 40 percent retained on the 12.7 mm sieve.

a)

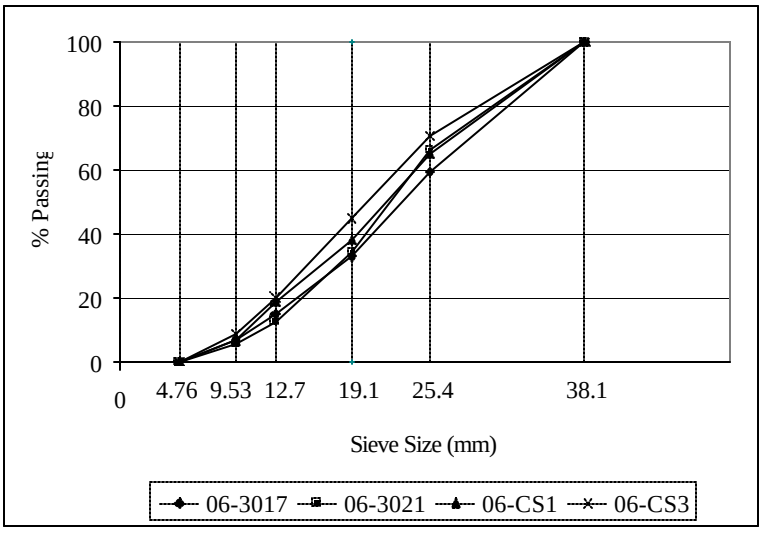

b)

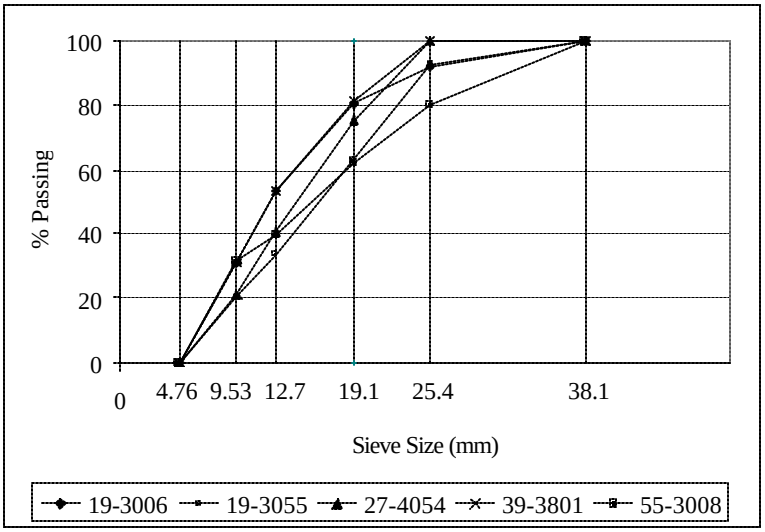

c)

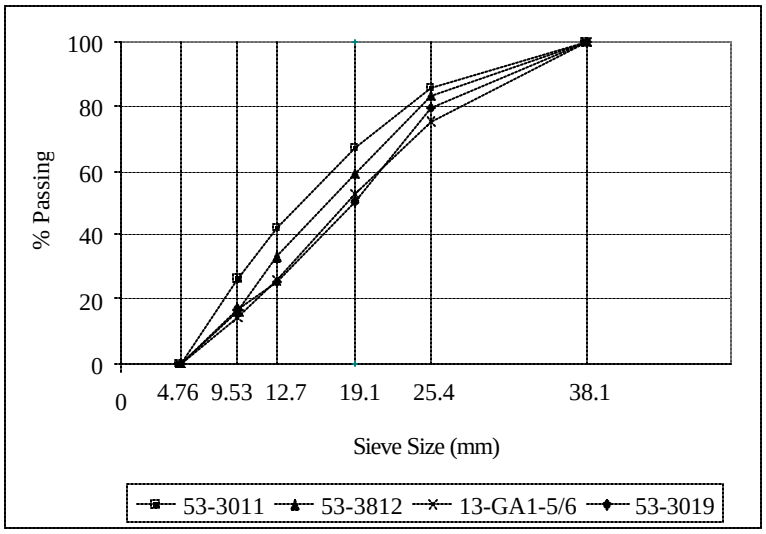

Figure 6.4.1a-c. *Coarse aggregate gradation curves. a)DNF zone, b)WF zone, and c)WNF and DF zones.*

6.4.2 Combined Fine and Coarse Aggregate Gradations

The coarse and fine aggregate gradation results as determined from the field cores are plotted in figure 6.4.1 as percent retained of combined aggregate gradations. They have been separated by climatic zone as the gradations appear to be related to regionally available sources of materials and climate zone requirements. These results show that the samples from the DNF and DF zones contain relatively high aggregate contents (46.3 to 53.2 percent by weight) in the size range of 12.7 to 25 mm (1/2 to 1 in). A higher content is also observed for aggregate size below 2.5 mm. This is particularly evident for the California sections 06-3017 and 06-3021 that contain very little material (2.88 to 4.74 percent by weight) in the intermediate size ranges (3.2 to 9.5 mm).

As compared with the specimens from the dry zones, the pavement sections from the WF and WNF zones generally have smaller grain sizes and less material retained on the larger sieves. Moreover, the aggregate distribution in the samples from the WF and the WNF zones generally plot within typical boundaries of the combined aggregate gradation curves.

In general, combined aggregate gradations in the WF zone are well graded. However, the aggregate distribution in one of the WF sections, 19-3055, is different from the others in that most of its aggregates (54 percent by weight) are between 6.1 mm (0.25 in) and 0.5 mm (0.02 in) in size. The highest aggregate contents in the other WF zone samples were observed on the 6.1-mm (0.25-in) sieve for sections 19-3006, 39-3801, and 55-3008, and on the 12.7-mm (0.5-in) sieve for section 27-4054. In the WF zone, very little aggregate is retained on the 25.4-mm (1-in) sieve (less than 4.1 percent by weight) for most sections. In one section, 55-3008, aggregate retained in this sieve is 12.4 percent by weight.

In the samples from the WNF sections, the maximum aggregate contents are retained on the 12.7-mm (0.5-in) sieve in sections 53-3812 and 13-GA1-5, and on the 6.1-mm (0.25-in) sieve for section 53-3011. Section 53-3011 contains less coarse material than 53-3812 and 13-GA1-5, but all three sections contain less material with aggregate sizes below 9.5 mm (0.375 in) than the WF sections.

a)

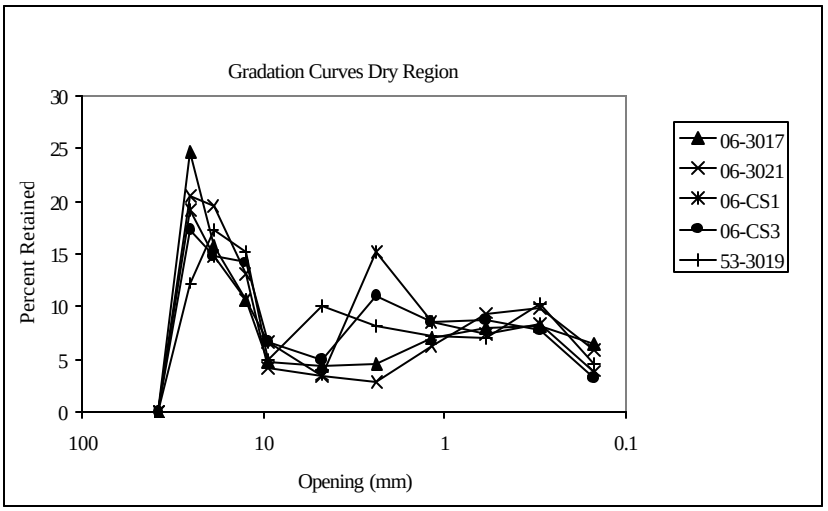

b)

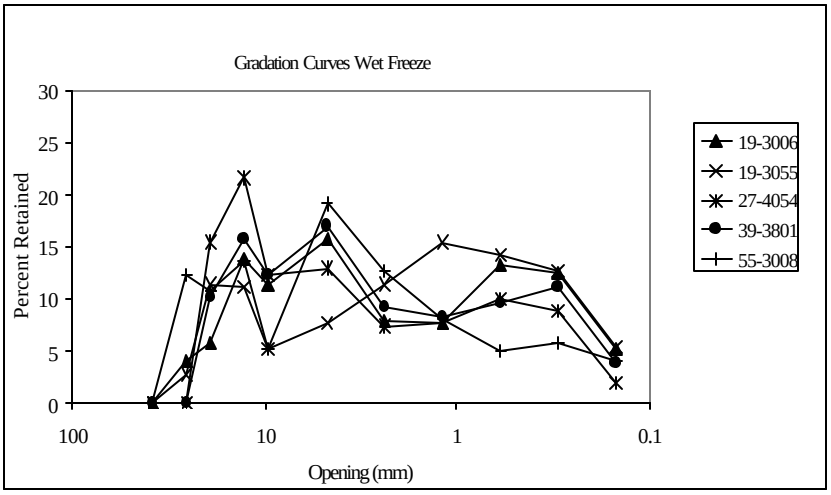

c)

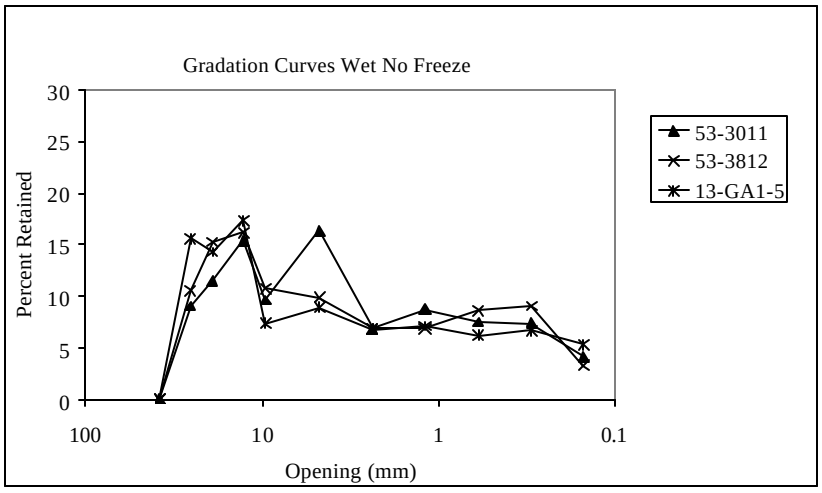

Figure 6.4.2 *Gradation curves for a) the DNF and DF zones, b) the WF zone, and c) WNF zone plotted in terms of percent weight retained.*

CHAPTER 7. DEVELOPMENT OF RECOMMENDATIONS

Project Background

In concrete applications other than pavements (e.g. bridges, columns for high rise buildings, off shore structures, etc.) there is a trend toward using higher strength. The advantages of higher compressive strength for structural applications are well understood. In pavement applications, high early strength concrete is used in special projects where it is convenient to minimize the interruption of traffic flow through congested areas. However, lacking good evidence of long-term performance benefits to be derived from additional strength, pavement engineers have been more reluctant to consider using higher than normal (28 MPa) strength PCC in typical pavement applications. Long-term pavement performance is affected by over 30 primary factors (table 1.4.1) in addition to concrete compressive strength.

It appears that the major benefit in using higher strength concrete is its improved resistance to chemical and physical deterioration as determined from fluid transport properties such as rapid chloride permeability and water permeability. Permeability is known to decrease several fold with increasing compressive strength. Thus, higher strength concrete would be expected to improve concrete spalling resistance at joints. This property is of major interest to SHA's in the wet-freeze regions, where spalling often is the major distress type, and repair and rehabilitation of the joint areas is expensive.

Project Objectives

In order to develop performance based specifications for the use of higher strength concrete in pavement applications, a materials study was undertaken to:

1. Determine the key concrete properties of Portland cement concrete (PCC) found in excellent performing, in-service, pavements (especially at joints.)

2. Determine the key PCC mix and materials characteristics and their proportions, responsible for the levels of the PCC properties.

3. Develop revised mix design procedures in order to provide concrete with the desired properties.

4. Develop prototype concrete mix designs, which will result in the production of concrete for use in pavements that possess these properties.

5. Identify test methods to measure these properties, which can be used for direct or indirect measure of key properties and mix features, needed to monitor the PCC quality level.

Project Tasks

Task A: This phase consisted of identifying the key PCC properties and materials characteristics known to play a role in PCC pavement performance. A synthesis report was developed based on literature review and preliminary analysis of PCC properties and pavement performance obtained primarily from the LTPP database. Based on these findings a select number of pavements were identified for detailed field and laboratory study in order to verify expected trends and/or develop new relations. The literature review is found in the interim report and is summarized in chapter 1.

The LTPP database and other available pavement project information were used to select pavements for detailed field and laboratory data collection and analysis in order to verify and further improve previously established trends. Further, gaps in current knowledge will be addressed. Several primary selection criteria were used such that a range of variables was investigated. These variables were PCC age (primarily PCC pavements older than 20 years), climate, traffic levels, distress levels and types, and strength levels. It was decided to concentrate the efforts on JPCP's.

Fifteen in-service concrete pavements ranging in age between 11 and 51 years, with traffic levels ranging between 3.9 million to over 23 million ESAL's were selected for detailed investigation. The selected fifteen test sections ranged from good to poor performing pavements, where the performance was determined from distress measurements of faulting, transverse cracking, and spalling according to the SHRP methods. The distress development over time was obtained from the LTPP database.

Six of these test sections from the DNF region were located California. These pavements were undowelled JPCP's, and they were all constructed on CTB and had variable joint spacings typical of California pavements. The California test sections were older pavements that at the time of investigation varied in age between 20 and 51 years. Three sections on the experimental test road, near Tracy, which had carried substantial traffic (16 million ESAL's), were selected to investigate the effects of strength and slab thickness on transverse cracking.

Five PCC pavements (four JPCP and one JRCP) were investigated in the WF climate ranging in age from 13 to 28 years. They were all LTPP test sites located in Ohio, Iowa, Wisconsin, and Minnesota. Three had doweled joints, and two were undoweled.

Three LTPP sections were selected from Washington as they had high field compressive strengths ranging from 57 to 79 MPa and had developed low levels of distress. Two sections were in the WNF climate, and one was in the DF climate (53-3019). A low strength and older JPCP in Georgia, located in the WNF climate, was selected, as it was almost distress-free despite its high age (25 years) and its high cumulative traffic (23 million ESAL's).

Task B: This was the data collection phase of the study. Field studies of the 15 pavements were conducted, and samples were tested in the laboratory for various properties. The field and laboratory test procedures are described in chapter 2. Results from the field and laboratory testing are presented in chapter 3 and the appendixes.

Task C: The field and laboratory results were analyzed in Chapters 4 through 6. The PCC properties (and their required levels) were determined, which are responsible for the good performance in JCP's of higher strength. Considering the key PCC properties, materials characteristics and mix design features were identified which produce these property levels.

Work carried out in Tasks A and B provides the basis for development of recommendations. Section 7.1 and 7.2, respectively, present major findings for PCC properties materials characteristics, and trends found with increasing strength. Mix design features and recommended additional design considerations are presented in section 7.3. In section 7.4 the effects of changing concrete properties and material characteristics on prototype mixes are discussed. Section 7.5 discusses additional PCC tests for improved quality and acceptance control.

7.1 Concrete Properties Necessary for Good Long-Term Performance

A major objective of this study was to determine key concrete properties and their effect on pavement performance. The key concrete properties found to relate to pavement performance were transport properties, strength, elastic modulus, coefficient of thermal expansion, drying shrinkage, and entrained air void system.

7.1.1 Long-Term PCC Properties

It is important to realize that long-term PCC properties were investigated. The average pavement age at time of testing was about 25 years. A substantial strength gain has occurred since time of construction as seen from the LTPP database values in table 7.1.1.

Early strength results from eight out of fifteen pavements clearly illustrate that they are regular strength highway concretes at the age of 28 days. As most of these concrete are good long-term performers it is clear that it is not necessary to achieve the long-term mechanical property levels at 28-days. However, it is important that substantial strength gain occurs in the field. This will vary for each cement type and environmental exposure conditions. Typically a Type II cement has higher later age strength gain as compared to a Type I. The environmental exposure conditions causing lower initial curing temperature is beneficial with respect to later age strength, and conditions associated with WF and WNF climates are beneficial in achieving substantial long-term strength gain based on analysis of the LTPP database. See section 5.1.

Table 7.1.1 *Field results of strength and elastic modulus from the LTPP database*

Climate	SHRP ID	State	Age at Testing (Days)	Flexural Strength (MPa)	Age at Testing (days)	Compressive Strength (MPa)	LTPP SURVEY (date)	Compressive Strength (MPa)	Tensile[1] Strength (MPa)	Elastic Modulus (MPa)
DNF	06-3017	CA					11/25/1991	44	5.0	28276
	06-3021	CA	14	3.79	14	25	11/18/1991	44	5.1	21034
	06-7456	CA	14	4.17	14	21	10/19/1995	50	5.7	29138
	CS1*	CA			28	27				
	CS3*	CA			28	31				
	I-10**	CA								
DF	53-3019	WA	14	5.60			4/21/1992	64	6.2	34138
WF	19-3006	IA	14	5.40	28	30		58	3.4	31552
	19-3055	IA	14	4.83	28	35	9/14/1993	59	3.9	23966
	27-4054	MN					2/28/1992	57	4.0	38276
	39-3801	OH	4	3.52	28	29		59	3.2	25862
	55-3008	WI			7	21	2/26/1992	72	4.7	46897
WNF	53-3011	WA	14	4.92			6/2/1992		7.0	36379
	53-3812	WA	14	3.39			6/1/1992		6.2	45690
	GA1-5/6**	GA								

* Data obtained from Caltrans field reports (sections not included in LTPP database)

** Section not included in LTPP database

[1] Most likely flexure strength

7.1.2 Long-Term Spalling Resistance in the WF climate

Spalling is the prevalent distress type in many older pavements in the WF climate region. Spalling is of major concern to SHA's as high severity joint deterioration often require expensive repair. Although, the spalling mechanisms are yet to be fully understood it is generally accepted that spalling is primarily related to durability and to a lesser extent to tensile strength (e.g. Sanadheera and Zollinger, 1995, and Titus-Glover et al., 1999).

A major finding of this study is that good drainage is a prerequisite for improved spalling resistance in the WF climate as drainage has a profound effect on the concrete pore saturation level at the slab base. Regardless of concrete permeability and the quality of entrained air void system, concrete cannot withstand prolonged continuous exposure to water as the capillary pores and air voids will become critically saturated. High saturation levels can initiate freeze-thaw damage. For cases of good drainage, long-term spalling at joints and free edges can be avoided by improving the resistance to water and salt transport using higher strength concrete. The major PCC properties needed for excellent long-term spalling resistance were found to be low permeability, entrained air (6 to 8.5 percent) and non-deleterious aggregates (i.e. F-T resistant, and not susceptible to AAR and sulfate attack).

Transport Properties Needed for Good Spalling Resistance

PCC transport properties such as permeability, chloride ion penetration resistance and water absorption can be critical to performance in freezing environments. In cases of poor drainage, increased PCC resistance to water transport helps avoid or delay critical saturation levels in the concrete and associated freeze-thaw deterioration of the paste. Other factors such as foundation drainage, aggregate soundness, and air void structure are also critical to spalling resistance.

In this study it was found that a PCC property, which was closely linked to transport properties, was compressive strength, irrespective of permeability test method. This is not surprising as both properties are closely tied to the porosity of the hydrated cement paste.

In order to achieve low permeability, a compressive strength level of 45 to 50 MPa is required. The field concretes with w/c ratios below about 0.45 were found to develop low permeability. (i.e. 2000 coulombs from RCPT method, 75×10^{-11} cm/sec using the Florida field water permeability test, and 0.1×10^{-16} m^2 using the Torrent air permeability technique). These levels were met for all of the test sections in the WF climate zone. In the remaining regions higher levels of permeability were observed. See discussions in sections 5.6 and 6.2.

Additional reduction in concrete permeability through increased compressive strength will occur. But for ultimate compressive strengths exceeding approximately 65 MPa the reduction in permeability is minor and would only provide slight improvements from a

durability point of view. A detailed discussion of the test results can be found in section 5.6 of this report.

In PCC's of higher w/c, such as the California, Georgia, and the Iowa PCC's, a through thickness permeability gradients were found. This was attributed to a higher local w/c ratio near the surface based on porosity measurements from mercury porosimetry.

The five concrete pavements investigated in the WF climate all had low permeability, suggesting that this property is important in long-term durability of concrete at exposed areas such as joints, cracks and free edges. One of these concretes, the Iowa LTPP section 19-3006, was selected since it out of all the LTPP test sections developed the highest amount of joint deterioration (i.e. spalling) despite having higher strength. The joint deterioration occurred from the bottom up and was found to be due to critical saturation of the air voids from long-term exposure to high moisture levels. This occurred due to poor drainage conditions creating a "bath-tub:" a slab on a poorly draining CTB and lacking longitudinal edge drains. This shows that low permeability is not sufficient in itself for good performance in a WF climate, and good drainage is of key importance in avoiding prolonged exposure to water.

The other Iowa concrete, LTPP section 19-3055, constructed on a granular base provided better drainage, and in this case its low permeability was sufficient. This pavement was distress free at joints and free edges despite its age (28 years). The Wisconsin pavement, also on a granular base and of an age of 22 years, was found to have higher strength (62 MPa) and very low permeability. Again, excellent PCC durability was found.

PCC Air Void Characteristics Needed for Good Spalling Resistance

Severe climatic exposure conditions such as freeze-thaw cycles combined with high moisture levels at the bottom of a concrete slab play a significant role with respect to PCC joint performance. As stated in ACI 201.2R, only good quality concrete with non-deleterious aggregates and appropriate amount of entrained air can survive freeze-thaw cycles. However, even good quality concrete may suffer freeze-thaw damage if the concrete is at a high level of saturation as observed for the Iowa test section, 19-3006. This study found that good to excellent freeze-thaw durability had been achieved when typical freeze-thaw requirements pertaining to the air void system and aggregate soundness were met. In most severe freeze-thaw climates (annual precipitation > 500 mm, annual freeze index > 150, and annual freeze-thaw cycles > 80), the characteristics of freeze-thaw durable PCC pavements were entrained air of 6 percent, spacing factor of less than 200 microns, specific surface area greater than 24 mm^2/mm^3, and non-deleterious reactive coarse aggregates. See section 5.7.

The five concrete pavements in the WF region are expected to be freeze-thaw durable, with the Ohio section, 39-3801, and the Iowa section, 19-3006, falling slightly below the recommended limit on minimum specific surface area. For the five concretes investigated the air content varies between 6.2 and 8.3 percent by volume. The calculated air void spacing factor varies between 51 and 178 microns, and the specific

surface area of air voids (a measure of the size of the air voids) varies between 22.4 and 40.6 mm^2/mm^3.

As discussed above the Iowa test section, 19-3006 has suffered from severe joint deterioration. Petrographic examination according to ASTM C 457 on the intact upper half of a core taken from a deteriorated joint showed that the smaller air voids (< 75 microns) were lined with a white crystalline deposit, which had rendered these voids ineffective. Thus, the minimum freeze-thaw requirements for both the spacing factor and the specific surface area were not met. The spacing factor was 221 microns and the specific surface area was 17.6 mm^2/mm^3. The concrete away from the joint had excellent air void characteristics with spacing factor of 102 microns, air content of 8.3 percent, and specific surface area of 22.4 mm^2/mm^3.

In climates outside the WF region, transport properties are not as critical as long as the aggregate are non-deleteriously reactive and the concrete is not subjected to prolonged exposure of high internal moisture levels activating deterioration mechanisms such as AAR. In this study concretes known to have AAR and other chemical distress were omitted from further investigation.

Mechanical related spalling distress may have been avoided due the associated increase in tensile strength with higher compressive strength PCC. However, this component of spalling is not fully understood, but in general higher long-term flexure strength is beneficial.

7.1.3 Improved Resistance to Fatigue Cracking

Transverse cracking in JPCP's can be the result of fatigue effects causing either bottom up or top-down cracking. Higher tensile strength is not required for excellent long-term performance in any climate because slab thickness is the effective parameter in controlling the fatigue resistance. The Iowa section 19-3055 located in the WF climate, and Georgia section 13-GA1-5 located in the WNF climate, had the lowest tensile strength in this study, yet they were found to have excellent long-term performance characteristics. These pavements were 28 and 26 years respectively at the time of this investigation, and the Georgia pavement had carried significant truck traffic (23 million ESAL's).

However, the concrete tensile strength affects the stress/strength ratio, which dictates the fatigue life. Therefore significant improvement in mid-panel transverse cracking resistance is expected by increasing the PCC's tensile strength. However, improved fatigue resistance can also be achieved by increasing slab thickness. It is estimated that a 25 mm (1 in.) increase in thickness from 225 mm (9 in.) to 250 mm (10 in.) will have the same effect as flexure strength increase of 0.70 MPa from 4.8 to 5.5 MPa (e.g. Yu et al, 1998). Each, of these alternatives may eliminate fatigue cracking as the failure mode provided that loss of support from pumping erosion does not occur. Other factors such as slab length and whether a stabilized base is bonded or unbonded have significant impact as well.

The high strength Washington JPCP, section 53-3812, on granular base fits the class of a high tensile strength (6 MPa in flexure) concrete, moderate slab thickness (225 mm), with significant traffic (12.8 million ESAL's) and no transverse cracking. The Wisconsin high strength JPCP section 55-3008, also on a granular base, has high tensile strength (6.1 MPa flexure) and consists of a 50 mm thicker slab (277 mm) and similar traffic (15.2 million ESAL's). Also, no transverse cracking has developed despite substantial slab settlement. It appears that higher tensile strength and greater thickness have played a major factor. Both these concretes were found to have lower w/c ratio (0.35 to 0.40) than is typically used for highway concrete.

Elastic modulus of concrete has a pronounced effect on the pavement deformation and curling/warping stresses. As elastic modulus increases the pavement slab deformation due to wheel loading decreases. However, curling/warping stresses increase proportional to concrete elastic modulus. A slightly increasing load-related stress occurs with increasing elastic modulus.

A strong correlation was found between elastic modulus and compressive strength based on field cores. The elastic modulus ranged from approximately 23,000 to 45,000 MPa while the compressive strength ranged from 33 to 75 MPa. See section 5.4. These results show that the elastic modulus increase is almost proportional to the increase in compressive strength, which was not expected based on the ACI-363 equation. Consequently, curling/warping stresses are more significant with increasing strength.

Top-Down Transverse Cracking Associated with Loss of Slab Support at Joints from Curling-Warping and Pumping Erosion

In the case of loss of support from curling-warping or pumping erosion, the critical slab loading position is at the transverse joint. In this case, axle loading near joint and corner of the slab causes maximum tensile stresses in the top of the slab at some distance away from the joint (Darter et al., 1995, and Khazanovich et al., 2000).

Over time, the loss of support due to pumping erosion combined with curling-warping phenomena creates large upward slab curvature and increased joint deflection during joint loading. In such event, greater slab thickness is an effective means of improving bending resistance and controlling transverse cracking (Darter et al., 1995).

Stress predictions by Khazanovich et al. (2000) based on finite element analysis show, that top-down transverse cracking can occur starting at the midslab outer edge for combinations of high axle loads at joints (i.e. tandem axle at a joint and a single axle at the other joint) and high built-in upward curvature. This loading condition locks both slab ends from rotating. This is especially a problem in cases where the axle spacing of a truck matches the joint spacing. This loading combination prevents slab rocking in short jointed slabs. The analysis showed that curling effects significantly influences top tensile stresses. For a given temperature gradient through the slab, the curling stress increases proportionally to the coefficient of thermal expansion and elastic modulus. Other factors, which have significant effect, include joint spacing and foundation stiffness.

When comparing a 75MPa concrete with a 33 MPa concrete, it was noted that the curling stresses predicted for the same temperature gradient was nearly 100 percent. This increase was attributed from the elastic modulus increasing from 24 to 47 GPa. Higher curling stresses would also arise from increased coefficient of thermal expansion (CTE). For the Tracy, California experimental project the high strength section had about a 40 percent increase in CTE as compared to the control concrete due to the increase in cement and paste content.

Figure 7.1.1 illustrates the permanent upward slab-base gap from curling-warping and pumping erosion effects for the Tracy experimental sections in California. The deflection profile from curling-warping is obtained from analysis of FWD slab deflection profile measurements in steps of 0.6 m (2 ft) in the traffic direction along the outer wheel-path (i.e. 0.6 to 0.9 m from outer edge). The profiles are shown for two consecutive slabs starting before the joint of the first slab and ending just after the second joint of the second slab. The analysis is based on the deflection profile shown in section 4.3 assuming that the midslab is in contact (i.e. reference point) and that the deflections at the joint, for a flat slab, would be similar at the deflections at midslab.

The upward curved slab shape is consistent with surface profile measurements as illustrated in chapter 4. The upward joint and crack deflection is similar for the three sections (CS 1, CS3 and 06-7456) varying between 50 and 150 microns. These results were obtained during a clear and sunny day October 29 and 30, 1998 between 9 AM and 1:30 PM. During that time the surface temperature increased from about 15 to about 28 °C while the deflection profiles remained nearly constant as seen for the thickened section, which was tested twice during this time period. This is evidence that a permanent gap exists between the slab and the base caused by combined curling-warping and base erosion. Base erosion was confirmed from cores taken at the joint and away from the joint as illustrated for the high strength section (CS3). See figure 7.1.2.

The results discussed in chapter 4 follow the expected trend from pumping effect on slab shape. It gradually curves upward towards each approach joint and falls off sharply on the leave joint side. This is consistent with buildup of fines on the approach joint side. At the same time, a sharp downward curvature on the leave side is consistent with expected effects from base erosion and with fault measurements. Further, these results suggest that slab cracking is predominantly expected at a distance of about 1.5 to 2.5 m (5 to 8 ft) from the leave joint, which is also in agreement with the observed crack location as discussed in section 4.3.

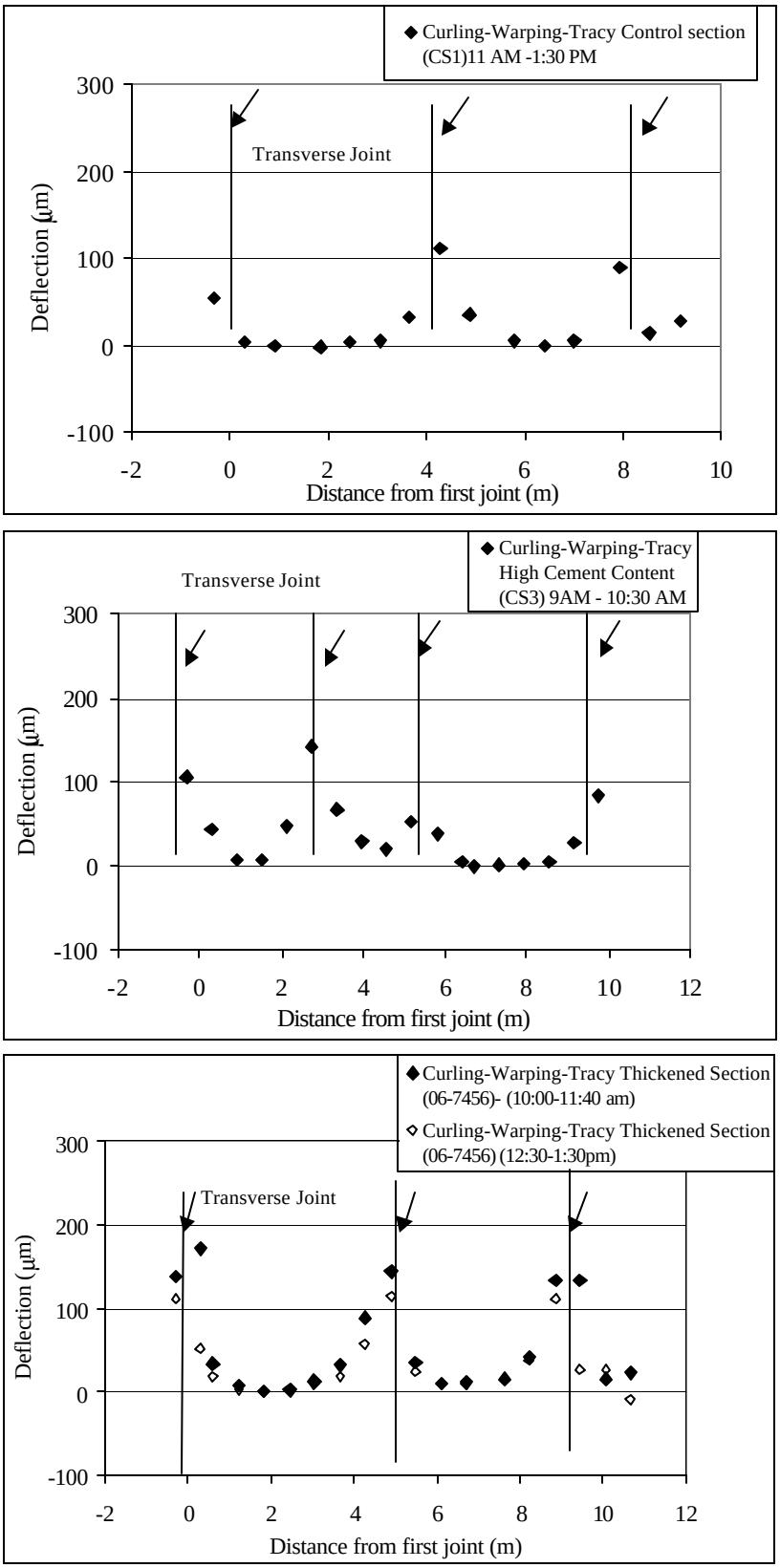

Figure 7.1.1 *Deflection profiles due to curling-warping of from the Experimental test road at Tracy, California.*

Figure 7.1.2 *Eroded CTB at joint. Decreasing erosion moving away from joint (left to right). Experimental test road at Tracy, California, with higher cement content.*

Moisture warping is also believed to have increased faulting, loss of slab support, and accelerated transverse cracking for the Iowa section 19-3006. The moisture warping has developed due to a poorly draining CTB base. The Iowa section had corner breaks at nearly every slab corner, typical for extensive loss of slab support.

The importance of good subsurface drainage in avoiding upward curvature from high moisture content at slab base near joints was investigated by Poblete et al. (1990). Also, Hveem, in a Caltrans report dating back to 1949, used profilograph measurements to demonstrate that vertical movements at slab ends from temperature and moisture differences in JPCP's increase over time. As a result the slab ends are curled or warped upward most of the time creating non-uniformity of contact and slab support. This mechanism causes pumping related distress when free water accumulates beneath the ends of a slab.

Darter et al. (1995) predicted using finite element analysis that slab thickness is a major factor in reducing the top tensile stress in cases of upward slab curvature and loss of slab support from curling-warping. This would explain why the thicker section (06-7456) of the Tracy experimental project has not developed transverse slab cracking despite similar losses of slab support as the other Tracy test sections.

The other extreme case of upward curling/warping is a slab on a soft foundation (i.e. low CBR subgrade), granular base, and undowelled joints. The Wisconsin section 55-3008 had developed extreme permanent upward curvature and joint faulting, but with only one slab cracked within the 153 m test section. This suggests that a PCC slab can "float" without breakup from traffic loads if the foundation is soft enough to maintain full support from curling and warping effects. Except for faulting, no other distress was found in the Wisconsin section, which is attributed to combinations of slab thickness (277 mm), flexure strength (6 MPa), excellent freeze-thaw resistance, durable aggregates, and low permeability (<1000 Coulombs RCPT).

The Georgia section was a lower strength concrete and dowelled JPCP on CTB and ATB. It was an excellent performer as it had not developed pumping erosion and associated upward curling. This suggests that the slab and base act together as a monolith, similar to German pavement design.

In summary, in cases of good design and construction practices, along with avoidance of loss of slab support, lower strength concrete can produce excellent long-term performance. However, if loss of support (pumping erosion and curling-warping) becomes significant, then higher strength PCC and/or greater slab thickness may be needed to control transverse cracking.

Premature Mid-Slab Transverse Cracking

Premature transverse cracking in PCC pavements is often associated with combinations of higher temperature at the time of construction and unfavorable environmental factors. These factors can affect the rate of hydration, strength gain, and moisture loss.

Within the first week after construction, rapid development of PCC properties occurs. These properties include coefficient of thermal expansion, elastic modulus, creep, shrinkage, and tensile strength occurs. These properties combined with environmental exposure conditions, timing of joint sawing, and slab restraint are important in avoiding mid slab transverse cracking. Creep and stress relaxation properties are significant during this time period. Beyond the first week the stress relaxation property is considerably reduced.

Concrete with a higher coefficient of thermal expansion and a higher elastic modulus is more sensitive to thermal gradient stresses known as curling stresses and moisture induced gradients from combined surface drying and/or high moisture level at the slab base at joints. Moisture warping develops over time, while slab deflections from curling follow a daily and seasonal cycle, with the maximum upward curvature at joints and corners (leading to increased joint deflection during heavy vehicle loading) occurs in the spring and summer at early morning hours when maximum thermal gradients are present (Hveem, 1949). Curling-warping, combined under certain unfavorable conditions, causes a permanent upward curved slab shape at the joints and corners. This together with water trapped at the slab-base interface from poor drainage and heavy vehicle loading starts the pumping mechanism resulting in joint faulting, corner breaks, loss of joint support, and eventually slab cracking. To combat pumping-erosion (pumping of fines) California adopted the practice of stabilizing base layers, hoping they would be erosion resistant. Hveem and Tremper (1957) concluded that concretes with reduced CTE and drying shrinkage potential are favorable for California weather conditions (warm and dry) leading to less upward curvature and improved long-term performance.

Additionally, concrete having higher CTE will undergo larger initial joint movement leading to increased crack width at joints. For certain coarse aggregate characteristics (soft aggregate and smaller top size) this can result in reduced load transfer efficiency (LTE) associated with aggregate interlock.

No correlation could be found between CTE and mechanical properties or aggregate type, which is probably due to the major effect that the cement paste content has on the CTE of concrete. CTE of the cement paste is 1.5 to 2 times that of the aggregate (FHWA LTPP-Program Reference Guide, 1996). In addition, variations in CTE can be significant within each aggregate type depending on mineral composition (Zoldners, 1971). CTE for dolomites ranges from 7.0 to 10.0 x $10^{-6}/^{o}$C, whereas granites and gneiss range from 6.5 to 8.5 x $10^{-6}/^{o}$C. These aggregate types were found in several concrete pavements for this project.

CTE values for concretes in California with cement contents of 307 kg/m^3 were about 9.8 x $10^{-6}/^{o}$C, increasing to 13.7 x $10^{-6}/^{o}$C for the higher cement content (418 kg/m^3) mix used at the Tracy test Road section 06-CS3. A 40 percent increase in cement content has resulted in about a 40 percent increase of CTE. Also, as seen from table 3.3.1, section 06-CS3 had a 10 percent higher elastic modulus (34,679 MPa) compared to the control concrete 06-CS1 (31,429 MPa).

The drying shrinkage property could not be determined on older field concretes as this property is irreversible for long-term environmental exposure. As high quality aggregates were found in the California concretes, and because the aggregate volume fraction was similar (75 percent of concrete), it is reasonable to assume that ultimate drying shrinkage has been similar for the control section (06-CS1) and the thickened section (06-7456) on the Tracy Test Road. However, the higher cement content concrete (06-CS3) is estimated to have substantially increased drying shrinkage as well as an increased CTE, although the actual amount of drying shrinkage is impossible to estimate as it depends on several factors (ACI 209). Based on the classical Pickett relation for aggregate volume effect on concrete shrinkage (Pickett, 1956), the higher cement content concrete (06-CS3) is estimated to have about 20 percent higher ultimate shrinkage than the control concrete 06-CS1.

Increased CTE and drying shrinkage are factors believed to have played a major role in the development of premature transverse cracking for the higher strength and higher cement content section (Tracy experimental project.) Caltrans distress survey showed that within one year, 42 percent of these slabs were cracked (Wells, 1993), while no cracking had occurred in the control concrete section of similar thickness or in the thickened section. The cumulative traffic at that point was about 0.31 million ESAL's. The number of cracks in this section remained constant until surveys stopped in 1990, at which point the estimated total traffic was 8.23 million ESAL's. During the period between one year after construction (1972) and 1980, 25 percent of the slabs in the control section (CS1) had developed transverse cracking. Number of cracks for both sections remained constant until 1990.

These results suggest that transverse slab cracking in the higher strength section (containing higher cement content) occurred due to restraint against contraction from thermal and drying shrinkage, and possibly late sawing, or curing problems or a combination of these factors. Premature distress is consistent with the higher CTE and shrinkage associated with higher cement and paste content of the mix.

7.1.4 PCC Properties Needed for Good Long-Term Resistance to Joint Faulting

This study findings show that joint faulting is a consequence of pumping erosion and/or slab settlement on soft foundation. Amount of joint faulting is, for a given climate and base/foundation type, primarily affected by heavy vehicle loading (i.e. ESAL's). See chapter 4 for more detail. These findings are in good agreement with a recent study by Titus-Glover et al., 1999, based on a comprehensive analysis of the LTPP database. It is apparent that PCC properties and materials characteristics play a secondary role through factors, which affect the rate of pumping (i.e. aggregate interlock and upward curvature from curling/warping).

Observations can be made regarding long-term aggregate interlock in the presence of upward curled joints based on the California sections, as they were undowelled. One site worth noting is the 51 year old test section on westbound I-10, in San Bernadino Co., near Los Angeles, where joint load transfer values were high (78 to 95 percent). This concrete had large gravel-like aggregates with a maximum size of 50 to 62 mm. This suggests that some types of coarse aggregate can improve LTE as they enhance the load-bridging action across a crack (e.g. Colley and Humphrey, 1967; and Nowlen, 1968; and Abdel-Maksoud et al., 1998). However, high variability in LTE was observed for the Tracy test sections probably associated with high variability in joint faulting and joint crack width from slab to slab.

7.2 Concrete Materials Characteristics Required to Produce the Above PCC Properties and Their Levels

PCC material characteristics and their required levels for achieving the necessary levels of PCC properties were determined. The key PCC material characteristics were w/c ratio, cement type and content, and coarse aggregate characteristics. The following discussions describe these factors in terms of the observations of this study.

7.2.1 Water-Cement Ratio

Water-cement ratio is the key mix characteristic controlling concrete strength (tensile and compressive). In most cases, the range was found to be typical of regular strength concrete pavements. See table 6.1.1. Using the LTPP database values and estimated w/c ratio values from water absorption tests, the w/c ratio ranged from 0.35 to 0.46 in the WF region, with an average of 0.42. The California PCC's located in the DNF region and the Georgia PCC in the WNF region had considerably higher w/c ratios. A range of about 0.46 to 0.67 was observed. The average w/c ratio for these concretes was 0.52. The WNF zone concretes from Washington (53-3812 and 53-3011) have low w/c ratios of about 0.40.

Lower w/c ratios were also associated with improved transport properties in the concretes. The data here suggests that one avenue for achieving high durability is by using a low w/c ratio. This is particularly valuable in the WF zone, where freeze-thaw resistance is needed. In the other climatic zones low permeability levels may be desired in order to protect the PCC from chemical deterioration.

As discussed in section 7.1, in the warm regions, PCC's with higher w/c ratios were found to have a permeability gradient (highest permeability at the slab surface), likely due to higher w/c ratios at the top of the slab compared to the bottom of the slab. Thus, these concretes are more exposed to moisture penetration near the pavement surface. This is discussed in detail in section 5.6. Lower w/c ratio concretes were seen to be both less permeable and more uniform through their thickness.

In chapter 6 it was shown that the compressive strength correlates well with w/c ratio despite the large differences in climate, and aggregate type and content. As seen in figure 6.2.1, an R^2 value of 0.80 was observed using regression with a simple power-curve. The w/c ratio was also related to elastic modulus and splitting tensile strength. However, the correlations were not as strong for these properties, as the R^2 values were below 0.40 from power-curve regressions.

7.2.2 Cement Type and Content

Not surprisingly, Type II (lower heat of hydration) Portland cements were found in warmer climates such as California, Georgia and even Washington State. The test sections in the WF climate used primarily Type I cements. The cement contents in these studied sections ranged from 252 to 418 kg/m^3 and averaged 328 kg/m^3.

The three highest compressive strength sections in this study (53-3812, 55-3008 and 53-3011) had similar cement contents, 335 kg/m^3, which is typical for pavement concrete. This indicates that higher strength can be achieved with typical mix proportions. The higher strength was obtained from combinations of slightly lower w/c ratio, excellent curing conditions, and good aggregates.

Many SHA's have traditionally designed pavements for a given slump, and have used cement content as the mechanism for increasing strength. A typical concrete mix contains 5.5(California) to 6 sacks (Michigan) of cement per cubic yard of concrete (307 to 335 kg/m^3). Often higher design strengths are obtained by increasing the cement content substantially. This was observed for the 7.5 sack (418 kg/m^3) mix used in the Tracy, California test section 06-CS3. While this approach is indeed effective in raising the strength, it may increase the tendency to cracking from increased CTE and shrinkage properties, as was the case in this section.

7.2.3 Coarse Aggregate Characteristics

In this study, coarse aggregate characteristics were found to significantly impact concrete properties in several areas, including aggregate interlock, fracture properties, and concrete durability to environmental attack.

Three different coarse aggregate groups were observed in the studied concretes: silicate rock gravel, dolomite/limestone, and crushed silicate rocks. The dolomite/limestone aggregates were used exclusively in concretes from the WF zone, most likely because of their local availability (test sections 19-3006, 19-3055, 27-4054, and 55-3008). The Ohio section 39-3801 contained a variety of coarse aggregate types, ranging from silicates and sandstone to limestone. The Georgia sections, 13-GA1-5 and 1-6, contained crushed granitic to granodioritic aggregates while the California and Washington State concretes mainly contained gravel of silicate rocks (test sections 06-3017, 06-3021, 06-7456, 06-CS1, 06-CS3, 06-I-10, 53-3019m 53-3011, 39-3801, and 53-3812).

Petrographic analysis showed that the aggregates had primarily remained chemically inert during placing of the concretes and their subsequent use. However, minor ASR was occasionally observed in the fine aggregate, particularly in Iowa section 19-3055, and Ohio section 39-3801. In the coarse aggregates ASR was rare and was only observed in Washington section 53-3019, and Ohio section 39-3801. It is concluded that high quality aggregates that are not deleteriously reactive (i.e. non reactive and freeze-thaw resistant) are important for long-term performance, particularly in aggressive environments like the WF climate zone.

The coarse aggregate gradations were very similar in the California concretes, which were significantly coarser than the gradations encountered in the other sections. The nominal maximum aggregate size was typically 38 mm in these sections with one section, 06-I10 as high as 62 mm. In general, these older concretes had well-graded aggregates of larger maximum particle size than commonly found in modern pavements. The nominal maximum aggregate size for the other studied sections ranged from 25 mm for PCC's in the WF climate to 38 mm in concretes outside the WF region. The smaller aggregates used in the WF region are consistent with D-cracking considerations. The gradations generally fell within the gradation limits of ASTM C 33.

It is noteworthy that the California combined (coarse and fine aggregate) gradations have 19 to 25 percent retained on the 25 mm sieve, which is beneficial for maintaining high load transfer through aggregate interlock. LTPP test section 55-3008 in Wisconsin had 12 percent retained on the 25 mm sieve, which is more than typically observed in PCC's in the WF region. This section is heavily faulted. It is speculated that large faulting and crack widths associated with slab settlement overshadow the effect of improved load transfer from larger aggregate size. Other factors such as the slabs being undoweled have contributed as well.

The presence of dowels and stiff foundations have been effective in maintaining high load transfer for the Iowa section 19-3006, and the Minnesota test section 27-4054, despite having only 0 to 4 percent retained on the 25 mm sieve.

The California PCC's were found to have excellent fracture resistance related to their gravel characteristics (strong and large size). The 51 year old California test section 06-I10, is an example of a low distress pavement with high traffic level (>16 million ESAL's), consisting of lower compressive strength (37.6 MPa) PCC with good splitting tensile strength (4.0 MPa). The large and strong gravel mix (top size of 50 to 62 mm) has ensured excellent load transfer (88 percent average) at joints and cracks and high fracture resistance (230 N/m). See table 4.2.1 and table 5.5.1.

7.3 Mix Design Procedures for Improved Long-Term Performance

Additional design considerations are proposed in order to improve the long-term pavement performance in terms of spalling and premature cracking. These distresses are categorized as durability issues related to environmental loading. The additional durability design considerations can be incorporated into current mix design procedures for proportioning normal concrete mixes.

This study also confirms several of the mix design considerations on materials related factors, which influence the durability of concrete pavements, resistance to environmental as well as traffic loading (e.g. Forster, 1997). Table 7.3.1 lists the mix and material factors confirmed in this study to significantly affect PCC properties. The mix factors were aggregates, cement, additives, and w/c ratios. This study focuses on the factors related to long-term PCC performance, and therefore table 7.3.1 does not elaborate on factors related to PCC workability, constructability, and economy.

Table 7.3.1 *Mix and material factors affecting PCC properties observed herein*

Mix Categories	**Material Characteristics**	**Affected PCC Properties**
Aggregates	Gradation, Maximum aggregate size	Elastic modulus, drying shrinkage (%paste), fracture resistance, brittleness, aggregate interlock
	Soundness	AAR resistance
	Strength (hardness)	Fracture resistance, brittleness, aggregate interlock
	Type	Coefficient of thermal expansion
Cements	Content	Coefficient of thermal expansion, strength, drying shrinkage
	Type	rate of strength gain
Additives	Air entraining	F-T resistance of the paste
w/c	level of:	ultimate strength, permeability, and elastic modulus

7.3.1 Mix Design Considerations for Improved Durability

Resistance to spalling is improved with low PCC permeability. Current design procedures (e.g. ACI 211) typically enforce a maximum w/c ratio of 0.45 and durable aggregates when the PCC is subjected to severe environmental loads (e.g. WF climates). This study found that in addition to the w/c ratio requirement that the level of permeability must also be specified and determined.

Further, this study found that several PCC's in the dry regions had a significant permeability gradient through the slab thickness with the highest permeability at the slab surface. Permeability gradients are believed to be caused by the tendency towards a more porous concrete near the surface when the mix w/c ratio is about 0.40 or greater. A more uniformly low permeability concrete was found for w/c ratios of about 0.40 or less.

In some cases a high early strength mix design is desired. It is common practice by SHA's to increase the cement content in order to achieve high early strength. Although it is generally known that such mix designs will lead to concrete with higher thermal stresses from heat of hydration as compared to regular cement contents. These concretes were found to have increased CTE, which further increases their early age (first 72 hours) cracking susceptibility. Later on drying shrinkage adds to these stresses, and combined effects can lead to premature cracking.

High early strength can also be obtained by lowering the w/c ratio rather than increasing the cement content. The reduction in w/c ratio to obtain 28-day strength values of 30 – 40 MPa can be achieved using combinations of water reducing admixtures and mineral additives, while maintaining typical cement contents (279 to 335 kg/m^3) (PCA 1995).

7.4 Prototype Concrete Mix Designs for Good Long-Term Jointed Concrete Pavement Performance

In section 7.3 modifications to the design considerations and procedures were discussed based on the mix and material characteristics needed for long-term performance. This section builds on the findings regarding PCC properties and the materials characteristics required to achieve excellent pavement performance, as presented in sections 7.1 and 7.2 respectively. In combination with the mix designs discussed in section 6, it is now possible to provide recommendations for prototype concrete mix designs for improved durability (i.e. spalling and premature transverse crack resistance) and improved structural capacity (i.e. improved fatigue resistance).

It is paramount that good practices must be followed during construction to ensure that the concrete mix designs will provide the intended improvement in long-term performance. The interaction of the concrete with the environment and any loading at early ages must be considered. As an example, heat generated during hydration must be estimated and combined with the effects of expected environmental conditions. Hot weather concreting requires special consideration, and changes in mix proportions may become necessary to prevent excessive internal temperatures, thermal gradients, and thermal stresses.

If these and other factors during the early life of the concrete are not considered, damage may occur that will prevent the concrete from attaining the intended design properties or design life.

Prototype mix designs, which are expected to meet these improved durability and structural capacity criteria are presented in tables 7.4.1 and 7.4.2. They are divided into two different climate groups (WF/DF) and (WNF/DNF). With the exceptions of the Washington concretes, they are divided into normal strength PCC and high strength PCC, as the mix designs were found to be typical for normal strength concrete (i.e. design strength less than 41.4 MPa (6000 psi)). These concretes were found to have ultimate in-service compressive strengths of up to 75 MPa and estimated flexure strength of about 6.0 MPa. Their w/c ratios were below 0.40. These concretes appear to have high resistance to spalling (despite low air content) and fatigue cracking.

Table 7.4.1 *Prototype mix designs for durable PCC pavements*

Climate Region	**Range of W/Cementitious ratio**	**Range of Cementitious Content (kg/m^3 (lb/cyd))**	**Cement Type**	**Minimum Air content in Hardened concrete (%)**	**Range of Coarse Aggregate (kg/m^3 (lb/cyd))**	**Range of Fine Aggregate (kg/m^3 (lb/cyd))**	**Target C/F ratio**
Regular Strength Mix Designs:							
WF/DF	0.40-0.45	≈335 (564)	I/IA or equivalent	6.0	990 -1280 (1669-2159)	564-839 (951-1407)	1.6
WNF/DNF	0.40-0.60	279-335 (470-564)	II/IIA or equivalent	No requirements	990 -1280 (1669-2159)	564-839 (951-1407)	1.6
High Strength Mix Designs:							
All	0.35-0.40	335-418 (564-705)	I A/II A or equivalent	6.0 in WF/DF	990 -1280 (1669-2159)	564-839 (951-1407)	1.6

Table 7.4.2 *Ultimate PCC properties for good long-term jointed concrete performance by climate region*

Climate Region	Range of Ultimate Compressive Strength (MPa)	Range of Ultimate Flexure Strength Range (MPa)	Range of Ultimate Elastic Modulus (GPa (10^6 psi))	Maximum RCPT Rating[1] (Coulombs)	Recommended Maximum CTE ($x10^{-6}$/°C)
Regular Strength Mix Designs:					
WF/DF	45-60	5.0-5.5	27.6-35 (4.0 - 5.0)	1000-2000 or low	10
WNF/DNF	35-60	4.5-5.5	25-35 (3.6-5.0)	2000-4000 (Moderate)	10
High Strength Mix Designs:					
	60-75	5.5-6.0	35-47 5.0-6.8)	100-1000 (Very low)	10

[1] If mineral additives such as fly ash or ground granulated slag are used, the water sorption test is recommended as well

7.4.1 Prototype Concrete Mix Designs and Ultimate PCC Properties for Improved Performance in the WF/DF Region

A major finding of this study was that regular strength concrete mixes are sufficient to provide good long-term spalling resistance in highway concrete in WF climates. A w/c ratio of about 0.45 or less is sufficient as the PCC will develop low long-term permeability, and a compressive strength of about 45 to 50 MPa. The minimum air content is about 6.0 percent, and the aggregate must be sound with respect to freeze-thaw and other durability attack.

Improving Performance by Increasing Strength

Increased 28-day strength above the typical design value of about 4.5 MPa (650 psi) may require combinations of lower w/c ratio, higher cement content, and water reducers. High strength concrete mixes with a 28-day compressive strength of 41.4 MPa (6000 psi) or higher typically contain higher than normal (335 kg/m^3) cement and paste contents. This places special demand on construction and curing methods to avoid early cracking.

Lowering w/c ratio

Lowering the w/c ratio to about 0.40 provides a more homogeneous concrete. This reduces the permeability gradient through the concrete thickness, which can leave the exposed surface vulnerable to environmental attacks (e.g. improving salt scaling resistance).

Lowering the w/c ratio has added benefits in terms of increased long-term fatigue resistance, as these concretes are expected to reach and exceed 5.5 MPa in ultimate

flexure strength. This corresponds to an additional 10 percent increase in long-term flexure strength as compared to a 28-day design value of 4.5 MPa (650 psi).

Adjusting Cement Type and Content

In the WF region it is adequate to use a Type I Portland cement, and a mix containing about 335 kg/m^3 (6 sack mix) cementitious material.

To achieve a higher than normal strength level (typically 4.5 MPa in flexure) it may be necessary to increase the cement content beyond the typical range of 300 to 335 kg/m^3 found in this study. The 418 kg/m^3 (7.5 sack) cement content mix of the high strength Tracy test section 06-CS3 had a reported 28-day compressive strength of 31 MPa, compared to 26 MPa for the 307 kg/m^3 (5.5 sack) cement content of the control concrete 06-CS1 (Spellman et al., 1973).

The cement contents and w/c ratios for an experimental JPCP in Detroit and the test sections from this study agree well with the PCA guidelines for required cement content and w/c ratio to achieve the expected strength levels (PCA, 1995). As an example, for air-entrained concrete containing Type I cement and regular cement content (i.e. about 335 kg/m^3), a 28-day compressive strength of 30 to 35 MPa can be expected for a 0.40 w/c ratio.

It must be noted, however, that increasing strength by increasing cement content may be detrimental to performance with respect to transverse cracking and faulting. Increasing cement content can significantly increase concrete shrinkage and CTE properties. These higher PCC levels can lead to transverse cracking from curling/warping due to loss of support, and/or loss of load transfer from excessive joint opening.

Mineral Additives

Due to the age of the studied sections, none contained mineral additives like fly ash or blast furnace slag. The use of mineral additives was therefore not within the scope of these investigations. However, modern mix designs frequently contain mineral additions. There is a wealth of literature on the benefits and detriments of mineral additives. Generally, though, it has been the experience of the investigators that mineral additives can be used as a partial replacement of cement to provide benefits such as added protection against chemical attacks like ASR, and reduced heat development during hydration. Excellent strength and low permeability can be achieved through the addition of mineral additives.

Minimum Requirements to Air Void System

For severe exposure conditions, ACI 211.1-91 recommends that the minimum total air content of concrete with a maximum aggregate size of 25 to 38 mm be in the range of 5.5 to 6 percent. Furthermore, air void spacing factor of less than 200 microns and specific surface area of air voids of 24 mm^2/mm^3 or greater are recommended. The air-entrained concretes from the WF climate region in this study all fall within these limits. These properties have sufficiently protected the studied pavements from freeze-thaw damage. Except in one case, where long-term saturation rendered the air void structure ineffective.

Aggregate Characteristics to be Considered in All Climates

Aggregate Soundness

Aggregate soundness is imperative for durable concrete. Aggregate soundness is the aggregate's resistance to all aspects of weathering and typically encountered chemical reactions. The weathering aspect includes heating and cooling, wetting and drying, and freezing and thawing. The chemical durability concerns reactions such as AAR. Thus aggregate soundness is important in all climates.

Aggregate Content, Size, and Gradation

In addition to aggregate soundness, the characteristics of the aggregates that have an important influence on proportioning concrete mixtures are particle size and distribution, content, and the shape and surface texture (PCA, 1998).

The aggregate volume content was found to be about 70 percent. This is consistent with low shrinkage. In addition, the weight ratio of coarse to fine aggregate was typically close to 60 percent coarse and 40 percent fine aggregates (C/F ratio about 1.6). These ratios are typical mix designs designed for pavements according to ACI 211 and PCA (1998).

This study showed that the older and higher strength PCC's contained larger maximum aggregate size than is typically used in today's conventional highway concrete. A larger top size has several advantages. First it reduces water and paste demand, leading to less drying shrinkage. The general guidelines for cement and water content versus maximum aggregate size can be used. As an example, an increase in maximum aggregate size from 25 to 50 mm generally results in a 15 percent reduction in cement and water content. For a 25 mm maximum size and 75 mm slump, a 335 kg/m^3 is sufficient for a non-air entrained concrete. For the concretes with the maximum nominal aggregate size of 38.1 mm and no air-entrainment, approximately 307 kg/m^3 of cement is required for a 75 mm slump concrete. These cement content levels were generally observed in this study for the test sections in California (06-3017, 06-3021, 06-7456, 06-CS1, and 06-I10). Second, tougher and larger sized aggregates provide better aggregate interlock and load transfer at joints and cracks for crack bridging. Furthermore, lower cement and paste content reduces CTE, and thus reduces joint crack width. Smaller crack width is important for maintaining long-term load transfer for any aggregate type and size.

It should be noted, however, that in severe climates maximum aggregate size may need to be limited for durability reasons. Increasing aggregate size can increase susceptibility to durability attacks, particularly for marginal quality aggregates.

Both fine and coarse aggregates in this study were found to be well-graded, and typically within ASTM C 33 grading limits. Therefore existing guidelines for aggregates according to ASTM C 33 and ACI 211 are necessary and adequate.

7.4.2 Prototype Concrete Mix Designs and Ultimate PCC Properties for Improved Performance in the WNF and DNF Regions

In the WNF/DNF regions spalling is not as prevalent, and more porous concretes can be used successfully. Based on this study, if the aggregate are AAR resistant, a w/c ratio of up to about 0.60 can provide excellent spalling resistance. Fatigue resistance is the major design factor. An ultimate flexure strength of about 4.5 MPa appears to be adequate in conjunction with sufficient slab thickness. Substantial improvement in fatigue resistance and ultimate flexure strength is achieved by reducing the w/c ratio below 0.60. A wide range in cement contents was found in the WNF/DNF region to provide excellent long-term performance ranging from 279 to 335 kg/m^3 (5 to 6 sack).

Lowering w/c ratio

In these regions the importance of permeability appears to be reduced as deicing salts and freeze-thaw cycles are not factors. However, in these hot, dry climates the advantage of lowering the w/c ratio would be to achieve a more homogeneous concrete. This reduces the permeability gradient through the concrete thickness, which can reinforce the concrete against environmental attacks. At the same time, in hot, dry climates workability requirements should be considered when selecting w/c ratio values. As discussed in section 7.4.1, it is an advantage to lower the w/c ratio to increase the PCC's fatigue resistance.

Cement Type and Content

Concretes in warmer climates such as in the WNF/DNF climates typically use a lower heat of hydration portland cement (Type II). In addition, these regions can typically use lower cement contents averaging 307 kg/m^3 as the resistance to fluid transport is often less of a concern.

In particular in dry regions, the potential for drying shrinkage should be addressed through minimizing the total paste content. As in the WF region, it is recommended to keep the paste content around 25 percent. As is also valid in the WF discussion, increasing the cement content can significantly increase the CTE. It was found in this study that CTE should be as low as possible. The typical range of 9 to 10 x 10^{-6}/°C was adequate for good performance.

7.5 Test Methods for Quality Acceptance and Control

This study has established several threshold levels for PCC properties and material characteristics, which were associated with good long-term performance in terms of spalling, transverse cracking, and faulting. Considering these findings, additional test methods are recommended to improve quality control and acceptance protocols.

The recommended tests should be performed in addition to already established quality control and acceptance measures employed by the various SHA's.

7.5.1 Test Methods for Improved Spalling Resistance

From this study it has been established that joint deterioration related to transport properties and freeze-thaw damage can be avoided when certain PCC properties and material characteristics met critical levels. In particular,

- PCC fluid transport is low.
- Air void content is about 6 to 8 percent.
- Ultimate compressive strength exceeds about 45 to 50 MPa.
- w/c ratio below about 0.45.
- Aggregates are not deleteriously reactive and are freeze-thaw resistant.

Transport Properties (Permeability and Chloride Resistance)

Low fluid transport properties (such as permeability) are fundamental to improved resistance to joint deterioration. This study found a strong relation between ultimate permeability values and compressive strength. Low permeability was achieved when the compressive strength exceeded 45 to 50 MPa. This is similar to, but somewhat lower than findings by Armaghani and Bloomquist (1994), who stated that the compressive strength must exceed 55 MPa to ensure that the PCC indeed has low permeability. Because the required compressive strength for low permeability is also dependent on the test method used, it is recommended that pre-construction testing be performed on the project specific concrete to establish a relationship between permeability and compressive strength. Field quality control and acceptance criteria can then be developed based on compressive strength values of test cylinders.

There are many permeability and transport property tests available. Two fluid transport test methods can be recommended based on this study. These are the rapid chloride permeability test (RCPT) and the water absorption test. However, no single transport property test gives an intrinsic material permeability value, and it is wise to use more than one test method. The RCPT in particular should be used with caution because it is an electro-chemical index test, and does not physically measure the transport of fluids. When used with OPC concretes with typical pavement mix designs, the RCPT is highly repeatable and reliable. On the other hand, the use of modern cements containing mineral additives may influence RCPT results.

Transport Properties of Concretes Containing Mineral Additives

Because none of the studied pavement sections were designed to contain mineral additives, inferences about the effect of mineral additives on transport properties must be drawn from the literature and laboratory data available to the research team from another study.

Concretes with a number of blended cement systems containing fly ash and blast furnace slag were cast and tested using the RCPT at 63, 91 and 270 days, and 3 years. These mixes had typical pavement mix designs, and contained between 20 and 25 percent mineral additives as a cement replacement. The concretes were air entrained to be suitable for the WF climate zone. The mixes included two different class F fly ashes, one type C fly ash, and one ground granulated blast furnace slag (GGBFS).

In figure 7.5.1 the RCPT results of the various blended systems are plotted against compressive strength, along with those of OPC's from the field and the laboratory study. A significant reduction in RCPT results is noted for blends of low to moderate strength over OPC's at similar strengths. In the figure all blend systems are lumped together into one relation for convenience. However, it is likely that each type and amount of mineral additive would exhibit a different RCPT and different strength relation.

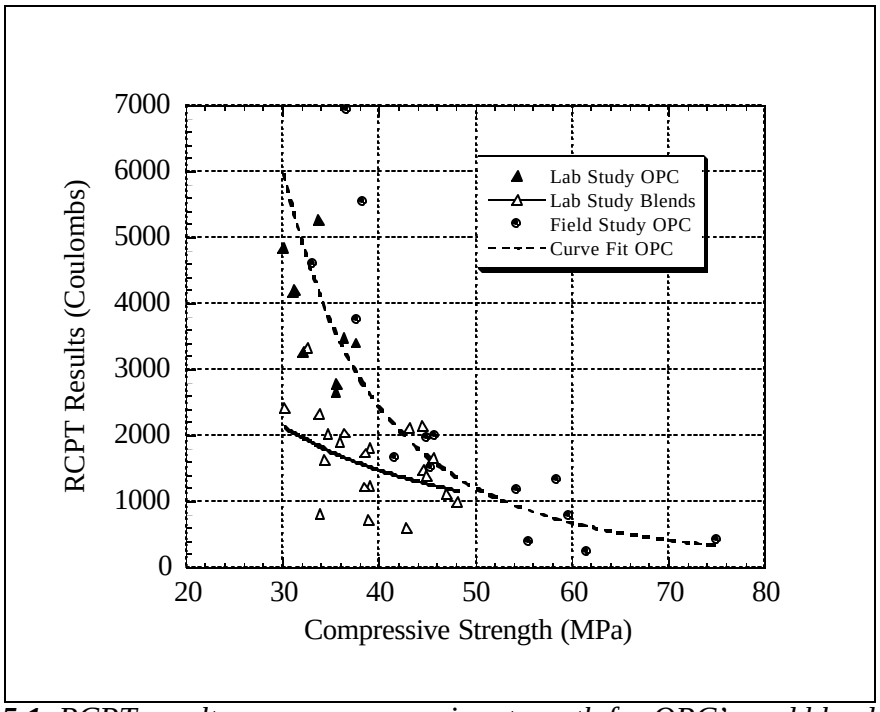

Figure 7.5.1 *RCPT results versus compressive strength for OPC's and blended cement systems from the field and laboratory studies.*

In recent years, though, a major concern has been raised about the RCPT. Researchers have found that the low RCPT measurements may not be caused by microstructure densification, but by changes in the pore solution chemistry (eg. Shi et al., 1998). These pore solution changes affect the electrical conductivity of the concrete, lowering measured RCPT values, but not the actual concrete permeability. As a result, a falsely low permeability is reported.

Figure 7.5.2 contains water absorption test data from the field study and from OPC and blended cement mixes in the laboratory study at 3 years. The significant decreases in transport seen with the RCPT are not visible here. All of the data here fall on one strength-permeability relation curve. Similar observations are made from the water permeability test. This indicates that the decreased RCPT results with blended systems are not primarily associated with a significant permeability decrease, but with some other mechanism. It is possible, for example that indeed the chloride ion penetration is significantly reduced with blended cements. However, permeability does not appear to be. A thorough study of the concrete microstructure and reaction processes would likely clear up the remaining uncertainty.

The absorptivity slope plotted here is obtained by taking the slope of the water uptake per unit area versus square root of time relationship, as described previously.

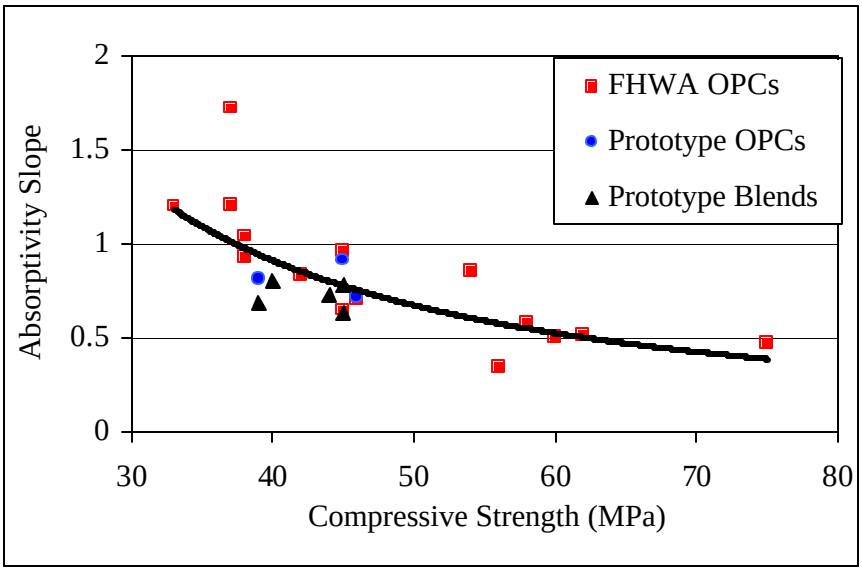

Figure 7.5.2 *Absorptivity slope versus compressive strength relation for field study and prototype mixes.*

Air Void System and Aggregate Soundness

Most SHA's already have established rigorous test methods for assuring adequate air void characteristics and sound aggregates. If post construction evaluation is desired, air void characteristics (air content, the spacing factor and specific surface area) can be determined in detail using the ASTM C 457 method. However, due to the detailed nature of this method, it is only recommended as a forensic tool. A good estimate of total air void content can also be gleaned from the relatively simple water absorption test, as described in chapter 6.

7.5.2 Test Methods for Improved Resistance to Transverse Cracking

This study found that transverse cracking could be avoided if the PCC slab has adequate strength and thickness, and if loss of support and large volumetric deformations are avoided as well. The observed PCC levels and material characteristics associate with improved resistance to transverse cracking are,

- PCC flexure strength exceeding 4.5 MPa when the slab thickness is adequate.
- Ultimate compressive strength exceeds about 33 MPa.
- CTE below 10.0 x 10^{-6}/°C.
- Drying shrinkage minimized with a paste content of about 25 percent (or about 28-30 percent including air).
- w/c ratio below about 0.60.
- Coarse aggregate tough and large sized.

Compressive Strength, Tensile Strength, and Elastic Modulus

Adequate strength is the controlling parameter for improved resistance to transverse cracking. The JPCP design procedures use the flexure strength as a design criterion. Current practice is often to establish a relationship between flexure strength and compressive strength, and then to base the field acceptance on the compressive strength measured from field cores. The main reasons for not using field beams are due to their large size and variability.

The PCC splitting tensile strength may serve as a better indicator of the PCC tensile capacity over its compressive strength. In general there is expected to be a stronger relation between flexure and splitting tensile strength, than between flexure and compressive strength.

It is, therefore, recommended that pre-construction testing be performed on the project specific concrete to establish a relationship between flexure strength and splitting tensile strength. Field quality control and acceptance can then be developed based on splitting tensile strength values of test cylinders from the field. Typically the same test equipment can be used to determine all the strength values. ASTM describes, in detail, the strength tests mentioned here.

In addition to PCC strength, the PCC elastic modulus is a key parameter in controlling the slab stresses. This study found that the ultimate elastic modulus increased proportionally to the ultimate compressive strength. This raises the need for determining the elastic modulus when higher strength concrete is used, as the elastic modulus increases more significantly than the increase in tensile capacity. This amplifies the significance of the elastic modulus as it could become a key input parameter for proper thickness design. Therefore, in the case of higher strength concrete, it is recommended that pre-construction testing be performed to establish the level of the elastic modulus associated with the PCC strength levels. The elastic modulus should be determined according to the current ASTM procedure.

Coefficient of Thermal Expansion

High CTE values were found associated with premature cracking. Therefore, it is recommended to keep CTE to a minimum. This study found that CTE values below 10.0 x $10^{-6}/^{o}$C were adequate. Based on the findings in this study, high CTE values become a concern when high cement contents are used. It is thus recommended to determine the concrete CTE when higher cement content is needed to obtain a desired level of strength. The test method is currently not an ASTM standard. However, the CTE test method developed by FHWA and used in this study has been accepted as a provisional standard by AASHTO. See chapter 2 for details.

PCC Resistance to Crack Propagation

Increasing strength has traditionally been viewed as increasing concrete brittleness. This study found that higher strength concrete may not become more brittle if tough coarse aggregates are selected. If higher strength is needed, the PCC fracture behavior can be optimized by proper coarse aggregate selection. The fracture energy test described in

chapter 2 of this report is an adequate measure of the resistance to crack propagation. This test is not currently an ASTM standard, however it is accepted and presented in detail by RILEM.

It was found that the ratio of fracture energy and splitting tensile strength can be used as an indicator of brittleness, and that the larger fracture energy to tensile ratio indicate tougher fracture behavior.

It is recommended that pre-construction tests be performed to establish which of the available aggregate sources would yield the toughest fracture behavior. The aggregates should be evaluated using the mix design and mix proportions intended for construction. The mix yielding the highest ratio should be selected, given that it also meets aggregate durability specifications.

7.5.3 Quality and Acceptance Control for Improved Resistance to Faulting

Faulting in this study has been linked primarily to foundation settlement and pumping erosion, both of which are structural level distresses. Thus, neither PCC properties nor material characteristics directly relate to faulting distress. At the same time, indirect relations to faulting are made with properties and materials characteristics that relate to improving load transfer across cracks and minimized pumping. As was described in the transverse cracking discussion above, the primary factors include large volumetric deformations and improved aggregate toughness. The test methods for these properties and characteristics have been discussed in section 7.5.2.

REFERENCES

AASHTO T 277 - 93 (1994). "Standard Method of Test for Electrical Indication of Concrete's Ability to Resist Chloride." *Standard Specifications for Transportation Materials and Methods of Sampling and Testing, Part II - Tests*, 16th Ed., American Association of State Highway and Transportation Officials, Washington, DC.

AASHTO (1986). *Guide for Design of Pavement Structures.* NCHRP Project 20-7/24, Vol. 2, American Association of State Highway and Transportation Officials.

AASHTO (1993). *Guide for Design of Pavement Structures - 1993*, Washington D.C. American Association of State Highway and Transportation Officials.

Abdel-Maksoud, M.G., Hawkins, N., and Barenberg, E. (1998). "Effect of geometric and mechanical properties of concrete joints on their cyclic shear response." Presented for the 1999 Federal Aviation Administration, Technology Transfer Conference.

ACI Committee 363 (1984). "State-of-the Art Report on High Strength Concrete." *ACI Journal*, Vol. 81, No. 4, Jul-Aug 1984, 364-411.

ACI Standard 211.1 (1989). "Recommended Practice for Selecting Proportions for Normal Weight Concrete." *ACI Manual of Concrete Practice, ACI*, Detroit, MI.

ACI Standard 318 (1994). "Durability Requirements, Section 4.2.1." *ACI Manual of Concrete Practice, ACI*, Detroit, MI.

ACI 360R-92 (1992). "Design of Slabs on Grade." Reported by ACI Committee 360, *ACI*, Detroit, MI.

Addis, B.J., ed. (1986). *Fulton's Concrete Technology.* Portland Cement Insitute, Midrand, South Africa.

Ahmad, S.H. (1994). "Short Term Mechanical Properties." *High Performance Concrete and Applications*, S.P. Shah and S.H. Ahmad, eds., Edward Arnold, London, UK, 27-64.

Aitcin, P.C., and Lessard, M. (1994). "Canadian Experience with Air-entrained High Performance Concrete." *Concrete International*, Vol. 16, No. 10, Oct 1994, pp. 35-38.

Aldea, C., Shah, S., and Karr, A. (1999). "Effect of Cracking on Water and Chloride Permeability of Concrete." *Journal of Materials in Civil Engineering*, Aug 1999, pp. 181-187.

Alungbe, G. D., Tia, M., and Bloomquist, D.C. (1990). "Effects of Aggregate, Water/Cement Ratio, and Curing on the Coefficient of Linear Thermal Expansion of

Concrete." *Transportation Research Record*, No. 1335, Transportation Research Board, pp. 44-51.

Armaghani, J., Romano, D., Bergin, M., and Moxley, J. (1994). "High Performance Concrete in Florida Bridges." *American Concrete Association Special Publication SP-140-1*, pp. 1-20.

Armaghani, J., and Bloomquist, D. (1994). "Development of Concrete Durability Specification and Ratings in Florida." *Transportation Research Record*, No. 1458, pp. 8-13.

Armaghani, J.M., and Bloomquist, D.G. (1993). "Durability Specification and Ratings for Concrete." *Concrete 2000*, R. Dhir and R. Jones, eds., E & FN Spon, pp. 23-36.

Armaghani, J.M., Larsen T.J., and Romano, D.C. (1992). "Aspects of Concrete Strength and Durability." *Transportation Research Record*, No. 1335, pp. 63-69.

ASTM C 39 - 94 (1995). "Standard Test Method for Compressive Strength of Cylindrical Concrete Specimens." *1995 Annual Book of ASTM Standards*, Vol. 04.02, Philadelphia, Pennsylvania.

ASTM C 457 - 90 (1995). "Standard Test Method for Microscopical Determination of Parameters of the Air-Void System in Hardened Concrete." *1995 Annual Book of ASTM Standards*, Vol. 04.02, Philadelphia, Pennsylvania.

ASTM C 469 - 94 (1995). "Standard Test Method for Modulus of Elasticity and Poisson's Ratio of Concrete in Compression." *1995 Annual Book of ASTM Standards*, Vol 04.02, Philadelphia, Pennsylvania.

ASTM C 496 - 90 (1995). "Standard Test Method for Splitting Tensile Strength of Cylindrical Concrete Specimens." *1995 Annual Book of ASTM Standards*, Vol. 04.02, Philadelphia, Pennsylvania.

ASTM C 856 - 83 (Re-approved 1988) (1995). "Standard Test Method for Petrographic Examination of Hardened Concrete." *1995 Annual book of ASTM Standards*, Vol. 04.02, Philadelphia, Pennsylvania.

ASTM C-1084 (1995). "Standard Test Method for Portland Cement Content of Hardened Hydraulic-Cement Concrete." *1995 Annual Book of ASTM Standards*, Vol. 04.02, Philadelphia, Pennsylvania.

ASTM C 1202 - 94 (1995). "Standard Test Method for Electrical Indication of Concrete's Ability to Resist Chloride Ion Penetration." *1995 Annual Book of ASTM Standards*, Vol. 04.02, Philadelphia, Pennsylvania.

Bache, H.H., and Vinding, I. (1990/1992). "Fracture Mechanics in Design of Concrete Pavements." *Proceedings, Second International Workshop on the Design and*

Evaluation of Concrete Pavements, CROW/PIARC, 4-5 October, Siguenza, Spain, pp. 139-164. (Also CBL reprint, CtO Aalborg Portland, Denmark -- in Danish.)

Benkelman, A.C. (1933). "Tests of Aggregate Interlock at Joints and Cracks." *Engineering News Record*, Vol. 3, No. 8, August 1933, pp. 227-232.

Bentz, D. et al. (1999) "Transport Properties and Durability of Concrete: Literature Review and Research Plan", NISTIR 6395, September 1999, pp.1-41.

Long, B., and Shatnawi, S. *"An Evaluation of Experimental PCC Pavement Design Features in California"*, TRB, 2000, pp.1-28.

Bjontegaard, O. (1999). "Thermal Dilation and Autogeneous Deformation as Driving Forces to Self-Induced Stresses in High Performance Concrete." Doctoral Thesis, The Norwegian University of Science and Technology.

Bradbury, R.D. (1938). *Reinforced Concrete Pavements.* Wire Reinforcement Institute, Washington, DC.

Bruinsma, J.E., Raja, Z.I., Snyder, M.B., and Vandenbosshe (1995). "Factors Affecting the Deterioration of Transverse Cracks in JRCP." Final Report, Contract 90-0973, to Michigan Department of Transportation. Michigan State University.

Buch, N., Frabizzio, M.A., and Hiller, J.E. (2000). "Factors Affecting Shear Capacity of Transverse Cracks in Jointed Concrete Pavements (JCP)." Final Report to Michigan Department of Transportation. Michigan State University.

Byrum, C.R., Hansen, W., and Kohn, S. (1997). "The effect of PCC Strength and Other Parameters on the Performance of PCC Pavements." *Sixth International Purdue Conference on Concrete Pavement Design and Materials for High Performance*, Vol. 1, pp. 373-393.

Carpinteri, A. (1986) "Mechanical Damage and Crack Growth in Concrete," Martinus nijhoff, Dordrecht. – as reference in Karihaloo (1995) p. 141.

Carrasquillo, R.L., Nilson, A.H. and Slate, F.O. (1981). "Properties of High Strength Concrete Subject to Short-Term Loads." *ACI Journal*, May-June 1981, pp. 171-178.

Colley, B.E., and Humphrey, H.A. (1967). "Aggregate Interlock at Joints in Concrete Pavements." *Highway Research Record*, No. 189, National Research Council, pp. 1-18.

Cramer, S.M., Hall, M., and Parry, J. (1995). "Effect of Optimized Total Aggregate Gradation on Portland Cement Concrete for Wisconsin Pavements." *Transportation Research Record,* No. 1478, July 1995, pp. 100-106.

CTA-Composite Testing and Analysis, Inc. (1998). *Design of Thermal Expansion Units,* Ann Arbor, Michigan.

Darter, M.I. (1977). *Design of Zero-Maintenance Plain Jointed Concrete Pavement: Vol. I-Development of Design Procedures.* FHWA, Report No. FHWA-RD-77-111.

Darter, M.I., and Barenberg, E.J. (1977). *Design of Zero-Maintenance Plain Jointed Concrete Pavement*. Report No. FHWA-RD-77-111., Vol. 1.

Darter, M.I., Peshkin, J.M., Snyder, M.B., and Smith, R.E. (1985). "Portland Cement Concrete Pavement Evaluation Systems – COPES." *National Cooperative Highway Research Program Report*, No. 227, Transportation Research Board, Washington DC.

Darter, M.I., Smith, K.D., and Peshkin, D.G. (1991). "Field-Calibrated Mechanistic-Empirical Models for Jointed Concrete Pavements." *Transportation Research Board,* No. 1307, National Research Council, Washington DC, pp. 143-153.

Darter, M.I., Hall. K.T., and Kuo, C-M (1994). *Support Under Concrete Pavements – Appendix E.* Prepared for National Cooperative Highway Research Program, Transportation Research Board, National Research Council, University of Illinois at Urbana-Champaign.

DataPave 97 (1997). *Long Term Pavement Performance (LTPP) Program Database*. US Department of Transportation, Federal Highway Administration.

Emborg, M. (1989). "Thermal Stresses in Concrete Structures at Early Ages." Doctoral Thesis, Lulea University of Technology.

FHWA (1996). *Determination of The Coefficient of Thermal Expansion of Portland Cement Concrete.* Draft.

FHWA (1995). *Performance of Concrete Pavements Containing Recycled Concrete Aggregate: Task B Draft Interim Report.* Prepared for the Federal Highway Administration by the University of Minnesota and ERES Consultants, Inc.

FHWA-SA-93-012-1992 (1992). *Report on the 1992 U.S. Tour of European Concrete Highways.* Federal Highway Administration, Publication No. FHWA-SA-93-012-1992.

Field Permeability Test (FPT) User's Manual. March, 1993.

Forster, S.W. (1997). "Concrete Materials and Mix Design for Assuring Durable Pavements." *Sixth International Purdue Conference on Concrete Pavement Design and Materials for High Performance,* Vol. 1, pp 111-118.

Foxworthy, P.T. (1985). "Concepts for the Development of a Nondestructive Testing and Evaluation System for Rigid Airfield Pavements." Ph.D. Thesis, University of Illinois at Urbana-Champaign.

Frabizzio, M.A., and Buch, N.J. (1999). "Investigation of Design Parameters Affecting Transverse Cracking in Jointed Concrete Pavements." *Transportation Research Board*, No. 1668, National Research Council, Washington DC, pp. 24-32.

Gan, G-L, Spry, P.G., Cody, R.D., and Cody, A.M. (1996). "Rim Formation in Iowa Highway Concrete Dolomite Aggregate: The Effects of Dedolomitization Reactions." *Environmental & Engineering Geoscience*, Vol. 2, No.1, Spring 1996, pp. 59-72.

Garboczi, E. (1990) "Permeability, Diffusivity, and Microstructural Parameters: A Critical Review," Cement and Concrete Research, Vol. 20, pp.591-601.

Giaccio, G., and Zerbino, R. (1998). "Failure Mechanism of Concrete – Combined Effects of Coarse Aggregates and Strength Level." *Advanced Cement Based Materials*, Elsevier Science Ltd., Vol. 7, pp. 41-48.

Gillespie, T.D., Karamihas, S.M., Sayers, M.W., Nasim, M.A., Hansen, W., and Ehsan, N. (1993). *Effects of Heavy-Vehicle Characteristics on Pavement Response and Performance.* Transportation Research Board, NCHRP Report 353, National Research Council, National Academy Press, Washington, DC.

Hansen, W., and Jensen, E.A. (2000). "Fracture Energy and Brittleness of Highway concrete: Effect of Coarse Aggregate Type and PCC Strength Level." *Cementing the Future, Center for Advanced Cement-Based Materials*, Spring 2000, Vol. 11, No. 2.

Hansen, W., Definis, A., Jensen, E., Byrum, C.R, Mohamed, A.R., Mohr, P., and Grove, G. (1998). *Investigation of Transverse Cracking On Michigan PCC Pavements over Open-Graded Drainage Course.* Final Report submitted to MDOT, University of Michigan.

Hansen, W., Mohamed, A. R., Byrum, C. R., and Jensen, E. (1998). "Effect of Higher Strength on Pavement Performance." *Proceedings, Materials Science of Concrete: The Sidney Diamond Symposium*, pp. 191-204.

Hearn, N., Hooton, D., and Mills, R. (1994). "Pore Structure and Permeability." *Tests and Properties of Concrete*, ASTM C 169, pp. 240-262.

Hillerborg, A. (1983). *Fracture Mechanics of Concrete.* "Chapter 4.1 Analysis of one single crack." Wittman, ed., Elsevier Science Publisher B.V., Amsterdam, pp. 223-249.

Holbrook, L.F., and Kuo, W.H. (1974). *General Evaluation of Current Concrete Pavement Performance in Michigan: Jointed Concrete Pavement Deterioration Considered as a Probability Process.* Michigan Research Laboratory Section, Michigan

Department of State Highways, Research Project 69 F-110, Research Report No. R-905.

Huang, Y. H. (1993). *Pavement Analysis and Design*. Prentice Hall, Englewood Cliffs, New Jersey.

Hveem, F.N. (1949) *"A Report of an Investigation to Determine Causes For Displacement and Faulting at the Joints in Portland Cement Concrete Pavements on California Highways"*, Caltrans, May 17, 1949.

Hveem, F.N., and Tremper, B. (1957). "Some Factors Influencing shrinkage of Concrete Pavements", ACI Journal, pp. 781-789, 1957.

Ioannides, A.M., and Korovesis, G.T. (1990). "Aggregate Interlock: A Pure Shear Load Transfer Mechanism." *Transportation Research Record*, No. 1286, Transportation Research Board, National Research Council.

Jensen, E.A, and Hansen, W. (2000). "Fracture Energy Test for Highway Concrete-Determining the Effect of Coarse Aggregate on Crack Propagation Resistance." *Transportation Research Record 1730,* pp. 10-16.

Kan, Y-C, and Swartz, S.E. (1995). "The effect of mix variables on concrete fracture mechanics parameters." *Fracture Mechanics of Concrete Structures, Proceedings FRAMCOS-2*, F.H. Wittmann, ed., AEDIFICATIO Publishers, Freiburg, Germany, pp. 111-118.

Karihaloo, B.L. (1995). *Fracture Mechanics & Structural Concrete.* Concrete Design & Construction Series, Longman Scientific & Technical, John Wiley & Sons, Inc., New York.

Kelleher, K., and Larson, R.M. (1989). "The Design of Plain Doweled Jointed Concrete Pavement." *Proceedings of the Fourth International Conference on Concrete Pavement Design and Rehabilitation*, Purdue University, West Lafayette, IN, April 1989.

Kleinschrodt, H.-D., and Winkler, H. (1986). *The Influence of Maximum Aggregate Size and the Size of Specimen on Fracture Mechanics Parameters, Fracture Toughness and Fracture Energy of Concrete.* F.H. Wittmann, ed., Elsivier Science Publishers B.V., Amsterdam, pp. 391-402.

Kosmatka, S.H., and Panarese, W.C. (1988/1992*). Design and Control of Concrete Mixtures.* 13th ed., PCA, Skokie, IL.

Kosmatka,S.H., Panarese W.C., Gissing,, K.D.,and MacLeod, N.F., (1995). *"Design and Control of Concrete Mixtures"*, Portland Cement Association. 1995.

Lane, S. (1994) "Thermal Properties of Aggregates," In *Significance of Tests and Properties of Concrete and Concrete-Making Materials*, Ed. Klieger, P., and Lamond, J.F. ASTM 04-169030-07, pp.438-445.

de Larrard, F., and Malier, Y. (1992). *High Performance concrete: From material to structure*. Y. Malier, ed., E & FN Spon, pp. 85-114.

Larson, R.M., Suneel, V., Forster, S. (1993). *Summary Report - U.S. Tour of European Concrete Highways (U.S. Tech) -- Follow-up tour of Germany and Austria*. FHWA-SA- 93-080, pp. 1-108.

"*Long-Term Pavement Performance-Program Reference Guide*"; Version 1.0, March 1996, Pavement Performance Division, Federal Highway Administration, 34 pp.

Mahoney, L.J., Pierce, L., Jackson, N., and Barenberg, E. (1991). "Urban Interstate Portland Cement Concrete Rehabilitation Alternatives for Washington State." WA-RD 202.1, p.350.

Marks, V.J. (1990). "An Overview of D-Cracking." *Nation D-Cracking Workshop Procedings,* Conducted by Kansas DOT and FHWA.

Marzouk, H. and Chen, C.W. (1995). "Fracture Energy and Tension Properties of High-Strength Concrete." *Journal of Materials in Civil Engineering*, Vol. 7, No. 2, May 1995, pp. 108-116.

Metha, P. (1990). "Durability of High Strength Concrete." Paul Klieger Symposium on Performance of Concrete, ACI SP-122, pp.19-27.

Mehta, P.K., and Aitcin, P.C. (1990). "Microstructural Basis of Selection of Materials and Mix Proportions for High-Strength Concrete." *High- Strength Concrete: Second International Symposium*, T.H. Weston, ed., ACI SP-121, pp. 89-108 and pp.265-286.

Mehta, P. and Monteiro, P.J.M. (1993). *Concrete: Structure, Properties, and Materials*. Second Edition, Prentice Hall, Inc., Englewood Cliffs, New Jersey.

Meyers, S.L. (1950). "Thermal Expansion Characteristics of Hardened Cement Paste and of Concrete." *Materials and Construction, Proc. Highway. Resesearch*., Board 30, 193.

Mindess, S., and Young, J. F. (1981). *Concrete.* Prentice-Hall, Inc., Englewood Cliffs, New Jersey.

Mobasher B., and Mitchell, T.M. (1988). "Laboratory Experience with the Rapid Chloride Permeability Test." *Permeability of Concrete,* ACI SP-108, pp. 117-144.

Mohamed, A.R., and Hansen, W. (1996). "Prediction of Stresses in Concrete Pavement Subjected Non-Linear Gradients." *Journal of Cement and Concrete Composites*, Vol. 18, pp. 381-387.

Mohamed, A.R., and Hansen, W. (1999). "Micromechanical Modeling of Crack-Aggregate Interaction in Concrete Materials." *Journal of Cement and Concrete Composites*.

Monteiro, P.J.M., and Helene, P.R.L. (1994). "Designing Concrete Mixtures for Desired Mechanical Properties and Durability, Concrete Technology: Past, Present and Future." *Proceedings of V.M. Malhotra Symposium*, K. Mehta, ed., ACI SP-144, pp. 519-543.

Neville, A.M. (1975). *Properties of Concrete.* Pitman Publishing Inc.

Neville, A.M. (1981). *Properties of Concrete.* Pitman Publishing Inc.

Neville, A.M. (1983). *Properties of Concrete.* 3rd Edition, The English Language Book Society and Pitman Publishing, London.

Neville, A.M. (1997) "Properties of Concrete", Wiley, pp.1-844.

NCHRP 1-26, (1990) *Calibrated Mechanistic Structural Analysis Procedures for Pavements.* Vol. 2, Appendices D.2.2-34, University of Illinois at Urbana-Champaign.

Nowlen, W.J. (1968). "Influence of Aggregate Properties on Effectiveness of Interlock Joints in Concrete Pavements." *Journal of the PCA*, Research and Development Laboratories, Vol. 10, No. 2, May 1968, pp. 2-8.

Ollivier, J., Massat, M., Parrot, L. (1995). "Parameters Influencing Transport Characteristics." *Performance Criteria for Concrete Durability*, RILEM Report No. 12, H. Hilsdorf and J. Kropp, eds., pp.33-96.

Owusu-Antwi, E.B., and Darter, M.I. (1994). "Early Results of the LTPP Concrete Pavement Data Analysis." *Third International Workshop on Design and Evaluation of Concrete Roads*, Vienna, Austria.

Packard, R.G., and Tayabji, S.D. (1985). "New PCA Thickness Design Procedure for Concrete Highway and Street Pavements." *Third International Conference on Concrete Pavement Design and Rehabilitation*, Purdue University, pp. 225-236.

PCA (1984). *Thickness Design for Concrete Highway and Street Pavements.* Portland Cement Association.

PCA (1988/91). "Design and Construction of Joints for Concrete Highways." *Concrete Paving Technology*, Portland Cement Association.

Peshkin, D.G., Smith, K.D., Darter, M.I, and Arnold, C. (1994). "Performance Evaluation of Experimental Pavement Designs at Clare, Michigan." *Transportation Research Record*, No. 1227, pp. 24-32.

Petersson, P. (1981). *Crack Growth and Development of Fracture Zones in Plain Concrete and Similar Materials*. Division of Building Materials, Lund Institute of Technology, Lund, Sweden.

Philleo, R.E. (1986) "Freezing and Thawing Resistance of High-Strength Concrete", NCHRP Report 129, pp.1-31.

Pickett, G.O., (1956). *"Effect of Aggregate on Shrinkage of Concrete and a Hypothesis Concerning Shrinkage"*, ACI Journal, January 1956, pp. 581-590.

Pittman, D.W. (1996). "Factors Affecting Joint Efficiency of Roller-Compacted Concrete Pavement Joints and Cracks." *Transportation Research Record*, No. 1525, National Research Council, Washington DC, pp. 10-20.

Poblete, M., Salsilli, R., Valenzuela, R., Bull, A., and Spratz, P. (1989). "Field Evaluation of Thermal Deformations in Undoweled PCC Pavement Slabs." *Transportation Research Record*, No. 1207.

Poblete, M., Ceza, P., Espinosa, D.R., Garcia, A., and Gonzalez, J. (1991). "Model of slab cracking for portland cement concrete pavements." *Transportation Research Record*, No. 1307, Transportation Research Board, National Research Council, Washington, DC.

Powers, T.C. (1945). "A Working Hypothesis for Further Studies of Frost Resistance of Concrete." *Proceedings*, American Concrete Institute, Vol. 41, pp. 245-272.

Powers T.C. & Brownyard T.L., (1948) "Studies of the Physical Properties of Hardened Portland Cement Paste", PCA Bulletin 22.

Powers, T.C. (1949). "The Air Requirement of Frost-Resistant Concrete." *Proceedings of the Highway Research Board*, Vol. 29, Highway Research Board, National Research Council, Washington, DC, pp. 184-211.

Price, W.H. (1951). "Factors Influencing Concrete Strength." *ACI Journal*, Feb 1951, pp. 417-432.

Rauhut, J. B., Lytton, R.L, and Darter, M.I. (1984). *Pavement Damage Functions for Cost Allocation*. Four Volumes, Report No. FHWA/RD-84/017-020, Federal Highway Administration, U.S. Department of Transportation, Washington, DC.

Rhodes, C.C. (1949). *Curing Concrete Pavements.* Michigan State Highway Department, Project 42 B-14(2), Report 145.

RILEM Committee FMC 50 (1985). "Determination of the fracture energy of mortar and concrete by means of the three-point bend tests on notched beams." Mater. Struct., 18.

Roesler, J.R., and Barenberg, E.J. (1998). "Fatigue of Concrete Beams and Slabs." Final report FHWA-IL-UI-265. University of Illinois Urbana, Illinois.

Roy, D.M., Silsbee, M.R., Sabol, S., and Scheetz, B.E. (1995). "Superior Microstructue of High-Performance Concrete for Long-Term Durability." *Transportation Research Record,* No. 1478, July 1995, pp. 11-19.

Schonlin, K., and Hilsdorf, H.K. (1988). "Permeability as a Measure of Potential Durability of Concrete - Development of a Suitable Test Apparatus." *Permeability of Concrete,* ACI SP-108, pp. 99-116.

Sellevold E.J., (1986) "Hardened Concrete-Determination of air/macro and gel/capillary porosity (PF-Method)," Report 01731, Norwegian Building Institute.

Senadheera, S.P., and Zollinger, D.G. (1994). "Framework for Incorporating Spalling in the Design of Concrete Pavements." *Transportation Research Record*, No. 1449, Transportation Research Board, National Research Council.

Senadheera, S.P. and D.G. Zollinger. (1995). "Influence of Coarse Aggregate in Portland Cement Concrete on Spalling of Concrete Pavements." Research Report 1244-11, Texas Transportation Institute, College Station, TX.

SHRP-P-338 (1993). *Distress Identification Manual for the Long-Term Pavement Performance Project*. Strategic Highway Research Program, National Research Council, Washington, DC.

Simpson, A.L., Rauhut, Jordahl, P.R., Owusu-Antwi, E.B., Darter, M.I., and Ahmad, R. (1994). "Early Analysis of LTPP General Pavement Studies Data, Volume 3: Sensitivity Analysis for Selected Pavement Distresses." Report No. SHRP-P-393. Strategic Highway Research Program, Washington, DC.

Smiley, D.L. (1995). "Michigan Department of Transportation-First Year Performance of The European Concrete Pavement on Northbound I-75-Detroit, Michigan." Research Report No. R-1338, pp. 1-20.

Smiley, D.L. (1996). "Michigan Department of Transportation-Second Year Performance of The European Concrete Pavement on Northbound I-75-Detroit, Michigan". Research Report No. R-1343, pp. 1-13.

Smiley, D.L. (1997). "Michigan Department of Transportation-Third Year Performance of The European Concrete Pavement on Northbound I-75-Detroit, Michigan." Internal MDOT document, March 18, pp. 1-6.

Smith, K.D., Peshkin, D.G., Darter, M.I., Mueller, A.L., and Carpenter, S.H. (1990). "Performance of Jointed Concrete Pavements: Volume I-Evaluation of Concrete Pavement Performance and Design Features." Report No. FHWA-RD-89-136, U.S. Department of Transportation, Federal Highway Administration.

Smith, K.D., Wade, M.J., Peshkin, D.G., Khazanovich, L., Yu, H.T., and Darter, M.I. (1995). *Performance of Concrete Pavements, Volume II - Evaluation of Inservice Concrete Pavements*, Report No. FHWA-RD-95-110, Federal Highway Administration, Washington, DC.

Smith, K.D., M.J., Wade, H. T. Yu, and M.I., Darter (1997). "Design Considerations for Improved JPCP Performance." *Sixth International Purdue Conference on Concrete Pavement Design and Materials for High Performance,* Vol. 1, pp. 89-109.

Soares, J.B., and Zollinger, D.G. (1997). "Strength Characterization and Basis for Sawcutting Requirements for Jointed Concrete Pavements." *Sixth International Purdue Conference on Concrete Pavement Design and Materials for High Performance*, Vol. 2.

Spellman, D.L.; Woodstrom, J.H.; Neal, B.F.; Mason, P.E. (1973) "Recent Experimental PCC Pavements In California", Caltrans, June 1973, pp.56.

Stark, D. (1991). *Handbook for the Identification of Alkali-Silica Reactivity in Highway Structures*. SHRP-C/FR-91-101, Nation Research Council, Washington, DC.

Sutherland, E.C., and Cashell, H.D. (1945). "Structural Efficiency of Transverse Weakened-Plane Joints." *Public Roads*, Vol. 24, No. 4, Apr-June 1945.

Tachibana, D., Imai, M., Yamazaki, N., Kawai, T., and Inada, Y. (1990). "High-Strength Concrete Incorporating Several Admixtures." *High- Strength Concrete: Second International Symposium*, ACI SP-121, T.H. Weston, ed., pp. 309-330.

Teller, L.W., and Bosley, H.L. (1930). "The Arlington Curing Experiments." *Public Roads Journal of Highway Research*, USDA, Vol. 10, No. 12.

Teller, L.W., and Sutherland, E.C. (1935). "Observed Effects of Variations in Temperature and Moisture on the Size, Shape, and Stress Resistance of Concrete Pavement Slabs." *Public Roads Journal of Highway Research*, USDA, Vol. 16, No. 9.

Till, R., Smiley, D., and Van Portfliet, R. (1994). "Demonstrating Innovative Concrete Pavement Concepts in Michigan" *Transportation Research News*, No. 174, pp. 14-18.

Titus-Glover, L., Owusu-Antwi, E.B., and Darter, M.I. (1999). "Design and Construction of PCC Pavements" FHWA-RD-98-113, U.S. Department of Transportation, Federal Highway Administration.

Titus-Glover, L., Owusu-Antwi, E.B., and Darter, M.I. (1999). "Design and Construction of PCC Pavements – Volume III: Improved PCC Performance Models." FHWA-RD-98-113, U.S. Department of Transportation, Federal Highway Administration.

Torrent, R. (1992). *A Two-chaber vacuum cell for measuring the coefficientof air-permeability of the concrete cover on site.* Materials & Structures, v. 25m n. 150, 1992, pp. 358-365

TRB (1986). *Strategic Highway Research Program - Research Plans.* Transportation Research Board, Final Report, Washington, DC.

Ulfkjær, J.P., Brincker, R., and Krenk, S. (1990). "Analytical Model for Complete Moment-Rotation Curves of Concrete Beams in Bending, Fracture Behavior and Design of Materials and Structures." (Proc 8th European Conf on Fracture, Turin, Italy 1990.) D. Firrao, ed., Engineering Materials Advisory Services, Warley, UK, Vol. 2, pp. 612-617. Also published elsewhere in 1992.

Van Dam, T.J. (1995). "The Impact of Climate, Load, and Materials on the Performance and Deterioration of GA Airports in Illinois." Ph.D. Thesis, University of Illinois Urbana-Champaign.

Van Wiji, A.J., Larralde, C.W.L., and Chen, W.F. (1989). "Pumping Prediction Model for Highway Concrete Pavements." *Journal of Transportation Engineering*, Vol. 115, No. 2, pp. 161-175.

Vervuurt, A. (1997). "Interface Fracture in Concrete." Ph.D Thesis, CIP-GEGEVENS KONINKLIJKE BIBILOTHEEK DEN HAAG.

Vesic, A.S. and Saxena, S.K. (1969). "Analysis of Structural Behavior of Road Test Rigid Pavements." *Highway Research Record*, No.291, pp. 156-158.

Weinfurter, J.A. et al. (1994). "Michigan Department of Transportation Construction of European Concrete Pavement on Northbound I-75-Detroit, Michigan." Research Report no. R-1333, pp. 1-27.

Wells, G.K. (1993). "Summary Report to Improve Jointed Plain Concrete Pavement (JPCP) Performance," Dec. 29.

Westergaard, H.M. (1926). "Stresses in Concrete Pavements Computed by Theoretical Analysis." *Public Roads Journal of Highway Research*, USDA, Vol. 7, No. 2.

Westergaard, H.M. (1927). "Analysis of Stresses in Concrete Roads Caused by Temperature." *Public Roads Journal of Highway Research*, USDA, Vol. 8, No. 3.

Yu, H.T., Darter, M.I., Smith, K.D., Jiang, J., and Khazanovich, L. (1996). "Performance of Concrete Pavements, Volume III – Improving Concrete Pavement Performance,

Final Report." Contract No. DTFH61-91-C-00053. Federal Highway Administration, McLean, VA.

Zia, P., Leming, M. L., and Ahmad S. H. (1991). *High Performance Concretes - A State of-the-Art Report*. Strategic Highway Research Program, SHRP-C/FR-91-103, National Research Council, Washington, DC.

Zhou, F.P., Barr, B.I.G., and Lydon, F.D. (1995). "Fracture Properties of High Strength Concrete with Varying Silica Fume Content and Aggregates." *Cement and Concrete Research*, Vol. 25, No. 3, pp. 543-552.

Zoldners, N.G. (1971). "Thermal Properties of Concrete Under Sustained Elevated Temperatures", Temperature and Concrete" in *Temperature and Concrete*, ACI SP-25, Detroit, MI, pp. 1-31.